Functional Studies of Thermosensitive Transient Receptor Potential (TRP) Ion Channel Regulation

by

Jacob Kenneth Hilton

A Dissertation Presented in Partial Fulfillment
of the Requirements for the Degree
Doctor of Philosophy

Approved April 2019 by the
Graduate Supervisory Committee:

Wade D. Van Horn, Chair
Giovanna Ghirlanda
Marcia Levitus

ARIZONA STATE UNIVERSITY

May 2019

ABSTRACT

All organisms need to be able to sense and respond to their environment. Much of this process takes place via proteins embedded in the cell membrane, the border between a living thing and the external world. Transient receptor potential (TRP) ion channels are a superfamily of membrane proteins that play diverse roles in physiology. Among the 27 TRP channels found in humans and other animals, TRP melastatin 8 (TRPM8) and TRP vanilloid 1 (TRPV1) are the primary sensors of cold and hot temperatures, respectively. They underlie the molecular basis of somatic temperature sensation, but beyond this are also known to be involved in body temperature and weight regulation, inflammation, migraine, nociception, and some types of cancer. Because of their broad physiological roles, these channels are an attractive target for potential therapeutic interventions.

This dissertation presents experimental studies to elucidate the mechanisms underlying TRPM8 and TRPV1 function and regulation. Electrophysiology experiments show that modulation of TRPM8 activity by phosphoinositide interacting regulator of TRP (PIRT), a small membrane protein, is species dependent; human PIRT attenuates TRPM8 activity, whereas mouse PIRT potentiates the channel. Direct binding experiments and chimeric mouse-human TRPM8 channels reveal that this regulation takes place via the transmembrane domain of the channel. Ligand activation of TRPM8 is also investigated. A mutation in the linker between the S4 and S5 helices is found to generally decrease TRPM8 currents, and to specifically abrogate functional response to the potent agonist icilin without affecting icilin binding.

The heat activation thermodynamics of TRPV1 are also probed using temperature-controlled electrophysiology. The magnitude of the gating enthalpy of human TRPV1 is found to be similar to other species reported in the literature. Human TRPV1 also features an apparent heat inactivation process that results in reduced heat sensitivity after exposure to elevated temperatures. The work presented in this dissertation sheds light on the varied mechanisms of thermosensitive TRP channel function and regulation.

To my family and friends

ACKNOWLEDGEMENTS

I am grateful to a multitude of people for making this not only possible, but also a grand adventure. I've had a great committee to help me along the way. I was lucky to be one of the first graduate students in Dr. Wade Van Horn's group, and he has been an excellent mentor and shaped me into a better scientist. Dr. Giovanna Ghirlanda gave me my first home and great experience as a rotation student, and Dr. Marcia Levitus taught me to appreciate the quantitative side of biology. They both have supported and encouraged me as my committee members. I have learned so much from the other faculty of the School of Molecular Sciences and the Biodesign Institute at ASU. I must also acknowledge some of my first scientific mentors, Dr. Emily Bates and Dr. Jeff Macedone, who inspired me as an undergraduate to continue in my scientific career.

My friends in the Van Horn lab group have been a pleasure to do science with. Minjoo Kim taught me how to run NMR experiments and has a welcome sense of humor and listening ear in times of frustration. Nick Sisco helped me think about these projects from different perspectives and gave helpful feedback in many lab group meetings. Dustin Luu was helpful in sharing his protein purification experience, and his generosity is always a bright spot. Camila Montano is a top-notch lab manager and lent a hand many times to make sure a dish of cells would be ready for experiments.

My family has been a bedrock of support over the years. I would not have taken this journey without the encouragement of my parents, Gary and Kengie Hilton. My family in Arizona, especially Shane and Megan Hilton, and Joe and Claudia Hilton, showed me the beauty of life in the desert and provided welcome breaks from life in the

lab. And I’m grateful to Hank and Barb Huey for their support and encouragement over the years.

Finally, I am grateful to Shannon, who made graduate school twice as fun as it should have been. She was there from the beginning to celebrate my successes, help me think about my work, and pick up my confidence after many failed experiments. Having her along for the ride amplified the peaks and dampened the troughs.

TABLE OF CONTENTS

Page

LIST OF TABLES xi

LIST OF FIGURES xii

CHAPTER

1 INTRODUCTION 1

1.1 References 7

2 UNDERSTANDING THERMOSENSITIVE TRANSIENT RECEPTOR POTENTIAL CHANNELS AS VERSATILE POLYMODAL CELLULAR SENSORS 9

2.1 Abstract 9

2.2 Introduction 9

2.3 TRP Channels Beyond Sensory Physiology 13

2.4 Variation in Thermosensitive TRP Channel Modulation 16

2.5 TRP Channels As Molecular Thermometers 22

2.6 On The Path to a Structural Biological Mechanism of TRP Thermosensing 27

2.7 Identifying a TRP Specific Thermosensor 29

2.8 References 38

3 PHOSPHOINOSITIDE-INTERACTING REGULATOR OF TRP (PIRT) HAS OPPOSING EFFECTS ON HUMAN AND MOUSE TRPM8 ION CHANNELS 52

3.1 Abstract 52

3.2 Introduction 53

CHAPTER Page

3.3 Results 55

3.3.1 PIRT Modulation of TRPM8 Is Species Dependent 55

3.3.2 PIRT Interacts Directly With the TRPM8 S1–S4 Domain 60

3.3.3 Functional Determinants of PIRT Modulation in the TRPM8 Transmembrane Domain 63

3.4 Discussion 65

3.5 Experimental Procedures 73

3.5.1 Cell Culture 73

3.5.2 Electrophysiology Measurements 74

3.5.3 Cell Surface Expression 75

3.5.4 Chimera Generation 77

3.5.5 Expression and Purification of hTRPM8 S1–S4 Domain and hKCNQ1-VSD 78

3.5.6 Expression and Purification of hPIRT 78

3.5.7 hTRPM8 S1–S4 Domain and hPIRT Pull-down Experiment 80

3.5.8 hPIRT-hTRPM8 S1–S4 Domain and KCNQ1-VSD NMR Titration 80

3.6 References 81

4 A MUTATION IN THE S4-S5 LINKER OF TRPM8 SELECTIVELY ABOLISHES ICILIN SENSITIVITY 87

4.1 Introduction 87

4.2 Experimental Methods 91

CHAPTER Page

4.2.1 Cell Culture 91

4.2.2 Electrophysiology 91

4.2.3 Expression Testing of the Human TRPM8 S1–S4 Domain 92

4.2.4 Expression of the S1–S4 Domain 94

4.2.5 Purification of the S1–S4 Domain 95

4.2.6 Nuclear Magnetic Resonance Spectroscopy 96

4.2.7 Circular Dichroism 97

4.3 Results and discussion 98

4.3.1 N852A Mutation Causes a General Decrease in TRPM8 Currents 98

4.3.2 Menthol and Icilin Sensitivity of the N852A Mutant 101

4.3.3 Purification of the TRPM8 S1–S4 Domain 106

4.3.4 Ligand Binding Measurements Using NMR 110

4.3.5 CD Measurements 114

4.4 Conclusion 117

4.5 Supplementary Information 119

4.5.1 NMR Processing scripts 119

4.5.1.1 fid.com Script from NMRPipe Conversion Utility (Version 2017.263.14.36) 119

4.5.1.2 nmrproc.com Script for nmrDraw 120

4.5.2 MatLab Peak Chemical Shift Calculation and Fitting Script 121

4.5 References 122

CHAPTER Page

5 THERMODYNAMICS AND ANTAGONISM OF THERMOSENSITIVE TRP CHANNELS 126

5.1 Introduction 126

5.2 Experimental Methods 126

5.2.1 Cell Culture 126

5.2.2 Generation of TRPM2–TRPM8 Chimeras 126

5.2.3 Plasmid and Mammalian Cell Transfection 128

5.2.4 Electrophysiology 128

5.3 TRPV1 Thermosensitivity 130

5.3.1 Introduction 130

5.3.2 Thermodynamics of TRPV1 Activation 131

5.3.3 Heat Inactivation of Human TRPV1 137

5.3.4 The R557A Mutation Abolishes TRPV1 Heat Sensitivity 140

5.4 Probing TRPM8 Cold Sensing With TRPM2-TRPM8 Chimeras 141

5.5 TRPM8 Compound 103 Antagonism 147

5.6 References 149

6 SUMMARY AND CONCLUSIONS 153

REFERENCES 156

APPENDIX

A SUPPLEMENT TO CHAPTER 3: ADDITIONAL HUMAN-MOUSE TRPM8 CHIMERA DATA 183

APPENDIX Page

B PUBLISHED PORTIONS 187

LIST OF TABLES

Table Page

2.1 Structures of TRP Channels and TRP Channel Domains 33

4.1 Literature Values of Menthol and Icilin EC_{50} for TRPM8 106

4.2 Expression Levels of TRPM8 S1–S4 Domain from Tested Cell Lines.....109

5.1 Literature Values for $\Delta H°$ of TRPV1 Gating 134

LIST OF FIGURES

Figure		Page
1.1	TRP Channel Evolutionary Relationships and Representative Structures	3
1.2	The Conserved Transmembrane Architecture of TRP Ion Channels	4
1.3	Whole-cell Patch-clamp Electrophysiology	6
2.1	Architecture of TRP Channels	11
2.2	Polymodal Modulation of Thermosensitive TRP Channels	13
2.3	Examples of Variation in TRP Channel Function Between Species	18
2.4	Reported Regions of TRP Channels Important for Thermosensing	24
2.5	Low Sequence Conservation in Human Thermosensitive TRP Channels	26
2.6	Residues of the Shaker Channel Modified to Confer Thermosensitivity	29
3.1	Human PIRT Attenuates Whole-cell Currents of Human TRPM8	56
3.2	Human and Mouse Species Dependent PIRT Regulation of TRPM8 Orthologs	58
3.3	Human TRPM8 Cell Surface Trafficking Is Not Affected by PIRT Expression	59
3.4	NMR Binding Studies of Human PIRT and TRPM8	62
3.5	Mouse-Human TRPM8 Chimeric Channels Regulated by Human PIRT	64
3.6	A Model of PIRT–TRPM8 Complex Stoichiometry	68
4.1	Locations of Mutated Residues in TRPM8	99
4.2	Electrophysiology Measurements of TRPM8 Mutants	100
4.3	Ratios of TRPM8-N852A Current Response to Cold and Menthol	101
4.4	Representative Tail Current Traces from TRPM8 and TRPM8-N852A	103
4.5	Determination of $I_{\mathrm{Tail,max}}$ From Tail Currents	105

Figure Page

4.6 Menthol and Icilin EC_{50} Values for TRPM8 and TRPM8-N852A.....105

4.7 TRPM8 S1–S4 Domain Expression Test Results.....108

4.8 Purification of TRPM8 S1–S4 Domain.....109

4.9 HSQC NMR Spectra of Wild-type and N852A TRPM8 S1–S4 Domain.....110

4.10 Overlay of HSQC NMR Spectra of Wild-type and N852A TRPM8 S1–S4.....111

4.11 Menthol Titration of Wild-type S1–S4 Domain.....112

4.12 Menthol Titration of N852A S1–S4 Domain.....113

4.13 Icilin Titration of Wild-Type and N852A S1–S4 Domain.....114

4.14 Circular Dichroism of TRPM8 S1–S4 Domain.....117

5.1 Modeled Ion Channel Open Probability Curves for Different Values of $\Delta H°$ 133

5.2 Electrophysiology Measurements to Determine $\Delta H°$ of TRPV1 Gating.....136

5.3 TRPV1 Temperature Ramps and Hysteresis.....138

5.4 The Role of R557 in TRPV1 Heat Sensitivity.....140

5.5 Sequence Alignment and Chimeras of TRPM8 and TRPM2.....144

5.6 Topology of TRPM2-TRPM8 Chimeric Channels.....145

5.7 Electrophysiology Measurements of TRPM2-TRPM8 Chimeras.....147

5.8 Chemical Structures of Menthol, Icilin, and Compound 103.....148

5.9 Inhibition of Menthol-evoked Currents by Compound 103.....149

A.1 hTRPM8[mM8-SD] Chimera Electrophysiology.....184

A.2 hTRPM8[mM8-TMD] Chimera Electrophysiology.....185

A.3 Summary of Human-Mouse TRPM8 Chimera Results.....186

CHAPTER 1

INTRODUCTION

Fundamental to life on earth is the ability of organisms to sense and respond to their environment. All cells, from unicellular bacteria and archaea to the hundreds of cell types in a human body, are enveloped in a lipid membrane that defines the cell boundary, encloses organelles, controls the internal environment and allows life-sustaining chemical reactions to take place. Embedded in this membrane are proteins that link the inner life of the cell with the outer world it lives in. These proteins have evolved to sense the internal and external environment, allow select ions and molecules to pass into or out of the cell, and respond to the environment in distinct ways.

Among these integral membrane proteins, ion channels are a diverse family of proteins that form pores in the membrane. Depending on the sequence and structure of the channel, these pores can be opened, or gated, in response to a wide variety of stimuli. Transient receptor potential (TRP) ion channels are a superfamily of channels that have evolved to fill an abundance of physiological functions. The first member of this family was identified in 1969, when Cosens and Manning reported a *Drosophila* mutant that lacked a sustained response to light during electroretinogram measurements [1]. In keeping with the traditional (albeit somewhat counterintuitive) practice in genetics of naming a gene for its loss-of-function mutant phenotype, the gene was later named transient receptor potential (*trp*), in reference to its momentary electrical response when exposed to light [2]. It wasn't until twenty years later that Montell and Rubin successfully cloned the *trp* gene and recognized it as an integral membrane protein, although its role in

the phototransduction pathway was still unclear[3]. Advances in isolating *Drosophila* photoreceptor cells by Hardie et al. [4] allowed for recording whole cell currents under controlled conditions, and using this technique it was soon discovered that the protein encoded by *trp* was a Ca^{2+}-permeant channel [5].

Since the discovery of that founding member of the TRP channel family, many other related channels have been discovered; currently 27 distinct TRP channels have been identified in humans (Figure 1.1, left). Based on sequence homology, these have been grouped into five subfamilies: TRPA, TRPV, TRPM, TRPC, and TRPML. Unlike other ion channel families, TRP channels show remarkable diversity in ion selectivity, structure, activation mechanisms, and physiological roles. Even within a subfamily, the channels can have widely divergent functional properties. For example, within the TRPM subfamily, TRPM8 activates at cold temperatures and is non-selectively permeable to both divalent and monovalent cations [6, 7], whereas TRPM5 is activated by warm temperatures and is selectively permeable to monovalent cations [8, 9]. Within the TRPV family, TRPV1 is activated by the pungent compound capsaicin [10], while other TRPV channels are unresponsive to this ligand. Besides functional diversity between different members of the superfamily, TRP channels have also evolved to be fine-tuned for a particular organism and its environment. For example, the temperature range and sensitivity of the cold-sensing channel TRPM8 is tuned to the body temperature set point and environmental temperature of a given organism; TRPM8 from cold-blooded frogs activates at lower temperatures compared to rodents and birds with their higher core body temperature [11]. Other branches of the animal kingdom have likewise “adjusted the

thermostat" by shifting the range of their thermosensing TRP channels [12]. Understanding the molecular basis of this functional diversity has been an overarching goal of the field over the past few decades.

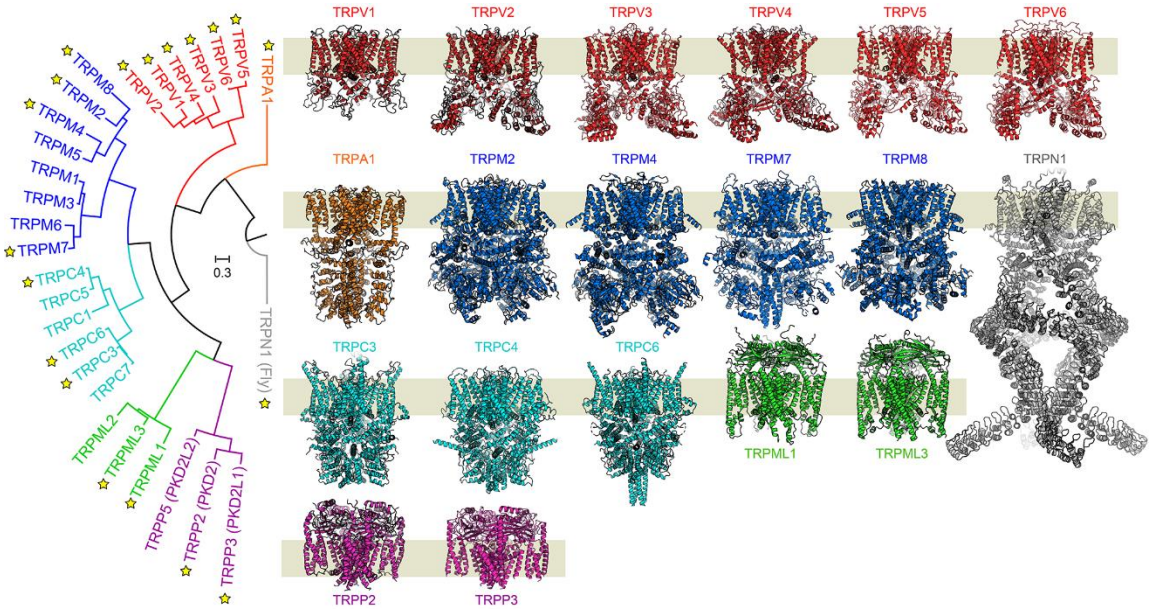

Figure 1.1 TRP channel evolutionary relationships and representative structures. Left, a phylogenetic tree of human TRP channels, including an ancestral non-mammalian TRPN1 channel (Gray). Yellow stars indicate that a structure of either the human or an ortholog channel has been determined. To date, at least two structures have been determined from each human TRP subfamily, with exception of TRPA1, where there is a lone human subfamily member. Representative structures have been determined for the entire vanilloid (TRPV) subfamily. The structures reveal a conserved general transmembrane architecture with highly diverse extramembrane loops and N- and C-terminal domains. The collective structural information has shaped understanding of how TRP channels gate in response to chemical and physical stimuli. TRPA is for ankyrin, -V for vanilloid, -M for melastatin, -C for canonical, -ML for mucolipin, -P for polycystic.

TRP channels are structurally diverse in their cytoplasmic N- and C-terminal domains (Figure 1.1, right), but they share a conserved transmembrane topology of six helices per subunit, termed the S1 through S6 helices. They share a general architecture with classical voltage-gated potassium (K_V) channels; the first four transmembrane helices (S1–S4) comprise a helical bundle homologous to the voltage-sensing domain of

K_Vs, while helices S5 and S6 form a pore domain. The channels are homotetramers, with the S5 and S6 helices forming the conducting pore in a domain-swapped configuration (Figure 1.2). Also similar to K_V channels, a short helical S4-S5 linker connects the S1–S4 domain to the pore domain and allows for functional coupling between the two domains. Finally, a feature conserved in all TRP channels and unique to the superfamily is a post-S6 amphipathic "TRP helix" that extends below the S1–S4 domain and interacts with the S4-S5 linker to modulate channel gating. In the last several years as cryo-electron microscopy has matured, TRP channel structures from each subfamily have been determined, confirming many of the features that had been hypothesized by functional studies while raising new questions.

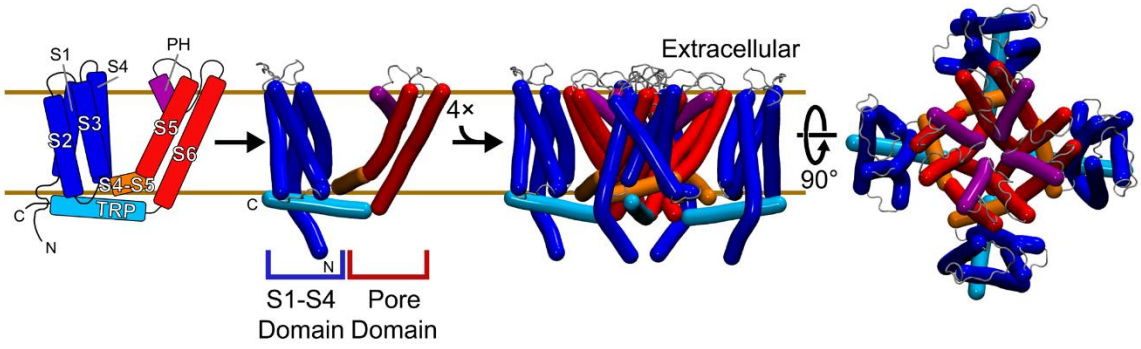

Figure 1.2 The conserved transmembrane architecture of TRP ion channels. A TRP channel monomer (left panels) contains six transmembrane helices, including two conserved structural domains. The S1-S4 (blue) domain forms a four-helix bundle. The last two transmembrane helices, S5 and S6, form the pore domain (PD, red) where the tetramer of the PD forms the conductance pathway of the channel. The S1-S4 domain and the PD are linked by an S4-S5 linker (orange). Two additional conserved helices are the pore helix (PH, violet) and the amphipathic TRP helix (cyan). A functional channel is composed of a domain-swapped tetramer, with the PD helices interacting with adjacent subunits (right panels). Structural and functional studies suggest that allosteric networks between binding, temperature sensing, and other stimuli regulate these channels.

The primary tool for investigating ion channel function is patch-clamp electrophysiology, first pioneered by the legendary Hodgkin and Huxley [13]. The studies presented in this work use the whole-cell patch clamp technique, which measures the total electrical currents through all ion channels in a cell under various conditions. In this technique, the channel of interest is biologically expressed and trafficking to a cell membrane. A fine-tipped glass pipette is filled with a solution that mimics the ionic concentrations of the intracellular environment, and an electrode is inserted into the pipette. The pipette is brought into contact with the membrane surface of an individual cell, and a tight seal is formed between a "patch" of the bilayer and the glass pipette, typically with more than gigaohm of resistance. The patch of membrane is torn away by applying negative pressure, giving the electrode access to the interior of the cell. A second electrode is placed outside the cell in an extracellular solution, and electronic equipment is used to clamp the membrane potential at a desired voltage (Figure 1.3). Any deviation from this voltage is quickly compensated by an injection of current; this current is measured and recorded. Measuring these currents under different conditions provides insight into ion channel selectivity and response to stimuli such as voltage, ligands, or temperature.

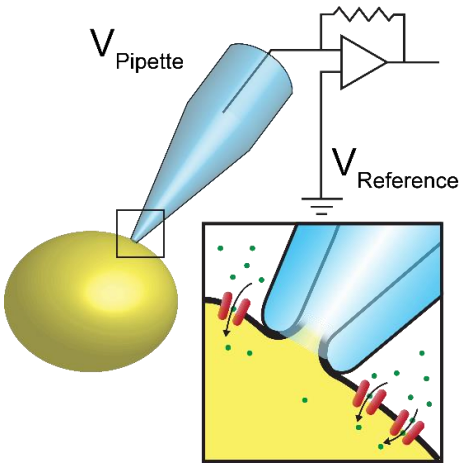

Figure 1.3 Whole-cell patch-clamp electrophysiology. After forming a seal between the glass pipette and the plasma membrane, tearing away the membrane patch under the pipette opening gives electrical access to the cell interior and allows for control of the potential across the membrane.

The work presented here focuses on two of the thermosensitive TRP channels: the cold-sensing channel TRPM8 and its heat-sensitive counterpart TRPV1. Chapter 2 presents a broad overview of TRP channel physiology and function, focusing particularly on thermosensing. This chapter also highlights techniques that can be used to study TRP channels, including X-ray crystallography, cryo-EM, nuclear magnetic resonance and fluorescence spectroscopy, and computational methods. Chapter 3 presents a study to investigate regulation of TRPM8 by PIRT, a small two-span membrane protein. The results of this study underscore the importance of the transmembrane domain in channel function and regulation, and they demonstrate a novel difference in PIRT modulation between species. Chapter 4 presents the identification of a point mutation in TRPM8 that causes a general attenuation of channel function and selectively abolishes response to the TRPM8 agonist icilin. Insights and possible interpretations of this effect are discussed. Chapter 5 discusses variously the measurement of TRPV1 heat activation energetics, an

attempt to probe the regions of TRPM8 involved in its cold temperature sensitivity, and a study of a novel TRPM8 antagonist. Finally, Chapter 6 summarizes the conclusions of this work and discusses future directions for further study.

1.1 References

1. Manning, A., and Cosens, D. J. (1969) Abnormal Electroretinogram from a *Drosophila* mutant. *Nature* **224**, 285-287

2. Minke, B., Wu, C., and Pak, W. L. (1975) Induction of photoreceptor voltage noise in the dark in *Drosophila* mutant. *Nature* **258**, 84-87

3. Montell, C., and Rubin, G. M. (1989) Molecular Characterization of the Drosophila *trp* Locus: A Putative Integral Membrane Protein Required for Phototransduction. *Neuron* **2**, 1313-1323

4. Hardie, R. C., Voss, D., Pongs, O., and Laughlin, S. B. (1991) Novel Potassium Channels Encoded by the *Shaker* Locus in Drosophila Photoreceptors. *Neuron* **6**, 477-486

5. Hardie, R. C., and Minke, B. (1992) The *trp* Gene is Essential for a Light-Activated Ca^{2+} Channel in Drosophila Photoreceptors. *Neuron* **8**, 643-651

6. McKemy, D. D., Neuhausser, W. M., and Julius, D. (2002) Identification of a cold receptor reveals a general role for TRP channels in thermosensation. *Nature* **416**, 52-58

7. Peier, A. M., Moqrich, A., Hergarden, A. C., Reeve, A. J., Andersson, D. A., Story, G. M., Earley, T. J., Dragoni, I., McIntyre, P., Bevan, S., and Patapoutian, A. (2002) A TRP Channel that Senses Cold Stimuli and Menthol. *Cell* **8** 705-715

8. Hofmann, T., Chubanov, V., Gudermann, T., and Montell, C. (2003) TRPM5 Is a Voltage-Modulated and Ca^{2+}-Activated Monovalent Selective Cation Channel. *Curr. Biol.* **13**, 1153-1158

9. Talavera, K., Yasumatsu, K., Voets, T., Droogmans, G., Shigemura, N., Ninomiya, Y., Margolskee, R. F., and Nilius, B. (2005) Heat activation of TRPM5 underlies thermal sensitivity of sweet taste. *Nature* **438**, 1022-1025

10. Caterina, M. J., Schumacher, M. A., Tominaga, M., Rosen, T. A., Levine, J. D., and Julius, D. (1997) The capsaicin receptor: a heat-activated ion channel in the pain pathway. *Nature* **389**, 816-824

11. Myers, B. R., Sigal, Y. M., and Julius, D. (2009) Evolution of Thermal Response Properties in a Cold-Activated TRP Channel. *PLoS One* **4**, e5741

12. Gracheva, E. O., and Bagriantsev, S. N. (2015) Evolutionary adaptation to thermosensation. *Curr. Opin. Neurobiol.* **34**, 67-73

13. Hodgkin, A. L., Huxley, A. F., and Katz, B. (1952) Measurement of current-voltage relations in the membrane of the giant axon of *Loligo*. *J. Physiol.* **116**, 424-448

CHAPTER 2

UNDERSTANDING THERMOSENSITIVE TRANSIENT RECEPTOR POTENTIAL CHANNELS AS VERSATILE POLYMODAL CELLULAR SENSORS

2.1 Abstract

Transient receptor potential (TRP) ion channels are eukaryotic polymodal sensors that function as molecular cellular signal integrators. TRP family members sense and are modulated by a wide array of inputs, including temperature, pressure, pH, voltage, chemicals, lipids, and other proteins. These inputs induce signal transduction events mediated by nonselective cation passage through TRP channels. In this review, we focus on the thermosensitive TRP channels and highlight the emerging view that these channels play a variety of significant roles in physiology and pathophysiology in addition to sensory biology. We attempt to use this viewpoint as a framework to understand the complexity and controversy of TRP channel modulation and ultimately suggest that the complex functional behavior arises inherently because this class of protein is exquisitely sensitive to many diverse and distinct signal inputs. To illustrate this idea, we primarily focus on TRP channel thermosensing. We also offer a structural, biochemical, biophysical, and computational perspective that may help to bring more coherence and consensus in understanding the function of this important class of proteins.

2.2 Introduction

TRP channels are a family of diverse ion channels with broad physiological roles found primarily in higher organisms. These protein channels share structural homology

with voltage-gated potassium and related ion channels (Figure 2.1). Since cloning and sequencing of the first transient receptor potential (TRP) ion channel in 1989, this protein superfamily has emerged as a diverse group of cellular sensors.[1] With the identification of temperature, gustatory, and mechano-sensing TRP channels in the late 1990s and early 2000s, TRP channels have been widely associated with sensory physiology. Many investigations have shown that in addition to significant roles in sensory biology, TRP channels are involved in a wide variety of physiological and pathophysiological roles. Unlike many protein families in which characteristic functional attributes identify family members, TRP channels are sufficiently evolutionarily diverse such that they are defined solely by their sequence, perhaps underscoring the ability of TRP channels to function in a variety of biological contexts.[2] In addition to high sequence and functional diversity among family members, individual TRP channels have been evolutionarily fine-tuned and multipurposed in a species dependent manner. This molecular speciation complicates comparative studies and seems to convolute attempts to elucidate molecular mechanisms. Compounding this, many TRP channels are modulated by a number of distinct stimuli.

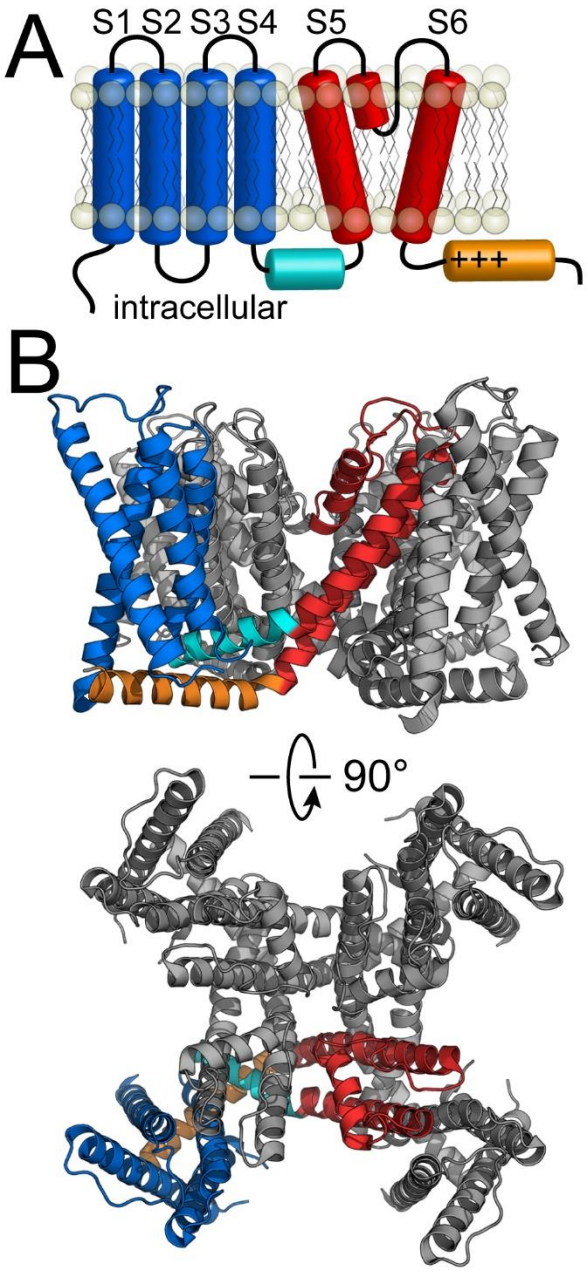

Figure 2.1 *Architecture of TRP channels.* A) The membrane domain structure of TRP channels is homologous to voltage-gated potassium channels. The sensor domain is comprised of helices S1-S4 (blue). This domain is linked to the pore domain S5-S6 transmembrane helices (red) by an S4-S5 α-helix linker (cyan). The C-terminal juxtamembrane region is comprised of an α-helical segment (orange) which includes a short segment of generally conserved basic residues that have been implicated in PIP_2 regulation of TRP channels. B) Structural view of the membrane regions of the functionally relevant tetrameric TRPV1 channel from 3J5P.pdb with the same coloring as panel A. The bottom panel is an extracellular view of the membrane regions of TRPV1.

The inherent polymodal modulation of themoTRP channels is illustrated by TRPV1, which is the most thoroughly studied family member (Figure 2.2). In humans, TRPV1 is the primary heat sensor and is activated by elevated temperatures.[3, 4] It is also activated by pH, changes in membrane potential (voltage), divalent cations (Mg^{2+} and Ca^{2+}), phosphoinositide lipids, a small membrane protein named PIRT, and perhaps mechanical force.[3, 5-10] TRPV1 is also directly and indirectly modulated by an array of natural and synthetic compounds, including capsaicin from spicy chili peppers, THC (Δ9-tetrahydrocannabinol) from cannabis, and a variety of toxins originating from spiders, fungi, and bacteria.[3, 11-15] While a given TRP channel may be sensitive to a wide variety of stimulatory inputs, TRPV1 and other TRP channels have evolved to fill specific species-dependent roles. For example, human and rodent TRPV1 channels are sensitive to capsaicin, while amphibian and avian TRPV1 are not.[16] Similarly, above physiological temperatures, human TRPV1 activates and thus fulfills its role as a molecular thermometer.[4] Vampire bats, on the other hand, utilize a truncated TRPV1 isoform in specialized organs to detect infrared radiation, allowing for thermal imaging of prey.[17]

This work briefly highlights the polymodal modulatory nature of thermosensitive TRP channels, the importance of these channels in roles outside of sensory biology, and uses this as a platform to examine controversial modes of modulation by proteins, lipids, and thermal stimuli. We suggest that the inherent diversity of TRP channels and their means of channel modulation give rise to apparently opposing experimental results.

Finally, we offer some yet to be investigated avenues that may help identify molecular mechanisms of thermosensation which have so far eluded previous investigations.

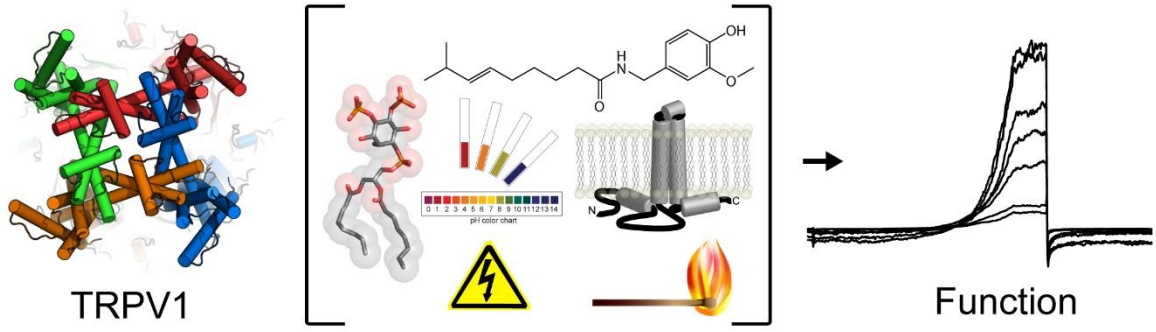

Figure 2.2 *Polymodal modulation of thermosensitive TRP channels.* TRPV1 is regulated, modulated, and gated by a variety of diverse stimuli. These include chemical compounds, such as capsaicin; lipids, such as phosphoinisitides; and membrane proteins, such as PIRT. In addition TRPV1 function is modulated by heat, voltage, and pH. The polymodal nature of TRPV1 modulation exemplifies a general feature of thermosensitive TRP channels.

2.3 TRP Channels Beyond Sensory Physiology

Of the 27 TRP channels identified in mammals, ten have been identified as thermosensors, or thermoTRP channels.[18] While many are familiar with TRPV1 and TRPM8, which function as heat and cold sensors respectively, a number of other TRP channels have been implicated as thermosensors, including TRPV2-V4, TRPA1, TRPM2, TRPM4, TRPM5 and TRPC5.[18, 19] These ion channels are well known as vanguards of the somatosensory system; however, research is increasingly revealing a wide variety of physiological roles beyond temperature and ligand sensing. Here, we highlight a few recent results that illustrate some of these diverse physiological roles.

TRPM8 is the primary cold sensor in higher organisms and several studies have shown that TRPM8 regulates body temperature.[20-23] Mice and rats experience a transient drop in core body temperature following administration of TRPM8

antagonists.[20, 22] This is apparently due to thermoregulatory systems of the brain misinterpreting the body's core temperature feedback system; consequently, thermogenesis factors such as vasoconstriction, oxygen consumption, brown adipose tissue thermogenesis, and cold-avoidance behavior are suppressed, resulting in a lower core temperature. Perhaps unsurprisingly, activation of TRPM8 channels by agonists, such as menthol and icilin, has an opposite physiological hyperthermic effect.[21, 23] The thermoregulatory effect of TRPM8 was shown to be connected to the cold hyperalgesia symptom of opiate withdrawal via a direct interaction with the opioid G-protein coupled receptor (GPCR), OPRM1.[24] Upon OPRM1 activation by morphine, TRPM8 and OPRM1 are co-internalized, resulting in a reduction of cold- and menthol-activated currents in vitro. In wild-type mice, morphine treatment causes cold analgesia, whereas TRPM8 knockout results in a decrease in this effect.[24] The thermoregulatory role of TRPM8 also has downstream physiological effects. In a recent study, TRPM8 activation in brown adipose tissue was shown to upregulate expression of a UCP1, the mitochondrial uncoupling protein that bypasses ATP synthesis and harnesses the transmembrane proton gradient to produce heat.[25] Further, mice fed a high fat diet supplemented with a TRPM8 agonist gained significantly less weight than non-supplemented mice, suggesting that TRPM8 plays a role in obesity and body weight regulation.[25]

TRPM8 has also been shown to be involved in insulin regulation. TRPM8 knockout mice exhibit increased rates of insulin clearance, which is apparently the result of increased liver expression of an insulin-degrading enzyme.[26] The precise

mechanism underlying this effect is unclear, given that TRPM8 is not expressed in either the pancreas or liver; however, TRPM8 afferent neurons do innervate the hepatic portal vein.[26] Taken together, while TRPM8 is best known for its role in cold thermosensation, it is implicated in a wide variety of physiologically important roles.

TRPV1 is a heat-activated channel that is also sensitive to a number of noxious stimuli.[27] It was the first human thermosensing channel identified, and is one of the most studied TRP channels. Its role in thermosensing is well established, but recent reports suggest more complex physiological roles. For example, TRPV1 knockout mice have longer lifespans and maintain a youthful metabolic profile, the downstream effects of inactivation of a calcium signaling cascade that results in improved glucose homeostasis.[28] In addition, TRPV1 expressed in osteoclasts is involved in regulating bone resorption via crosstalk with GPCR cannabinoid receptors. Mice models of osteoporosis with either genetic or pharmacological inactivation of TRPV1 have restored osteoclast quiescence and improved bone density and morphology.[29]

TRPM2 is activated by H_2O_2 and other agents that produce reactive oxygen species (ROS), in addition to intracellular adenosine diphosphate ribose (ADPr). It is involved in a diverse array of physiological roles, and new roles continue to be identified. Recently, TRPM2 was shown to play an important role in neuritogenesis during embryonic brain development.[30] In this process, axonal growth and retraction must be properly balanced as the brain is shaped. Neurons that lack TRPM2 activity have significantly longer neurites than native cells.[30] This study also linked TRPM2 to the lysophosphatidic acid (LPA) signaling pathway, which is known to induce neurite

retraction. LPA activates poly-ADPr polymerase 1, which results in increased production of ADPr, an endogenous activator of TRPM2.[30]

TPRM2 is also expressed in mucosal mast cells, where it is involved in the degranulation process in response to antigen stimulation. Oda and coworkers demonstrated that TRPM2-mediated calcium influx is important in this process, and TRPM2 inhibition improved symptoms in a mouse model of food allergy.[31]

Finally, Numata et al. demonstrated that ADPr- and cyclic ADPr-induced TRPM2 currents were identical to hypertonicity-activated currents in HeLa cells.[32] Further experiments revealed that a splice variant of TRPM2 is likely the hypertonicity-induced cation channel in HeLa cells. TRPM2 appears to be activated downstream of CD38, an ectoenzyme responsible for exporting ADPr and cADPR out of the cell. siRNA knockdown of both TRPM2 and CD38 significantly reduced regulatory volume increase in response to hypertonic challenge.[32] While the nature of the crosstalk between CD38 and TRPM2 remains unclear, the finding suggests an interesting role of TRPM2 in cell volume regulation, an important factor in cell proliferation and apoptosis.

These highlights are just a few of the extensive roles thermosensitive TRP channels play in diverse aspects of physiology, but are far from a comprehensive list.[33] Nonetheless, thermoTRP channels clearly play significant roles beyond sensory physiology.

2.4 Variation in Thermosensitive TRP Channel Modulation

Surprising differences in modulation have been documented between thermosensitive TRP orthologues, even in closely related species (Figure 2.3). TRPA1 is

a prime example of species dependent differences, which has probably contributed to the controversy surrounding this channel's function.[34] TRPA1 is a chemical and thermosensitive nociceptor in animals. Sequence variation between species likely accounts for the observed differences in identified in TRPA1 function. As an example, human and mouse TRPA1 share 80% sequence identity, though lower conservation is found between more distantly related species. TRPA1 serves as a heat sensor for reptiles while it is reportedly a cold sensor in rodents and other mammals.[35, 36] A screen of potential new TRPA1 antagonists revealed that trichloro(sulfanyl)ethyl benzamides inhibit human TRPA1, but some of the compounds elicited far smaller inhibitory effects on rat TRPA1, while others even activated it, demonstrating differential pharmacological profiles between the two species' channels.[37] Similarly, caffeine activates mouse TRPA1 but inhibits human TRPA1; the mouse channel activation by caffeine can be reversed to inhibition by a single point mutation.[38-40] There is substantial evidence for evolutionary differentiation of mammalian TRPA1 from other animals: pit vipers express TRPA1 as an infra-red sensor, and TRPA1 appears to be a heat sensor in *Drosophila melanogaster.*[41-43] Indeed, the function of TRPA1 as a nociceptor is well-conserved throughout many species, but there are many examples of species-dependent differences: for a more thorough analysis of this literature, refer to the review by Chen and Kim.[44]

In addition to clear functional differences for TRP channels between species, it is clear that specific isoforms of TRP channels expand functional properties for a given channel in a given species. This idea is highlighted in *Drosophila* TRPA1 studies that carefully characterized four channel isoforms.[42, 45] Two *Drosophila* TRPA1 isoforms

are heat sensitive while the other two isoforms are not temperature sensitive. Interestingly, the *Drosophila* TRPA1 isoforms exhibit differential expression profiles, apparently physiologically tailored to either heat- or pain-sensing neurons.

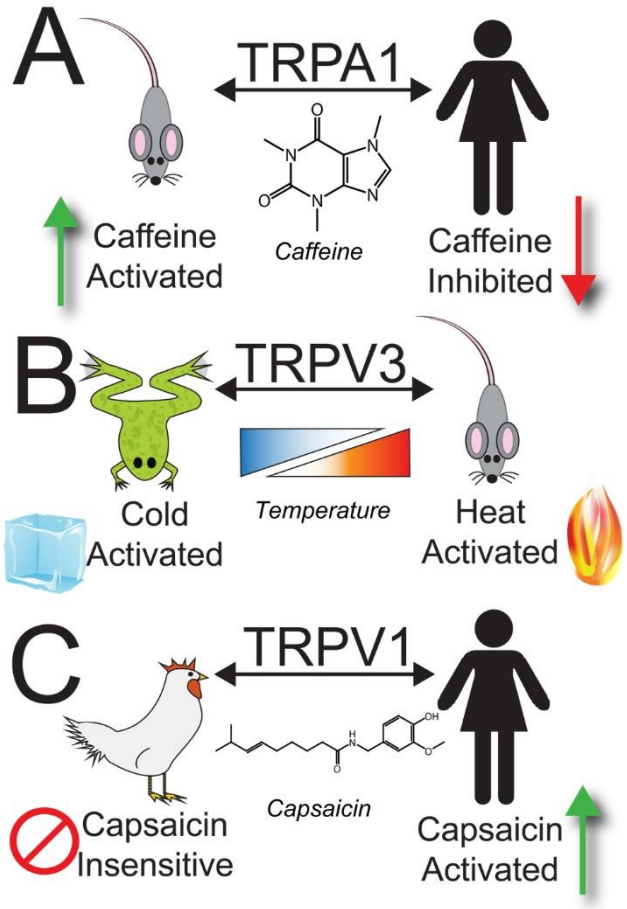

Figure 2.3 *Examples of variation in TRP channel function between species*. A) Caffeine activates mouse TRPA1, but attenuates the activity of human TRPA1. B) Evolutionary divergence has produced cold-sensitive TRPV3 in Western Clawed Frogs, whereas TRPV3 has been implicated as a heat sensor in mice and other mammals. C) Avian orthologues of TRPV1 are insensitive to capsaicin, a key agonist of the mammalian channel.

While TRPA1 is a particularly rich example of apparent speciation and complex regulation, it is not unique in this regard. The IR sensitive TRPA1 found in pit vipers is not the only TRP channel that has evolved to fill this functional niche: in vampire bats, a

TRPV1 isoform serves a similar function.[46] Western clawed frogs developed a cold-sensitive TRPV3, whereas mammalian TRPV3 is likely a heat sensor.[47] There is conflicting evidence on TRPV3 and TRPV4 contributions to heat sensitivity that may potentially be explained by strain differences in mice.[48]

Species dependent pharmacology has been shown for many compounds for a number of thermosensitive TRP channels. A putative TRPM8 orthologue in clawed frogs is activated by menthol, but with fine-tuned thermosensitivity across a much lower temperature range than the mouse and rat channels.[49] Similarly, chickens and other avians express TRPV1 orthologues that are insensitive to capsaicin, a key agonist of the mammalian channel.[50] The candidate anti-inflammatory compound JYL-1421 blocks capsaicin responses in rat TRPV1, but not in the human or monkey channels.[51] Likewise, phorbol 12-phenylacetate 13-acetate 20-homovanillate (PPAHV) is a strong agonist of rat TRPV1, but has no discernable effect on human TRPV1.[52] Zebrafish TRPV1 orthologues lack residues that are likely essential for endocannabinoid binding, suggesting that zebrafish TRPV1 may be insensitive to endocannabinoids known to interact with the mammalian channels.[53] Rat and mouse TRPV2 are activated by 2-aminoethoxydiphenyl borate (2-APB), a known modulator of many TRPs and store-operated calcium channels, but human TRPV2 is not responsive at all.[54]

Even for well-established endogenous regulators, a given thermosensitive TRP channel's modulatory profile can be complicated. In the case of PIP_2 (phosphatidylinositol 4,5-bisphosphate), an endogenous inner-leaflet membrane lipid known to interact with many ion channels and most TRPs, several channels have

produced conflicting accounts of activation and inactivation. There is emerging and broad agreement that PIP_2 activates TRPV1 in a physiologically relevant context.[55] However, experiments with PIP_2 in artificial liposomes produce an inhibitory effect.[56] This may be explained by the fact that these liposomes do not exhibit the leaflet segregation of PIP_2 found in natural membranes, so the localization of PIP_2 in these experiments may not accurately reflect the endogenous biological context. However, the sensitivity of functional data to such minute differences demonstrates the intrinsic diversity of TRP channel modulation at a fundamental level. A TRP-like *Drosophila melanogaster* channel (dTRPL) has been reported to be both inhibited and strongly activated by PIP_2.[57, 58] Similarly, TRPC4 may exhibit isoform-specific interaction with PIP_2.[59] For a thorough analysis of these issues, see Rohacs' 2014 review of phosphoinositide regulation of TRP channels.[55]

In 2008, Dong et al. characterized a small two-span membrane TRP channel modulatory protein named PIRT (phosphoinositide interacting regulator of TRP), analogous to other β-subunits like the KCNE family for voltage-gated potassium channels.[9] In these studies PIRT activated TRPV1 channels, and PIRT knockout mice showed reduced sensitivity to heat and capsaicin. PIRT has since been implicated in pruritus, or itch sensation, with PIRT knockout mice exhibiting minimal scratching in response to injection of histamine and non-histamine pruritogens.[60] A more recent report revealed that PIRT also potentiates TRPM8 currents in a manner similar to TRPV1; PIRT knockout mice exhibited impaired response to cold temperatures, while electrophysiology recordings showed increased current density in response to cold or

menthol stimuli when PIRT was co-expressed with TRPM8.[61] These results reveal another layer of complexity in thermosensitive TRP channel modulation and given the diverse physiological roles of TRP channels, potentially this functional heterogeneity is achieved by modulatory proteins, including PIRT.

Interestingly, like TRP channels, PIRT contains a putative PIP_2-binding site. Initially it was proposed to be necessary for PIP_2-mediated activation of TRPV1.[9] However, later work by Carmen et al. called that conclusion into question, as inside-out excised patches showed that PIRT had no effect on PIP_2-dependent TRPV1 activation.[8] In any case, from in vivo studies PIRT seems to modulate TRPV1 activity, but questions about the interplay, interactions, and intricacies between channel, PIRT, and PIP_2 remain to be answered. For example, PIRT was shown to bind directly to TRPV1,[9] but the binding site and stoichiometry of this interaction have yet to be elucidated, and the role of the phosphoinositide-binding region of PIRT is unclear.

Differential modulation has been demonstrated in multiple thermosensitive TRP channels, suggesting that it is not an incidental feature of a few family members. Perhaps these distinct modulatory modes have allowed them to function as polymodal sensors well beyond the realm of sensory biology. This issue presents a potential problem for functional studies of TRP channels, because it can be difficult to discern spurious results from genuine differences in systems. Further study and careful analysis must be devoted to differential modulation of TRP channels to habilitate animal models and further drug development.

2.5 TRP Channels As Molecular Thermometers

One of the most interesting features of some TRP channel family members is their functional role in thermosensing. TRP channel thermosensitivity is an intrinsic property of the proteins, which are directly activated or gated by temperature. This is evidenced by purified channels reconstituted into artificial membranes. Rohacs and coworkers expressed and purified full-length rat TRPM8 from *E. coli*, which was incorporated into a 3:1 POPC:POPE planar bilayer and subjected to single channel electrophysiology measurements. Their results show that TRPM8 purified and reconstituted in a non-biological bilayer produces cold-evoked currents with steep temperature dependence similar to results observed in cell membranes.[62] Similarly, Julius and coworkers have expressed and purified a truncated functional form of rat TRPV1 from Sf9 insect cells. The resulting protein was incorporated into soybean polar lipid extract-based liposomes for electrophysiology measurements probing thermal sensitivity.[4] The outcomes mirror those seen from recombinant TRPM8 studies and indicate that elevated temperature produces direct activation of TRPV1. These results clearly show that thermosensitivity is an inherent property of these channels. Despite the inherent thermosensitivity of TRPM8 and TRPV1 (and presumably the other thermosensitive TRP channels), to date there is no coherent understanding of the temperature-dependent mechanism at the molecular level. Notwithstanding, a number of important ideas, frameworks, and mechanisms have been proposed, including experimentally testable hypotheses.[27, 63-65]

Part of the challenge in identifying a mechanism for TRP channel thermosensation arises because the nature of the protein region (or regions) used to sense

temperature has not been isolated. A number of studies have reported on regions that affect TRP thermosensitivity. In aggregate, the outcomes of these studies do not isolate a specific region or domain and are generally contradictory.[64] The resulting regions are spread throughout the channels both in sequence and structure space (Figure 2.4). For example, a number of studies have identified the N-terminal extra-membrane ankyrin repeat domains (ARD) of TRPV1 and TRPA1 as being involved in thermosensation. However, TRPM8 has no ARDs and TRPA1 has significantly more ARDs than TRPV1. This result suggests that either the ARDs are not key to thermosensing, or indicates that the TRPM8 thermosensing mechanism is distinct from TRPV1 and TRPA1, which admittedly could be the case as the channels are relatively divergent (TRPV1 and TRPM8 share about 11% sequence identity). Indeed, thermoTRP channels in general have low sequence homology, even between members of the same family (Figure 2.5). The lack of consensus between functional studies intended to isolate regions and mechanisms of thermosensing TRP channels has interesting implications in its own right. It either suggests that unlike other ion channel properties, such as voltage- or ligand-dependent channel activation and ion selectivity (which are driven by localized structural regions), TRP channel thermosensation may be delocalized over structural space dependent on a new, yet to be identified mechanism. An alternative explanation for the challenges in isolating a TRP channel thermosensor is that using mutations, chimeras, and/or truncations may not be the most viable method to probe thermosensation mechanisms since these changes generally have unknown and unintended

thermodynamic consequences, which can result in energetic perturbations that change the functional output without inherently perturbing thermosensation.[63]

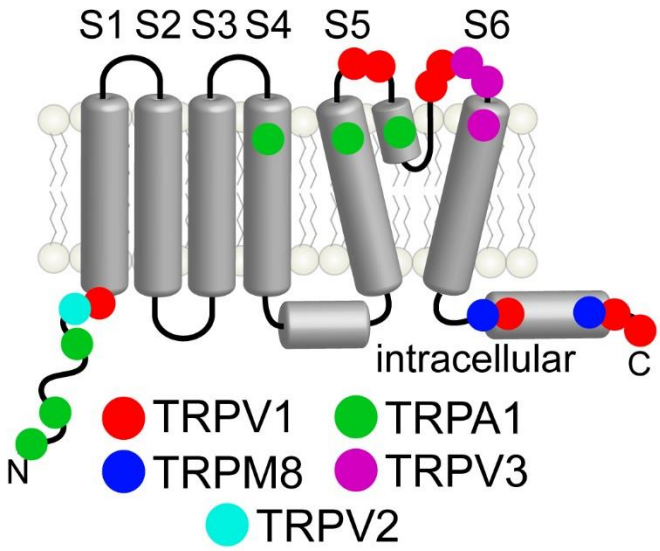

Figure 2.4 *Reported regions of TRP channels important for thermosensing.* For a number of TRP channels various regions have been implicated as crucial to thermosensing. Thermosensing regions are plotted on the monomer topology diagram of a generic TRP channel. Colors represent different thermosensitive TRP channels as follows: TRPV1 (red),[66-73] TRPM8 (blue),[68, 74] TRPA1 (green),[35, 40, 42, 75, 76] TRPV3 (purple),[69, 77] and TRPV2 (cyan).[66] Each colored circle represents a published account of a region involved in thermosensing.

Arising from the challenges in isolating a temperature-sensitive domain or sub-domain, the hypothesis has emerged that perhaps TRP thermosensing regions are structurally dispersed over multiple domains. Notwithstanding, important strides to understanding thermosensation are forthcoming. It is clear from quantitative electrophysiology-based thermodynamic studies that TRP channels have relatively large magnitude changes in enthalpy ($\Delta H \geq \pm 100$ kcal/mol) upon channel activation.[78, 79] The magnitudes of ΔH are more than an order of magnitude larger than for many other reported proteins undergoing conformational change, and are similar to the reported

values for classical protein unfolding studies.[80] Interestingly, for the cold sensing protein TRPM8 ΔH of activation is exothermic ($\Delta H < 0$), suggestive of an enthalpy driven activation as given by $\Delta G = \Delta H - T\Delta S$. On the other hand, for the heat sensing TRPV1, ΔH is endothermic, which suggests that the free energy of activation is entropy driven. The free energy of activation for thermosensitive TRP channels is similar to other ion channels (~10 kcal/mol), which demands that the large ΔH of thermosensitive TRP channels is compensated by significant changes in entropy (ΔS).[81] To this end, Clapham and Miller have proposed a thermodynamic model of TRP thermosensitivity mirroring early protein folding studies where the temperature dependent conformational change of these channels is driven by a change in heat capacity (ΔC_p).[63] Historical protein studies have found that temperature dependent enthalpies and entropies are common and arise from a change in heat capacity. At a given temperature (T) the ΔH can be related to a reference enthalpy (ΔH°) at the reference temperature (T°) as a function of ΔC_p:

$$\Delta H = \Delta H^\circ + \Delta C_p (T - T^\circ)$$

Similarly a temperature dependent change in entropy, ΔS, includes a ΔC_p term:

$$\Delta S = \Delta S^\circ + \Delta C_p ln\left(\frac{T}{T^\circ}\right)$$

These temperature-dependent thermodynamic entities give rise to non-linear protein stability curves, which dictates how ΔG varies as a function of temperature:

$$\Delta G = \Delta H^\circ - T\Delta S^\circ + \Delta Cp\left(T - T^\circ - Tln\left(\frac{T}{T^\circ}\right)\right)$$

Thus, changes in heat capacity can impact the temperature dependence of conformational changes, including potentially that of thermosensing TRP channels.[82]

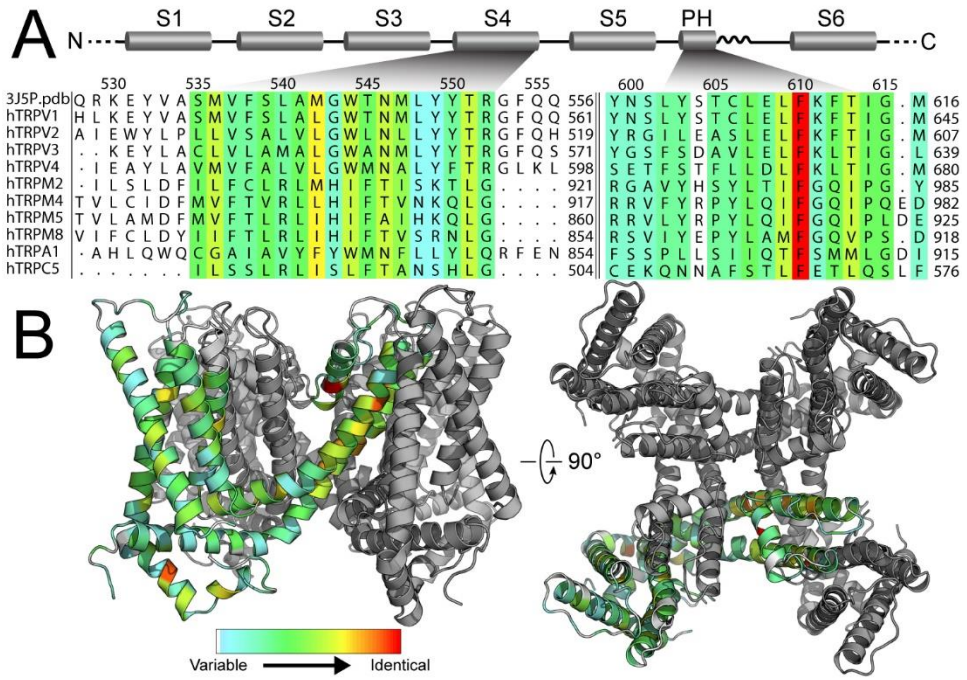

Figure 2.5 *Low sequence conservation in human thermosensitive TRP channels* . A) A multiple sequence alignment of the S4 and pore (PH) helices in known human TRP thermosensors represented using ALINE.[83] These two helices were chosen because, unlike strongly voltage-gated channels, the S4 helix is relatively poorly conserved in TRP channels, whereas the pore helix (PH) appears to contain the only residue that is absolutely conserved in the transmembrane region of human thermoTRPs. There is little to no homology in the loop regions, and limited homology in the helices. This alignment was generated using ClustalX[84] to iteratively add multiple sequences to a pairwise structural alignment of human TRPM8 to the apo structure of rat TRPV1 (3J5P) generated using MUSTANG.[85] Sequence similarity is indicated with a color spectrum from cyan to red using ALSCRIPT Calcons.[86] White, cyan, and red indicate subthreshold conservation, low conservation, and absolutely conserved residues, respectively. B) The sequence conservation is mapped to membrane regions of rTRPV1 structure using the same colors as above.

One prominent feature of the ΔC_p-dependent thermosensing hypothesis is that both positive and negative enthalpies of TRPM8 and TRPV1 can be explained thermodynamically because transitions that have changes in heat capacity between states

have, by definition, protein stability curves that are non-linear where transitions can be either enthalpy or entropy driven, analogous to protein heat and cold denaturation. The most important outcome of this hypothesis is that it can be tested experimentally. It is clear from early protein folding studies what underlies changes in heat capacity. These underpinnings include changes in electrostatics, secondary structure, etc. However, it has been recognized for decades that changes in heat capacity usually correlate extremely well with changes in solvation. For example, a hydrophobic residue transitioning to a hydrophilic environment results in a large and positive ΔC_p. Moreover, changes in solvent accessibility are observable in experimental and computational studies which may provide a method to link the existing thermodynamics to structural investigations.

2.6 On the Path to a Structural Biological Mechanism of TRP Thermosensing

Understanding thermodynamic measurements in terms of structure is at best inherently challenging. However, the emerging progress in TRP channel structural biology suggests optimism. The Cheng and Julius labs recently reported three high-resolution structures of a truncated but functional rat TRPV1 channel in apo– and agonist–bound states.[87, 88] Their structures are the first to include membrane regions of a TRP channel at high resolution, and their studies highlight important features of agonist dependent channel gating. While seminal to understanding TRP channel function, the structures do not elucidate anything in particular regarding TRPV1 thermosensation. In addition to the recent TRPV1 structures, there are a handful of other low resolution structures and high resolution structural domains from some TRP family members as detailed in Table 2.1.

Beyond thermosensitive TRP channels, there are a number of other proteins and nucleic acids that have physiologically relevant temperature dependent responses, which may provide insight into TRP channel thermosensitivity.[89-91] One relevant example is DesK, a bacterial histidine-kinase thermosensor. DesK is a bifunctional membrane enzyme that is regulated between kinase and phosphatase activities by changes in temperature. Recent studies indicate that the temperature dependent switch in DesK is a membrane proximal helical segment that transitions between coil and helix conformations.[92] Interestingly, this conformational change alters the solvent accessibility of a patch of hydrophilic residues to and from the membrane, suggesting a mechanism that would produce significant changes in heat capacity (ΔC_p) as has been proposed for TRP channel thermosensing.[63]

Recently, Chanda and coworkers used rational protein design on the Shaker voltage gated potassium channel ($K_v1.2$), engineering significantly increased thermosensitivity at magnitudes on par with thermosensitive TRP channels.[93] The Shaker channel was used because it is well-studied and has negligible inherent temperature sensitivity. At the heart of the design principle was the idea that the ΔC_p could be changed and thus thermosensitivity altered by modifying the polarity of residues that undergo a change in solvent accessibility as a function of gating. Chanda and coworkers focused on mutating the membrane interfacial residues of the S1-S3 helices and charge bearing S4 helix residues of the voltage-sensing domain and were able to confer temperature sensitivity to the Shaker channel (Figure 2.6). The outcome of this work supports the hypothesis that TRP channel thermosensitivity has a strong

dependence on ΔC_p. Similarly, the outcomes suggest that alterations of a single structural domain, like the voltage-sensing domain of the Shaker channel, are sufficient to confer thermosensitivity.

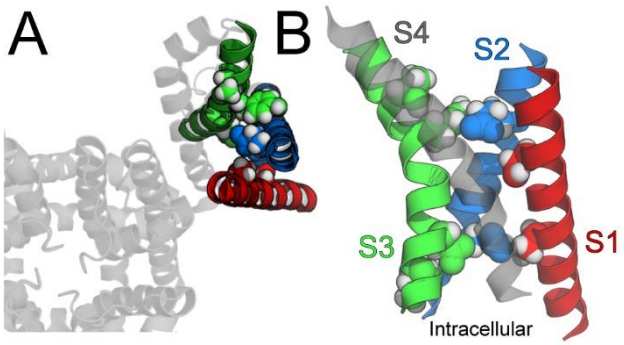

Figure 2.6 *Residues and regions of the Shaker channel modified to confer thermosensing functionality.* A) An extracellular view of a portion of the pore domain (bottom left) with the voltage-sensing domain (upper right) from the Shaker channel. Residues that were rationally mutated in helices S1-S3 are highlighted; these mutations generally increase temperature sensitivity of a non-thermosensing channel. These residues are posited to change solvent accessibility with domain conformational changes and are focused around the interface of the S4 helix. B) Close-up view of the residues mutated to increase thermosensitivity of Shaker. The reduction in S4 charged residues significantly increased thermosensitivity. The S4 helix is colored gray and is transparent.

2.7 Identifying a TRP Specific Thermosensor

The only conserved structural domains in all thermosensing TRP channels are the pore and sensor domains (S5-S6 and S1-S4 helices respectively). As a result, it should be possible to employ a "divide and conquer" approach to overexpress these (and other) structural domains of TRP channels on the path to identifying a thermosensor structural domain. Given the apparent thermodynamic similarities between thermosensing proteins and protein unfolding, one can tap into the immense and well-developed field of protein folding to gain mechanistic and thermodynamic insight into thermosensing, including answering the basic question of whether thermosensing is accomplished by a specific

domain or is diversified over many structural domains and ultimately what the nature and magnitude of the temperature dependent conformational changes are.

Calorimetry data would be the gold standard for identifying and validating a thermosensing region. In particular, differential scanning calorimetry (DSC) provides a direct measurement of the molar heat capacity as a function of temperature which can be used to detect the change in enthalpy of the temperature dependent transition. DSC data can also provide the midpoint of the transition temperature and with further analysis the change in entropy and free energy. These values would be directly comparable to existing values obtained from functional studies and therefore very useful to potentially confirm the isolation of a thermosensing domain. There are downsides to this approach. The main limitation is that with a modern sensitive DSC instrument, one would still likely need milligram levels of pure and folded protein to ensure accurate and reliable calorimetry data, the same quantities needed for NMR and X-ray structural studies.

In the absence of calorimetry data, reversible temperature dependent conformational changes can be measured by a handful of spectroscopic techniques (circular dichroism, fluorescence, NMR, etc.) and subjected to van't Hoff analysis to obtain estimates of the changes in enthalpy, entropy, and heat capacity. For example, far ultraviolet circular dichroism (CD) offers a relatively sensitive, label-free, and straightforward method to subject potential thermosensing proteins and domains to thermodynamic analysis.[94] For far UV CD to properly detect a temperature transition, there must be a change in secondary structure, which seems likely if the structural transition is similar to DesK.

In addition to DSC and CD measurements, solution NMR is well-suited to thermosensing studies for a number of reasons. Both voltage-sensing and pore domains from other channels have been investigated by solution NMR.[95-97] The benefits for solution NMR are that the experiments are capable of probing atomic resolution protein dynamics over biological time scales, including the millisecond timescale regime where protein conformational changes generally occur. This information could be used in comparative studies of thermosensitive TRP channels to validate the outcomes with existing electrophysiology data. Lastly, modern NMR hardware makes it straightforward to probe structure, dynamics, and thermodynamics in a temperature dependent manner from zero to eighty degrees Celsius, making this technique particularly promising for TRP thermosensing studies. One classic study made use of relaxation dispersion experiments to probe conformational dynamics and energetics between states of a membrane bound enzyme.[98] Such methods would be very relevant to a TRP channel thermosensing domain. While it is unlikely with current methods that solution NMR could be used to determine the structure of a full-length TRP channel, it is feasible to determine the structures of the sensor domain or a tetrameric pore domain at distinct temperatures.

In addition to NMR structural studies, advances in other structural techniques suggest that either cryo-electron microscopy (EM) or X-ray crystallography could potentially be able to determine the structure of a full-length thermosensing channel in distinct states. It is clear from the work of Cheng and Julius that high resolution cryo-EM is applicable to TRP channel structure determination. With new advances in EM

software, which includes the ability to perform single particle reconstruction on conformationally heterogeneous samples, and the use of time-resolved cryo-EM instrumentation, which can freeze samples on the order of milliseconds, it may be possible to trap and determine the structures of TRP channels in distinct conformations as a function of temperature.[87, 99]

One last promising structural technique that could have important implications for understanding the mechanism of thermosensitive TRP channels is the use of time-resolved serial femtosecond X-ray crystallography (SFX). This emerging technique relies on intense femtosecond pulses from an X-ray laser that interact with a stream of small protein crystals causing X-ray diffraction prior to sample destruction. A recent example coupled time-resolved SFX with a yellow light laser to specifically activate photosystem (PS) II, resulting in the ability to probe structurally the PSII conformational changes associated with water-splitting which is central to photosynthesis.[100] Modifications on this theme, where instead of a light to activate PSII, one could modulate the temperature, perhaps by altering the distance between sample injector and X-ray laser, could give way to probing structurally the conformational changes central to TRP channel thermosensitivity. Given the advances in understanding of TRP channels and membrane protein structural biology, it seems likely that it is only a matter of time before the mechanism of TRP thermosensing emerges.

Table 2.1 Structures of TRP channels and TRP channel domains.

Channel	Source	Domain studied[a]	Expression system	Method	Resolution (Å)	PDB code
TRPV1[87, 88, 101-103]	Rat	ARD (101-364) +ATP	*E.coli* BL21 (DE3)	X-ray	2.7	2PNN
		C-terminal (767-801)+ CaM	*E.coli* BL21 (DE3)	X-ray	1.95	3SUI
		full length*	*S.cerevieae* BJ5457	Cryo-EM	19	N/A
		near full length (110-603//627-764)	Baculovirus transduction in HEK293S GnTI$^-$	Cryo-EM	3.4	3J5P
		+DkTx and RTx†			3.8	3J5Q
		+ Capsaicin†			4.2	3J5R
TRPV2[104-106]	Rat	full length	*S.cerevieae* BJ5457	Cryo-EM	13.6	5688[b]
	Human	ARD(68-319)	*E.coli* DL41	X-ray	1.7	2F37
	Rat	ARD (75-321)	*E.coli* BL21 (DE3)	X-ray	1.65	2ETB
TRPV3[107]	Mouse	ARD (118-367)	Rosetta (DE3)	X-ray	1.95	4N5Q
TRPV4[108, 109]	Human	ARD(149-397) +ATP	*E.coli* BL21 (DE3)	X-ray	2.85	4DX1
	Rat	full length‡	Baculovirus-infected Sf9 cells	Cryo-EM	35	N/A
TRPV6[110]	Mouse	ARD (44-265)	*E.coli* BL21 (DE3)	X-ray	1.7	2RFA
TRPA1[111]	Mouse	full length§	*S.cerevieae* BJ5457	Negative-stain EM	16	5334[b]
TRPM2[112]	Human	full length‡	HEK 293	Negative-stain EM	28	N/A
TRPM7[113, 114]	Rat	coiled-coil (1230-1282)	*E.coli* BL21 (DE3)pLysS	X-ray	2.0	3E7K
	Mouse	alpha-kinase (1549-1828)	Baculovirus-infected Sf9 cells	X-ray	2.8	1IAJ
TRPC3[115]	Mouse	full length	HEK 293	Cryo-EM	15	N/A
TRPP2[116, 117]	Human	coiled-coil (833-872)	Rosetta2 (DE3)	X-ray	1.9	3HRN 3HRO
	Human	EF hand (720-796)	BL21(DE3) codon Plus RIL	NMR	1.9[c]	2KQ6
	Human	EF hand (680-796)	BL21(DE3)	NMR	4.2[c]	2KLD 2KLE
TRPP3[118]	Human	coiled-coil (699-743)	Rosetta (DE3)	X-ray	2.8	4GIF

[a]Numbers indicate residues used for structural studies. ARD and CaM stand for the ankyrin repeat domain and calmodulin binding domain, respectively. Full length or near full length channels were reconstituted in various artificial hydrophobic environments such as (*) n-decyl-B-D-maltoside, (†) Amphipol A8-35, (‡) n-dodecyl-B-D-maltoside and (§) Fos-choline 12. [b]Reference numbers for the EMDataBank. [c]Predicted equivalent resolution.[119]

X-ray crystallography and cryo-EM may provide structures at medium to high resolution, and NMR can reveal a structural, dynamic, and thermodynamic context. Computational approaches can yield complementary insights to these and other experimental approaches previously discussed. Computer simulations take static protein structures as input but are able to reveal the details of conformational changes, protein-

membrane, or protein-solvent interactions at the atomic level and can also provide dynamic information.[120] Computer simulation output is often sufficient to construct mechanistic molecular models. Computational methods model the interactions between atoms with physical or heuristic inter-atomic interaction potentials and utilize computational algorithms to sample the conformational dynamics of a given channel.

The gold standard of these studies are molecular dynamics (MD) simulations which provide a means to computationally explore the dynamics of structural models of, for instance, a TRP channel embedded in a lipid bilayer.[121] Based on atomic resolution experimental structures, MD simulations show the interactions of the channel with the solvent (ions and water molecules) and the membrane lipids, and allow for qualitative and quantitative analysis of thermodynamic and kinetic properties of the channel. [122-125] To date, few TRP channel MD studies have been carried out due to the lack of reliable atomic-resolution input structures, although a number of studies combined experiments with short (<20 ns) simulations of TRPV1 models based on Kv, HCN, or the KcsA channel structures. [74, 126-128] The first atomic resolution structures were published in late 2013, and as a result, the first MD simulations based on these experimental input structures are only now beginning to emerge.[87, 129] Recently, the TRPV1 selectivity filter of the isolated pore structure was studied to probe its interaction with sodium, potassium and calcium ions.[130] This study concludes that the selectivity filter of TRPV1 is highly flexible and hypothesizes that the cryo-EM observed selectivity filter is not optimized for ion conductance.[129] Another recent study combined experimental mutagenesis, electrophysiology, and MD simulations to identify a binding

site for $PI(4,5)P_2$.[131] These studies utilized equilibrium MD simulations of a few hundred nanoseconds that explicitly contained all atoms of the protein, lipid and solvent molecules. Similar simulations will continue to yield further insights, especially when carried out over longer time scales to increase sampling of solvent and protein degrees of freedom. Unbiased equilibrium MD is particularly useful since no specific assumptions are made about the protein of interest and the system evolves naturally, driven by thermal fluctuations. However, due to their high computational demands, equilibrium MD is currently limited to tens of microseconds on standard supercomputers and hundreds of microseconds on special purpose machines.[132] Importantly, enhanced sampling methods can be employed to obtain equilibrium properties over longer timescales, including conformation changes underlying channel gating.[133-136] MD-based methods also exist to compute thermodynamic information that may be useful to correlate experimental observables such as single channel conductance or thermodynamics with structural conformational changes.[137, 138] Because TRP channels are temperature sensitive, temperature-based ensemble methods, such as temperature replica exchange (typically coupled with Hamiltonian exchange), are of particular interest.[139, 140] Non-equilibrium MD simulations that include the membrane potential have been used to study ion permeation of other channels in a voltage-dependent manner and have yielded observables such as completer current-voltage curves and ion selectivity, as well as new insights into voltage sensor dynamics.[141-144] Thus, computational methods have demonstrated their usefulness in bridging the gap between structure and function, in

particular for ion channels, and therefore present another meaningful technique to dissect the function of thermosensitive TRP channels.

One of the primary questions that needs to be addressed by these techniques is whether the thermosensitivity of TRP channels is governed by discrete modular domains or distributed throughout the channel in smaller, structurally unrelated regions. As explained earlier, random mutagenesis studies have so far not yielded definite conclusions for distinguishing these two models. Testing the dispersed thermosensing hypothesis will require high-resolution structural information from full-length or near full-length native channels to identify regions of the channel that are involved in temperature-dependent conformational change. The cryo-EM or X-ray crystallography techniques discussed above could provide high-resolution insight into these changes. Residues or regions that are identified as potential contributors to channel thermosensitivity could then be probed and tested functionally in a hypothesis-driven approach. Chowdhury et al. demonstrated an excellent example of such an approach by utilizing the wealth of structural information on the Shaker channel to rationally guide experiments.[93] In this context, one of the major challenges limiting fundamental TRP studies is the ability to produce sufficient quantities of pure, reconstituted, and biologically-relevant TRP channels and related domains. As this hurdle is overcome, more biophysical, structural, and computational investigations will follow, yielding new insight into this important class of proteins.

As pointed out earlier, thermosensitive TRP channels are inherently susceptible to multiple distinct stimuli. In addition, a number of studies have identified TRP channel

orthologs with species dependent functionality. The TRP channel activation and modulation landscape is further expanded by reports of isoforms and heteromultimerization with additional diversified functional output.[145] It thus stands to reason that TRP channels are exquisitely balanced for sensitivity to a variety of distinct inputs, which likely is at the heart of reported challenges isolating and identifying mechanisms associated with PIP_2, PIRT, and thermosensing based gating. This idea is supported by recent molecular phylogenetic studies that indicate TRP channels originally evolved in non-neuronal cells and later in animal evolution acquired neuronal functionality associated with sensory biology.[146] The intrinsic plasticity of TRP channels notwithstanding, important inroads are being made pointing towards a more complete understanding of how these proteins are integrated into many diverse physiologically important signal transduction pathways.

In addition to providing a brief synopsis of the state of thermosensing TRP channel studies, we offer a perspective of a few structural and biophysical methods that should complement the existing functional electrophysiology data that has been foundational for the current understanding of these fascinating channels. These types of studies are needed to test specific hypotheses that have recently emerged and will hopefully lead to a better understanding of the molecular intricacies of thermosensation, with a long term view of elucidating how these channels not only sense temperature, but also by what means they are able to integrate numerous diverse stimuli.

2.8 References

1. Montell, C., and Rubin, G. M. (1989) Molecular Characterization of the Drosophila trp locus: A Putative Integral Membrane Protein Required for Phototransduction. *Neuron* **2**, 1313-1323

2. Montell, C., Birnbaumer, L., Flockerzi, V., Bindels, R. J., Bruford, E. A., Caterina, M. J., Clapham, D. E., Harteneck, C., Heller, S., Julius, D., Kojima, I., Mori, Y., Penner, R., Prawitt, D., Scharenberg, A. M., Schultz, G., Shimizu, N., and Zhu, M. X. (2002) A Unified Nomenclature for the Superfamily of TRP Cation Channels. *Mol. Cell* **9**, 229-231

3. Caterina, M. J., Schumacher, M. A., Tominaga, M., Rosen, T. A., Levine, J. D., and Julius, D. (1997) The capsaicin receptor: a heat-activated ion channel in the pain pathway. *Nature* **389**, 816-824

4. Cao, E., Cordero-Morales, J. F., Liu, B., Qin, F., and Julius, D. (2013) TRPV1 channels are intrinsically heat sensitive and negatively regulated by phosphoinositide lipids. *Neuron* **77**, 667-679

5. Voets, T., Droogmans, G., Wissenbach, U., Janssens, A., Flockerzi, V., and Nilius, B. (2004) The principle of temperature-dependent gating in cold- and heat-sensitive TRP channels. *Nature* **430**, 748-754

6. Cao, X., Ma, L., Yang, F., Wang, K., and Zheng, J. (2014) Divalent cations potentiate TRPV1 channel by lowering the heat activation threshold. *J. Gen. Physiol.* **143**, 75-90

7. Lukacs, V., Thyagarajan, B., Varnai, P., Balla, A., Balla, T., and Rohacs, T. (2007) Dual regulation of TRPV1 by phosphoinositides. *J. Neurosci.* **27**, 7070-7080

8. Ufret-Vincenty, C. A., Klein, R. M., Hua, L., Angueyra, J., and Gordon, S. E. (2011) Localization of the PIP2 sensor of TRPV1 ion channels. *J. Biol. Chem.* **286**, 9688-9698

9. Kim, A. Y., Tang, Z., Liu, Q., Patel, K. N., Maag, D., Geng, Y., and Dong, X. (2008) Pirt, a phosphoinositide-binding protein, functions as a regulatory subunit of TRPV1. *Cell* **133**, 475-485

10. Prager-Khoutorsky, M., Khoutorsky, A., and Bourque, C. W. (2014) Unique interweaved microtubule scaffold mediates osmosensory transduction via physical interaction with TRPV1. *Neuron* **83**, 866-878

11. De Petrocellis, L., Ligresti, A., Moriello, A. S., Allarà, M., Bisogno, T., Petrosino, S., Stott, C. G., and Marzo, V. D. (2011) Effects of cannabinoids and

cannabinoid-enriched Cannabis extracts on TRP channels and endocannabinoid metabolic enzymes. *Br. J. Pharmacol.* **163**, 1479-1494

12. Bohlen, C. J., Priel, A., Zhou, S., King, D., Siemens, J., and Julius, D. (2010) A bivalent tarantula toxin activates the capsaicin receptor, TRPV1, by targeting the outer pore domain. *Cell* **141**, 834-845

13. Szallasi, A., Jonassohn, M., Acs, G., Biro, T., Acs, P., Blumberg, P. M., and Sterner. (1996) The stimulation of capsaicin-sensitive neurones in a vanilloid receptor-mediated fashion by pungent terpenoids possessing an unsaturated 1,4-dialdehyde moiety. *Br. J. Pharmacol.* **119**, 283-290

14. McVey, D. C., and Vigna, S. R. (2005) The Role of Leukotriene B4 in Clostridium difficile Toxin A-Induced Ileitis in Rats. *Gastroenterology* **128**, 1306-1316

15. Shimizu, T., Shibata, M., Toriumi, H., Iwashita, T., Funakubo, M., Sato, H., Kuroi, T., Ebine, T., Koizumi, K., and Suzuki, N. (2012) Reduction of TRPV1 expression in the trigeminal system by botulinum neurotoxin type-A. *Neurobiology of Disease* **48**, 367-378

16. Jordt, S. E., and Julius, D. (2002) Molecular Basis for Species-Specific Sensitivity to "Hot" Chili Peppers. *Cell* **108**, 421-430

17. Gracheva, E. O., Cordero-Morales, J. F., Gonzalez-Carcacia, J. A., Ingolia, N. T., Manno, C., Aranguren, C. I., Weissman, J. S., and Julius, D. (2011) Ganglion-specific splicing of TRPV1 underlies infrared sensation in vampire bats. *Nature* **476**, 88-91

18. Saito, S., and Tominaga, M. (2014) Functional diversity and evolutionary dynamics of thermoTRP channels. *Cell Calcium*

19. Zimmermann, K., Lennerz, J. K., Hein, A., Link, A. S., Kaczmarek, J. S., Delling, M., Uysal, S., Pfieifer, J. D., Riccio, A., and Clapham, D. E. (2011) Transient receptor potential cation channel, subfamily C, member 5 (TRPC5) is a cold-transducer in the peripheral nervous system. *Proc. Natl. Acad. Sci. U. S. A.* **108**, 18114-18119

20. Almeida, M. C., Hew-Butler, T., Soriano, R. N., Rao, S., Wang, W., Wang, J., Tamayo, N., Oliveira, D. L., Nucci, T. B., Aryal, P., Garami, A., Bautista, D., Gavva, N. R., and Romanovsky, A. A. (2012) Pharmacological blockade of the cold receptor TRPM8 attenuates autonomic and behavioral cold defenses and decreases deep body temperature. *J. Neurosci.* **32**, 2086-2099

21. Ding, Z., Gomez, T., Werkheiser, J. L., Cowan, A., and Rawls, S. M. (2008) Icilin induces a hyperthermia in rats that is dependent on nitric oxide production and NMDA receptor activation. *European Journal of Pharmacology* **578**, 201-208

22. Gavva, N. R., Davis, C., Sonya, G. L., Rao, S., Wang, W., and Zhu, D. X. (2012) Transient receptor potential melastatin 8 (TRPM8) channels are involved in body temperature regulation. *Molecular Pain* **8**, 36

23. Knowlton, W. M., Daniels, R. L., Palkar, R., McCoy, D. D., and McKemy, D. D. (2011) Pharmacological blockade of TRPM8 ion channels alters cold and cold pain responses in mice. *PLoS One* **6**, e25894

24. Shapovalov, G., Gkika, D., Devilliers, M., Kondratskyi, A., Gordienko, D., Busserolles, J., Bokhobza, A., Eschalier, A., Skryma, R., and Prevarskaya, N. (2013) Opiates modulate thermosensation by internalizing cold receptor TRPM8. *Cell reports* **4**, 504-515

25. Ma, S., Yu, H., Zhao, Z., Luo, Z., Chen, J., Ni, Y., Jin, R., Ma, L., Wang, P., Zhu, Z., Li, L., Zhong, J., Liu, D., Nilius, B., and Zhu, Z. (2012) Activation of the cold-sensing TRPM8 channel triggers UCP1-dependent thermogenesis and prevents obesity. *Journal of molecular cell biology* **4**, 88-96

26. McCoy, D. D., Zhou, L., Nguyen, A. K., Watts, A. G., Donovan, C. M., and McKemy, D. D. (2013) Enhanced insulin clearance in mice lacking TRPM8 channels. *American journal of physiology. Endocrinology and metabolism* **305**, E78-88

27. Vriens, J., Nilius, B., and Voets, T. (2014) Peripheral thermosensation in mammals. *Nature reviews. Neuroscience* **15**, 573-589

28. Riera, C. E., Huising, M. O., Follett, P., Leblanc, M., Halloran, J., Van Andel, R., de Magalhaes Filho, C. D., Merkwirth, C., and Dillin, A. (2014) TRPV1 pain receptors regulate longevity and metabolism by neuropeptide signaling. *Cell* **157**, 1023-1036

29. Rossi, F., Bellini, G., Torella, M., Tortora, C., Manzo, I., Giordano, C., Guida, F., Luongo, L., Papale, F., Rosso, F., Nobili, B., and Maione, S. (2014) The genetic ablation or pharmacological inhibition of TRPV1 signalling is beneficial for the restoration of quiescent osteoclast activity in ovariectomized mice. *Br. J. Pharmacol.* **171**, 2621-2630

30. Jang, Y., Lee, M. H., Lee, J., Jung, J., Lee, S. H., Yang, D. J., Kim, B. W., Son, H., Lee, B., Chang, S., Mori, Y., and Oh, U. (2014) TRPM2 mediates the lysophosphatidic acid-induced neurite retraction in the developing brain. *European Journal of Pharmacology* **466**, 1987-1998

31. Oda, S., Uchida, K., Wang, X., Lee, J., Shimada, Y., Tominaga, M., and Kadowaki, M. (2013) TRPM2 contributes to antigen-stimulated Ca^{2+} influx in mucosal mast cells. *European Journal of Pharmacology* **465**, 1023-1030

32. Numata, T., Sato, K., Christmann, J., Marx, R., Mori, Y., Okada, Y., and Wehner, F. (2012) The DeltaC splice-variant of TRPM2 is the hypertonicity-induced cation channel in HeLa cells, and the ecto-enzyme CD38 mediates its activation. *J. Physiol.* **590**, 1121-1138

33. Kaneko, Y., and Arpadd, S. (2014) Transient receptor potential (TRP) channels: a clinical perspective. *Br. J. Pharmacol.* **171**, 2474-2507

34. Story, G. M., Peier, A. M., Reeve, A. J., Eid, S. R., Mosbacher, J., Hricik, T. R., Earley, T. J., Hergarden, A. C., Andersson, D. A., Hwang, S. W., McIntyre, P., Jegla, T., Bevan, S., and Patapoutian, A. (2003) ANKTM1, a TRP-like Channel Expressed in Nociceptive Neurons, Is Activated by Cold Temperatures. *Cell* **112**, 819-829

35. Chen, J., Kang, D., Xu, J., Lake, M., Hogan, J. O., Sun, C., Walter, K., Yao, B., and Kim, D. (2013) Species differences and molecular determinant of TRPA1 cold sensitivity. *Nat. Commun.* **4**, 2501

36. Saito, S., Banzawa, N., Fukuta, N., Saito, C. T., Takahashi, K., Imagawa, T., Ohta, T., and Tominaga, M. (2014) Heat and noxious chemical sensor, chicken TRPA1, as a target of bird repellents and identification of its structural determinants by multispecies functional comparison. *Mol. Biol. Evol.* **31**, 708-722

37. Klionsky, L., Tamir, R., Gao, B., Wang, W., Immke, D., Nishimura, N., and Gavva, N. (2007) Species-specific pharmacology of Trichloro(sulfanyl)ethyl benzamides as transient receptor potential ankyrin 1 (TRPA1) antagonists. *Molecular Pain* **3**, 39

38. Nagatomo, K., Ishii, H., Yamamoto, T., Nakajo, K., and Kubo, Y. (2010) The Met268Pro Mutation of Mouse TRPA1 Changes the Effect of Caffeine from Activation to Suppression. *Biophys. J.* **99**, 3609-3618

39. Nagatomo, K., and Kubo, Y. (2008) Caffeine activates mouse TRPA1 channels but suppresses human TRPA1 channels. *Proc. Natl. Acad. Sci. U. S. A.* **105**, 17373-17378

40. Jabba, S., Goyal, R., Sosa-Pagán, J. O., Moldenhauer, H., Wu, J., Kalmeta, B., Bandell, M., Latorre, R., Patapoutian, A., and Grandl, J. (2014) Directionality of temperature activation in mouse TRPA1 ion channel can be inverted by single-point mutations in ankyrin repeat six. *Neuron* **82**, 1017-1031

41. Geng, J., Liang, D., Jiang, K., and Zhang, P. (2011) Molecular evolution of the infrared sensory gene TRPA1 in snakes and implications for functional studies. *PLoS One* **6**

42. Kang, K., Panzano, V. C., Chang, E. C., Ni, L., Dainis, A. M., Jenkins, A. M., Regna, K., Muskavitch, M. A. T., and Garrity, P. A. (2012) Modulation of TRPA1 thermal sensitivity enables sensory discrimination in Drosophila. *Nature* **481**, 76-80

43. Viswanath, V., Story, G. M., Peier, A. M., Petrus, M. J., Lee, V. M., Hwang, S. W., Patapoutian, A., and Jegla, T. (2003) Ion channels: Opposite thermosensor in fruitfly and mouse. *Nature* **423**, 822-823

44. Chen, J., and Kym, P. R. (2009) TRPA1: the species difference. *J. Gen. Physiol.* **133**, 623-625

45. Zhong, L., Bellemer, A., Yan, H., Honjo, K., Robertson, J., Hwang, R. Y., Pitt, G. S., and Tracey, W. D. (2012) Thermosensory and Nonthermosensory Isoforms of Drosophila melanogaster TRPA1 Reveal Heat-Sensor Domains of a ThermoTRP Channe. *Cell Rep* **1**, 43-55

46. Gracheva, E. O., Cordero-Morales, J. F., González-Carcacía, J. A., Ingolia, N. T., Manno, C., Aranguren, C. I., Weissman, J. S., and Julius, D. (2011) Ganglion-specific splicing of TRPV1 underlies infrared sensation in vampire bats. *Nature* **476**, 88-91

47. Saito, S., Fukuta, N., Shingai, R., and Tominaga, M. (2011) Evolution of vertebrate transient receptor potential vanilloid 3 channels: opposite temperature sensitivity between mammals and western clawed frogs. *PLoS Genet.* **7**, e1002041

48. Huang, S., Li, X., Yu, Y., Wang, J., and Caterina, M. (2011) TRPV3 and TRPV4 ion channels are not major contributors to mouse heat sensation. *Molecular Pain* **7**, 37

49. Myers, B. R., Sigal, Y. M., and Julius, D. (2009) Evolution of Thermal Response Properties in a Cold-Activated TRP Channel. *PLoS One* **4**, e5741

50. Jordt, S.-E., and Julius, D. (2002) Molecular Basis for Species-Specific Sensitivity to "Hot" Chili Peppers. *Cell* **108**, 421-430

51. Papakosta, M., Dalle, C., Haythornthwaite, A., Cao, L., Stevens, E. B., Burgess, G., Russell, R., Cox, P. J., Phillips, S. C., and Grimm, C. (2011) The chimeric approach reveals that differences in the TRPV1 pore domain determine species-specific sensitivity to block of heat activation. *J. Biol. Chem.* **286**, 39663-39672

52. Phillips, E., Reeve, A., Bevan, S., and McIntyre, P. (2004) Identification of Species-specific Determinants of the Action of the Antagonist Capsazepine and the Agonist PPAHV on TRPV1. *J. Biol. Chem.* **279**, 17165-17172

53. McPartland, J. M., Glass, M., Matias, I., Norris, R., and Kilpatrick, C. W. (2007) A shifted repertoire of endocannabinoid genes in the zebrafish (Danio rerio). *Mol. Genet. Genomics* **277**, 555-570

54. Neeper, M. P., Liu, Y., Hutchinson, T. L., Wang, Y., Flores, C. M., and Qin, N. (2007) Activation Properties of Heterologously Expressed Mammalian TRPV2 EVIDENCE FOR SPECIES DEPENDENCE. *J. Biol. Chem.* **282**, 15894-15902

55. Rohacs, T. (2014) Phosphoinositide Regulation of TRP Channels. *Handbook of Experimental Pharmacology* **223**, 1143-1176

56. Cao, E., Cordero-Morales, Julio F., Liu, B., Qin, F., and Julius, D. (2013) TRPV1 Channels Are Intrinsically Heat Sensitive and Negatively Regulated by Phosphoinositide Lipids. *Neuron* **77**, 667-679

57. Estacion, M., Sinkins, W. G., and Schilling, W. P. (2001) Regulation of Drosophila transient receptor potential-like (TrpL) channels by phospholipase C-dependent mechanisms. *J. Physiol.* **530**, 1-19

58. Huang, J., Liu, C.-H., Hughes, S. A., Postma, M., Schwiening, C. J., and Hardie, R. C. (2010) Activation of TRP Channels by Protons and Phosphoinositide Depletion in Drosophila Photoreceptors. *Curr. Biol.* **20**, 189-197

59. Otsuguro, K.-i., Tang, J., Tang, Y., Xiao, R., Freichel, M., Tsvilovskyy, V., Ito, S., Flockerzi, V., Zhu, M. X., and Zholos, A. V. (2008) Isoform-specific Inhibition of TRPC4 Channel by Phosphatidylinositol 4,5-Bisphosphate. *J. Biol. Chem.* **283**, 10026-10036

60. Patel, K. N., Liu, Q., Meeker, S., Undem, B. J., and Dong, X. (2011) Pirt, a TRPV1 modulator, is required for histamine-dependent and -independent itch. *PLoS One* **6**, e20559

61. Tang, Z., Kim, A., Masuch, T., Park, K., Weng, H., Wetzel, C., and Dong, X. (2013) Pirt functions as an endogenous regulator of TRPM8. *Nat. Commun.* **4**, 2179

62. Zakharian, E., Cao, C., and Rohacs, T. (2010) Gating of transient receptor potential melastatin 8 (TRPM8) channels activated by cold and chemical agonists in planar lipid bilayers. *J. Neurosci.* **30**, 12526-12534

63. Clapham, D. E., and Miller, C. (2011) A thermodynamic framework for understanding temperature sensing by transient receptor potential (TRP) channels. *Proc. Natl. Acad. Sci. U. S. A.* **108**, 19492-19497

64. Voets, T. (2014) TRP channels and thermosensation. *Handbook of Experimental Pharmacology* **223**, 729-741

65. Feng, Q. (2014) Temperature sensing by thermal TRP channels: thermodynamic basis and molecular insights. *Curr. Top. Membr.* **74**, 19-50

66. Yao, J., Liu, B., and Qin, F. (2011) Modular thermal sensors in temperature-gated transient receptor potential (TRP) channels. *Proc. Natl. Acad. Sci. U. S. A.* **108**, 11109-11114

67. Grandl, J., Kim, S. E., Uzzell, V., Bursulaya, B., Petrus, M., Bandell, M., and Patapoutian, A. (2010) Temperature-induced opening of TRPV1 ion channel is stabilized by the pore domain. *Nature neuroscience* **13**, 708-714

68. Brauchi, S., Orta, G., Salazar, M., Rosenmann, E., and Latorre, R. (2006) A hot-sensing cold receptor: C-terminal domain determines thermosensation in transient receptor potential channels. *J. Neurosci.* **26**, 4835-4840

69. Kim, S. E., Patapoutian, A., and Grandl, J. (2013) Single residues in the outer pore of TRPV1 and TRPV3 have temperature-dependent conformations. *PLoS One* **8**, e59593

70. Vlachova, V., Teisinger, J., Sušánková, K., Lyfenko, A., Ettrich, R., and Vyklicky, L. (2003) Functional Role of C-Terminal Cytoplasmic Tail of Rat Vanilloid Receptor 1. *J. Neurosci.* **23**, 1340-1350

71. Yang, F., Cui, Y., Wang, K., and Zheng, J. (2010) Thermosensitive TRP channel pore turret is part of the temperature activation pathway. *Proc. Natl. Acad. Sci. U S A* **107**, 7083-7088

72. Cui, Y., Yang, F., Cao, X., Yarov-Yarovoy, V., Wang, K., and Zheng, J. (2012) Selective disruption of high sensitivity heat activation but not capsaicin activation of TRPV1 channels by pore turret mutations. *J. Gen. Physiol.* **139**, 273-283

73. Valente, P., Garcia-Sanz, N., Gomis, A., Fernandez-Carvajal, A., Fernandez-Ballester, G., Viana, F., Belmonte, C., and Ferrer-Montiel, A. (2008) Identification of molecular determinants of channel gating in the transient receptor potential box of vanilloid receptor I. *FASEB journal : official publication of the Federation of American Societies for Experimental Biology* **22**, 3298-3309

74. Brauchi, S., Orta, G., Mascayano, C., Salazar, M., Raddatz, N., Urbina, H., Rosenmann, E., Gonzalez-Nilo, F., and Latorre, R. (2007) Dissection of the

components for PIP_2 activation and thermosensation in TRP channels. *Proc. Natl. Acad. Sci. U. S. A.* **104**, 10246-10251

75. Caordero-Morales, J. F., Gracheva, E. O., and Julius, D. (2011) Cytoplasmic ankyrin repeats of transient receptor potential A1 (TRPA1) dictate sensitivity to thermal and chemical stimuli. *Proc. Natl. Acad. Sci. U. S. A.* **108**, E1184-E1191

76. Wang, H., Schupp, M., Zurborg, S., and Heppenstall, P. A. (2013) Residues in the pore region of Drosophila transient receptor potential A1 dictate sensitivity to thermal stimuli. *J. Physiol.* **591**, 185-201

77. Grandl, J., Hu, H., Bandell, M., Bursulaya, B., Schmidt, M., Petrus, M., and Patapoutian, A. (2008) Pore region of TRPV3 ion channel is specifically required for heat activation. *Nature neuroscience* **11**, 1007-1013

78. Brauchi, S., Orio, P., and Latorre, R. (2004) Clues to understanding cold sensation: thermodynamics and electrophysiological analysis of the cold receptor TRPM8. *Proc. Natl. Acad. Sci. U. S. A.* **101**, 15494-15499

79. Yao, J., Liu, B., and Qin, F. (2010) Kinetic and energetic analysis of thermally activated TRPV1 channels. *Biophys. J.* **99**, 1743-1753

80. Privalov, P. L. (1997) Thermodynamics of protein folding. *J. Chem. Thermodyn.* **29**, 447-474

81. Liu, B., Hui, K., and Qin, F. (2003) Thermodynamics of Heat Activation of Single Capsaicin Ion Channels VR1. *Biophys. J.* **85**, 2988-3006

82. Becktel, W. J., and Schellman, J. A. (1987) Protein Stability Curves. *Biopolymers* **26**, 1859-1877

83. Bond, C. S., and Schuttelkopf, A. W. (2009) ALINE: a WYSIWYG protein-sequence alignment editor for publication-quality alignments. *Acta crystallographica. Section D, Biological crystallography* **65**, 510-512

84. Larkin, M. A., Blackshields, G., Brown, N. P., Chenna, R., McGettigan, P. A., McWilliam, H., Valentin, F., Wallace, I. M., Wilm, A., Lopez, R., Thompson, J. D., Gibson, T. J., and Higgins, D. G. (2007) Clustal W and Clustal X version 2.0. *Bioinformatics* **23**, 2947-2948

85. Konagurthu, A. S., Whisstock, J. C., Stuckey, P. J., and Lesk, A. M. (2006) MUSTANG: a multiple structural alignment algorithm. *Proteins* **64**, 559-574

86. Barton, G. J. (1993) ALSCRIPT: a tool to format multiple sequence alignments. *Protein engineering* **6**, 37-40

87. Liao, M., Cao, E., Julius, D., and Cheng, Y. (2013) Structure of the TRPV1 ion channel determined by electron cryo-microscopy. *Nature* **504**, 107-112

88. Cao, E., Liao, M., Cheng, Y., and Julius, D. (2013) TRPV1 structures in distinct conformations reveal activation mechanisms. *Nature* **504**, 113-118

89. *Thermal Sensors, Current Topics in Membranes*. (2014) Vol. 74, Islas, L. D., and Qin, F., Elsevier, Amsterdam

90. de Mendoza, D. (2014) Temperature sensing by membranes. *Annual review of microbiology* **68**, 101-116

91. Shapiro, R. S., and Cowen, L. E. (2012) Thermal control of microbial development and virulence: molecular mechanisms of microbial temperature sensing. *mBio* **3**, e00238-00212

92. Inda, M. E., Vandenbranden, M., Fernandez, A., de Mendoza, D., Ruysschaert, J. M., and Cybulski, L. E. (2014) A lipid-mediated conformational switch modulates the thermosensing activity of DesK. *Proc. Natl. Acad. Sci. U. S. A.* **111**, 3579-3584

93. Chowdhury, S., Jarecki, B. W., and Chanda, B. (2014) A molecular framework for temperature-dependent gating of ion channels. *Cell* **158**, 1148-1158

94. Greenfield, N. J. (2006) Using circular dichroism collected as a function of temperature to determine the thermodynamics of protein unfolding and binding interactions. *Nat Protoc* **1**, 2527-2535

95. Chill, J. H., Louis, J. M., Miller, C., and Bax, A. (2006) NMR study of the tetrameric KcsA potassium channel in detergent micelles. *Protein Sci.* **15**, 684-698

96. Butterwick, J. A., and MacKinnon, R. (2010) Solution structure and phospholipid interactions of the isolated voltage-sensor domain from KvAP. *J. Mol. Biol.* **403**, 591-606

97. Peng, D., Kim, J. H., Kroncke, B. M., Law, C. L., Xia, Y., Droege, K. D., Van Horn, W. D., Vanoye, C. G., and Sanders, C. R. (2014) Purification and structural study of the voltage-sensor domain of the human KCNQ1 potassium ion channel. *Biochemistry* **53**, 2032-2042

98. Hwang, P. M., Bishop, R. E., and Kay, L. E. (2004) The integral membrane enzyme PagP alternates between two dynamically distinct states. *Proc. Natl. Acad. Sci. U. S. A.* **101**, 9618-9623

99. White, H. D., Thirumurugan, K., Walker, M. L., and Trinick, J. (2003) A second generation apparatus for time-resolved electron cryo-microscopy using stepper motors and electrospray. *J. Struct. Biol.* **144**, 246-252

100. Kupitz, C., Basu, S., Grotjohann, I., Fromme, R., Zatsepin, N. A., Rendek, K. N., Hunter, M. S., Shoeman, R. L., White, T. A., Wang, D., James, D., Yang, J. H., Cobb, D. E., Reeder, B., Sierra, R. G., Liu, H., Barty, A., Aquila, A. L., Deponte, D., Kirian, R. A., Bari, S., Bergkamp, J. J., Beyerlein, K. R., Bogan, M. J., Caleman, C., Chao, T. C., Conrad, C. E., Davis, K. M., Fleckenstein, H., Galli, L., Hau-Riege, S. P., Kassemeyer, S., Laksmono, H., Liang, M., Lomb, L., Marchesini, S., Martin, A. V., Messerschmidt, M., Milathianaki, D., Nass, K., Ros, A., Roy-Chowdhury, S., Schmidt, K., Seibert, M., Steinbrener, J., Stellato, F., Yan, L., Yoon, C., Moore, T. A., Moore, A. L., Pushkar, Y., Williams, G. J., Boutet, S., Doak, R. B., Weierstall, U., Frank, M., Chapman, H. N., Spence, J. C., and Fromme, P. (2014) Serial time-resolved crystallography of photosystem II using a femtosecond X-ray laser. *Nature* **513**, 261-265

101. Lau, S. Y., Procko, E., and Gaudet, R. (2012) Distinct properties of Ca^{2+}-calmodulin binding to N- and C-terminal regulatory regions of the TRPV1 channel. *J. Gen. Physiol.* **140**, 541-555

102. Lishko, P. V., Procko, E., Jin, X., Phelps, C. B., and Gaudet, R. (2007) The ankyrin repeats of TRPV1 bind multiple ligands and modulate channel sensitivity. *Neuron* **54**, 905-918

103. Moiseenkova-Bell, V. Y., Stanciu, L. A., Serysheva, II, Tobe, B. J., and Wensel, T. G. (2008) Structure of TRPV1 channel revealed by electron cryomicroscopy. *Proc. Natl. Acad. Sci. U. S. A.* **105**, 7451-7455

104. Huynh, K. W., Cohen, M. R., Chakrapani, S., Holdaway, H. A., Stewart, P. L., and Moiseenkova-Bell, V. Y. (2014) Structural insight into the assembly of TRPV channels. *Structure* **22**, 260-268

105. Jin, X., Touhey, J., and Gaudet, R. (2006) Structure of the N-terminal ankyrin repeat domain of the TRPV2 ion channel. *J. Biol. Chem.* **281**, 25006-25010

106. McCleverty, C. J., Koesema, E., Patapoutian, A., Lesley, S. A., and Kreusch, A. (2006) Crystal structure of the human TRPV2 channel ankyrin repeat domain. *Protein Sci.* **15**, 2201-2206

107. Shi, D. J., Ye, S., Cao, X., Zhang, R., and Wang, K. (2013) Crystal structure of the N-terminal ankyrin repeat domain of TRPV3 reveals unique conformation of finger 3 loop critical for channel function. *Protein Cell* **4**, 942-950

108. Inada, H., Procko, E., Sotomayor, M., and Gaudet, R. (2012) Structural and biochemical consequences of disease-causing mutations in the ankyrin repeat domain of the human TRPV4 channel. *Biochemistry* **51**, 6195-6206

109. Shigematsu, H., Sokabe, T., Danev, R., Tominaga, M., and Nagayama, K. (2010) A 3.5-nm structure of rat TRPV4 cation channel revealed by Zernike phase-contrast cryoelectron microscopy. *J. Biol. Chem.* **285**, 11210-11218

110. Phelps, C. B., Huang, R. J., Lishko, P. V., Wang, R. R., and Gaudet, R. (2008) Structural analyses of the ankyrin repeat domain of TRPV6 and related TRPV ion channels. *Biochemistry* **47**, 2476-2484

111. Cvetkov, T. L., Huynh, K. W., Cohen, M. R., and Moiseenkova-Bell, V. Y. (2011) Molecular architecture and subunit organization of TRPA1 ion channel revealed by electron microscopy. *J. Biol. Chem.* **286**, 38168-38176

112. Maruyama, Y., Ogura, T., Mio, K., Kiyonaka, S., Kato, K., Mori, Y., and Sato, C. (2007) Three-dimensional reconstruction using transmission electron microscopy reveals a swollen, bell-shaped structure of transient receptor potential melastatin type 2 cation channel. *J. Biol. Chem.* **282**, 36961-36970

113. Fujiwara, Y., and Minor, D. L., Jr. (2008) X-ray crystal structure of a TRPM assembly domain reveals an antiparallel four-stranded coiled-coil. *J. Mol. Biol.* **383**, 854-870

114. Yamaguchi, H., Matsushita, M., Nairn, A. C., and Kuriyan, J. (2001) Crystal structure of the atypical protein kinase domain of a TRP channel with phosphotransferase activity. *Mol. Cell* **7**, 1047-1057

115. Mio, K., Ogura, T., Kiyonaka, S., Hiroaki, Y., Tanimura, Y., Fujiyoshi, Y., Mori, Y., and Sato, C. (2007) The TRPC3 channel has a large internal chamber surrounded by signal sensing antennas. *J. Mol. Biol.* **367**, 373-383

116. Petri, E. T., Celic, A., Kennedy, S. D., Ehrlich, B. E., Boggon, T. J., and Hodsdon, M. E. (2010) Structure of the EF-hand domain of polycystin-2 suggests a mechanism for Ca^{2+}-dependent regulation of polycystin-2 channel activity. *Proc. Natl. Acad. Sci. U. S. A.* **107**, 9176-9181

117. Yu, Y., Ulbrich, M. H., Li, M. H., Buraei, Z., Chen, X. Z., Ong, A. C., Tong, L., Isacoff, E. Y., and Yang, J. (2009) Structural and molecular basis of the assembly of the TRPP2/PKD1 complex. *Proc. Natl. Acad. Sci. U. S. A.* **106**, 11558-11563

118. Yu, Y., Ulbrich, M. H., Li, M. H., Dobbins, S., Zhang, W. K., Tong, L., Isacoff, E. Y., and Yang, J. (2012) Molecular mechanism of the assembly of an acid-sensing receptor ion channel complex. *Nat. Commun.* **3**, 1252

119. Berjanskii, M., Zhou, J., Liang, Y., Lin, G., and Wishart, D. S. (2012) Resolution-by-proxy: a simple measure for assessing and comparing the overall quality of NMR protein structures. *Journal of biomolecular NMR* **53**, 167-180

120. Orozco, M. (2014) A theoretical view of protein dynamics. *Chemical Society reviews* **43**, 5051-5066

121. Dror, R. O., Dirks, R. M., Grossman, J. P., Xu, H., and Shaw, D. E. (2012) Biomolecular simulation: a computational microscope for molecular biology. *Annual review of biophysics* **41**, 429-452

122. Denning, E. J., and Beckstein, O. (2013) Influence of lipids on protein-mediated transmembrane transport. *Chem. Phys. Lipids* **169**, 57-71

123. Khalili-Araghi, F., Gumbart, J., Wen, P.-C., Sotomayor, M., Tajkhorshid, E., and Schulten, K. (2009) Molecular dynamics simulations of membrane channels and transporters. *Curr. Opin. Struct. Biol.* **19**, 128-137

124. Koehler Leman, J., Ulmschneider, M. B., and Gray, J. J. (2015) Computational modeling of membrane proteins. *Proteins* **83**, 1-24

125. Stansfeld, P. J., and Sansom, M. S. P. (2011) Molecular simulation approaches to membrane proteins. *Structure* **19**, 1562-1572

126. Fernandez-Ballester, G., and Ferrer-Montiel, A. (2008) Molecular modeling of the full-length human TRPV1 channel in closed and desensitized states. *The Journal of membrane biology* **223**, 161-172

127. Kornilov, P., Peretz, A., Lee, Y., Son, K., Lee, J. H., Refaeli, B., Roz, N., Rehavi, M., Choi, S., and Attali, B. (2014) Promiscuous gating modifiers target the voltage sensor of K(v)7.2, TRPV1, and H(v)1 cation channels. *FASEB journal : official publication of the Federation of American Societies for Experimental Biology* **28**, 2591-2602

128. Susankova, K., Ettrich, R., Vyklicky, L., Teisinger, J., and Vlachova, V. (2007) Contribution of the putative inner-pore region to the gating of the transient receptor potential vanilloid subtype 1 channel (TRPV1). *J. Neurosci.* **27**, 7578-7585

129. Cao, E., Liao, M., Cheng, Y., and Julius, D. (2013) TRPV1 structures in distinct conformations reveal activation mechanisms. *Nature* **504**, 113-118

130. Darré, L., Furini, S., and Domene, C. (2015) Permeation and Dynamics of an Open-Activated TRPV1 Channel. *J. Mol. Biol.* **427**, 537-549

131. Poblete, H., Oyarzún, I., Olivero, P., Comer, J., Zuñiga, M., Sepulveda, R. V., Báez-Nieto, D., González Leon, C., González-Nilo, F., and Latorre, R. (2015) Molecular Determinants of Phosphatidylinositol 4,5-Bisphosphate (PI(4,5)P2) Binding to Transient Receptor Potential V1 (TRPV1) Channels. *J. Biol. Chem.* **290**, 2086-2098

132. Shaw, D. E., Dror, R. O., Salmon, J. K., Grossman, J. P., Mackenzie, K. M., Bank, J. A., Young, C., Deneroff, M. M., Batson, B., Bowers, K. J., Chow, E., Eastwood, M. P., Ierardi, D. J., Klepeis, J. L., Kuskin, J. S., Larson, R. H., Lindorff-Larsen, K., Maragakis, P., Moraes, M. A., Piana, S., Shan, Y., and Towles, B. (2009) Millisecond-scale molecular dynamics simulations on Anton. in *SC '09: Proceedings of the Conference on High Performance Computing Networking, Storage and Analysis*, ACM, New York, NY, USA

133. Liwo, A., Czaplewski, C., Ołdziej, S., and Scheraga, H. A. (2008) Computational techniques for efficient conformational sampling of proteins. *Curr. Opin. Struct. Biol.* **18**, 134-139

134. Okamoto, Y. (2004) Generalized-ensemble algorithms: enhanced sampling techniques for Monte Carlo and molecular dynamics simulations. *J. Mol. Graphics Modell.* **22**, 425-439

135. Seyler, S. L., and Beckstein, O. (2014) Sampling of large conformational transitions: Adenylate kinase as a testing ground. *Molec. Simul.* **40**, 855-877

136. van der Vaart, A. (2006) Simulation of conformational transitions. *Theor. Chem. Acc.* **116**, 183-193

137. Chodera, J. D., Mobley, D. L., Shirts, M. R., Dixon, R. W., Branson, K., and Pande, V. S. (2011) Alchemical free energy methods for drug discovery: progress and challenges. *Curr. Opin. Struct. Biol.* **21**, 150-160

138. Roux, B., Allen, T., Bernèche, S., and Im, W. (2004) Theoretical and computational models of biological ion channels. *Quart. Rev. Biophys.* **37**, 15-103

139. Sugita, Y., and Okamoto, Y. (1999) Replica-exchange molecular dynamics method for protein folding. *Chem. Phys. Lett.* **314**, 141-151

140. Wang, L., Friesner, R. A., and Berne, B. J. (2011) Replica exchange with solute scaling: a more efficient version of replica exchange with solute tempering (REST2). *J. Phys. Chem. B* **115**, 9431-9438

141. Jensen, M. Ø., Jogini, V., Borhani, D. W., Leffler, A. E., Dror, R. O., and Shaw, D. E. (2012) Mechanism of Voltage Gating in Potassium Channels. *Science* **336**, 229-233

142. Köpfer, D. A., Song, C., Gruene, T., Sheldrick, G. M., Zachariae, U., and de Groot, B. L. (2014) Ion permeation in K^+ channels occurs by direct Coulomb knock-on. *Science* **346**, 352-355

143. Tarek, M., and Delemotte, L. (2013) Omega currents in voltage-gated ion channels: what can we learn from uncovering the voltage-sensing mechanism using MD simulations? *Acc Chem Res* **46**, 2755-2762

144. Ulmschneider, M. B., Bagnéris, C., McCusker, E. C., Decaen, P. G., Delling, M., Clapham, D. E., Ulmschneider, J. P., and Wallace, B. A. (2013) Molecular dynamics of ion transport through the open conformation of a bacterial voltage-gated sodium channel. *Proc. Natl. Acad. Sci. U. S. A.* **110**, 6364-6369

145. Venkatachalam, K., and Montell, C. (2007) TRP Channels. *Annu. Rev. Biochem.* **76**, 387-417

146. Peng, G., Shi, X., and Kadowaki, T. (2014) Evolution of TRP channels inferred by their classification in diverse animal species. *Molecular phylogenetics and evolution* **84**, 145-157

CHAPTER 3

PHOSPHOINOSITIDE-INTERACTING REGULATOR OF TRP (PIRT) HAS OPPOSING EFFECTS ON HUMAN AND MOUSE TRPM8 ION CHANNELS

3.1 Abstract

Transient receptor potential melastatin 8 (TRPM8) is a cold-sensitive ion channel with diverse physiological roles. TRPM8 activity is modulated by many mechanisms, including an interaction with the small membrane protein phosphoinositide-interacting regulator of TRP (PIRT). Here, using comparative electrophysiology experiments, we identified species-dependent differences between the human and mouse TRPM8–PIRT complexes. We found that human PIRT attenuated human TPRM8 conductance, unlike mouse PIRT, which enhanced mouse TRPM8 conductance. Quantitative Western blot analysis demonstrates that this effect does not arise from decreased trafficking of TRPM8 to the plasma membrane. Chimeric human/mouse TRPM8 channels were generated to probe the molecular basis of the PIRT modulation, and the effect was recapitulated in a pore domain chimera, demonstrating the importance of this region for PIRT-mediated regulation of TRPM8. Moreover, recombinantly expressed and purified human TRPM8 S1–S4 domain (comprising transmembrane helices S1–S4, also known as the sensing domain, ligand-sensing domain, or voltage sensing-like domain) and full-length human PIRT were used to investigate binding between the proteins. NMR experiments, supported by a pulldown assay, indicated that PIRT binds directly and specifically to the TRPM8 S1–S4 domain. Binding became saturated as the S1–S4:PIRT mole ratio approached 1. Our results have uncovered species-specific TRPM8 modulation by PIRT.

They provide evidence for a direct interaction between PIRT and the TRPM8 S1–S4 domain with a 1:1 binding stoichiometry, suggesting that a functional tetrameric TRPM8 channel has four PIRT-binding sites.

3.2 Introduction

Transient receptor potential melastatin 8 (TRPM8) is a temperature sensitive ion channel that activates at temperatures below 25 °C; it is considered the primary cold sensor in mammals [1, 2]. Besides temperature, TRPM8 activity is modulated by a variety of stimuli, including small molecules (the most well-known of which is menthol), pH, and the phospholipid phosphoinositide 4,5-bisphosphate (PIP_2) [3, 4]. Although TRPM8 function is typically considered in the context of sensory physiology, TRPM8 also has important roles in other physiological processes such as pain [5], core body temperature regulation [6-8], body weight regulation [9], vasoconstriction regulation [10], and osmolality sensing [11]. Understanding the regulation of TRP channel activity, including TRPM8, is currently an area of much investigation and debate.

TPRM8 activity is also modulated by PIRT, a small two-span membrane protein [12, 13]. PIRT was originally identified as a regulator of TRPV1, and it is exclusively expressed in dorsal root ganglia, trigeminal ganglia, and enteric neurons of the peripheral nervous system [14]. PIRT knockout mice exhibit impaired temperature response to both hot and cold temperatures, and electrophysiology and calcium imaging studies demonstrated that both TRPM8 and TRPV1 activity are enhanced in the presence of PIRT [12, 14]. In addition, PIRT was shown to contribute to visceral pain sensation [15], bladder activity regulation [16], and TRPV1-dependent and -independent itch (pruritus) sensation [17],

suggesting broader physiological roles and underscoring the biological importance of this modulatory protein. Coimmunoprecipitation experiments show that PIRT interacts with TRPV1 and TRPM8, suggesting that the regulation is mediated via a direct interaction with the channel [14]. Cell surface trafficking experiments indicate that enhanced channel activity in mice is not caused by changes in expression levels or channel trafficking, supporting the idea that PIRT enhances channel activity by interacting directly with the channels rather than increasing the number of channels in the membrane [12, 14]. More recently, it was shown that PIRT works synergistically with PIP_2 to enhance TRPM8 currents by increasing conductance at the single channel level [13]. However, the details of this interaction including the binding site and stoichiometry of PIRT to TRPM8 are unknown.

Notably, these studies were carried out using mouse models and apparently heterologous expression of the mouse *Pirt* and *Trp* channel genes. TRP channels exhibit remarkable functional and sequence diversity not only between different channels in the family, but also between orthologs, i.e. the same gene product from different species [18, 19]. These differences can manifest as important selected features between species; for example, the thermosensitivity of different species of TRPM8 is evolutionarily tuned to the appropriate temperature range based on organismal core body temperature and environment [20], and avian TRPV1 is insensitive to capsaicin, a potent agonist of the mammalian ortholog, which allows for seed disbursement [19].

The results of this study focus on the human TRPM8 and PIRT gene products and for the first time reveal that in contrast to the increased conductance seen in the mouse proteins,

human TRPM8 currents are attenuated in the presence of human PIRT. Analogous to previously published mouse studies, human PIRT does not reduce human TRPM8 cell-surface expression. Additionally, nuclear magnetic resonance (NMR) chemical shift perturbation and *in vitro* pull-down experiments show that PIRT binds specifically to the S1–S4 domain of TRPM8, with a 1:1 stoichiometry. Transmembrane domain chimeras of human/mouse TRPM8 showed that residues in the transmembrane domain (helices S1-S6), and in particular the pore domain (S5-S6), are the basis for modulation by PIRT and the species differences observed. These results shed light on the PIRT–TRPM8 interaction and reveal that the PIRT–TRPM8 complex has evolved in a species-dependent manner.

3.3 Results

3.3.1 PIRT Modulation of TRPM8 Is Species Dependent

Whole-cell patch-clamp electrophysiology was used to measure current responses of human embryonic kidney (HEK) 293 cells that were transiently transfected with either human *TRPM8* and human *PIRT* or human *TRPM8* and empty vector (Fig. 3.1A). Current responses to voltage steps from -100 to +100 mV were recorded using a standard step protocol (Fig. 3.1D). At ambient room temperature (~23 °C), recordings of cells transfected with both human *TRPM8* and human *PIRT* resulted in significantly reduced currents compared to cells transfected with human *TRPM8* and an empty pIRES2-DsRed vector at voltages of +60 mV and above; at +100 mV, cells transfected with human *PIRT* showed on average ~69% of the current measured from cells expressing hTRPM8 alone.

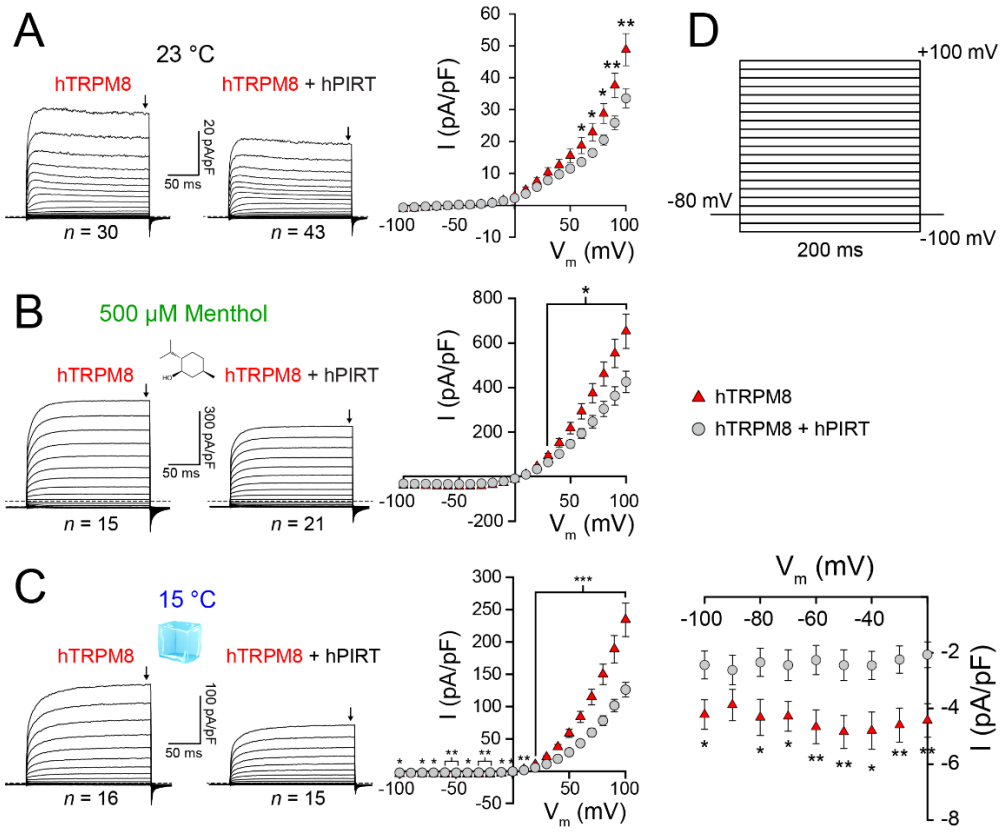

Figure 3.1 Human PIRT attenuates whole-cell currents of human TRPM8. (A) Average current traces and current-voltage plot of whole-cell patch-clamp electrophysiology recordings of HEK-293 cells expressing hTRPM8 or hTRPM8 and hPIRT taken at ambient temperature (23 ± 1 °C). Current-voltage plots are of steady-state current values taken from the time point indicated by an arrow in the average current traces. At ambient temperature, hTRPM8 currents are significantly attenuated at voltages above +60 mV when coexpressed with hPIRT. (B) Upon stimulation with saturating menthol concentrations (500 µM), hTRPM8 currents are significantly attenuated at voltages above +30 mV. (C) Cold-evoked currents were significantly attenuated at all measured voltages with the exception of -90 mV. An expanded view of negative potentials (bottom right) shows that hPIRT significantly attenuates cold-evoked currents at physiological membrane potentials. (D) The voltage step protocol used to record current responses from -100 to +100 mV in 10 mV steps with a holding potential of -80 mV between steps. Statistical significance was determined using a two-tailed Student's *t*-test; single asterisk indicates $p < 0.5$, double asterisk indicates $p < 0.01$. Red triangles represent cells transfected with human *TRPM8* and empty control vector DNA; gray circles represent cells transfected with human *TRPM8* and human *PIRT* DNA. Error bars represent standard error of the mean.

We further tested hPIRT modulation of hTRPM8 in the more physiologically relevant context of low temperature and menthol stimuli. In the presence of a TRPM8 saturating concentration of menthol (500 μM) [21], current from human *PIRT* transfected cells is significantly reduced at and above +30 mV, with ~65% of the maximum current observed at +100 mV (Fig. 3.1B). At 15 °C, a TRPM8 saturating temperature, human *PIRT*-transfected cells exhibited significantly attenuated currents at all measured voltages except -90 mV. At +100 mV, cells expressing hPIRT exhibited ~54% of the current evoked from TRPM8 alone (Fig. 3.1C). Temperature dependent inward hTRPM8 currents were significantly reduced at physiological voltages (Fig. 3.1C). Statistical significance was determined by an unpaired Student's *t*-test; a minimum of 15 and maximum of 43 cells were measured for these conditions and clearly specified in Figure 3.1.

Mouse PIRT (mPIRT) has previously been established as an endogenous regulator of TRPM8 that enhances TRPM8 currents [12]. Using whole-cell patch-clamp experiments, we were able to reproduce these results using the mouse orthologs, with mTPRM8 currents significantly higher in the presence of mPIRT. We note that the hTRPM8 currents are about twice the magnitude of mTRPM8 currents when PIRT was not expressed, highlighting the inherent functional differences between the two TRPM8 orthologs (Fig. 3.2A). Cross species expression of PIRT with TRPM8 (e.g. hTRPM8/mPIRT) did not result in significant differences in currents (Fig. 3.2B).

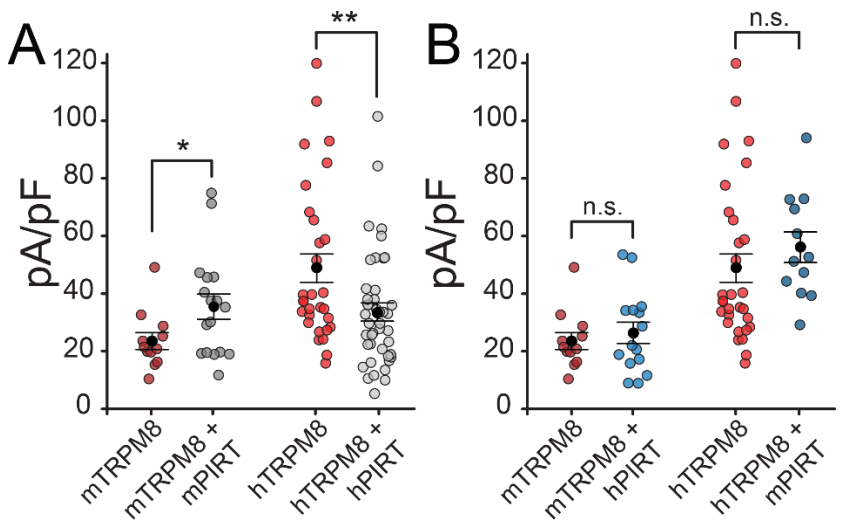

Figure 3.2 Human and mouse species dependent PIRT regulation of TRPM8 orthologs. (A) Comparison of steady state current density measured at room temperature (23 ± 1 °C) from HEK-293 cells coexpressing either mouse or human TRPM8 and PIRT. The presence of mouse PIRT increases current compared to TRPM8 alone, whereas human PIRT has an opposite, attenuating effect. (B) Comparison of TRPM8 currents in the presence and absence of PIRT from the opposite species. No significant difference can be detected between the two conditions. This is likely the result of an intermediate effect. Currents were measured at +100 mV at the same steady state time point indicated in Figure 3.1. (mTRPM8, n = 12; mTRPM8+mPIRT, n = 17; mTRPM8+hPIRT, n = 15; hTRPM8, n = 30; hTRPM8+hPIRT, n = 43; hTRPM8+mPIRT, n = 12)

Previous studies have shown that TRP channel activity can be modulated by associated proteins that regulate channel trafficking to the membrane [22]. To test whether hPIRT affects hTRPM8 trafficking, we performed cell-surface expression experiments on HEK-293 cells transfected with human *TRPM8* alone or with human *TRPM8* and human *PIRT*. Western blot quantification from three independent experiments showed no significant difference in hTRPM8 plasma membrane expression levels in the presence and absence of hPIRT expression, confirming that hPIRT does not affect hTRPM8 membrane trafficking (Fig. 3.3A). This agrees with previous similar studies of the mouse orthologs, which show that mouse TRPM8 membrane trafficking is

also not affected by mouse PIRT coexpression and that mouse PIRT increases single channel conductance [12-14].

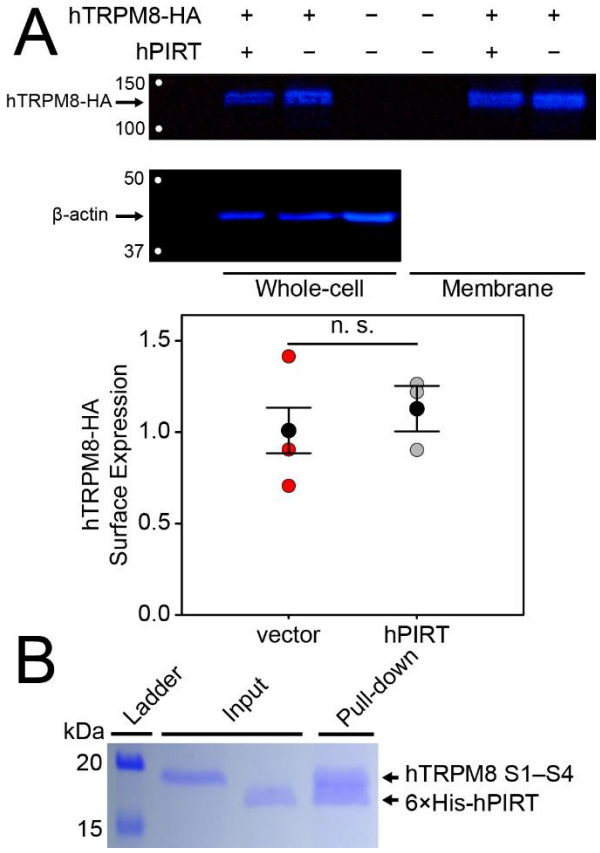

Figure 3.3 Human TRPM8 cell-surface trafficking is not affected by PIRT expression, and the purified proteins directly interact under in vitro conditions. (A) Representative Western blot from trafficking experiments. hTRPM8 cell-surface expression was measured by biotinylation and purification of surface proteins followed by western blotting. Negative signs indicate conditions in which cells were transfected with empty vector. The blot shows similar surface expression levels in the presence and absence of hPIRT. Three experiments were repeated using independently transfected cells, and the results are presented in the scatter plot. Black circles represent average expression level, and error bars represent standard error of the mean. (B) Human PIRT directly binds the TRPM8 VSLD. 6×His-hPIRT was mixed with the tag-cleaved hTRPM8 S1–S4 domain and the complex was bound to a Ni-NTA column. Coomassie stained SDS-PAGE revealed that hTRPM8 S1–S4 domain coelutes with PIRT, indicating that the two proteins bind directly.

3.3.2 PIRT Interacts Directly With the TRPM8 S1–S4 Domain

Previously reported co-immunoprecipitation studies indicate that mTRPM8 and mPIRT interact in the context of HEK-293 cells [12]. In particular, the C-terminal 26 residues of PIRT were shown to bind to both TRPV1 and TRPM8; additionally, a glutathione S-transferase-tagged form of the PIRT C-terminus was shown to modulate currents from these two channels [12, 14]. However, a follow-up study using mTRPV1 and mPIRT fused to fluorescent proteins detected no FRET signal [23]. To date, nothing has been published regarding which regions of TRPV1 or TRPM8 interact with PIRT. To further probe the molecular basis of the TRPM8/PIRT complex, we performed an in vitro pull-down experiment. Given that PIRT is a small transmembrane protein, we reasoned that it likely interacts with a transmembrane region within TRPM8. TRP channels have a transmembrane topology similar to voltage-gated potassium channels, with six transmembrane helices that form an S1–S4 domain and a pore domain (S5–S6 helices) [18]. Using purified hPIRT and hTRPM8 S1–S4 domain, where only the hPIRT protein contained a histidine affinity tag, the two proteins were mixed, bound to Ni-NTA resin, washed extensively (>50 column volumes) and eluted from the column. Analysis of the eluted fractions by SDS-PAGE showed that both hPIRT and hTRPM8 S1–S4 domain were eluted from the mixture, demonstrating that hPIRT interacts directly with hTRPM8 S1–S4 domain as shown in Figure 3.3B. The pull-down experiment was performed twice and had consistent results in showing the hTRPM8 S1–S4 domain–hPIRT interaction.

To further study this interaction, we performed an NMR titration of ^{15}N-labeled hPIRT with hTRPM8 S1–S4 domain. We used ^{1}H,^{15}N TROSY-HSQC experiments to

measure ^{1}H and ^{15}N chemical shifts of hPIRT with increasing concentrations of hTRPM8 S1–S4 domain (Fig. 3.4, A and C). A number of hPIRT resonances exhibited significant chemical shift perturbation (Δδ) with increasing hTRPM8 S1–S4 domain concentration. Figure 3.4 highlights two representative resonances (Fig. 3.4B) and plots the change in chemical shift (Δδ) as a function of hTRPM8:hPIRT mole ratio (Fig. 3.4D). Fitting a single binding site model to these plots shows that binding becomes saturated as the molar ratio approaches 1 (Fig. 3.4D). The saturating chemical shift changes of these resonances indicate that the perturbation is the result of direct and specific binding interactions. The calculated K_d values for the two highlighted resonances were near a molar ratio of ~0.5. As a negative control, we expressed and purified the voltage sensing domain of KCNQ1 (KCNQ1-VSD), a voltage-gated potassium channel that is structurally homologous to TRPM8 but has not been shown to be modulated by PIRT. The TROSY-HSQC titration data of hPIRT and KCNQ1-VSD (Fig. 3.4, E and F) indicates that hPIRT does not bind to KCNQ1 as there is non-saturating and minimal chemical shift perturbation identified in this control experiment. These data confirm the pull-down experimental results and show that hPIRT binds specifically and directly to the hTRPM8 S1–S4 domain with a 1:1 binding stoichiometry.

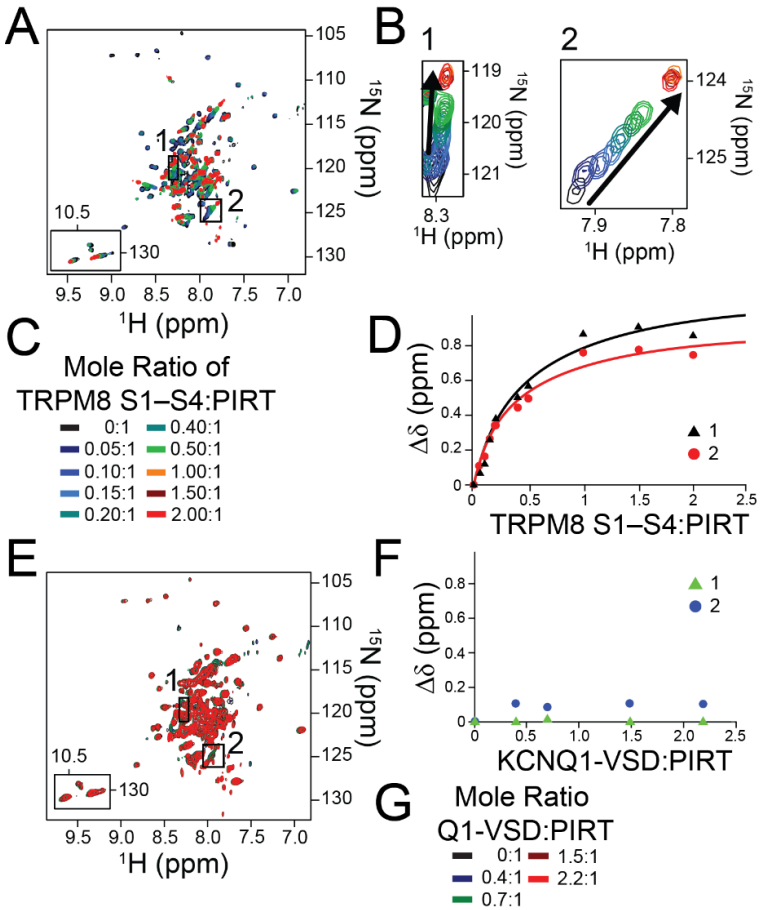

Figure 3.4 NMR studies show that human PIRT directly binds to the TRPM8 S1–S4 domain. Titration of ^{15}N-labeled hPIRT with unlabeled hTRPM8 S1–S4 domain. (A) Overlaid ^{1}H, ^{15}N TROSY-HSQC spectra from samples with varying hTRPM8 S1–S4 domain:hPIRT mole ratios from zero to two. Individual amino acid resonance chemical shift perturbations are highlighted by boxes 1 and 2. The chemical shifts of these resonances show evidence of saturable binding at elevated TRPM8 S1–S4 domain concentrations. (B) Expanded view of the chemical shift perturbations highlighted in panel A; note that in box 2 of panel B the spectral contours are raised such that the resonances are more easily observed. (C) The mole ratio legend for the titration of hPIRT with hTRPM8 S1–S4 domain. (D) Normalized change in chemical shift (Δδ) values from both resonances were plotted as a function of hTRPM8 S1–S4 domain:hPIRT mole ratio. The data were fit to a single binding site model using the equation $f(\Delta\delta) = (\Delta\delta)(\Delta\delta_{max})/(K_d + \Delta\delta)$. K_d values for resonances 1 and 2 were calculated to be 0.50 ± 0.11 and 0.41 ± 0.07, respectively, both with r^2 coefficients of 0.98. (E) Overlaid ^{1}H, ^{15}N TROSY-HSQC spectra from samples with varying concentrations of the KCNQ1 voltage sensing domains (VSD). The lack of PIRT chemical shift perturbation upon addition of the KCNQ1-VSD suggests that it does not interact with PIRT. (F) An equivalent $\Delta\delta$ plot for KCNQ1-VSD:PIRT showing that there is no significant chemical shift perturbation to the corresponding PIRT resonances from panel A upon addition of KCNQ1-VSD to PIRT. (G) Concentration legend for the PIRT–KCNQ1-VSD titration.

3.3.3 Functional Determinants of PIRT Modulation in the TRPM8 Transmembrane Domain

Chimeric ion channels have proven a valuable research tool for identifying molecular bases of channel regulatory mechanisms and of functional differences between orthologues.[19, 24-26]. To probe the functional determinants of TRPM8 modulation by PIRT, we generated a series of mouse and human TRPM8 chimeras to search for regions that give rise to species-specific phenotypes. The transmembrane core is known to be the nexus of TRP channel integration of stimuli. Because of this and the concise nature of PIRT, we chose to focus our search on this region, and we generated a series of transmembrane domain (TMD) chimeras. Based on sequence homology with other TRP channels for which cryo-EM structures have been solved, we defined the TMD as residues 672-1012. Within this region, there are only 11 residues that are different between mouse and human TRPM8. A recently determined cryo-EM structure of F. albicollis TRPM8 allowed us to map these residues to specific regions in the channel (Fig. 3.5A) [27]. Two divergent residues are found in the helical pre-S1 domain, four in the S2 helix, three in the pore loop, one in the S6 helix, and one in the TRP helix. We mutated residues in mTRPM8 to the corresponding residues found in hTRPM8 to generate three chimeric channels: mTRPM8$_{hTMD}$, which includes all eleven residues from hTRPM8; mTRPM8$_{hS1S4}$, which includes only hTRPM8 residues from the voltage sensor-like domain; and mTRPM8$_{hPD}$, which includes hTRPM8 residues from the pore domain and TRP helix (Fig. 3.5B). We performed electrophysiology measurements to

determine whether these chimeras reproduce the human phenotype in the presence of human PIRT.

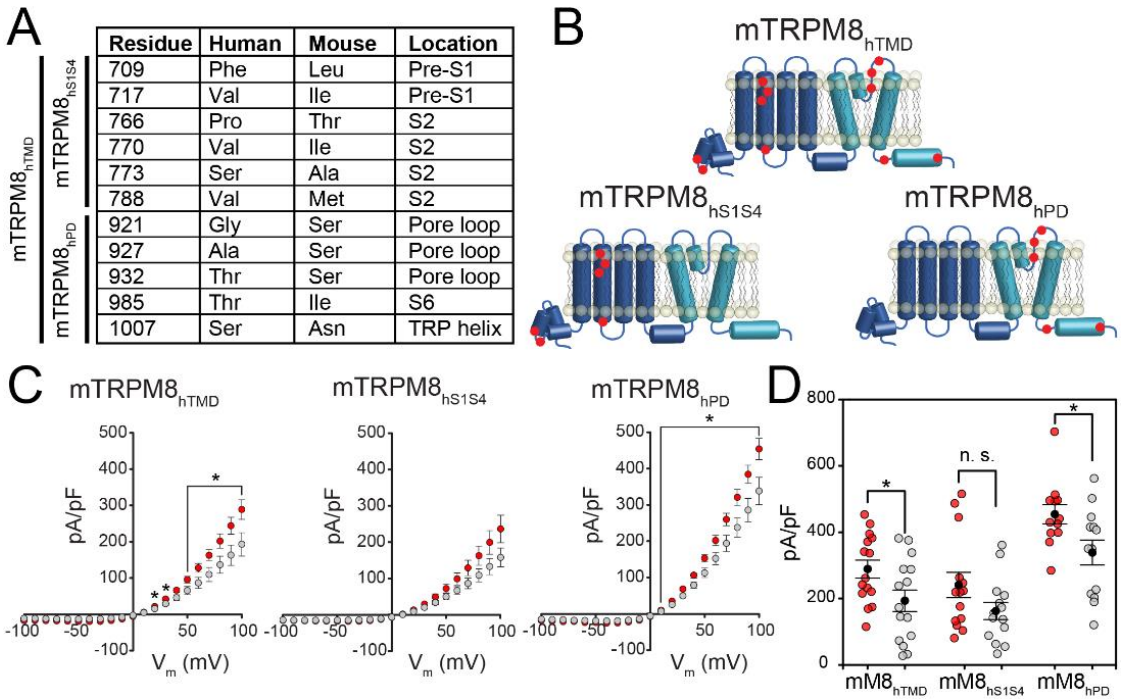

Residue	Human	Mouse	Location
709	Phe	Leu	Pre-S1
717	Val	Ile	Pre-S1
766	Pro	Thr	S2
770	Val	Ile	S2
773	Ser	Ala	S2
788	Val	Met	S2
921	Gly	Ser	Pore loop
927	Ala	Ser	Pore loop
932	Thr	Ser	Pore loop
985	Thr	Ile	S6
1007	Ser	Asn	TRP helix

Figure 3.5 Mouse-human chimeric channels demonstrate functional determinants of TRPM8 modulation by PIRT (A) Divergent residues in the transmembrane domains of human and mouse. (B) Topology plots illustrating the locations of divergent residues in each chimeric construct. The full transmembrane domain has eleven mutations, the VSLD has six, and the pore domain has three. (C) Current-voltage plots showing attenuation of currents when chimeric channels are coexpressed with hPIRT. Measurements were made at ambient temperature (~23 °C) in the presence of 500 µM menthol ($mTRPM8_{hTMD}$, n = 15; $mTRPM8_{hTMD}$+hPIRT, n = 15; $mTRPM8_{hS1S4}$, n = 14; $mTRPM8_{hS1S4}$+hPIRT, n = 14; $mTRPM8_{hPD}$, n = 12; $mTRPM8_{hPD}$+hPIRT, n = 13). (D) Jitter plot of steady-state current density from individual cells at +100 mV in the presence of 500 µM menthol. Human PIRT significantly attenuates current response from $mTRPM8_{hTMD}$ and $mTRPM8_{hPD}$ chimeras. Average current from $mTRPM8_{hS1S4}$ channels is also lower but not to a significant degree. All error bars represent standard error of the mean. Red circles represent cells transfected with TRPM8 and vector, grey circles represent cells transfected with TRPM8 and hPIRT, and black circles represent average current density.

The $mTRPM8_{hTMD}$ construct produced a phenotype similar to hTRPM8 in the presence of hPIRT. When coexpressed with hPIRT, the channel exhibited 67 ± 13% of the current density without hPIRT at 100 mV with 500 µM menthol; this is close to the

reduction observed with wild-type hTRPM8 and hPIRT (vector only, n = 15; hPIRT, n = 15; p = 0.03). This channel exhibited no difference in current when expressed with or without mPIRT, suggesting that the TMD plays a key role in the modulatory effect (Fig. 3.5C). The mTRPM8$_{hS1S4}$ channel also exhibited a decreased average current density to 67 ± 13% of the current without hPIRT; however, a Student's t-test resulted in a higher p-value (vector only, n = 14; hPIRT, n = 14; p = 0.1) (Fig. 3.5C). Finally, mTRPM8$_{hPD}$ showed significantly decreased current density to 75 ± 10% of the current without hPIRT (vector only, n = 12; hPIRT, n = 13; p = 0.03) (Fig. 3.5C). Taken together, these results point to the transmembrane domain, and particularly the pore domain, as key functional determinants of TRPM8 modulation by PIRT.

Intriguingly, the mTRPM8$_{hPD}$ chimera showed significantly increased currents compared to the other chimeras (Fig. 3.5D). An ANOVA test showed significant difference between the three groups (p = 0.0001; F = 11.4121) and a Tukey HSD test showed significant difference between mM8$_{hPD}$ and mM8$_{hS1S4}$ (p = 0.004), and between mM8$_{hPD}$ and mM8$_{hTMD}$ (p = 0.0002), but not between mM8$_{hS1S4}$ and mM8$_{hTMD}$ (p = 0.6). Wild-type mTRPM8 current density was also significantly lower compared to wild-type hTRPM8; thus, the five mutations in the pore domain and TRP helix are sufficient to confer higher, human-like current density to the mTRPM8 chimera.

3.4 Discussion

PIRT has previously been shown in behavioral knock-out mice studies to be important in thermosensation via regulation of the thermosensitive TRP channels TRPV1 and TRPM8, demonstrating that the biophysical effects of PIRT on TRPM8 are

functionally significant at the organismal level [12, 14]. These studies focused on mouse orthologs of both the Trp channel and Pirt genes. Here, we present data from the human orthologs and show that the human PIRT–TRPM8 interaction results in an opposite modulatory effect compared to the mouse proteins.

Previous studies have investigated PIRT binding with TRP channels. Dong and coworkers expressed the first 53 residues of the N-terminus and the last 26 residues of the C terminus fused to GST tags and performed a pull down assay with mouse TRPV1 and TRPM8. Their results indicate that the PIRT C- and N-termini bind strongly and weakly to the two TRP channels, respectively [14]. However, as whole cell lysate was used, this data does not rule out an indirect interaction with other partner proteins in the complex. A second study by Gordon and coworkers used a Förster Resonance Energy Transfer (FRET) approach where fluorescent proteins were genetically fused to the termini of TRPV1 and PIRT and the fluorescent signal was measured in HEK-293 cells [23]. No FRET signal was observed; nevertheless, the lack of FRET signal does not necessarily rule out an association between the proteins, as this negative result could potentially occur for a number of reasons, such as suboptimal structural arrangement of the fluorophores [23]. The lack of FRET could arise because the fluorophore was fused to the C-terminus of PIRT, which is implicated in TRP channel binding [14]. Also, given the relatively small size of PIRT (~15 kDa) compared to the size of the YFP fluorophore (~26 kDa), it is possible that the C-terminal tag could sterically interfere with the TRPV1-PIRT interaction.

Our data indicate that the TRPM8 S1–S4 domain binds specifically with PIRT in a 1:1 binding stoichiometry. This association is demonstrated using two different methods that show a direct interaction between the two proteins. In functioning TRP channels, the S1–S4 domain is positioned at the periphery of the tetrameric channel with the conducting pore in the center. The molecular mechanism of TRP channel gating is currently under investigation; however, the gating mechanism of similarly structured voltage-gated potassium (K_V) channels is better established. It is known that the S4 helix within the voltage sensing domain of K_V channels is responsible for opening the gate upon membrane depolarization [28]. Thus from an evolutionary standpoint it is possible that the structurally homologous S1–S4 domain of TRP channels is involved in channel gating. Recent studies of TRPM8 and TRPV1 identify the respective S1–S4 domains as central to ligand binding and activation [29, 30]. The 1:1 stoichiometry we observed suggests a possible mechanism of fine-tuning TRPM8 activity; each channel has four S1–S4 domains, so it may be possible that up to four PIRT proteins can interact with the channel (Fig. 3.6). Different levels of PIRT expression could result in varying degrees of attenuation for the human channel (or activation for the mouse channel), as has recently been shown with K_V channel-interacting proteins [31].

Mounting evidence points to the complex role of regulatory proteins in TRP channel function. Gkika et al. recently reported a family of TRPM8-associated proteins found in prostate cells [22]. These TRP channel-associated factors (TCAFs) regulate TRPM8 trafficking to the plasma membrane as well as kinetic states at the single channel level [22]. Weng et al. reported that a protein known as Tmem100 enhances TRPA1

activity by modulating the physical association of a TRPA1–TRPV1 complex, thus interfering with TRPV1-mediated inhibition of TRPA1 [32]. Interestingly, a Tmem100 mutant was found to have the inverse effect, inhibiting TRPA1 activity by enhancing the association between TRPA1 and TRPV1 [32]. Based on this result, a synthetic peptide mimicking the Tmem100 mutant was designed and found to reduce pain behaviors induced by mustard oil, a TRPA1 agonist [32]. Like PIRT, Tmem100 is a small two-span membrane protein and is evolutionarily related to PIRT with 27% sequence identity between the human paralogs. In addition to TRP channel function being modulated by proteins like TCAFs and PIRTs, there is emerging evidence that PIRT is an endogenous regulator of P2X purinergic receptors [16, 33]. As with TRP channels, P2X receptors are considered promising therapeutic targets and highlight the possibility of developing therapeutics based on targeting modulatory proteins such as PIRT.

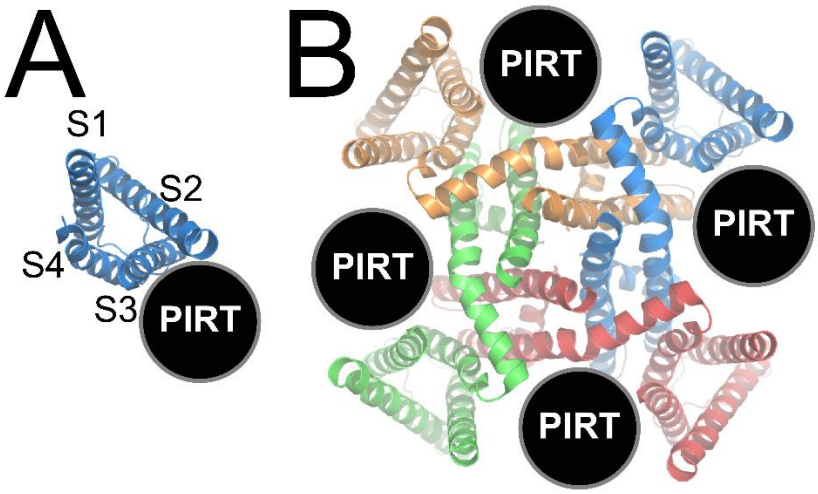

Figure 3.6 A model of PIRT–TRPM8 complex stoichiometry. (A) Based on NMR titration data, PIRT binds the TRPM8 S1–S4 domain with a 1:1 stoichiometry. (B) Functional channels are homotetramers, suggestive that up to four PIRT proteins can simultaneously bind TRPM8. Thus, the number of PIRT proteins bound is a possible mechanism of further fine-tuning the channel activity.

In addition to TRP channels, many ion channels have been shown to be regulated by modulatory subunits. The voltage-sensitive channel KCNQ1 ($K_V7.1$) is regulated in diverse ways by KCNE subunits, which are single span integral membrane proteins [34]. The five members of the KCNE family are known to modulate multiple different K_V channels, resulting in changes in properties including current density, pharmacology, and activation and inactivation kinetics [35]. For example, KCNQ1 activation is dramatically slowed and current density increased when associated with KCNE1, whereas KCNE4 completely abolishes KCNQ1 currents [36, 37]. This functional relationship is further complicated by the fact that KCNE1 and KCNE4 can also co-associate with KCNQ1 to form heteromultimeric complexes [38]. Mutations in these subunits disrupt native currents and are associated with inherited cardiac arrhythmias including long QT syndrome, underscoring the physiological importance of ion channel modulation [39]. Another example is the β-subunits of BK channels [34]. In cochlear hair cells, differential expression of β1 and β4 subunits is a mechanism of tuning BK channels to facilitate appropriate electrical oscillation frequency [40, 41], whereas the β2 subunit is responsible for inactivating BK channels in adrenal chromaffin cells [42]. Regulation by modulatory proteins is a well-established mechanism of enhanced functional diversity of ion channels; a single type of channel can be adapted for different roles in different tissue or cell types. TRP channels are likewise widely expressed and have diverse physiological roles; modulatory proteins like PIRT and Tmem100 (PIRT2) appear to be an additional mechanism that enhances functional diversity.

Previous studies have shown that the C-terminus of PIRT binds to both TRPV1 and TRPM8, and the PIRT C-terminus also binds to PIP_2, a known regulator of TRP channel function [4, 14, 23]. In particular, the proximal C-terminus of TRPV1 has been implicated in regulation by PIP_2 [23]. A FRET-based assay using the proximal C-terminal region fused to a cyan fluorescent protein showed a FRET signal when mixed with fluorescently labeled PIP_2, indicating that this region binds PIP_2. Deletion or neutralization of basic residues in this region eliminated TRPV1 capsaicin-activated currents; however, it was unclear whether this was due to disruption of PIP_2 binding or unrelated changes in channel trafficking or function. Cryo-EM structures of TRPV1 provide additional insight; the PIP_2-binding region identified by Gordon and coworkers is found at the end of a juxtamembrane helix following the S6 helix, near a region that is conserved in TRP channels called the TRP box, which protrudes beneath the S1–S4 domain [23, 43]. This supports the notion that the S1–S4 domain might be involved in channel regulation by PIP_2. The proximal C-terminal region of TRPV1 has also been shown to bind to PIP_2; this region is conserved across TRPV and TRPM channel families, and so the mechanism of PIP_2 regulation may also be conserved [4, 23].

Our data show that PIRT binds specifically to the TRPM8 S1–S4 domain. Recently, cryo-EM structures of TRP channels from all subfamilies have become available. A general feature of these structures is that the aforementioned proximal C-terminal putative PIP_2 binding site extends beneath the S1–S4 domain, placing them in close proximity. Also, TRPV family studies recently identified a potentially distinct phosphoinositide binding site where PIP_2 binds residues in the S4 helix and S4–S5 linker

of PIP_2 sensitive TRPV family channels [44, 45]. Taken together, these results suggest a possible regulatory mechanism in which PIRT and PIP_2 interact and exert their modulatory effects near the VSLD. Our data also suggest possible differences in channel activation mechanisms between cold, menthol, and voltage stimulation. Under cold stimulation, hPIRT expression resulted in attenuated current response even at physiological negative voltages (Fig. 3.1C), whereas menthol and room temperature currents were only affected at positive voltages (Fig. 3.1, A and B).

The transmembrane domain of TRP channels is an important functional nexus. For example, recent studies have elucidated that TRPM8-mediated thermosensitivity species differences in hibernating rodents can be recapitulated by swapping only six residues within the TRPM8-TMD, similar to the number of divergent residues between mouse and human TRPM8 in our experiments [24]. Previous studies have shown that species differences between a small number of residues in the transmembrane core give rise to capsaicin sensitivity in TRPV1 and icilin sensitivity in TRPM8 [19, 25]. Additionally, the transmembrane domain of TRPA1 is sufficient to recapitulate temperature and agonist response of this channel [46, 47]. Given the importance of the transmembrane core in TRP channel function, we focused our search on this region. Human and mouse TRPM8 have few sequence differences, but electrophysiology measurements from chimeric channels demonstrate that these few differences have significant functional consequences. Swapping the eleven human mutations in the transmembrane core produced a channel that recapitulated the human phenotype of TRPM8 attenuation by hPIRT, indicating key functional determinants are found in these

residues. Narrowing the chimeric region to the S1–S4 domain resulted in somewhat attenuated currents, whereas the pore domain chimera had significantly attenuated currents. Considering these results together with our data showing that PIRT binds the TRPM8 S1–S4 domain, it is possible that this domain is important for binding while most of the functional effect is produced in the pore domain. Besides interactions with hPIRT, swapping the three disparate residues found in the pore loop and TRP helix of hTRPM8 into mTRPM8 produced a channel that exhibited significantly increased overall current magnitudes compared to the TMD and S1–S4 chimeras. The region these residues are found in is unresolved in the Ficedula albicollis TRPM8 cryo-EM structure, but it is clear they are in the pore loop following the pore helix [27]. In structures of TRPM4, where equivalent post pore helix residues are resolved, these residues are outside of the selectivity filter, so they likely do not directly determine channel conductance [48-50].It is noteworthy that this increase in conductance is not seen in the $mTRPM8_{hTMD}$ chimera, which also includes the pore loop and TRP helix changes. This is possibly a consequence of the spatial arrangement of these residues, as the TRP helix extends beneath the S1–S4 domain and plays a key role in channel gating regulation [27].

Species divergence has been well documented in other TRP channels [18-20, 51, 52]. In particular, TRPM8 orthologs have significant differences in temperature sensitivity as a result of species-specific evolutionary pressure from environmental factors and thermoregulation [20, 24, 53]. Given this speciation it seems likely that a modulatory protein like PIRT would also be under evolutionary pressure to fine tune a given TRP channel for a particular environmental niche. As PIRT is expressed

exclusively in the peripheral nervous system [14], its physiological interaction with TRPM8 may be limited to modulating thermosensation, and the differences between modulation of human and mouse TRPM8 by PIRT could reflect the different thermosensation requirements of the two species.

TRP channels, including TPRM8 are functionally diverse both within an organism and across species. Small modulatory proteins such as PIRT may provide a partial explanation for how a single TRP channel is physiologically repurposed for a variety of cellular needs.

3.5 Experimental Procedures

3.5.1 Cell Culture

Human embryonic kidney (HEK) 293 cells (ATCC CRL-1573) were authenticated by polymorphic genetic marker testing (DNA Diagnostics Center Medical). Cells were cultured in growth medium consisting of 90% Dulbecco's modified Eagle's medium, 10% fetal bovine serum, 100 $U \cdot mL^{-1}$ penicillin-streptomycin, and 2 mM L-glutamine (Gibco). Cells were cultured in 35 mm polystyrene dishes (Falcon) experiments at 37 °C in the presence of 5% CO_2. Cells were transiently co-transfected with human or mouse gene orthologs of pIRES2-TRPM8-EGFP and either ortholog of pIRES2-PIRT-DsRed or, as a negative control, the empty pIRES2-DsRed plasmid. These constructs express bicistronic mRNA with an internal ribosome entry site (IRES) positioned between the gene of interest (TRPM8 or PIRT) and the fluorescent protein reporter gene (EGFP or DsRed) such that the reporter is not covalently fused to the protein of interest. Transient transfection was achieved using Fugene 6 transfection

reagent (Promega) and 0.5 μg of each plasmid in a 35 mm dish (Falcon) at a ratio of 3 μL transfection reagent per μg of plasmid. HEK-293 cells were authenticated by polymorphic genetic marker testing (DNA Diagnostics Center Medical).

3.5.2 Electrophysiology Measurements

Forty-eight hours after transfection, cells were released from culture dishes by brief exposure to 0.25% trypsin/EDTA and resuspension in supplemented DMEM; cells were then plated on glass coverslips and allowed to recover for 1–2 h at 37 °C in 5% CO_2. Cells that exhibited yellow (green and red markers) fluorescence, indicating successful co-transfection of both plasmids, were selected for electrophysiology measurements. Whole-cell voltage-clamp current measurements were performed using an Axopatch 200B amplifier (Axon Instruments) and pClamp 10.3 software (Axon Instruments). Data was acquired at 2 kHz and filtered at 1 kHz. Patch pipettes were pulled using a P-2000 laser puller (Sutter Instruments) from borosilicate glass capillaries (World Precision Instruments) and heat-polished using a MF-830 microforge (Narishige). Pipettes had resistances of 2–5 MΩ in the extracellular solution. A reference electrode was placed in a 2% agar bridge made with a composition similar to the extracellular solution. Experiments were performed at 23 ± 1 °C unless otherwise noted. Cells were placed in a chamber with extracellular solution containing (in mM) NaCl 132, KCl 4.8, $MgCl_2$ 1.2, $CaCl_2$ 2, HEPES 10, and glucose 5, with the pH adjusted to 7.4 using NaOH and the osmolality adjusted to 310 mOsm using sucrose. Pipettes were filled with a solution containing (in mM) K^+ gluconate 135, KCl 5, $MgCl_2$ 1, EGTA 5, and HEPES 10; pH was adjusted to 7.2 with KOH, and osmolality was adjusted to 300 mOsm using

sucrose. Chemicals were obtained from Sigma-Aldrich. Osmolality was measured using a Vapro 5600 vapor pressure osmometer (Wescor). At least 15 cells were recorded for each condition. Unpaired two-tailed Student's t-tests were performed to determine statistical significance, and differences were considered significant at $p < 0.05$ as indicated by a single asterisk (*). A double or triple asterisk indicates $p < 0.01$ or $p < 0.001$, respectively.

For temperature controlled experiments, extracellular solution was cooled using a Peltier-based perfusion system (ALA Scientific). For menthol perfusion experiments, a menthol stock solution was prepared by dissolving menthol in ethanol at a concentration of 100 $mg \cdot mL^{-1}$. This stock was then diluted with extracellular solution to 500 μM menthol.

3.5.3 Cell Surface Expression

A C-terminal human influenza hemagglutinin (HA) epitope tagged construct of hTRPM8 was generated. The tag sequence was as follows: YPYDVPDYA. An additional glycine residue was added before the tag sequence to promote structural flexibility. Functionality of the construct was verified by cold and menthol sensitivity in whole-cell patch-clamp experiments where it behaved like wild-type TRPM8 (data not shown). HEK-293 cells were cultured in 100 mm dishes as described above. Three sets of five dishes were transfected with pIRES2-hTRPM8-HA-EGFP/pIRES2-hPIRT-DsRed, pIRES2-hTRPM8-HA-EGFP/pIRES2-DsRed (a positive control), or empty vectors (pIRES2-EGFP/pIRES2-DsRed, a negative control). After ~42 hr, cells were washed twice with cold PBS (pH 7.4) and incubated with agitation in 0.5 $mg \cdot mL^{-1}$ sulfo-NHS-

SS-biotin (Thermo Scientific) in PBS for 30 min at 4 °C. Cells were further washed three times in cold PBS, incubated with quenching solution (100 mM glycine in PBS) for 5 min, and then washed two additional times with cold PBS. Cells were lysed in 600 µL RIPA buffer (150 mM NaCl, 5 mM EDTA, 50 mM Tris, 1% NP-40 substitute **(**4-Nonylphenyl-polyethylene glycol)**,** 0.5% sodium deoxycholate, 0.1% SDS, pH 7.4) and incubated with tumbling at 4 °C for 15 min. Lysate was centrifuged for 10 min at 14,000 ×g at 4 °C. Protein concentration of the lysate was measured by BCA assay (Thermo Fisher), and a normalized volume of lysate was added to 150 µL (75 µL bed volume) NeutrAvidin UltraLink resin (Thermo Scientific). Lysate was tumbled overnight at 4 °C. Supernatant was collected, and resin was washed with RIPA buffer. Surface-expressed biotinylated protein was eluted in 2× SDS-PAGE loading dye and analyzed by SDS-PAGE and western blot.

For hTRPM8 detection, the membrane was probed with a mouse monoclonal anti-HA primary antibody (Thermo catalog #26183, lots #QK218547 and #SA244939) diluted to 1:1000. For loading control, mouse anti-beta-actin primary antibody (Thermo catalog #MA5-15739, lots #QH220961 and #SF253548) was diluted to 1:2000. In both cases, horse anti-mouse IgG secondary antibody (Cell Signaling Technology catalog #7076, lot #32) was diluted to 1:1500. Blots were developed with Clarity ECL blotting substrate (Bio-Rad) according to manufacturer protocol. Blot chemiluminescence was directly imaged using a Nikon D610 DSLR camera and Nikkor 50mm f/1.4G lens and the overall image exposure was adjusted with Adobe Camera Raw, in part after Khoury et al. [54]. Signal intensity was quantified using ImageJ, where the hTRPM8-HA intensity was

normalized to that of the β-actin loading control from the same sample. Blots were imaged using a Nikon D610 DSLR camera and Nikkor 50mm f/1.4G lens and processed using Photoshop [54]. In an effort to minimize experimental bias, the trafficking studies are from three independent sets of experiments that were carried out on independently transfected dishes of cells on different days.

3.5.4 Chimera Generation

Human and mouse TRPM8 sequences were aligned using Clustal Omega. Chimeric regions were swapped with the pIRES2 vector using MEGAWHOP PCR [55]. The initial primer sequences for generating megaprimers are as follows: $mTRPM8_{hTMD}$: forward, GTCTATTCATTATCCCCTTAGTGGGCTGTGGCTTTGTATCATTTAG; reverse, GACAACGAAGGGGAAGGGGATGTTTAGGCGGCTGCAGTACTCCTGCAC; $mTRPM8_{hS1S4}$: forward, GTCTATTCATTATCCCCTTAGTGGGCTGTGGCTTTGTATCATTTAG; reverse, AACGTTCCATAGGTCGGTGAAATAATTCACTCCGTTTACGTACCACTGTCTCACTTC; $mTRPM8_{hPD}$: forward, GGAGATGGATCTTCCGCTCTGTCATCTATGAGCCCTACCTGGCCATGTTC reverse, GACAACGAAGGGGAAGGGGATGTTTAGGCGGCTGCAGTACTCCTGCAC. Megaprimers were generated using PCR and purified using an agarose gel purification kit (Qiagen). Purified chimera plasmid DNA were verified by Sanger sequencing and transfected into HEK293 cells for electrophysiology experiments as described above.

3.5.5 Expression and Purification of hTRPM8 S1–S4 Domain and hKCNQ1-VSD

Overexpression of the hTRPM8 S1–S4 domainwas carried out as previously described and used in PIRT binding studies [29]. Briefly, N-terminal 10×His tagged hTRPM8 S1–S4 domain was expressed and purified using a Ni^{2+}-NTA column. The 10×His tag was removed by cleaving with restriction grade thrombin (Novagen). Following thrombin cleavage, hTRPM8 S1–S4 domain was again flowed over a Ni^{2+}-NTA column to eliminate uncleaved 10×His-hTRPM8 S1–S4 domain.

The voltage sensing domain of the human KCNQ1 potassium channel (hKCNQ1-VSD) was expressed and purified according to a previously published protocol and used as a negative control in PIRT NMR binding studies [56].

3.5.6 Expression and Purification of hPIRT

Recombinant hPIRT was expressed with a 6×Histidine tag on the N-terminus in a pET16b vector and grown in BL21 Star (DE3) Escherichia coli at 25 °C in M9 minimal media with 100 µg/mL ampicillin and enriched with 1 g/L (^{15}N) ammonium chloride. 0.5 mM IPTG was used to induce expression of hPIRT at OD_{600nm} of 0.6, and cells were allowed to express for 20 h.

Cells were harvested by 6000 × g centrifugation at 4 °C. The resulting cell pellets were resuspended in a lysis buffer (75 mM Tris-HCl, 300 mM NaCl, 0.2 mM EDTA, pH 7.7) with 20 mL per gram of cell pellet. Lysozyme (0.2 mg/mL), RNase (0.02 mg/mL), DNase (0.02 mg/mL), 1 mM phyenylmethanesulfonyfluoride (PMSF, Sigma-Aldrich), and 5 mM magnesium acetate were added and the solution and tumbled for 30 min at room temperature. Cells were then lysed by sonication using a Misonix Ultrasonic Liquid

Processor at 4 °C with a 50% duty cycle (5 s on, 5 s delay). Empigen (Sigma-Aldrich) was then added to 3.5% (v/v) and the lysate was allowed to rotate at 4 °C for 30 min. The cellular lysate was then centrifuged for 20 min at 20,000 ×g; the pellet was then discarded and the supernatant was used for PIRT purification. Ni-NTA Superflow resin (QIAGEN; 2 mL of resin/g of cell pellet) was added to the supernatant and allowed to rotate at 4 °C for 30 min. The resin and supernatant mixture was then packed into a chromatography column and washed with 10 column volumes of primary buffer (40 mM HEPES, 300 mM NaCl, 3% v/v Empigen pH 7.5). Ten column volumes of secondary buffer (1.5% Empigen, 30 mM imidazole, 40 mM HEPES, 300 mM NaCl, pH 7.5) was then used to wash nonspecific binding proteins from the resin. This was followed by five column volumes of tertiary buffer (0.2% DPC, 25 mM sodium phosphate, pH 7.2) used to exchange detergents from Empigen to dodecylphosphocholine (DPC, Avanti Polar Lipids). Lastly, the protein was eluted from the resin with an elution buffer (0.5% DPC, 300 mM imidazole, 25 mM sodium phosphate, pH 7.8). All of the buffers used for chromatography contained 2.2 mM beta-mercaptoethanol (Sigma-Aldrich) that was added immediately prior to purification.

Following nickel affinity chromatography, hPIRT was subjected to ion exchange chromatography. The high concentration of imidazole, 300 mM, was decreased to <1 mM by ultrafiltration, using an Amicon Ultra-15 centrifugal filter unit with 10 kDa cutoff. The protein solution was then bound to a 1 mL cation exchange column (GE Healthcare, HiTrap SP FF) using an AKTA Pure FPLC with low salt buffer (0.2% DPC, 50 mM HEPES, 50 mM NaCl, pH 7.5) and eluted with high salt buffer (0.5% DPC, 50

mM HEPES, 1 M NaCl, pH 7.5). After purification steps, total yield of hPIRT was ~2 mg per liter of minimal media. For NMR experiments, the resulting eluent was then buffer exchanged to phosphate buffer (20 mM sodium phosphate, 0.5 mM EDTA, and pH 6.5) using an Amicon Ultra-4 centrifugal filter unit with 10 kDa cutoff to a final volume of 180 µl with a resulting concentration of 0.5 mM protein. The sample plus 4 µl (2% v/v) of D_2O were loaded into a 3 mm NMR tube (Bruker).

3.5.7 hTRPM8 S1–S4 Domain and hPIRT Pull-down Experiment

To test whether hTRPM8 S1–S4 domain and hPIRT directly interact in vitro, hTRPM8 S1–S4 domain and 6×His-hPIRT were expressed in E. coli and purified in 25 mM Na_2HPO_4, pH 7.3 containing approximately 1% DPC (ca. 28 mM which is about nineteen times the CMC). 50 µg each of hTRPM8 S1–S4 domain (after thrombin cleavage and removal of the 10×His tag) and 6×His-hPIRT were mixed with continuous tumbling for 12 h at room temperature. This was followed by incubation with 100 µl of Ni-NTA resin for 2 h at room temperature. After Ni-NTA interaction, unbound protein in the supernatant was separated by centrifugation at 3000 × g for 2 min using a benchtop centrifuge (Thermo Scientific). Protein-bound Ni-NTA resin was washed with 6 mL (60 column volumes) of 25 mM Na_2HPO_4, pH 7.3 buffer containing 0.25% DPC (w/v, ~7 mM) followed by elution of the bound protein using the same buffer containing 500 mM imidazole. The eluted protein fractions were analyzed on 16% tris-glycine SDS-PAGE.

3.5.8 hPIRT-hTRPM8 S1–S4 Domain and KCNQ1-VSD NMR Titration

For ^{15}N-labeled hPIRT, ^{1}H,^{15}N-TROSY-HSQC experiments were acquired at 40 °C on a Bruker 850 MHz (^{1}H) spectrometer with a helium cooled 5 mm TCI cryoprobe

and Avance III HD console. 128 transients, with 2048 points in the direct and 128 points in the indirect dimension, of hPIRT without the hTRPM8 S1–S4 domain were recorded and analyzed as the initial titration point. After the initial titration point was recorded, the sample was removed and TRPM8 S1–S4 domain added to the desired mole ratio and concentrated to 180 µl; iterations of this were done to produce several titration points at mole ratios ranging from 0:1 to 2:1 hTRPM8 S1–S4 domain:hPIRT. As a negative control, the same protocol was performed with the KCNQ1-VSD.

NMR data were processed in NMRPipe and analyzed with CcpNmr Analysis [57, 58]. The change in chemical shifts ($\Delta\delta$) were plotted and compared to reference resonances, where $\Delta\delta = [(\Delta\delta_H)^2 + [0.2(\Delta\delta_N)]^2]^{1/2}$. Dissociation constants were extracted using the nlinfit function in Matlab R2013a and a single binding site model with the equation $f(x) = (x)(B_{max})/(K_d + x)$, where B_{max} is the maximal change in chemical shift observed for a given resonance upon saturation with ligand (hTRPM8 S1–S4 domain), K_d is the dissociation constant, *x* is the hTRPM8 S1–S4 domain:hPIRT ratio, and *f*(*x*) is correlated to the absolute value of the change in chemical shift ($\Delta\delta$).

3.6 References

1. McKemy, D. D., Neuhausser, W. M., and Julius, D. (2002) Identification of a cold receptor reveals a general role for TRP channels in thermosensation. *Nature* **416**, 52-58

2. Peier, A. M., Moqrich, A., Hergarden, A. C., Reeve, A. J., Andersson, D. A., Story, G. M., Earley, T. J., Dragoni, I., McIntyre, P., Bevan, S., and Patapoutian, A. (2002) A TRP Channel that Senses Cold Stimuli and Menthol. *Cell* **108**, 705-715

3. Andersson, D. A., Chase, H. W., and Bevan, S. (2004) TRPM8 activation by menthol, icilin, and cold is differentially modulated by intracellular pH. *J. Neurosci.* **24**, 5364-5369

4. Rohacs, T. (2014) Phosphoinositide Regulation of TRP Channels. *Handb. Exp. Pharmacol.* **223**, 1143-1176

5. Knowlton, W. M., Daniels, R. L., Palkar, R., McCoy, D. D., and McKemy, D. D. (2011) Pharmacological blockade of TRPM8 ion channels alters cold and cold pain responses in mice. *PLoS One* **6**, e25894

6. Almeida, M. C., Hew-Butler, T., Soriano, R. N., Rao, S., Wang, W., Wang, J., Tamayo, N., Oliveira, D. L., Nucci, T. B., Aryal, P., Garami, A., Bautista, D., Gavva, N. R., and Romanovsky, A. A. (2012) Pharmacological blockade of the cold receptor TRPM8 attenuates autonomic and behavioral cold defenses and decreases deep body temperature. *J. Neurosci.* **32**, 2086-2099

7. Ding, Z., Gomez, T., Werkheiser, J. L., Cowan, A., and Rawls, S. M. (2008) Icilin induces a hyperthermia in rats that is dependent on nitric oxide production and NMDA receptor activation. *European Journal of Pharmacology* **578**, 201-208

8. Gavva, N. R., Davis, C., Lehto, S. G., Rao, S., Wang, W., and Zhu, D. X. D. (2012) Transient receptor potential melastatin 8 (TRPM8) channels are involved in body temperature regulation. *Mol. Pain* **8**, 36

9. Ma, S., Yu, H., Zhao, Z., Luo, Z., Chen, J., Ni, Y., Jin, R., Ma, L., Wang, P., Zhu, Z., Li, L., Zhong, J., Liu, D., Nilius, B., and Zhu, Z. (2012) Activation of the cold-sensing TRPM8 channel triggers UCP1-dependent thermogenesis and prevents obesity. *J. Mol. Cell Biol.* **4**, 88-96

10. Sun, J., Yang, T., Wang, P., Ma, S., Zhu, Z., Pu, Y., Li, L., Zhao, Y., Xiong, S., Liu, D., and Zhu, Z. (2014) Activation of cold-sensing transient receptor potential melastatin subtype 8 antagonizes vasoconstriction and hypertension through attenuating RhoA/Rho kinase pathway. *Hypertension* **63**, 1354-1363

11. Quallo, T., Vastani, N., Horridge, E., Gentry, C., Parra, A., Moss, S., Viana, F., Belmonte, C., Andersson, D. A., and Bevan, S. (2015) TRPM8 is a neuronal osmosensor that regulates eye blinking in mice. *Nat. Commun.* **6**, 7150

12. Tang, Z., Kim, A., Masuch, T., Park, K., Weng, H., Wetzel, C., and Dong, X. (2013) Pirt functions as an endogenous regulator of TRPM8. *Nat. Commun.* **4**, 2179

13. Tang, M., Wu, G. Y., Dong, X. Z., and Tang, Z. X. (2016) Phosphoinositide interacting regulator of TRP (Pirt) enhances TRPM8 channel activity in vitro via increasing channel conductance. *Acta Pharmacol. Sin.* **37**, 98-104

14. Kim, A. Y., Tang, Z., Liu, Q., Patel, K. N., Maag, D., Geng, Y., and Dong, X. (2008) Pirt, a phosphoinositide-binding protein, functions as a regulatory subunit of TRPV1. *Cell* **133**, 475-485

15. Wang, C., Wang, Z., Yang, Y., Zhu, C., Wu, G., Yu, G., Jian, T., Yang, N., Shi, H., Tang, M., He, Q., Lan, L., Liu, Q., Guan, Y., Dong, X., Duan, J., and Tang, Z. (2015) Pirt contributes to uterine contraction-induced pain in mice. *Mol. Pain* **11**, 57

16. Gao, X. F., Feng, J. F., Wang, W., Xiang, Z. H., Liu, X. J., Zhu, C., Tang, Z. X., Dong, X. Z., and He, C. (2015) Pirt reduces bladder overactivity by inhibiting purinergic receptor P2X3. *Nat. Commun.* **6**, 7650

17. Patel, K. N., Liu, Q., Meeker, S., Undem, B. J., and Dong, X. (2011) Pirt, a TRPV1 modulator, is required for histamine-dependent and -independent itch. *PLoS One* **6**, e20559

18. Hilton, J. K., Rath, P., Helsell, C. V., Beckstein, O., and Van Horn, W. D. (2015) Understanding thermosensitive transient receptor potential channels as versatile polymodal cellular sensors. *Biochemistry* **54**, 2401-2413

19. Jordt, S.-E., and Julius, D. (2002) Molecular Basis for Species-Specific Sensitivity to "Hot" Chili Peppers. *Cell* **108**, 421-430

20. Myers, B. R., Sigal, Y. M., and Julius, D. (2009) Evolution of Thermal Response Properties in a Cold-Activated TRP Channel. *PLoS One* **4**, e5741

21. Janssens, A., and Voets, T. (2011) Ligand stoichiometry of the cold- and menthol-activated channel TRPM8. *J. Physiol.* **589**, 4827-4835

22. Gkika, D., Lemonnier, L., Shapovalov, G., Gordiencko, D., Poux, C., Bernardini, M., Bokhobza, A., Bidaux, G., Degerny, C., Verreman, K., Guarmit, B., Benahmed, M., de Launoit, Y., Bindels, R. J. M., Pla, A. F., and Prevarskaya, N. (2015) TRP channel-associated factors are a novel protein family that regulates TRPM8 trafficking and activity. *J. Cell Biol.* **208**, 89-107

23. Ufret-Vincenty, C. A., Klein, R. M., Hua, L., Angueyra, J., and Gordon, S. E. (2011) Localization of the PIP2 sensor of TRPV1 ion channels. *J. Biol. Chem.* **286**, 9688-9698

24. Matos-Cruz, V., Schneider, E. R., Mastrotto, M., Merriman, D. K., Bagriantsev, S. N., and Gracheva, E. O. (2017) Molecular Prerequisites for Diminished Cold Sensitivity in Ground Squirrels and Hamsters. *Cell reports* **21**, 3329-3337

25. Chuang, H. H., Neuhausser, W. M., and Julius, D. (2004) The super-cooling agent icilin reveals a mechanism of coincidence detection by a temperature-sensitive TRP channel. *Neuron* **43**, 859-869

26. Kroncke, B. M., Van Horn, W. D., Smith, J., Kang, C., Welch, R. C., Song, Y., Nannemann, D. P., Taylor, K. C., Sisco, N. J., George, A. L., Jr., Meiler, J.,

Vanoye, C. G., and Sanders, C. R. (2016) Structural basis for KCNE3 modulation of potassium recycling in epithelia. *Sci. Adv.* **2**, e1501228

27. Yin, Y., Wu, M., Zubcevic, L., Borschel, W. F., Lander, G. C., and Lee, S. Y. (2018) Structure of the cold- and menthol-sensing ion channel TRPM8. *Science* **359**, 237-241

28. Jensen, M. Ø., Jogini, V., Borhani, D. W., Leffler, A. E., Dror, R. O., and Shaw, D. E. (2012) Mechanism of Voltage Gating in Potassium Channels. *Science* **336**, 229-233

29. Rath, P., Hilton, J. K., Sisco, N. J., and Van Horn, W. D. (2016) Implications of Human Transient Receptor Potential Melastatin 8 (TRPM8) Channel Gating from Menthol Binding Studies of the Sensing Domain. *Biochemistry* **55**, 114-124

30. Yang, F., Xiao, X., Cheng, W., Yang, W., Yu, P., Song, Z., Yarov-Yarovoy, V., and Zheng, J. (2015) Structural mechanism underlying capsaicin binding and activation of the TRPV1 ion channel. *Nat. Chem. Biol.* **11**, 518-524

31. Zhou, J., Tang, Y., Zheng, Q., Li, M., Yuan, T., Chen, L., Huang, Z., and Wang, K. (2015) Different KChIPs Compete for Heteromultimeric Assembly with Pore-Forming Kv4 Subunits. *Biophys. J.* **108**, 2658-2669

32. Weng, H. J., Patel, K. N., Jeske, N. A., Bierbower, S. M., Zou, W., Tiwari, V., Zheng, Q., Tang, Z., Mo, G. C., Wang, Y., Geng, Y., Zhang, J., Guan, Y., Akopian, A. N., and Dong, X. (2015) Tmem100 Is a Regulator of TRPA1-TRPV1 Complex and Contributes to Persistent Pain. *Neuron* **85**, 833-846

33. Guo, W., Sui, Q. Q., Gao, X. F., Feng, J. F., Zhu, J., He, C., Knight, G. E., Burnstock, G., and Xiang, Z. (2016) Co-localization of Pirt protein and P2X2 receptors in the mouse enteric nervous system. *Purinergic Signalling*

34. Sun, X., Zaydman, M. A., and Cui, J. (2012) Regulation of Voltage-Activated K(+) Channel Gating by Transmembrane beta Subunits. *Front. Pharmacol.* **3**, 63

35. McCrossan, Z. A., and Abbott, G. W. (2004) The MinK-related peptides. *Neuropharmacology* **47**, 787-821

36. Barhanin, J., Lesage, F., Guillemare, E., Fink, M., Lazdunski, M., and Romey, G. (1996) K_VLQT1 and IsK (minK) proteins associate to form the I_{Ks} cardiac potassium current. *Nature* **384**, 78-80

37. Grunnet, M., Jespersen, T., Rasmussen, H. B., Ljungstrøm, T., Jorgensen, N. K., Olesen, S.-P., and Klaerke, D. A. (2002) KCNE4 is an inhibitory subunit to the KCNQ1 channel. *J. Physiol.* **542**, 119-130

38. Manderfield, L. J., and George, A. L., Jr. (2008) KCNE4 can co-associate with the I_{Ks} (KCNQ1-KCNE1) channel complex. *FEBS J.* **275**, 1336-1349

39. Abbott, G. W., and Goldstein, S. A. N. (2002) Disease-associated mutations in KCNE potassium channel subunits (MiRPs) reveal promiscuous disruption of multiple currents and conservation of mechanism. *FASEB journal : official publication of the Federation of American Societies for Experimental Biology* **16**, 390-400

40. Ramanathan, K., Michael, T. H., Jiang, G.-J., Hiel, H., and Fuchs, P. A. (1999) A Molecular Mechanism for Electrical Tuning of Cochlear Hair Cells. *Science* **283**, 215-217

41. Bai, J. P., Surguchev, A., and Navaratnam, D. (2011) beta4-subunit increases Slo responsiveness to physiological Ca2+ concentrations and together with beta1 reduces surface expression of Slo in hair cells. *Am. J. Physiol. Cell Physiol.* **300**, C435-446

42. Martinez-Espinosa, P. L., Yang, C., Gonzalez-Perez, V., Xia, X. M., and Lingle, C. J. (2014) Knockout of the BK beta2 subunit abolishes inactivation of BK currents in mouse adrenal chromaffin cells and results in slow-wave burst activity. *J. Gen. Physiol.* **144**, 275-295

43. Liao, M., Cao, E., Julius, D., and Cheng, Y. (2013) Structure of the TRPV1 ion channel determined by electron cryo-microscopy. *Nature* **504**, 107-112

44. Gao, Y., Cao, E., Julius, D., and Cheng, Y. (2016) TRPV1 structures in nanodiscs reveal mechanisms of ligand and lipid action. *Nature* **534**, 347-351

45. Velisetty, P., Borbiro, I., Kasimova, M. A., Liu, L., Badheka, D., Carnevale, V., and Rohacs, T. (2016) A molecular determinant of phosphoinositide affinity in mammalian TRPV channels. *Scientific reports* **6**, 27652

46. Survery, S., Moparthi, L., Kjellbom, P., Hogestatt, E. D., Zygmunt, P. M., and Johanson, U. (2016) The N-terminal Ankyrin Repeat Domain Is Not Required for Electrophile and Heat Activation of the Purified Mosquito TRPA1 Receptor. *J. Biol. Chem.* **291**, 26899-26912

47. Moparthi, L., Survery, S., Kreir, M., Simonsen, C., Kjellbom, P., Hogestatt, E. D., Johanson, U., and Zygmunt, P. M. (2014) Human TRPA1 is intrinsically cold- and chemosensitive with and without its N-terminal ankyrin repeat domain. *Proc. Natl. Acad. Sci. U. S. A.* **111**, 16901-16906

48. Winkler, P. A., Huang, Y., Sun, W., Du, J., and Lu, W. (2017) Electron cryo-microscopy structure of a human TRPM4 channel. *Nature* **552**, 200-204

49. Duan, J., Li, Z., Li, J., Santa-Cruz, A., Sanchez-Martinez, S., Zhang, J., and Clapham, D. E. (2018) Structure of full-length human TRPM4. *Proc. Natl. Acad. Sci. U. S. A.* **115**, 2377-2382

50. Autzen, H. E., Myasnikov, A. G., Campbell, M. G., Asarnow, D., Julius, D., and Cheng, Y. (2018) Structure of the human TRPM4 ion channel in a lipid nanodisc. *Science* **359**, 228-232

51. Saito, S., Fukuta, N., Shingai, R., and Tominaga, M. (2011) Evolution of vertebrate transient receptor potential vanilloid 3 channels: opposite temperature sensitivity between mammals and western clawed frogs. *PLoS Genet.* **7**, e1002041

52. Chen, J., Kang, D., Xu, J., Lake, M., Hogan, J. O., Sun, C., Walter, K., Yao, B., and Kim, D. (2013) Species differences and molecular determinant of TRPA1 cold sensitivity. *Nat. Commun.* **4**, 2501

53. Gracheva, E. O., and Bagriantsev, S. N. (2015) Evolutionary adaptation to thermosensation. *Curr. Opin. Neurobiol.* **34**, 67-73

54. Khoury, M. K., Parker, I., and Aswad, D. W. (2010) Acquisition of chemiluminescent signals from immunoblots with a digital single-lens reflex camera. *Anal. Biochem.* **397**, 129-131

55. Miyazaki, K. (2011) MEGAWHOP Cloning: A Method of Creating Random Mutagenesis Libraries via Megaprimer PCR of Whole Plasmids. *Methods in Enzymology* **498**, 399-406

56. Peng, D., Kim, J. H., Kroncke, B. M., Law, C. L., Xia, Y., Droege, K. D., Van Horn, W. D., Vanoye, C. G., and Sanders, C. R. (2014) Purification and structural study of the voltage-sensor domain of the human KCNQ1 potassium ion channel. *Biochemistry* **53**, 2032-2042

57. Delaglio, F., Grzesiek, S., Vuister, G. W., Zhu, G., Pfeifer, J., and Bax, A. (1995) NMRPipe - A Multidimensional Spectral Processing System Based on UNIX Pipes. *Journal of biomolecular NMR* **6**, 277-293

58. Vranken, W. F., Boucher, W., Stevens, T. J., Fogh, R. H., Pajon, A., Llinas, P., Ulrich, E. L., Markley, J. L., Ionides, J., and Laue, E. D. (2005) The CCPN data model for NMR spectroscopy: Development of a software pipeline. *Proteins: Struct., Funct., Bioinf.* **59**, 687-696

CHAPTER 4

A MUTATION IN THE S4-S5 LINKER OF TRPM8 SELECTIVELY ABOLISHES ICILIN SENSITIVITY

4.1 Introduction

TRPM8 is activated by an array of small molecule ligands. Such "cooling compounds" are familiar to anyone who has tried a breath mint or applied a cooling gel to an injury. These compounds, such as menthol, activate TRPM8-expressing neurons, mimicking the sensation of cool temperatures. Besides menthol, other known TRPM8 agonists include menthol derivatives such as menthyl lactate and WS-12, as well as the "super-cooling" agent icilin. Icilin is structurally unrelated to menthol and its activation of TRPM8 has distinct properties. It requires Ca^{2+} as a cofactor, and TRPM8 response to icilin is pH dependent; extracellular pH values below ~6.2 completely inhibit the icilin response, whereas menthol response is unaffected [1, 2].

Identifying the binding sites and unraveling the mechanisms of TRPM8 agonists has long been a challenge to the field. Early studies using random mutagenesis identified residues that seemed to be crucial to menthol activation. Functional experiments showed that the mutations Y745H in S1 and Y1005F in the TRP helix reduced or eliminated menthol sensitivity while the channel remained cold sensitive, suggesting that these residues are key to menthol sensitivity [3]. However, chimeric channels in which short (2-5 amino acids) sequences in this region from TRPM2, the menthol-insensitive nearest relative of TRPM8, were exchanged into TRPM8 did not show a specific effect on menthol sensitivity. This suggests that other residues or structural elements are important.

In another study, mutating the charged R842 residue in the S4 helix to a neutral amino acid significantly decreased menthol affinity for the channel. Radioligand displacement studies with ^{3}H-menthol showed that both the Y745H and the R842A mutants had decreased affinity for the ligand [4].

Residues important for icilin activation of the channel have also been identified. Using comparative functional studies between chicken TRPM8, which is insensitive to icilin, and icilin-sensitive rat TRPM8, Chuang et al. found that a single residue in position 805 accounts for the difference [2]. This residue is a glycine in mammalian TRPM8 channels, but alanine in avian orthologs. The A805G mutation in chicken TRPM8 conferred robust icilin sensitivity on the channel; whereas the converse mutation in rat TRPM8 abolished the icilin response. Two other residues, N799 and D802 at the bottom of the S3 helix, were also found to be critical to icilin activation. Recent TRPM structures make it clear that these two residues are part of a Ca^{2+}-binding site that also includes E782 and Q785 at the bottom of S2 that are conserved in TRPM2, TRPM4, TRPM5, and TRPM8 [5-7].

Recently determined cryo-EM structures of TRPM8 bound to WS-12 or icilin are consistent with these results [8]. The ligands are bound inside the S1–S4 helical bundle; WS-12 is within interacting distance of the Y745, Y1005, and R842 residues mentioned above that are involved in menthol sensitivity. The structures also shed light on icilin interactions with the channel. The calcium binding site formed by E782, Q785, N799, and D802 is confirmed in these structures. While icilin does not directly interact with calcium, binding of calcium appears to induce a conformational change to accommodate

icilin binding. Additionally, icilin binding is accompanied by a transition from α-helical to 3_{10}-helical structure at the bottom of the S4 helix, causing the side chains of H844 and R842 to rotate toward the center of the S2–S4 domain within interacting distance of the ligand. This interaction with H844 likely explains the pH dependence of TRPM8 sensitivity to icilin.

These results are beginning to clarify the binding sites and mechanisms of TRPM8 agonists, but other studies complicate the picture. In a later study that used nuclear magnetic resonance spectroscopy to directly measure menthol binding to the isolated S1-S4 domain of TRPM8, binding affinity was not affected in either the Y745H or the R842H mutants [9]. Recently determined cryo-EM structures of TRPM2, TRPM4, TRPM7, and TRPM8 confirm that the Y745 and R842 residues are structurally conserved in the TRPM subfamily, yet TRPM8 is the only TRPM channel sensitive to these cooling compounds. Furthermore, an isoform of TRPM8 identified in the endoplasmic reticulum of keratinocytes is completely missing the S1 and S2 helices, including Y745 in S1, yet this truncated isoform retains sensitivity to cold and to cooling compounds including menthol, icilin, and WS-12 [10]. Therefore, other structural or allosteric mechanisms are likely involved in activation of TRPM8 by cooling agents.

In contrast to the murky understanding of TRPM8 ligand activation, TRPV1 activation by vanilloid ligands has been studied more extensively and the mechanism is much clearer. Cryo-EM structures show that vanilloid ligands, including the agonists capsaicin and resiniferatoxin, and the antagonist capsazepine, bind in a hydrophobic pocket between the S1–S4 domain and the S5/S6 pore helices [11, 12]. Computational

studies support this notion and give detailed insight into the mechanism of activation upon capsaicin binding [13, 14]. The ligand binds with the vanillyl head pointing down into the pocket between S3, S4, and the S4-S5 linker, while the aliphatic tail extends upward and samples nonspecific van der Waals interactions with the residues lining the pocket. The oxygen atom in the amide neck forms a specific hydrogen bond interaction with T551 of S4, while the head interacts with S513 at the base of S3 and forms a hydrogen bond with E571 in the S4-S5 linker. This pulls the linker toward the bound capsaicin molecule, dragging S6 along with it and opening the lower gate of the channel [13]. This initiates a conformational wave that eventually propagates to the upper gate in the selectivity filter, opening the channel [14]. Lending credence to these results, the principles elucidated in these studies were used to successfully engineer vanilloid sensitivity into TRPV2 and TRPV3 channels, which are not naturally sensitive to vanilloids [15-17].

TRP channels share highly conserved structural homology in the transmembrane region, including the vanilloid binding region discussed above. Given this homology across TRP channels, the importance of the S4-S5 linker in gating mechanisms of both TRPV1 and voltage-gated channels, and a demonstrated role for this region in TRPM8 menthol sensitivity specifically [4], it is possible that residues within this region are important for ligand binding in TRPM8. To test this hypothesis, in this study several residues in this region of TRPM8 were tested to determine whether they have a role in ligand sensing by the channel.

4.2 Experimental Methods

4.2.1 Cell Culture

HEK-293 cells (ATCC cell line CRL-1573) were cultured in 35 mm dishes at 37 °C in DMEM supplemented with 10% fetal bovine serum, 2 mM L-glutamine, 4.5 $mg \cdot mL^{-1}$ glucose, and 100 $mg \cdot mL^{-1}$ penicillin and streptomycin. Cultures were maintained in the presence of 5% CO_2. All reagents were obtained from Life Technologies. Cells were plated in 35 mm dishes at ~30% confluency one day before transfection. Human TRPM8 was cloned into a pIRES2-EGFP vector, and cells were transiently transfected with 0.5 µg of plasmid in a 3:1 Fugene(µL):DNA(µg) ratio 36-48 h before electrophysiology experiments were performed.

4.2.2 Electrophysiology

Transfected cells were trypsinized with 0.25% trypsin for 60 sec, then replated on glass coverslips 1–2 hours prior to electrophysiology measurements. Successfully transfected cells were identified with EGFP epifluorescence. Coverslips were placed in extracellular solution consisting of (in mM) NaCl 132, KCl 4.8, $MgCl_2$ 1.2, $CaCl_2$ 2, HEPES 10, and glucose 5; pH was adjusted to 7.4 with NaOH and osmolality was adjusted to 310 mOsm with sucrose. Borosilicate glass pipettes were pulled using a laser puller (Sutter Instruments P-2000) and were filled with intracellular solution comprising (in mM) K^+ gluconate 135, KCl 5, $MgCl_2$ 1, EGTA 5, and HEPES 10, with pH adjusted to 7.2 using KOH, and osmolality adjusted to 300 mOsmol using sucrose. Osmolality of the solutions was measured with a Vapro 5600 vapor pressure osmometer (Wescor). Pipettes had resistances of 2–5 MΩ when placed in extracellular solution, with a

reference electrode placed in 2% agar salt bridge made from extracellular solution without glucose. Whole-cell patch-clamp experiments were performed using an Axopatch 200B amplifier and pClamp 10.3 software (Molecular Devices). Data was acquired at 2 kHz, filtered at 1 kHz, and digitized with a Digidata 1440a digitizer (Molecular Devices).

For ligand experiments, (1R,2S,5R)-(−)-menthol (Sigma) and icilin (Cayman Chemical) were dissolved in stock solutions of DMSO at 650 mM,and 100 mM respectively, then diluted to the given concentrations in extracellular solution. For icilin experiments, intracellular solution was made without EGTA and with addition of 50 μM $CaCl_2$. Temperature was controlled by perfusing pre-cooled extracellular solution through an HCPC perfusion cube (ALA Scientific).

4.2.3 Expression Testing of the Human TRPM8 S1–S4 Domain

The S1–S4 domain of human TRPM8 (residues P716–P855) was cloned into a pET16b vector with the following 10xHis tag and thrombin cleavage site sequence preceding the N-terminal end: MGHHHHHHHHHHGLVPRGS. The plasmid was transformed into seven different *E. coli* cell lines for expression testing: BL21(DE3), BL21(DE3) Star, C41(DE3), Rosetta 2(DE3), C43(DE3) Rosetta2, BL21(DE3) CodonPlus RP, and BL21(DE3) LOBSTR. Transformed cells were tested for expression at 37 °C, 25 °C, and 18 °C, and with inducing IPTG concentrations of 0.3, 0.5, and 1 M.

For 37 °C expression testing, 5 mL starter cultures of LB with appropriate antibiotic added were inoculated with a single colony from each of the transformed lines. Cultures were grown overnight for ~17 h with 250 rpm shaking. The next morning, 100 mL cultures of M9 minimal media in 250 mL volume baffled flasks were inoculated with

all 5 mL of starter culture and grown at 37 °C with 250 rpm. M9 media consisted of 12.8 g $Na_2HPO_4 \cdot 7H_2O$, 3 g KH_2PO_4, 0.5 g NaCl, and 1 g NH_4Cl per liter of media. The pH was adjusted to 7.0 with 6 M HCl, media was autoclaved and cooled, then supplemented to a final concentration of 0.4% glucose, 2 mM $Mg(SO_4)_2$, 0.1 mM $CaCl_2$, 1x MEM Vitamins Mix, and 5 µM metals mix ($FeCl_3$, $CuSO_4$, $MnSO_4$, and $ZnSO_4$). OD_{600} was checked every ~30min until it reached ~0.8. Three 5 mL aliquots were taken from the 100 mL cultures of each cell line, and IPTG was added to 0.3, 0.5, or 1 mM final concentration so that each cell line had one of each concentration. As a negative control, 1 mL of pre-induced culture was taken and centrifuged to pellet the cells, then supernatant was discarded and the pellet was stored at -80 °C. Cultures were allowed to express for 4 h, then the final OD_{600} was measured 0.5 mL of each culture was pelleted and stored at -80 °C.

For 25 °C expression testing, 5 mL LB starter cultures with antibiotic added were inoculated with a single colony in the morning and allowed to grow for 7–9 h. Larger 100 mL M9 media cultures were inoculated with 250 µL (for fast growing cell lines BL21(DE3), BL21(DE3) Star, C41(DE3), BL21(DE3) CodonPlus RP, and BL212(DE3) LOBSTER) or with 400 µL (for slow growing cell lines Rosetta 2(DE3), and C43(DE3) Rosetta2) of starter culture and grown overnight at 37 °C with 225 rpm shaking for ~14 h. When OD_{600} reached ~0.8, cultures were induced with IPTG as described above and allowed to express for 24 h before harvesting.

For 18 °C expression testing, cultures were prepared the as described for 25 °C above, except the 100 mL M9 cultures were inoculated with 1.5 mL starter culture for

fast-growing lines and 2 mL for slow-growing lines. Cultures were grown at 18 °C with 225 rpm shaking for ~14 h, and induced for 48 h and harvested as described above.

For quantification by Western blot, pellets were resuspended in lysis buffer (50 mM Na_2HPO_4 300 mM NaCl, 0.5% DM, 2/0.2/0.2 mg/mL lysozyme/DNase/RNase, 2.5 mM magnesium acetate, pH 7.5) at a ratio of 100 µL per OD_{600} unit at the time of harvest. Samples were incubated at room temperature 5-10 min, then lauroylsarcosine was added from 10% stock to a final concentration of 1%. Samples were incubated another 5-10 min at room temperature, then SDS loading dye was added to 1x. To quantify expression, 50 µL of each sample were run through a nitrocellulose membrane using a dot blot apparatus (Bio-Rad). Protein was detected using a mouse anti-HIS tag primary antibody (Abgent) and anti-mouse IgG HRP-linked secondary antibody (Cell Signaling Technology) with a standard Western blot procedure. The blot was visualized using Clarity Western ECL substrate (Bio-Rad) and imaged with a Nikon D610 DSLR camera and Nikkor 50-mm f/1.4G lens. The image was processed with ImageJ and quantified with the Protein Array Analyzer for ImageJ.

4.2.4 Expression of the S1–S4 Domain

The plasmid was transformed into the BL21 (DE3) Lobstr cell line [18]. The next morning, 5 mL of LB media for each planned liter of culture was inoculated with a single colony and grown for ~8 h at 37 °C and 250 rpm shaking. M9 minimal media was prepared as described above and 0.1 mM ampicillin was added. Each liter was inoculated with 3–4 mL of primary culture, then grown at 18 °C and 250 rpm shaking overnight. Once cultures reached OD_{600} ~0.6 (usually within ~16 h), they were induced with 0.15

mM IPTG and were maintained at 18 °C with 250 rpm shaking for an additional 40–48 h. Cells were harvested by centrifugation at 6000×g for 15 min, resulting in a pellet size of 4–5 g per liter of culture. Pellets were stored at -80 °C until purification.

4.2.5 Purification of the S1–S4 Domain

For NMR samples, 15–20 g of cell pellet were purified. Cells were resuspended in 6.5 mL of lysis buffer (75 mM Tris-HCl, 300 mM NaCl, 0.2 mM EDTA, pH 7.7) per gram of cell pellet. Lysis buffer was then supplemented with 0.15 mg/mL lysozyme, .015 mg/mL DNase, 0.015 mg/mL RNase, 5 mM magnesium acetate, and 1 mM PMSF. Lysate was tumbled for 30 min at room temperature, then sonicated for 7.5 min with 55% amplitude and 5 sec on / 5 sec off duty cycle (Sonicator brand). Empigen was added to 3% concentration, then lysate was tumbled at room temperature for 1 h to extract membrane proteins. Lysate was centrifuged at 18,000×g for 30 min at 4 °C, then supernatant was removed and tumbled with 0.5 mL pre-equilibrated Ni-NTA resin (Qiagen) per 50 mL lysate for ~2 h at 4 °C. Resin was transferred to a column and washed with 25 column volumes of Buffer A (40 mM HEPES, 300 mM NaCl, pH 7.5) with 1% Empigen, then with 25 column volumes of Buffer A with 1% Empigen and 50 mM imidazole. Detergent was exchanged by washing with 20 CV of Buffer B (25 mM Na_2HPO_4, pH 7.8) with 0.05% LPPG (Anatrace). Finally, protein was eluted in 10 mL Buffer B with 0.05% LPPG and 500 mM imidazole.

Eluted protein was exchanged to thrombin cleavage buffer (20 mM Tris, 100 mM NaCl, pH 8.0) using a 10 kDa cutoff Amicon Ultra centrifugal filter (Millipore). Protein was concentrated to ~250 µL, then diluted with 3 mL thrombin cleavage buffer for 4

cycles, until the concentration of imidazole was <0.1 mM. Thrombin buffer was added to a final volume of 1 mL, then 4 U of thrombin was added and the sample was tumbled at room temperature for ~20 h. The sample was then tumbled with Ni-NTA for 30–60 min, flowthrough was collected and the resin was washed with an additional 2 mL of thrombin buffer with 0.05% LPPG added. Flowthrough and wash fractions were combined and concentrated to 0.5 mL with a 10 kDa cutoff centrifugal filter.

The concentrated sample was purified by gel filtration on a 33 cm XK 16 Superdex S200 column (GE Healthcare) pre-equilibrated with NMR buffer (25 mM Na_2HPO_4, 0.5 mM EDTA, pH 6.5, 0.05% LPPG). Protein generally eluted in a peak at 36–42 mL volume. Protein purity was verified with SDS-PAGE and Coomassie staining. Pure fractions were combined and concentrated for further experiments, and protein concentration was determined using a BCA assay. Protein identity was confirmed by trypsin digestion and LC-MS/MS (MS Bioworks), resulting in 12 unique peptides and 31% sequence coverage (44/142 amino acids).

4.2.6 Nuclear Magnetic Resonance Spectroscopy

Protein was expressed and purified as described above, but $^{15}NH_4Cl$ (Cambridge Isotope Laboratories) was used in the M9 buffer to produce ^{15}N-labeled S1–S4 domain. NMR experiments were carried out at 37 °C in a 3 mm NMR tube with 180 µL sample on a Bruker 850 MHz ^{1}H Avance III HD spectrometer with a 5 mm TCI cryoprobe. Protein concentrations were typically 100–200 µM, with LPPG concentrations of ~1.4%. ^{1}H, ^{15}N TROSY-HSQC experiments were performed with varying concentrations of menthol or icilin. Concentrated stocks of ligands were dissolved in DMSO, such that the

final concentration of added DMSO in the NMR sample of the last titration point did not exceed 4%. The data were processed in NMRPipe and analyzed in CcpNmr. The chemical shift perturbation was calculated by the following equation:

$$\Delta\delta = [\Delta\delta_{\mathrm{H}}{}^{2} + 0.2(\Delta\delta_{\mathrm{N}}{}^{2})]^{1/2}$$

in which $\Delta\delta_H$ and $\Delta\delta_N$ are respectively the proton and nitrogen chemical shift position differences between the resonance at the initial titration point and a given ligand concentration. Δδ values were plotted as a function of ligand concentration and fit to the single binding site model:

$$\Delta\delta = (\Delta\delta_{\mathrm{max}})(x)/(K_{\mathrm{d}} + x)$$

where $(\Delta\delta)_{max}$ is maximum chemical shift perturbation, *x* is the mol % of menthol, and Δδ is the absolute value of the change in chemical shift at a given concentration.

4.2.7 Circular Dichroism

Circular Dichroism (CD) samples were prepared in NMR buffer with a final concentration of 0.2 mg/mL S1–S4 domain. Spectra were recorded on a Jasco J-710 spectropolarimeter, and temperature was controlled using a peltier device (Jasco). CD spectra were acquired from 190–250 nm with 100 mDeg sensitivity, data pitch of 0.5 nm, and scanning speed of 50 nm/min. Menthol stock was dissolved in 50% ethanol. Five scans were acquired per condition and signal averaged for each spectrum. Blank spectra were measured in NMR buffer alone or with 10 mol% menthol added. Data was processed using CDtoolX [19].

4.3 Results and discussion

4.3.1 N852A Mutation Causes a General Decrease in TRPM8 Currents

At the time of initial identification of potential ligand-binding residues, a TRPM8 structure had not yet been determined. Therefore, a homology model of human TRPM8 based on the cryo-EM structure of rat TRPV1 was used [20]. Based on their apparent location in the ligand binding pocket of the homologous TRPV1 channel, four residues were identified as likely to be involved in ligand binding and the following point mutations were made: L699H at the bottom of S1, V755H at the bottom of S2, and N852A and G854H at the bottom of S4 near the S4-S5 linker (Figure 4.1A). Later, a cryo-EM structure of TRPM8 from the collared flycatcher bird, *Ficedula albicollis*, was published by Yin et al. [8]. An updated model of human TRPM8 shows that L699 is actually found in a pre-S1 juxtamembrane helical region, V755 is near the top of S1, and N852 and G854 are still near the S4-S5 linker as originally predicted (Figure 4.1B). After heterologous expression of each mutant in HEK-293 cells, whole-cell currents were measured to determine their activity. As shown in Figure 4.2A, three of these mutants (L699H, V755H, and G854A) showed no significant increase in current response compared to untransfected HEK-293 cells. These mutants also showed no sensitivity to 500 μM menthol or application of extracellular solution pre-cooled to 15 °C. Most likely, these three mutations result in nonfunctional channels, either by disrupting trafficking to the plasma membrane or abolishing the ability of the channel to gate. In contrast, the N852A mutation did result in a functional channel that was sensitive to both menthol and cold (Figure 4.2B,C).

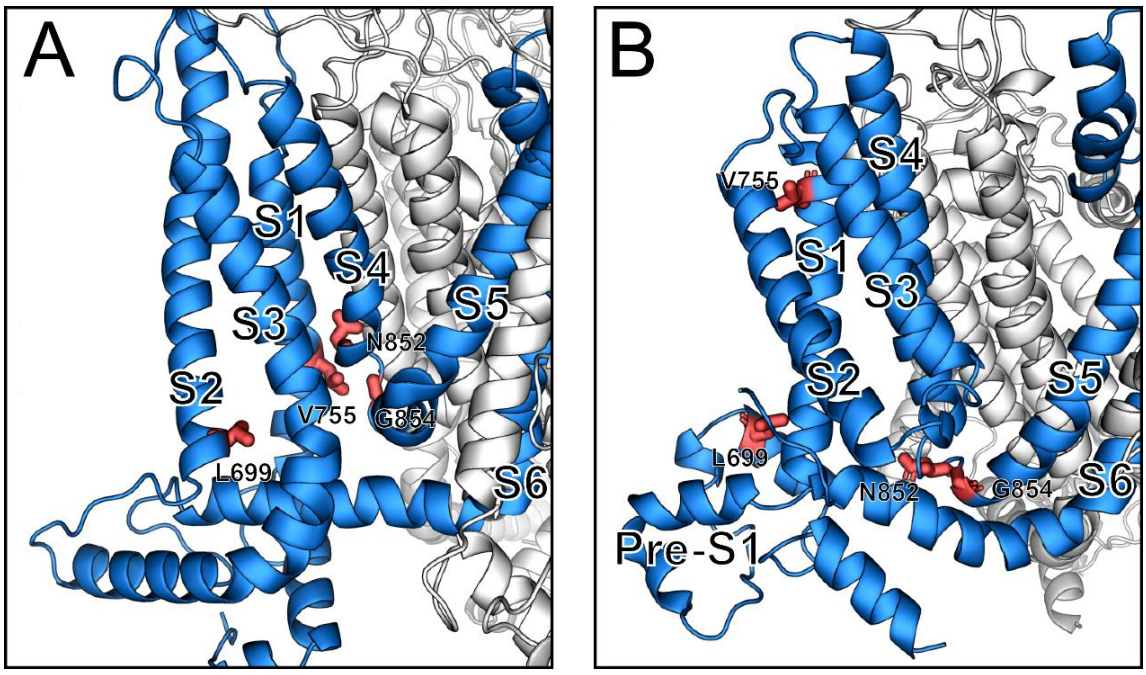

Figure 4.1 Locations of mutated residues. (A) Homology model of human TRPM8 based on a cryo-EM structure of rat TRPV1. Residues were chosen from this model based on vicinity to the known vanilloid TRPV1 binding pocket and are highlighted here in red. (B) Updated homology model of human TRPM8 based on the cryo-EM structure of Ficedula albicollis TRPM8. Based on this model, L699 and V755 are far away from the proposed binding pocket near the S4-S5 linker.

TRPM8-N852A current magnitudes were significantly reduced compared to wild-type TRPM8. Currents evoked by a +100 mV voltage pulse at 23 °C were reduced by a factor of 0.36 ± 0.06 compared to wild-type TRPM8 currents measured at ambient temperature. A decreased response to a similar degree was also observed in both menthol- and cold-evoked currents, which were reduced by factors of 0.52 ± 0.08 and 0.38 ± 0.11 respectively (Figure 4.3A). Comparing the ratios of cold and menthol activation from TRPM8-N852A to the wild-type channel showed that both stimuli activate the mutant to a similar degree as the wild type, with no significant difference between the TRPM8-N852A and wild-type ratios (Figure 4.3B).

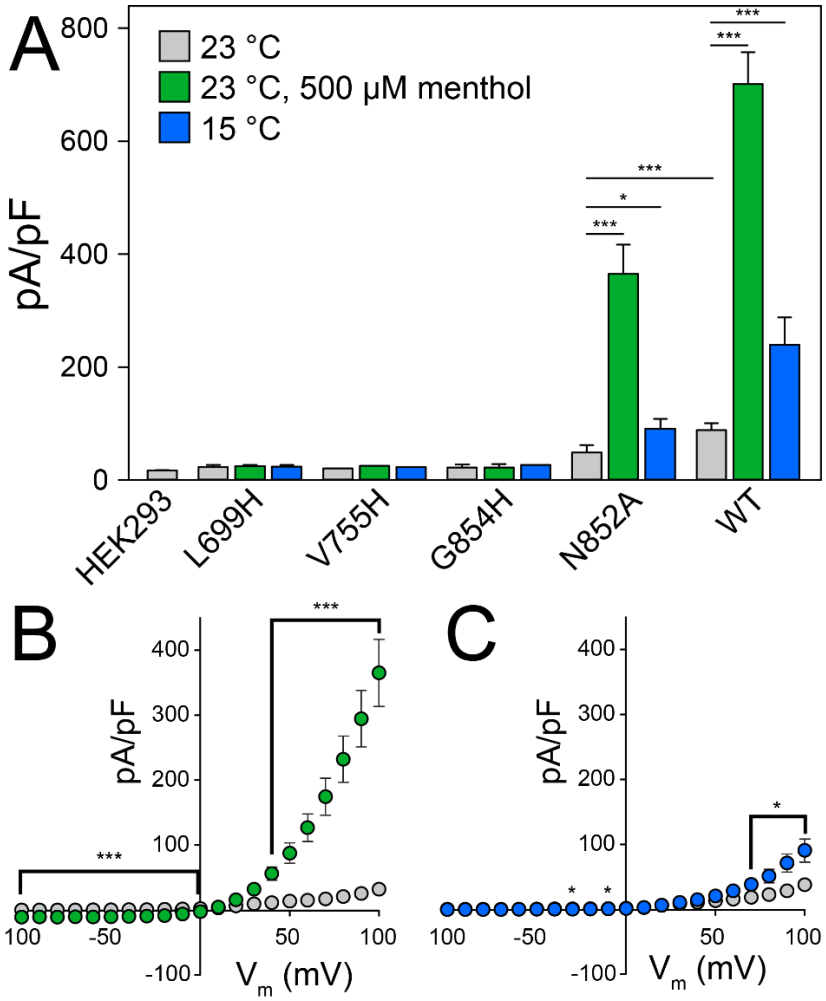

Figure 4.2 Electrophysiology measurements of mutant TRPM8 channels. (A) Steady-state current magnitudes during a +100 mV pulse. Current magnitude from untransfected HEK-293 cells (n = 9) is shown for comparison. L699H (n = 3), V755H (n = 1), and G854H (n = 4) mutations resulted in apparently non-functional channels. The N852A (n = 13) mutation resulted in a functional channel that was sensitive to both menthol (n = 13, p <0.0001) and cold (n = 8, p = 0.013). Wild-type TRPM8 (n = 8) is shown for comparison. TRPM8-N852A exhibited significantly smaller currents than wild-type TRPM8 at room temperature without menthol (p <0.0001). (B) Current-voltage plot of TRPM8-N852A at room temperature in the absence (gray) or presence (green) of 500 µM menthol. (C) Current-voltage plot of TRPM8-N852A at room temperature (gray) or 15 °C (blue). All error bars represent standard error of the mean; (*) signifies $p < 0.05$, and (***) signifies $p < 0.001$.

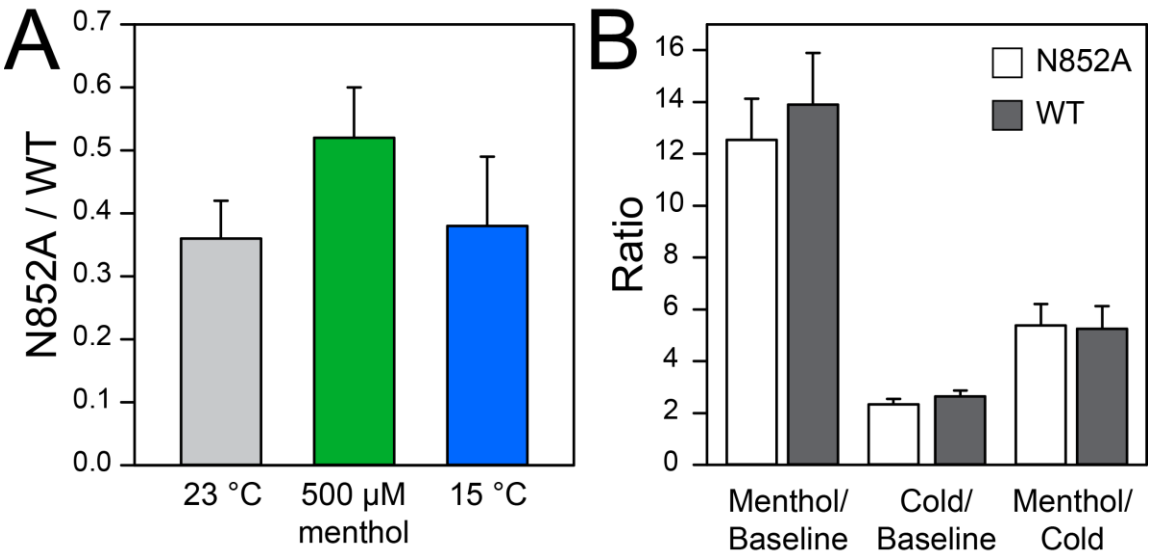

Figure 4.3 (A) Ratios of TRPM8-N852A steady-state current response to wild-type current response during a +100 mV pulse. At room temperature, mutant current density is decreased by a factor of 0.36 ± 0.06. Menthol response decreased by 0.52 ± 0.08, and cold response by 0.38 ± 0.11. (B) the ratio of cold- and menthol-evoked current responses at +100 mV is similar between the wild-type and TRPM8-N852A channels.

4.3.2 Menthol and Icilin Sensitivity of the N852A Mutant

To further investigate the effect of the N852A mutation on ligand response in the channel, electrophysiology experiments were performed to measure the EC_{50} values of menthol and icilin. For menthol experiments, tail currents were measured after a voltage prepulse to determine whether the mutation affects the open probability of the channel in response to the ligand [21]. One common method of measuring tail currents involves a voltage step protocol in which a prepulse to various potentials is applied, followed closely by a fast pulse to a constant potential (Figure 4.4A). The channels take some amount of time to respond to this second potential, and the current that flows during this time is related to the kinetics of channel closing. For voltage-sensitive channels, as larger prepulse potentials are applied, the tail current begins to saturate as the number of open

channels approaches a maximum. Tail current magnitude can then be normalized to this maximum, giving the open probability at a given potential:

$$P_{\mathrm{Open}}(V) = \frac{I_{\mathrm{Tail}}(V)}{I_{\mathrm{Tail,max}}} \quad (1)$$

In this equation, $I_{\mathrm{Tail}}(V)$ is the measured tail current magnitude at a given prepulse potential and $I_{\mathrm{Tail,\ max}}$ is the tail current magnitude at very high prepulse potentials. Because TRP channels are only mildly voltage sensitive, this maximum value was determined by the projection of fitting the tail currents after a +160 mV prepulse at a range of menthol concentrations to a single binding site model, as illustrated in Figure 4.5.

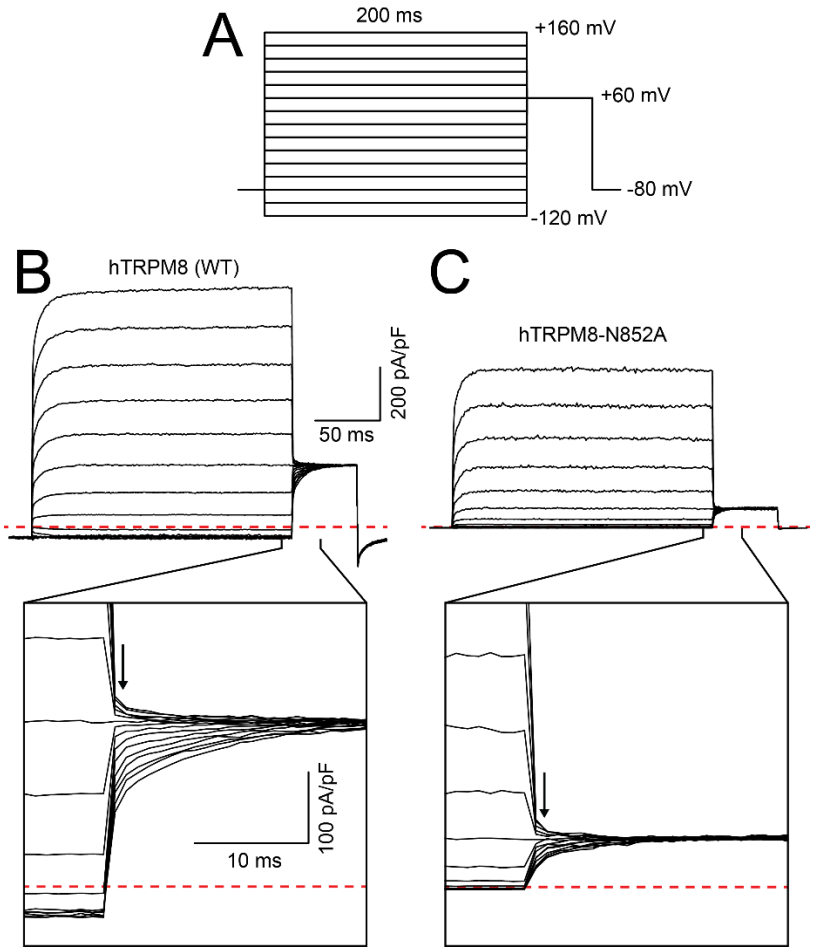

Figure 4.4 Representative current traces for wild-type TRPM8 and TRPM8-N852A in the presence of 500 µM menthol. (A) Voltage protocol used to measure tail currents. Membrane potential was held at -80 mV prior to a voltage pulse in a series of steps from -120 mV to +160 mV, then to +60 mV to record tail currents. (B) current traces from wild-type and (C) N852A channels. Red dashed line represents 0 pA/pF. Insets with arrows show the tail currents at +60 mV.

This method resulted in a menthol EC_{50} value of 46.5 ± 8.3 µM for the wild-type channel after a +100 mV prepulse, while EC_{50} for TRPM8-N852A under the same conditions was right-shifted more than twofold to 114 ± 12 µM, suggesting that the mutation does affect the open probability of the channel in response to menthol (Figure 4.6A).

As discussed above, icilin activation of TRPM8 has features distinct from menthol, including calcium and pH dependence. Additionally, in contrast to menthol, icilin-evoked currents desensitize relatively quickly, making it difficult to obtain sustained steady-state recordings [2]. Therefore, to measure EC_{50} for icilin, another approach had to be used. In this approach, membrane potential was clamped at +60 mV and continuous recordings were made while icilin solutions of a range of concentrations were perfused across the cell. Maximum currents at each icilin concentration were then taken from the current traces. Currents were then normalized and fit to a single-binding site model to obtain EC_{50} values. Whereas the wild-type channel showed robust response to icilin with an EC_{50} of 3 ± 1 μM, the response was almost completely abolished in the N852A mutant such that a EC_{50} could not be determined (Figure 4.6B). These results indicate that the mutation has an effect beyond merely decreasing channel trafficking to the membrane; if this were the case, EC_{50} values would be maintained despite a decreased current magnitude. As shown in Table 4.1, the EC_{50} values measured for wild-type TRPM8 in this study are in the general range of those reported in literature. The polymodal nature of this channel can cause measurements to vary considerably due to factors like expression conditions, ambient temperature, and the species from which the gene originates.

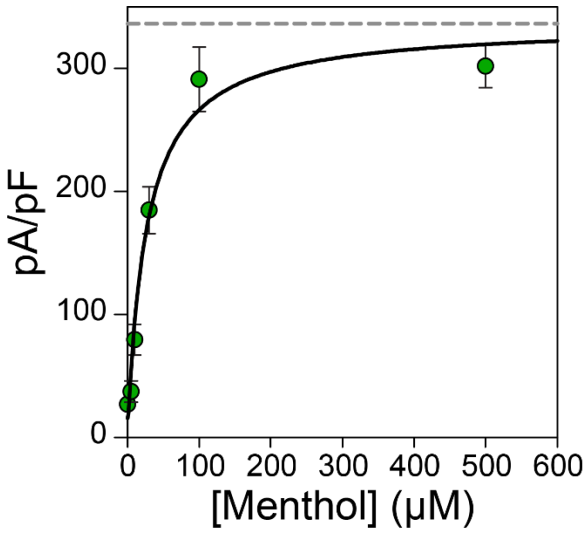

Figure 4.5 Determination of $I_{\text{Tail, max}}$ from the fit of tail currents following a +160 mV prepulse. Data was fit to the single binding site equation $I = \frac{I_{\text{Tail,max}} \times [\text{menthol}]}{\text{EC}_{50} + [\text{menthol}]}$. The projected $I_{\text{Tail,max}}$ is shown by the dashed gray line and in this case has a value of 336.4 pA/pF.

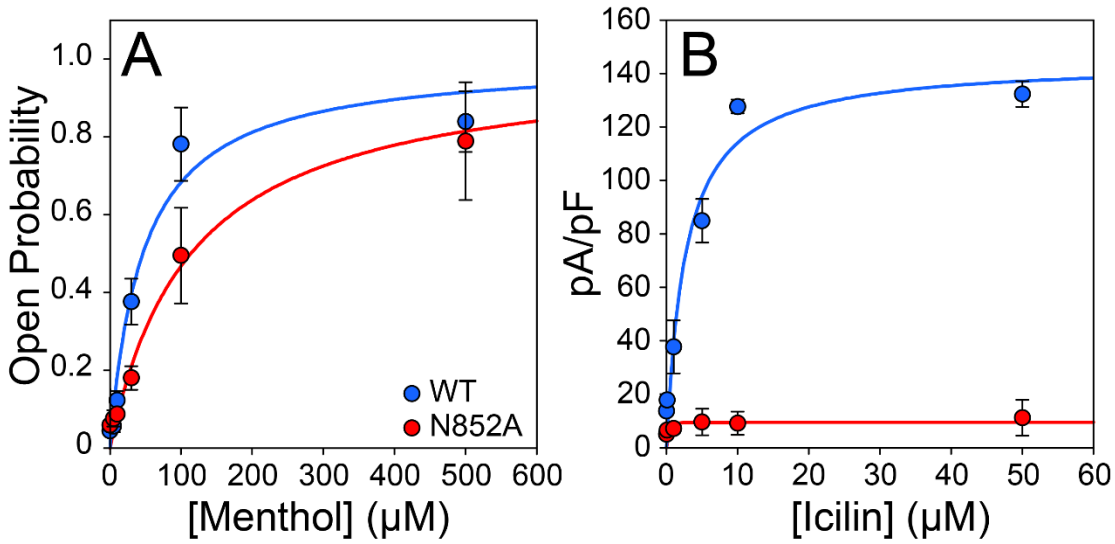

Figure 4.6 (A) Dose-response curves for menthol activation of wild-type TRPM8 (EC_{50} = 46.5 ± 8.3 μM, *n* =5, blue) or TRPM8-N852A (EC_{50} = 114 ± 12 μM *n* = 4, red). (B) Dose-response curves for icilin activation of wild-type TRPM8 (EC_{50} = 3 ± 1 μM, *n* =2, blue) or TRPM8-N852A (EC_{50} could not be determined, *n* = 2, red).

Table 4.1 Literature values of menthol and icilin EC_{50} for TRPM8

Compound	Species	Expression system	Technique	EC_{50}	Reference
Menthol	Human	HEK-293	Electrophysiology	46.5 ± 8.3 μM	This study
	Human	HEK-293	Electrophysiology	27.4 μM	[4]
	Human	HEK-293	Ca^{2+} imaging	10.4 μM	[22]
	Rat	Dissociated trigeminal neurons	Electrophysiology	80 ± 2.4 μM	[23]
	Rat	*X. laevis* oocytes	Electrophysiology	66.7 ± 3.3 μM	[23]
	Rat	Purified from *E. coli*	Electrophysiology	111.8 ± 2.4 μM	[24]
	Rat	*X. laevis* oocytes	Electrophysiology	62.1 ± 3.1 μM	[2]
	Mouse	CHO cells	Ca^{2+} imaging	101 ± 13 μM	[1]
	Mouse	*X. laevis* oocytes	Electrophysiology	196 ± 22 μM	[25]
	Chicken	*X. laevis* oocytes	Electrophysiology	15.0 ± 1.2 μM	[2]
	Ficedula albicollis	HEK-293T cells	Electrophysiology	28.0 ± 4.4 μM	[7]
Icilin	Human	HEK-293	Electrophysiology	3 ± 1 μM	This study
	Mouse	CHO cells	Ca^{2+} imaging	125 ± 30 nM	[1]
	Mouse	*X. laevis* oocytes	Electrophysiology	7 ± 3 μM	[25]
	Human	HEK-293	Ca^{2+} imaging	1.4 μM	[22]

4.3.3 Purification of the TRPM8 S1–S4 Domain

Two possible explanations for the decreased agonist response in the N852A mutant are 1) decreased ligand binding affinity or 2) disruption of coupling between ligand binding and channel gating, affecting the energetics of channel gating. To test the first possibility, the TRPM8 S1–S4 domain (hM8-SD) was expressed and purified from an *E. coli* cell line for direct binding experiments using nuclear magnetic resonance spectroscopy.

Because membrane proteins tend to express in low quantities, to determine the conditions that would yield the most protein an array of expression conditions were tested on a small scale. To facilitate purification, the S1–S4 domain of human TRPM8 (residues P716–P855) was cloned into a pET16b expression vector with a 10xHis tag followed by a thrombin cleavage site. Expression in 7 different cell lines at 18, 25, and 37 °C, and with inducing IPTG concentrations of 0.3, 0.5, and 1 M were tested for a total of 63 different conditions as described in the methods section above. The results were quantified, and the highest yield was determined to be from BL21(DE3) CodonPlus RP at 25 °C and with 0.3 M IPTG (Figure 4.7). However, further expression tests identified that the BL21(DE3) Lobstr cell line at 18 °C produced more consistent results with fewer contaminating proteins during the purification process. Furthermore, given the trend of decreased IPTG concentration yielding more protein (Table 4.2), additional trials found that a concentration between 0.1 and 0.2 mM IPTG produced the most consistently high yields.

To purify the construct, whole-cell lysate was initially purified with Ni-NTA. The 10xHis tag was removed by thrombin cleavage, and a second purification step was performed by rebinding the sample to Ni-NTA resin and collecting the flowthrough containing the cleaved S1–S4 domain. A final purification by size exclusion chromatography resulted in a sample pure enough for NMR experiments (Figure 4.8A). The identity of the purified product was confirmed by LC-MS/MS, with 31% of the sequence identified in 12 unique peptides (Figure 4.8B). The far-UV circular dichroism spectrum of the purified protein shows minima at ~220 and 208 nm, as expected for a

folded helical protein (Figure 4.8C). Typically, 1 L of culture yielded a pellet size of 4–5 g and ~45 µg of purified hM8-SD per gram of cell pellet. The same expression conditions were used for both the wild type and the N852A mutant constructs.

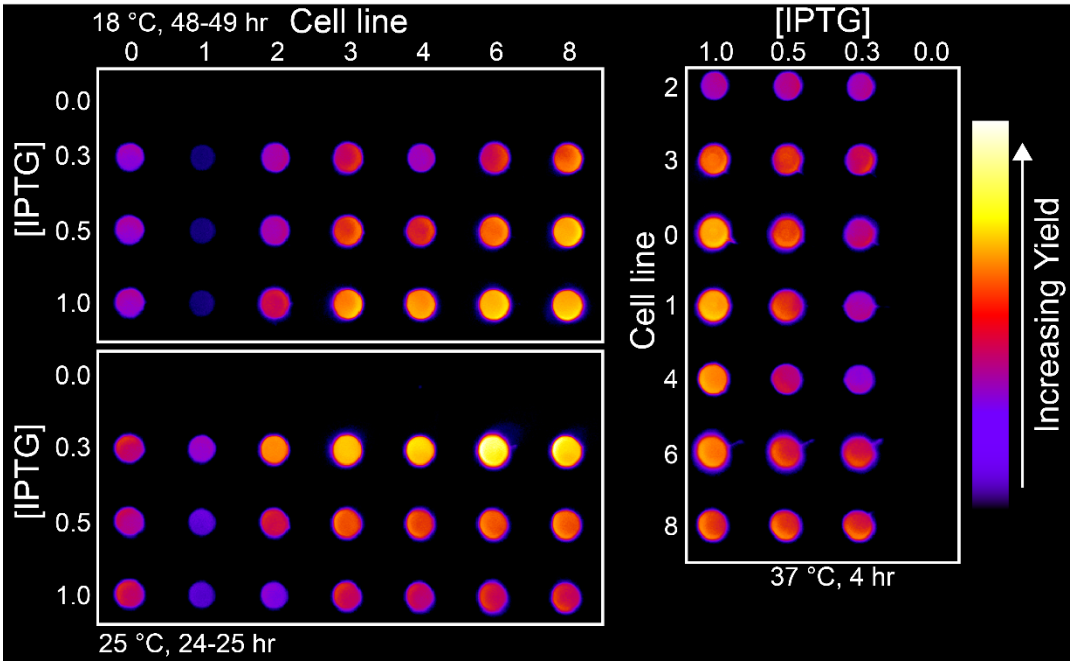

Figure 4.7 Expression testing of the TRPM8 S1–S4 domain. Cell lines are numbered as: 0, BL21(DE3); 1, BL21(DE3) Star; 2, C41(DE3); 3, Rosetta 2(DE3); 4, C43(DE3) Rosetta2; 6, BL21(DE3) CodonPlus RP; 8 BL21(DE3) LOBSTR.

Table 4.2 Expression levels of TRPM8 S1–S4 domain under various conditions.

	[IPTG] (mM)	Cell Line						
		0	1	2	3	4	6	8
18 °C	0.3	0.21	0.06	0.26	0.39	0.24	0.42	0.52
	0.5	0.24	0.06	0.28	0.49	0.43	0.59	0.72
	1.0	0.26	0.06	0.41	0.64	0.66	0.79	0.79
25 °C	0.3	0.34	0.21	0.56	0.77	0.72	1.00	0.86
	0.5	0.30	0.14	0.36	0.49	0.47	0.52	0.53
	1.0	0.35	0.13	0.18	0.36	0.34	0.42	0.41
37 °C	0.3	0.37	0.29	0.24	0.38	0.24	0.51	0.47
	0.5	0.58	0.53	0.28	0.45	0.35	0.57	0.50
	1.0	0.79	0.79	0.24	0.54	0.62	0.75	0.51

Signal intensity was quantified using ImageJ. The numbers were normalized to the highest value, and the color gradient from red to white to blue represents the lowest to highest signal intensity. Cell lines are numbered as in Figure 4.7.

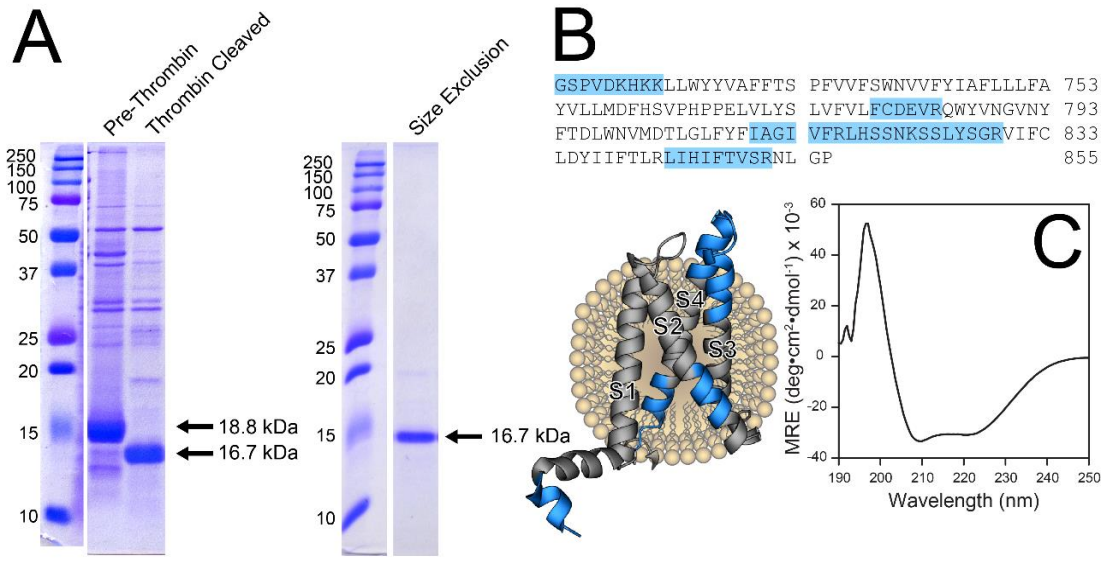

Figure 4.8 (A) Representative gels showing the purification of TRPM8 S1–S4 domain, with bands at the expected molecular weights. (B) Segments highlighted in blue in the sequence and shown on the structure were identified by LC-MS/MS. Peptides identified at both the N and C termini confirm successful expression of the full S1–S4 domain. (C) The far-UV circular dichroism spectrum features minima at ca. 220 and 208 nm and a maximum at ca. 195 nm, typical of a helical protein.

4.3.4 Ligand Binding Measurements Using NMR

$^{1}H,^{15}N$-TROSY HSQC experiments were performed using ^{15}N-labeled hM8-SD in LPPG micelles. The resulting NMR spectrum showed well-dispersed resonances in the 7.0–8.6 ppm range of the ^{1}H dimension, typical of a well-folded helical membrane protein (Figure 4.9) [26]. The quality of the spectrum was an improvement compared to a previously used construct [9] and was amenable to monitoring chemical shift perturbations during ligand titrations. The S1–S4-N852A mutant was also expressed and purified, and it likewise gave a well-dispersed HSQC spectrum (Figure 4.9). Most of the resonances in the two spectra overlaid closely, indicating a largely conserved global fold of the two constructs (Figure 4.10). However, a few resonances showed changes in chemical shift, suggesting local differences in fold or dynamics as a result of the N852A mutation.

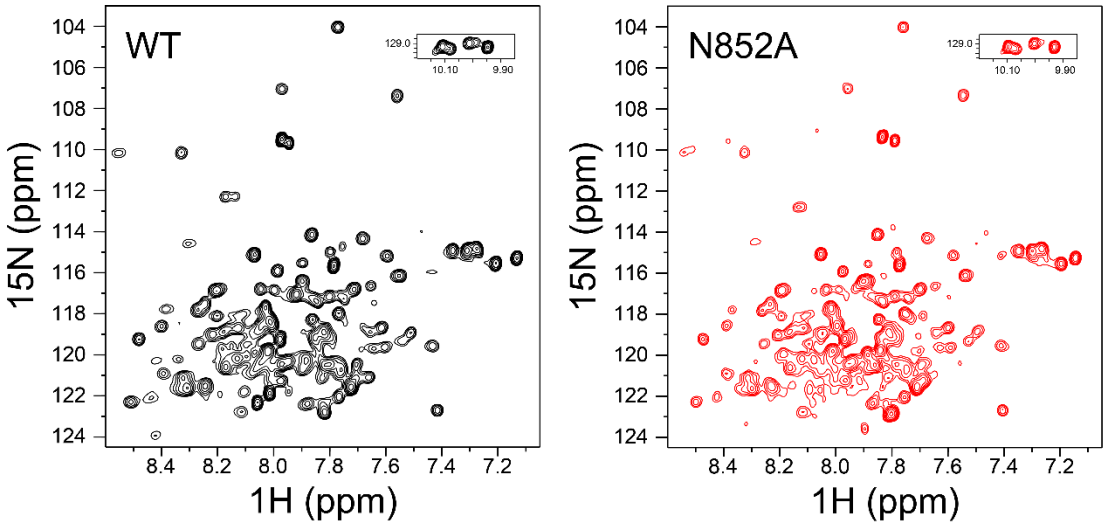

Figure 4.9 NMR spectra of wild-type (left, black) and N852A (right, red) TRPM8 S1–S4 domain. Both spectra show well-dispersed peaks in a range typical of helical membrane proteins. Spectra were recorded with 32 scans at 37 °C and pH 6.5. LPPG concentrations were ~1.1–1.4 %.

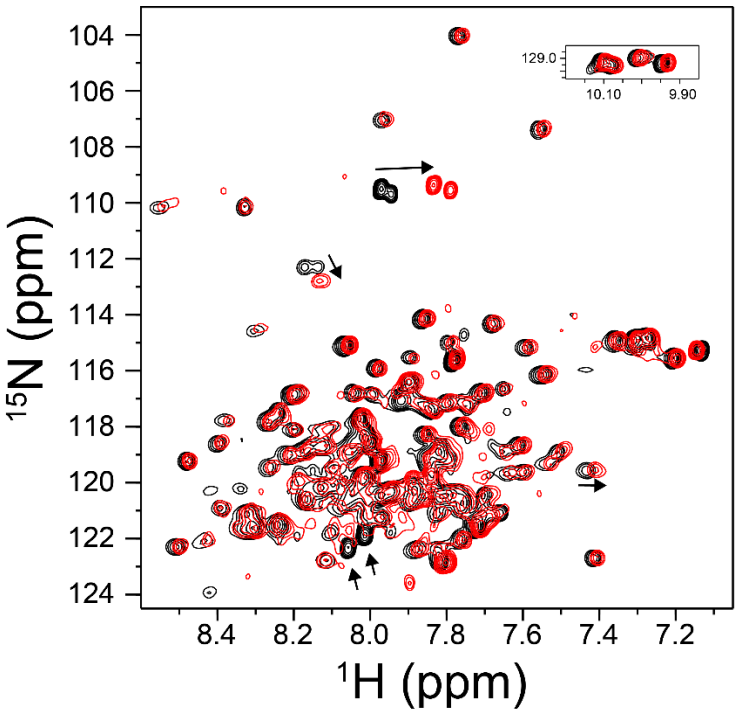

Figure 4.10 Overlay of the same spectra shown in Figure 4.9 (black, WT; red, N852A). Major differences between the two spectra are indicated with arrows. The two spectra largely agree; only a few residues showed sizable chemical shift changes, indicating a conserved global fold with local differences in fold or dynamics due to the N852A mutation.

To directly measure binding and establish ligand affinity for the wild-type sensing domain, a menthol titration was performed up to 10 mole percent menthol, where mole percent was defined as follows:

$$\frac{\text{moles ligand}}{\text{moles ligand} + \text{moles LPPG} + \text{moles hM8-SD}} \times 100 \qquad 1$$

Because the ligands used are hydrophobic and only slightly soluble in water (menthol, 0.42mg/mL [27], icilin ~0.1 mg/mL), mole percent is a more appropriate measure of the ligand concentration accessible by the protein in a detergent micelle, and has been used in similar cases in the literature [9, 28, 29]. The menthol titration showed evidence of ligand binding at two resonances in the spectrum (Figure 4.11). The same menthol titration was

carried out on the S1–S4-N852A. Looking at the two peaks that showed binding in the wild-type protein, one of the peaks did exhibit a saturating binding isotherm with a K_d increased to 0.9 ± 0.3, while the second fit poorly to the single site binding model (Figure 4.12). These results may suggest disruption of menthol binding.

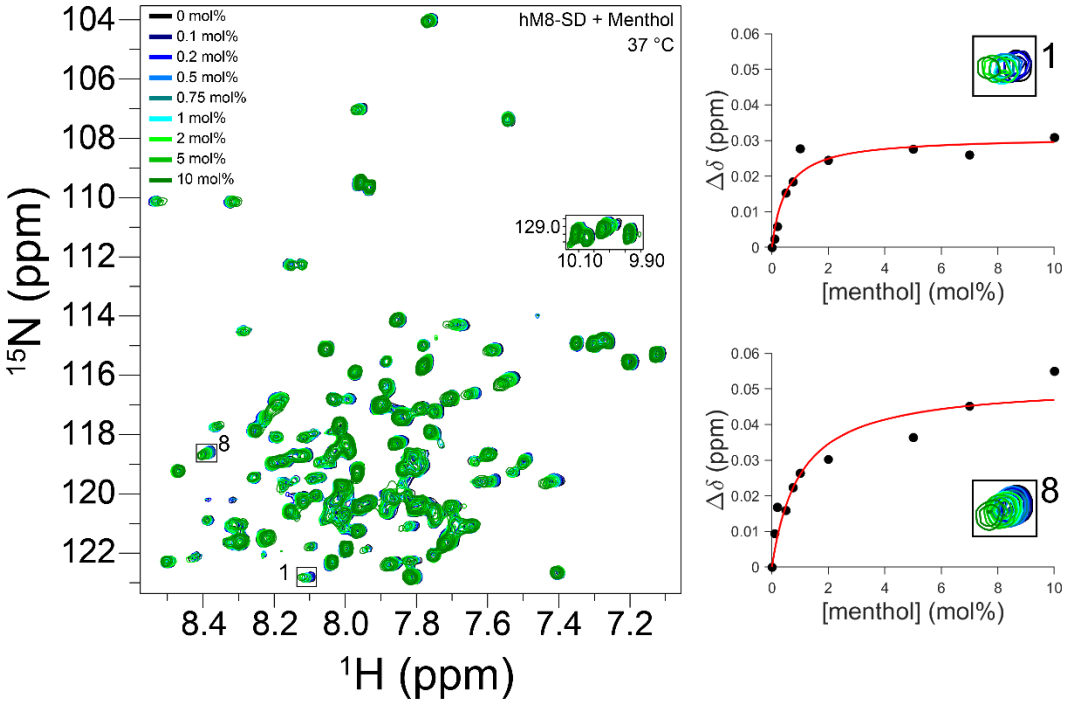

Figure 4.11 Menthol titration of wild-type S1–S4 domain. Two resonances highlighted here exhibited saturating binding behavior. Peak 1 had a calculated K_d of 0.5 ± 0.2 mol %, while the K_d for peak 8 was calculated to be 1.0 ± 0.3 mol %.

Icilin titrations were also carried out for both the wild-type and N852A proteins. In this case, four peaks were identified that showed saturating binding isotherms. Icilin is a more potent agonist than menthol; as described above the EC_{50} for menthol is ~15-fold larger than for icilin in electrophysiology experiments. Consistent with this, the K_d of icilin in the wild-type S1–S4 domain as measured by NMR is approximately an order of magnitude lower than for menthol (Figure 4.13). An icilin titration with S1–S4-N852A

also showed binding affinity similar to the wild-type. Thus, the diminished icilin response of the mutant cannot be explained by a decrease in binding affinity.

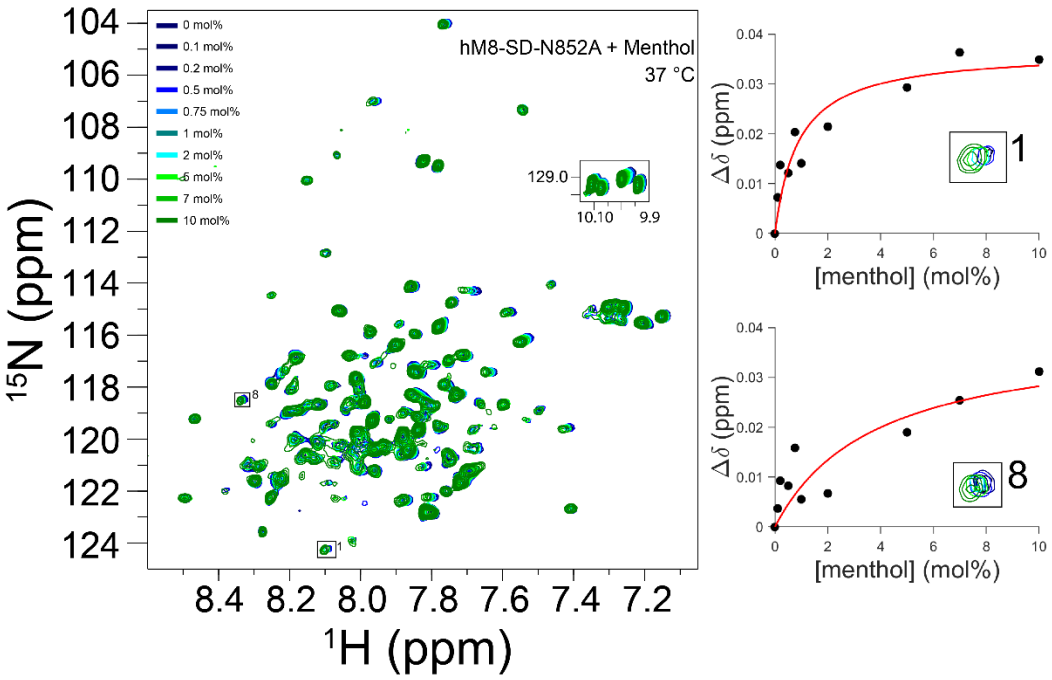

Figure 4.12 Menthol titration of S1–S4-N852A. The corresponding resonances from the wild-type titration are also shown here; peak 1 had an increased K_d of 0.9 ± 0.3, and peak 8 did not fit well to a single binding site model.

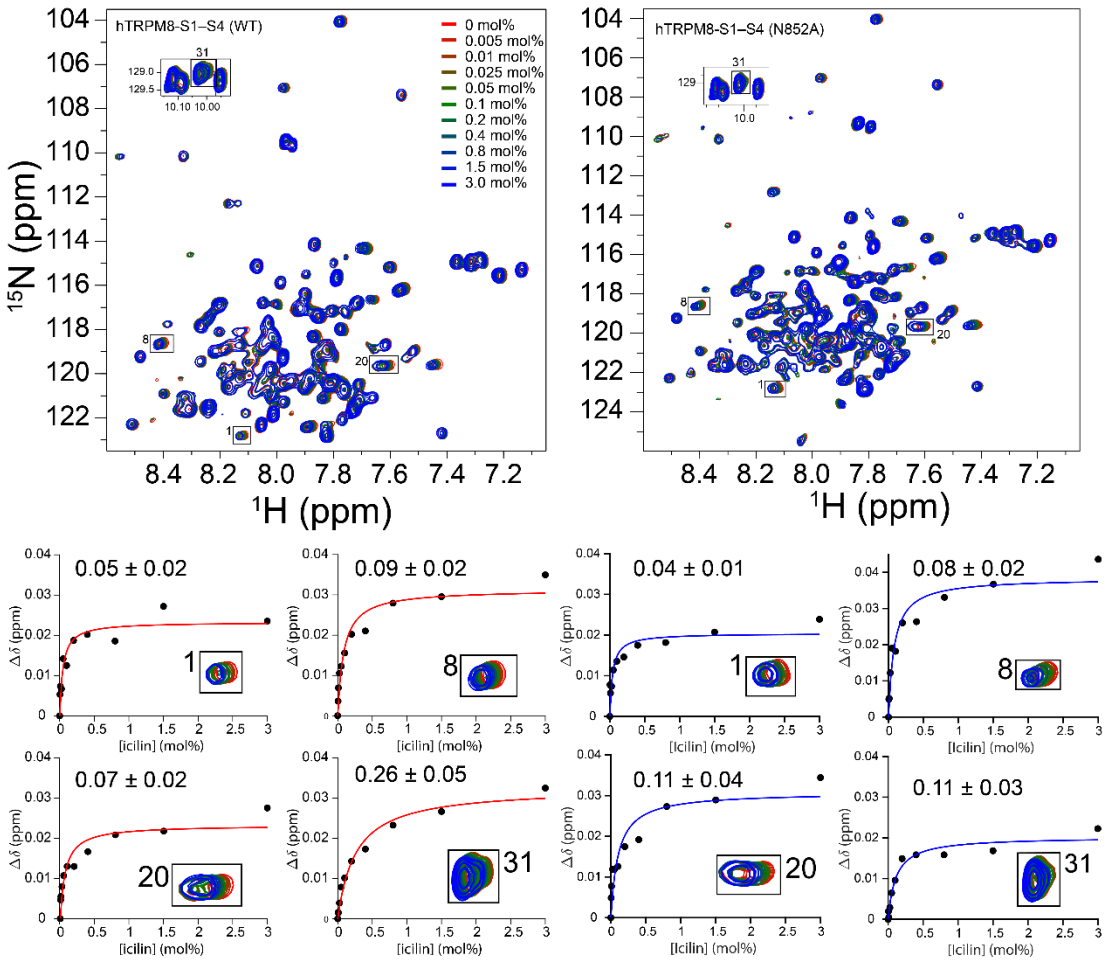

Figure 4.13 Icilin titration of the S1–S4 domain. The spectrum from wild-type is shown on the top left, and the N852A mutant spectrum is on the top right. Four peaks were identified that show saturating binding curves in both constructs. The calculated K_d in mol % from the fit to a single binding site model is shown in the top left of each curve. Curves from the wild-type are shown in red; those from N852A are shown in blue. The K_d values from corresponding peaks are similar in the wild-type and mutant constructs, indicating that the N852A mutation does not affect icilin binding.

4.3.5 CD Measurements

Activation of the TRPM8 channel involves a conformational change that causes the central pore to open. Based on recent TRPM8 structures, icilin binding in the S1–S4 domain causes changes in the transmembrane domain; specifically, the S5 helix bends away from the pore, the S1–S4 domain rotates away from the pore domain, and the TRP

helix rotates and tilts downward [8]. Most relevant here, the bottom of S4 undergoes a transition from an α-helix to a tighter 3_{10}-helix. These movements allow for conformational shifts in the pore domain that lead to ion permeation.

To monitor any changes in secondary structure of the TRPM8 S1–S4 domain as a result of ligand binding, far-UV circular dichroism (CD) spectroscopy measurements were carried out. An increase or decrease in helical content upon ligand binding can be observed as an increase or decrease the 208 and 220 nm peaks. As shown in Figure 4.14A, there was no clear effect on secondary structure from addition of menthol up to 10 mole percent. Thus, binding of this ligand appears not to significantly affect the helical content of this construct. This is in contrast to an hM8-SD construct that includes the N-terminal juxtamembrane helices, which showed a significant decrease in the 208 and 220 nm peaks with addition of 10 mole percent menthol [9].

The effect of temperature on the secondary structure of the hM8-SD construct was also tested. CD spectra were measured from 10 to 57 °C, a temperature range that covers the physiological TRPM8 channel thermal response. Although a general decrease in the two peaks was observed with increasing temperature, this effect follows a linear trend as would be expected from the thermal expansion of any helical peptide before it reaches an unfolding transition [30, 31]. However, the slope of the trends is slightly different; the 222 nm peak loses more intensity than the 207 nm peak with increasing temperature (Figure 4.14B). It has been shown that the intensity ratio of the 220 nm peak to the 208 nm peak can be indicative of the type of helix in a peptide. α-helices tend to have a ratio close to 1, whereas 3_{10} helices are theoretically predicted and have been measured to have

a 222/207 ratio around 0.4 [32-34]. Additionally, the positive peak around 195 nm is predicted to be significantly lower for a 3_{10} helix compared to an α-helix. As shown in Figure 4.14C and D, as the temperature increases, both the 222/207 ratio and the 197 nm peak tend toward decreasing values as would be expected for increasing 3_{10}-helical content. As mentioned above, the cryo-EM structures of ligand bound TRPM8 show that the bottom of S4, from R842 to S849, forms a 3_{10} helix. This would represent ~6% of the hM8-SD construct. The CD data presented here is consistent with a small increase in 3_{10}-helical content at higher temperatures. However, this would be an unexpected result given that at higher temperatures the full channel would be in a closed state, whereas the ligand-bound structures suggest that the 3_{10} helix forms upon channel activation by ligands.

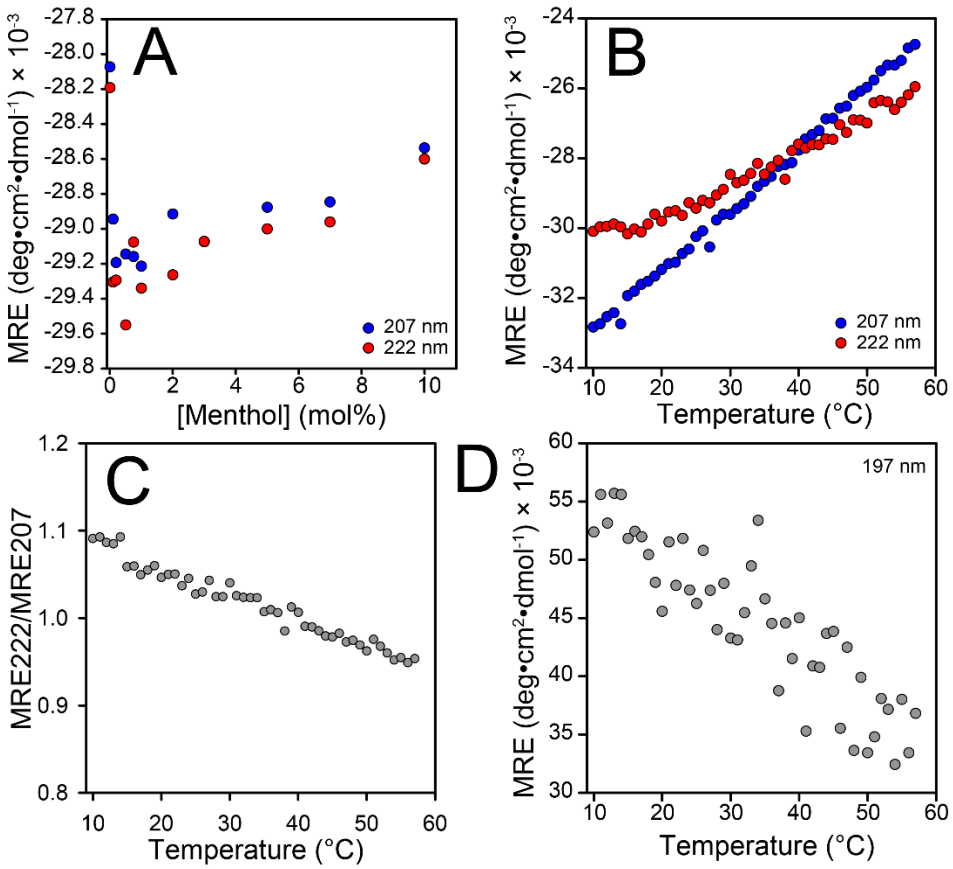

Figure 4.14 Circular dichroism of TRPM8 S1–S4 domain. (A) Minima values of peaks at 207 and 222 nm. The 207 nm peak loses more intensity compared to the 222 nm peak as a function of increasing temperature, possibly reflecting a decrease in α-helical content. (B) Peak intensity at 197 nm decreases as a function of temperature. (C) The ratio of 222/207 nm peaks decreases with temperature, consistent with formation of a 3_{10} helix. (D) A menthol titration showed no specific trend, indicating either that menthol does not bind to this construct or that menthol binding does not significantly affect helical content.

4.4 Conclusion

The N852A mutation was shown to have a general attenuating effect on TRPM8 activity. Current response to cold and menthol stimuli were reduced by a similar amount, suggesting decreased sensitivity to these stimuli. Strikingly, icilin response of the mutant was severely diminished, whereas menthol still showed appreciable activation. This result highlights the distinct activation mechanism of these two agonists, despite recent cryo-

EM structures that demonstrate similar binding sites [8]. Menthol binding affinity for the mutant construct was similar to the wild-type at one of the resonances, with a K_d of 0.9 ± 0.3 compared to 0.5 ± 0.2. However, another resonance that showed binding to the wild-type did not show binding in the mutant, suggesting that menthol binding was somewhat disrupted by the N852A mutation. In contrast, icilin binding affinity was similar for both constructs. Therefore, the decreased sensitivity of the channel for the two agonists appears to be the result of an effect other than ligand binding affinity.

N852 is found at the lower end of the S4 helix as it connects to S5. Cryo-EM structures of icilin-bound TRPM8 reveal that the ligand binds inside the S1–S4 helical bundle in a way unlikely to directly interact with N852, consistent with the NMR data presented here. Additionally, the structures suggest that the side chains of H845 and Arg 842, both at the bottom of S4, interact with icilin. These interactions are facilitated by a transition from α-helical to 3_{10}-helical structure in the C-terminal end of S4 when icilin is bound, shifting the register and placing H844 on the same side of the helix as R842, with both side chains pointing in toward the binding pocket. Neither of these residues interact with the bound WS-12 ligand; indeed, mutating H845 to alanine resulted in a dramatic decrease in icilin sensitivity without affecting WS-12 response. In the apo TRPM8 and WS-12 bound structures, N852 caps the C-terminal end of the α-helical S4; the nitrogen in the side chain forms a hydrogen bond with the backbone carbonyl of T848 in S4. In the icilin-bound structure, this hydrogen bond is broken and N852 is shifted to a short linker loop between S4 and S5 as a result of the tighter turn in S4. Furthermore, breaking of the N852-T848 hydrogen bonding interaction frees the adjacent R851 residue to interact with

PIP_2, an essential cofactor for TRPM8 activation. One possibility that could explain the differential effect of the N852A mutation on menthol and icilin sensitivity is that this mutation disrupts this α- to 3_{10}-helical transition, which would prevent H845 from interacting with icilin.

Several experiments could be done to build on this work. The S1–S4 construct described here gives NMR spectra of sufficient quality that most of the resonances could be assigned with 3D NMR experiments. Ligand-bound cryo-EM structures provide a snapshot of the binding pocket, but NMR analysis with resonances assigned would reveal residues that directly interact with the ligand and provide quantitative information about binding affinity. Given that the structures suggest that icilin interacts with H845 and R842, assigning these resonances and carrying out ligand binding studies would confirm whether this is the case. Mutating H845 to alanine did decrease icilin response in the channel, but NMR would confirm whether this functional affect is the result of decreased binding affinity or some other effect from the mutation.

4.5 Supplementary Information

4.5.1 NMR Processing Scripts

4.5.1.1 fid.com Script from NMRPipe Conversion Utility (Version 2017.263.14.36)

```
#!/bin/csh

bruk2pipe -in ./ser \
  -bad 0.0 -ext -aswap -AMX -decim 1960 -dspfvs 20 -grpdly 67.9862976074219  \
  -xN              2048  -yN              128  \
  -xT              1024  -yT               64  \
  -xMODE           DQD  -yMODE  Echo-AntiEcho  \
  -xSW         10204.082  -ySW         2585.315  \
  -xOBS          850.279  -yOBS          86.168  \
  -xCAR            4.641  -yCAR        117.953  \
```

```
  -xLAB            HN  -yLAB           15N  \
  -ndim            2  -aq2D        Complex  \
  -out ./test.fid -verb -ov

sleep 1

#!/bin/csh
```

4.5.1.2 nmrproc.com Script for nmrDraw

```
set nodelist = (  11ppm 6ppm  )

set lbHz    =  1.0
set g1      =  15
set g2      =  20
set off     =  0.33
set pow     =  2
set p0      =  -67.8
set p1      =   0.0
set c       =   0.5
set extX1   = 11.0ppm
set extXN   = 6.4ppm



nmrPipe -in test.fid \
| nmrPipe -fn POLY -time                              \
#| nmrPipe -fn LP -b -pred 20  -fix -ord                        \
| nmrPipe  -fn GM -g1 $g1 -g2 $g2 -g3 0.05 -c 0.75 -one           \
| nmrPipe  -fn ZF -zf 2 -auto                          \
| nmrPipe  -fn FT -auto                          \
| nmrPipe -fn BASE -nl $nodelist                       \
| nmrPipe  -fn PS -p0 $p0  -p1 $p1 -di -verb        \
| nmrPipe  -fn POLY -auto                        \
| nmrPipe -fn EXT -x1 $extX1 -xn $extXN -sw          \
| nmrPipe  -fn TP                                \
#| nmrPipe -fn LP -fb -pred 50 -ord                     \
| nmrPipe  -fn SP -off $off -end 0.98 -pow $pow -c 0.5       \
| nmrPipe  -fn ZF -zf 2 -auto                          \
| nmrPipe  -fn FT -auto                          \
| nmrPipe  -fn PS -p0 90.00 -p1 0.00 -di -verb        \
#| nmrPipe  -fn POLY -auto                        \
       -ov -out test.ft2
```

4.5.2 MatLab Peak Chemical Shift Calculation and Fitting Script

```
%%read in the files (keep in the same format as exported from CCPN
clc
close all
clear
warning('off')
files=dir('*txt');
j=readtable(files(1).name,'Delimiter','\t');
n=size(files);

%Calculate Delta-delta for each peak position
for i = 1:n
    j=readtable(files(i).name,'Delimiter','\t');
    N=j.PositionF1;
    H=j.PositionF2;
    dH=(H(:)-H(1)).^2;
    dN=0.2*(N(:)-N(1)).^2;
    Dd(:,i)=sqrt(dH+dN);
end
%% Correlate peak position to ligand concentration and fit to single
binding site Hill equation

x=[0 0.005 0.01 0.025 0.05 0.1 0.2 0.4 0.8 1.5 3.0]; %values of ligand
concentration

fit=@(b,x) b(1).*x./(b(2)+x);
xData=x(:);
yData=Dd(:,1);
beta0=[max(yData),0];
[beta,R,J,CovB,MSE]=nlinfit(xData,yData,fit,beta0)


%%
close all

%generate figures with fit line plotted
 for i = 1:n
    [xData yData]=prepareCurveData(xData,Dd(:,i));

    fit=@(b,x) b(1).*x./(b(2)+x);
    yData=Dd(:,i);
    beta0=[max(yData),0];
    [beta,R,J,CovB,MSE]=nlinfit(xData,yData,fit,beta0)
    standev=sqrt(diag(CovB));
    SSresidual=sum(R.^2);
    SStotal=sum((yData-mean(yData)).^2);
    rsquare=1-(SSresidual/SStotal)

    h=figure(i);
    xfit=linspace(min(xData),max(xData));
    g=plot(xData,yData,'o',xfit,fit(beta,xfit));
```

```
    kd(:,i)=beta(:,2);
    standard_error(:,i)=standev(2);
    rsquares(:,i)=rsquare;

set(gca,'TickDir','out','Box','off','Color','none','TickLength',[0.025
0.1],'FontSize',14,'LineWidth',2,'FontName','Arial')
    g(1).MarkerSize=10;
    g(1).MarkerFaceColor=[0 0 0];
    g(1).MarkerEdgeColor='none';
    g(2).Color=[0 0 1];
    g(2).LineWidth=2;
    %ylim([0 0.045]); %undo comment and add a y limit if needed
    xlabel('[Icilin] (mol%)','FontSize',22)
    ylabel('\Delta\delta (ppm)','FontSize',22)
    saveas(h,sprintf('./plots/FIG_%d.pdf',i)); % will create FIG1,
FIG2,...

end
disp('done')
```

4.5 References

1. Andersson, D. A., Chase, H. W., and Bevan, S. (2004) TRPM8 activation by menthol, icilin, and cold is differentially modulated by intracellular pH. *J. Neurosci.* **24**, 5364-5369

2. Chuang, H. H., Neuhausser, W. M., and Julius, D. (2004) The super-cooling agent icilin reveals a mechanism of coincidence detection by a temperature-sensitive TRP channel. *Neuron* **43**, 859-869

3. Bandell, M., Dubin, A. E., Petrus, M. J., Orth, A., Mathur, J., Hwang, S. W., and Patapoutian, A. (2006) High-throughput random mutagenesis screen reveals TRPM8 residues specifically required for activation by menthol. *Nature neuroscience* **9**, 493-500

4. Voets, T., Owsianik, G., Janssens, A., Talavera, K., and Nilius, B. (2007) TRPM8 voltage sensor mutants reveal a mechanism for integrating thermal and chemical stimuli. *Nat. Chem. Biol.* **3**, 174-182

5. Autzen, H. E., Myasnikov, A. G., Campbell, M. G., Asarnow, D., Julius, D., and Cheng, Y. (2018) Structure of the human TRPM4 ion channel in a lipid nanodisc. *Science* **359**, 228-232

6. Huang, Y., Winkler, P. A., Sun, W., Lu, W., and Du, J. (2018) Architecture of the TRPM2 channel and its activation mechanism by ADP-ribose and calcium. *Nature* **562**, 145-149

7. Yin, Y., Wu, M., Zubcevic, L., Borschel, W. F., Lander, G. C., and Lee, S. Y. (2018) Structure of the cold- and menthol-sensing ion channel TRPM8. *Science* **359**, 237-241

8. Yin, Y., Le, S. C., Hsu, A. L., Borgnia, M. J., Yang, H., and Lee, S. Y. (2019) Structural basis of cooling agent and lipid sensing by the cold-activated TRPM8 channel. *Science* **363**, eaav9334

9. Rath, P., Hilton, J. K., Sisco, N. J., and Van Horn, W. D. (2016) Implications of Human Transient Receptor Potential Melastatin 8 (TRPM8) Channel Gating from Menthol Binding Studies of the Sensing Domain. *Biochemistry* **55**, 114-124

10. Bidaux, G., Borowiec, A. S., Gordienko, D., Beck, B., Shapovalov, G. G., Lemonnier, L., Flourakis, M., Vandenberghe, M., Slomianny, C., Dewailly, E., Delcourt, P., Desruelles, E., Ritaine, A., Polakowska, R., Lesage, J., Chami, M., Skryma, R., and Prevarskaya, N. (2015) Epidermal TRPM8 channel isoform controls the balance between keratinocyte proliferation and differentiation in a cold-dependent manner. *Proc. Natl. Acad. Sci. U. S. A.* **112**, E3345-E3354

11. Cao, E., Liao, M., Cheng, Y., and Julius, D. (2013) TRPV1 structures in distinct conformations reveal activation mechanisms. *Nature* **504**, 113-118

12. Gao, Y., Cao, E., Julius, D., and Cheng, Y. (2016) TRPV1 structures in nanodiscs reveal mechanisms of ligand and lipid action. *Nature* **534**, 347-351

13. Yang, F., Xiao, X., Cheng, W., Yang, W., Yu, P., Song, Z., Yarov-Yarovoy, V., and Zheng, J. (2015) Structural mechanism underlying capsaicin binding and activation of the TRPV1 ion channel. *Nat. Chem. Biol.* **11**, 518-524

14. Yang, F., Xiao, X., Lee, B. H., Vu, S., Yang, W., Yarov-Yarovoy, V., and Zheng, J. (2018) The conformational wave in capsaicin activation of transient receptor potential vanilloid 1 ion channel. *Nat. Commun.* **9**, 2879

15. Zhang, F., Hanson, S. M., Jara-Oseguera, A., Krepkiy, D., Bae, C., Pearce, L. V., Blumberg, P. M., Newstead, S., and Swartz, K. J. (2016) Engineering vanilloid-sensitivity into the rat TRPV2 channel. *eLife* **5**, e16409

16. Zhang, F., Swartz, K. J., and Jara-Oseguera, A. (2019) Conserved allosteric pathways for activation of TRPV3 revealed through engineering vanilloid-sensitivity. *eLife* **8**, e42756

17. Yang, F., Vu, S., Yarov-Yarovoy, V., and Zheng, J. (2016) Rational design and validation of a vanilloid-sensitive TRPV2 ion channel. *Proc. Natl. Acad. Sci. U. S. A.* **113**, E3657-3666

18. Andersen, K. R., Leksa, N. C., and Schwartz, T. U. (2013) Optimized E. coli expression strain LOBSTR eliminates common contaminants from His-tag purification. *Proteins* **81**, 1857-1861

19. Miles, A. J., and Wallace, B. A. (2018) CDtoolX, a downloadable software package for processing and analyses of circular dichroism spectroscopic data. *Protein Sci.* **27**, 1717-1722

20. Liao, M., Cao, E., Julius, D., and Cheng, Y. (2013) Structure of the TRPV1 ion channel determined by electron cryo-microscopy. *Nature* **504**, 107-112

21. Talavera, K., and Nilius, B. (2011) Electrophysiological Methods for the Study of TRP Channels. in *TRP Channels* (Zhu, M. X. ed.), CRC Press/Taylor & Francis, Boca Raton, FL. pp

22. Bödding, M., Wissenbach, U., and Flockerzi, V. (2007) Characterisation of TRPM8 as a pharmacophore receptor. *Cell Calcium* **42**, 618-628

23. McKemy, D. D., Neuhausser, W. M., and Julius, D. (2002) Identification of a cold receptor reveals a general role for TRP channels in thermosensation. *Nature* **416**, 52-58

24. El-Arabi, A. M., Salazar, C. S., and Schmidt, J. J. (2012) Ion channel drug potency assay with an artificial bilayer chip. *Lab Chip* **12**, 2409-2413

25. Sherkheli, M. A., Vogt-Eisele, A. K., Bura, D., Márques, L. R. B., Gisselmann, G., and Hatt, H. (2010) Characterization of Selective TRPM8 Ligands and their Structure Activity Response (S.A.R) Relationship. *J. Pharm. Pharm. Sci.* **13**, 242-253

26. Gong, X. M., Franzin, C. M., Thai, K., Yu, J., and Marassi, F. M. (2007) Nuclear Magnetic Resonance Structural Studies of Membrane Proteins in Micelles and Bilayers. *Methods Mol. Biol.* **400**, 515-529

27. Wakita, K., Yoshimoto, M., Miyamoto, S., and Watanabe, H. (1986) A Method for Calculation of the Aqueous Solubility of Organic Compounds by Using New Fragment Salubility Constants. *Chem. Pharm. Bull.* **34**, 4663-4681

28. Barrett, P. J., Song, Y., Van Horn, W. D., Hustedt, E. J., Schafer, J. M., Hadziselimovic, A., Beel, A. J., and Sanders, C. R. (2012) The Amyloid Precursor Protein Has a Flexible Transmembrane Domain and Binds Cholesterol. *Science* **336**, 1168-1171

29. Barrett, P. J., Song, Y., Van Horn, W. D., Hustedt, E. J., Schafer, J. M., Hadziselimovic, A., Beel, A. J., and Sanders, C. R. (2012) Structural studies of

the transmembrane C-terminal domain of the amyloid precursor protein (APP): does APP function as a cholesterol sensor? *Biochemistry* **47**, 9428– 9446

30. López-Arenas, L., Solís-Mendiola, S., and Hernández-Arana, A. (1999) Estimating the Degree of Expansion in the Transition State for Protein Unfolding: Analysis of the pH Dependence of the Rate Constant for Caricain Denaturation. *Biochemistry* **38**, 15936-15943

31. Consalvi, V., Chiaraluce, R., Giangiacomo, L., Scandurra, R., Christova, P., Karshikoff, A., Knapp, S., and Ladenstein, R. (2000) Thermal unfolding and conformational stability of the recombinant domain II of glutamate dehydrogenase from the hyperthermophile *Thermotoga maritima*. *Protein engineering* **13**, 501-507

32. Manning, M. C., and Woody, R. W. (1991) Theoretical CD studies of polypeptide helices: examination of important electronic and geometric factors. *Biopolymers* **31**, 569-586

33. Toniolo, C., Polese, A., Formaggio, F., Crisma, M., and Kamphuis, J. (1996) Circular Dichroism Spectrum of a Peptide 3_{10}-Helix. *J. Am. Chem. Soc.* **118**, 2744-2745

34. Banerjee, R., and Sheet, T. (2017) Ratio of ellipticities between 192 and 208 nm (R_1): An effective electronic circular dichroism parameter for characterization of the helical components of proteins and peptides. *Proteins* **85**, 1975-1982

CHAPTER 5

THERMODYNAMICS AND ANTAGONISM OF THERMOSENSITIVE TRP CHANNELS

5.1 Introduction

Beyond the core work presented in previous chapters, I also completed several smaller projects investigating TRPV1 and TRPM8 activity. Here I present three of those projects. The first is a set of electrophysiology experiments probing the thermodynamics of TRPV1 heat activation. The second is an attempt to locate regions important for TRPM8 cold sensing by testing TRPM2/TRPM8 chimeric channels. Finally, I present measurements to quantify the potency of a novel TRPM8 antagonist.

5.2 Experimental Methods

5.2.1 Cell Culture

HEK-293 cells (ATCC cell line CRL-1573) were cultured in 35 mm dishes at 37 °C in DMEM with 10% fetal bovine serum, 2 mM L-glutamine, 4.5 $mg \cdot ml^{-1}$ glucose, and 100 $mg \cdot ml^{-1}$ each of penicillin and streptomycin in the presence of 5% CO_2. All reagents were obtained from Life Technologies.

5.2.2 Generation of TRPM2–TRPM8 Chimeras

Chimeric regions were swapped with the pIRES2 vector using MEGAWHOP PCR [1]. To generate megaprimers, the following initial primer sequences were used:

hTRPM2[M8-TMD]S0-TRP:

Forward:

CTCGCCCTGGAGGCCAAGGACATGAAGTTTGTGTCTCACCCTGGGGTCCAGA

ATTTTCTTTC

Reverse:

CAGGTGGCTGAGGAGGATGAAGGGGGGCGGGATATTGAGGCGGCTGCAGTA

CTC

hTRPM2[M8-PD]S4/S5-TRP:

Forward:

TACCATCAGTAAGACGCTGGGGCCCAAGATCATCATGCTGCAGAGGATGCTG

ATCG

Reverse:

CAGGTGGCTGAGGAGGATGAAGGGGGGCGGGATATTGAGGCGGCTGCAGTA

CTC

hTRPM2[M8-PD]S4/S5-S6:

Forward:

TACCATCAGTAAGACGCTGGGGCCCAAGATCATCATGCTGCAGAGGATGCTG

ATCG

Reverse:

GCGCTGGAACTTCCAAATCTGGTCCGTGTGCTCCTGCACGGTGCCCACCGTGT

AGCCAAAC

hTRPM2[M8-PD]S5-S6:

Forward:

GCGGATGATGAAGGACGTCTTCTTCTTCCTCTTCCTGTTTGCGGTGTGGATGG

TGGCCTTTG

Reverse:

GCGCTGGAACTTCCAAATCTGGTCCGTGTGCTCCTGCACGGTGCCCACCGTGT
AGCCAAAC.

Megaprimers were generated using PCR and purified using an agarose gel purification kit (Qiagen). Purified megaprimers were then used to generate chimeric genes in a second round of PCR. Purified chimera plasmids were verified by Sanger sequencing and transfected into HEK-293 cells for electrophysiology experiments as described below.

5.2.3 Plasmid and Mammalian Cell Transfection

A pIRES-2 plasmid also containing the EGFP gene was used as a vector for all ion channel genes. This construct produces bicistronic mRNA containing an internal ribosome entry site (IRES) between the two genes, allowing for the independent translation of the channel and the EGFP reporter. Cells were transiently transfected with 0.5 µg DNA using FuGENE 6 transfection reagent (Promega) in a 1:3 µg DNA:µL FuGENE ratio 48 h before electrophysiology measurements were performed.

5.2.4 Electrophysiology

Transfected cells were released from the culture dish surface by briefly exposing them to 0.25% trypsin-EDTA (Thermo) and resuspending in supplemented DMEM. Cells were plated on glass coverslips and incubated for 1-2 h at 37 °C. Whole-cell voltage-clamp measurements were performed with an Axopatch 200B amplifier and pClamp 10.3 software (Molecular Devices). Data was acquired at 2 kHz, filtered at 1 kHz, and digitized using a Digidata 1440a digitizer (Molecular Devices). Patch pipettes were

pulled from borosilicate glass capillaries (World Precision Instruments) using a P-2000 laser puller (Sutter Instruments) and heat polished with a MF-830 microforge (Narashige), resulting in resistances of 2-5 MΩ. A reference electrode was inserted into a salt bridge composed of 2% agar in extracellular solution. Glass coverslips plated with cells were placed in a chamber and covered with extracellular solution containing 132 mM NaCl, 5 mM KCl, 1 mM $MgCl_2$, 2 mM $CaCl_2$, 10 mM HEPES, and 5 mM glucose. The pH of the solution was adjusted to 7.4 using NaOH and osmolality was adjusted to 310 mOsm using sucrose. Pipette solution contained 315 mM K+ gluconate, 5 mM KCl, 1 mM $MgCl_2$, 5 mM EGTA, and 10 mM HEPES, with pH adjusted to 7.2 using KOH and osmolality adjusted to 300 mOsm using sucrose. Osmolality was measured using a Vapro 5600 vapor pressure osmometer (Wescor). Temperature was controlled by perfusing preheated or cooled extracellular solution using an HCPC perfusion system and HCT-10 temperature controller (ALA Scientific), which heats or cools solution by supplying a specified voltage to a Peltier device through which perfusion solution flows. The HCPC has an internal thermistor to maintain a specified temperature, but this value does not accurately report on the temperature of the solution as it exits the capillary. To calibrate the temperature for electrophysiology experiments, a calibration curve was generated by identifying the voltage necessary to maintain a given solution temperature for values between 5 °C and 50 °C, in 5 °C increments. The temperature of the solution exiting the capillary was measured directly and the requisite voltage was noted. The calibration curve was almost perfectly linear in the 5–50 °C range. A line was fit to the data and the

resulting equation was used to calculate the voltage input required for the desired temperature.

For TRPM8 inhibition experiments, (1R,2S,5R)-(−)-menthol (Sigma) was dissolved in DMSO at a concentration of 650 mM and diluted to 500 µM in extracellular solution. Compound 103 was also dissolved in DMSO to 3.6 mM, then diluted to 1 µM in extracellular solution also containing 500 µM menthol. A serial dilution of compound 103 in 500 µM menthol-containing extracellular solution was performed to make solutions with the given concentration of inhibitor. Solutions were perfused using an Automate Multi-barrel Perfusion Pencil.

5.3 TRPV1 Thermosensitivity

5.3.1 Introduction

Transient Receptor Potential Vanilloid 1 (TRPV1) is a heat sensitive ion channel that is involved in a variety of physiological processes. The channel activates at elevated temperatures, with a half-maximal temperature of ~42 °C [2]. TRPV1 was the first of several thermosensitive ion channels discovered that allow somatic sensation of temperature in metazoans [3]. The channel is intrinsically heat sensitive, requiring no secondary messengers or cofactors [4]. The mechanism of thermosensation by the channel is not clearly understood, and it has been the subject of much investigation and debate since its initial discovery.

Thermosensitive TRP channels have evolved to sense a wide range of temperatures depending on the species and physiological context. For example, vampire bats express a shortened isoform of TRPV1 in their infrared-sensing trigeminal nerve

fibers that responds to a much lower temperature range, with a $T_{1/2}$ of ~34 °C, compared to ~42 °C for rat TRPV1 [5]. This drastic difference in thermosensing is caused by a C-terminal truncation of 62 residues. The short isoform is co-expressed with the canonical TRPV1 sequence in vampire bat trigeminal nerves, and measurements from heterologously co-expression of the two isoforms produced an intermediate thermal response. At the other end of the spectrum, TRPV1 from heat-tolerant squirrels and camels shows very little heat sensitivity; this physiological adaptation appears to be the basis of their ability to inhabit otherwise inhospitable environments [6]. The molecular basis of this loss of thermosensitivity comes down to a single amino acid change in one of the ankyrin repeat of the N terminus [6]. Evolutionary pressure also extends to other thermosensitive TRP channels; for example, the cold sensitivity of TRPM8 is correlated with the core body temperature of a species, with TRPM8 from cold water-dwelling frogs having a temperature response shifted to lower temperatures [7]. Winter hibernating rodents have also adapted to survival in cold temperatures in part due to attenuated cold response from their TRPM8 orotholog [8].

As shown in Table 5.1, literature values for the $\Delta H°$ of TRPV1 gating are highly variable. Furthermore, to date, there are no published values for the human TRPV1 ortholog. Given this variation and the paucity of data on the thermodynamic properties of human TRPV1, this study sought to measure the enthalpy of gating in human TRPV1.

5.3.2 Thermodynamics of TRPV1 Activation

Upon heating, a conformational change takes place in the TRPV1 channel, opening the ion-conducting pore and initiating action potentials that the brain interprets

as heat sensation. The details of this conformational change remain to be resolved, but the fundamental thermodynamic properties have been measured using electrophysiology techniques. Following is a brief treatment of the thermodynamics of thermosensing ion channel gating.

The open probability (P_O) of an ion channel can be described by a two-state sigmoidal Boltzmann function [9]:

$$P_O = \frac{1}{1 + e^{\frac{\Delta H^\circ}{RT} - \frac{\Delta S^\circ}{R}}} \quad (1)$$

From this equation, it can be seen that the temperature dependence of ion channel opening is related to the enthalpy change of channel opening. This sigmoidal curve is defined by two parameters: the midpoint of the curve ($T_{1/2}$, or the point at which P_O is equal to 0.5), and the steepness of the curve. Solving for $T_{1/2}$ shows that the midpoint will always be equal to $\Delta H^\circ/\Delta S^\circ$. Differentiating the function with respect to 1/T gives the relationship:

$$\frac{dP_O}{d\left(\frac{1}{T}\right)} = -P_O(1 - P_O)\frac{\Delta H^\circ}{R} \quad (2)$$

Thus, the steepness of the curve is determined by the value of ΔH°. All ion channels are nominally sensitive to temperature if a wide enough temperature range is considered, but to be biologically useful a thermosensing channel must have a narrow temperature range over which it will move from P_O near zero to P_O close to unity. In other words, the slope of its temperature response curve will be relatively steep. Figure 5.1 illustrates two instances of Equation 1 plotted with the same $T_{1/2}$ value but different values of ΔH°; the steeper red curve has a higher ΔH° than the shallower black curve. Temperature sensitive

TRP channels are therefore expected to have a relatively high $\Delta H°$ of channel opening compared to temperature insensitive channels. For comparison, $\Delta H°$ for the C-type inactivation process of the canonical voltage-gated potassium channel Shaker has been measured at ~17 kcal/mol [10], while $\Delta H°$ of nerve Na^+ channel opening was measured to be ~24 kcal/mol [11]. In contrast, $\Delta H°$ for TRPV1 activation has been measured in the range of ~65 to 150 kcal/mol, depending on the species and the conditions under which it is measured (Table 5.1). To determine the enthalpy of gating of human TRPV1 and place it in the context of published measurements of other species, temperature-controlled electrophysiology experiments were carried out.

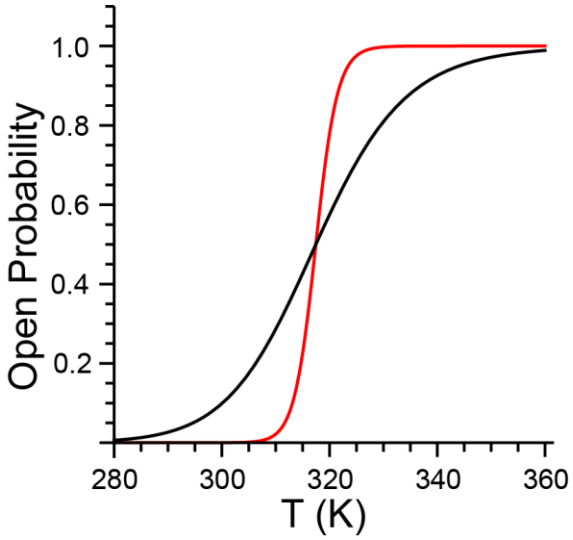

Figure 5.1 Calculated open probability curves for a temperature-sensitive channel (red, $\Delta H°$ = 98 kcal/mol) compared to a temperature-insensitive channel (black, $\Delta H°$= 24 kcal/mol). The red curve uses a value for TRPV1 gating enthalpy determined in this study, while the black curve uses a value for Na^+ channels [11].

Table 5.1 Literature values for $\Delta H°$ of TRPV1 channel gating.

Reference	$\Delta H°$ (kcal/mol)	Potential (mV)	Method	TRPV1 species	Protein Origin/ Membrane Type
This Study	98 ± 12	+60	Whole-cell	Human	HEK293/HEK293
[12]	64.9[a]	-70	Whole-cell	Rat	HEK293/HEK293
[13]	150 ± 13	-60	Inside-out	Rat	*X. laevis*/ *X. laevis*
[14]	26.8	+80	Inside-out	Murine	HEK293/HEK293
[2]	101 ± 4 65 ± 6	-60, +60	Outside-out	Rat	HEK293/HEK293
[15]	90 ± 3	-60	Whole-cell	Rat	HEK293/HEK293
[4]	86.2 ± 3.9	-60	Proteoliposome patch	Rat	Sf9 Insect cells/Soybean polar lipids
[16]	155	+100	Single-channel planar lipid bilayers	Rat	HEK293/3:1 POPC:POPE
[17]	65 ± 5.7[a]	-60	Whole-cell	Rat	*X. laevis*/ *X. laevis*
[18]	88 ± 8	+60	Inside-out	Rat	HEK293/HEK293

[a]The reported temperature coefficient (Q_{10}) was converted to $\Delta H°$ according to $\Delta H \approx 20 \ln Q_{10}$ [19].
[b] Protein was purified and reconstituted in proteoliposomes.

Human TRPV1 was heterologously expressed in HEK-293 cells, and whole-cell measurements were made at a range of temperatures from 20 °C up to ~50 °C. These measurements were made using two different experiments; in both methods, temperature was controlled by perfusing pre-warmed bath solution over the cells as currents were recorded. For the first set of experiments, cells were perfused until temperature and current was stable, then current was recorded with a voltage pulse at +60 mV (Figure 5.2A). These measurements were made from 20 °C to 50 °C in 5 °C increments. Steady state current magnitudes were plotted as a function of temperature.

Under steady state conditions, the channel can be considered in equilibrium between the open and closed states, with equilibrium constant *K*, which can be written as the fraction of the concentration of the open state (α):

$$K = \frac{[\text{open}]}{[\text{closed}]} = \frac{\alpha}{1-\alpha} \quad (3)$$

K is also related to the change in Gibb's free energy between the open and closed states in the familiar equation:

$$\Delta G° = -RT\ln(K) \quad (4)$$

$\Delta G°$ is related to the change in enthalpy ($\Delta H°$) and entropy ($\Delta S°$) between states:

$$\Delta G° = \Delta H° - T\Delta S° \quad (5)$$

At the midpoint temperature ($T_{1/2}$) of the transition between open and closed states, the concentrations of the two states are equal, *K* is equal to 1, and $\Delta G°$ is equal to 0 by equation 4. Then according to equation 5 $\Delta S°$ can be written in terms of $T_{1/2}$:

$$\Delta S° = \frac{\Delta H°}{T_{\frac{1}{2}}} \quad (6)$$

Combining equations 4, 5, and 6, *K* can be written in terms of the change in enthalpy ($\Delta H°$), temperature (*T*), and midpoint temperature ($T_{1/2}$):

$$K = e^{\left(\frac{\Delta H°}{RT}\right)\left(\frac{T}{T_{\frac{1}{2}}}-1\right)} \quad (7)$$

Rearranging equation 3 yields:

$$\alpha = \frac{K}{1+K} \quad (8)$$

Assuming that the measured steady-state current is directly proportional to the number of open channels, the following mathematical description can be written:

$$I = \alpha(I_{max} - I_{min}) + I_{min} \quad (9)$$

where I is the current at a given temperature, I_{max} is the maximum measured current, and I_{min} is the smallest measured current. Whole-cell measurements of heterologously expressed channels in HEK-293 cells always feature a baseline amount of current from endogenous ion channels. Fitting steady state current measured at range of temperatures to this two-state model yields values for the enthalpy change of the closed to open transition (which reflects the slope of the sigmoidal curve, a measure of the temperature sensitivity of the channel) and the midpoint temperature (which reflects the temperature range over which the channel is sensitive). Fitting steady-state currents to equation 9 yielded a $\Delta H°$ of 98 ± 12 kcal/mol (Figure 5.2B), in the general range of values previously reported in the literature (Table 5.1).

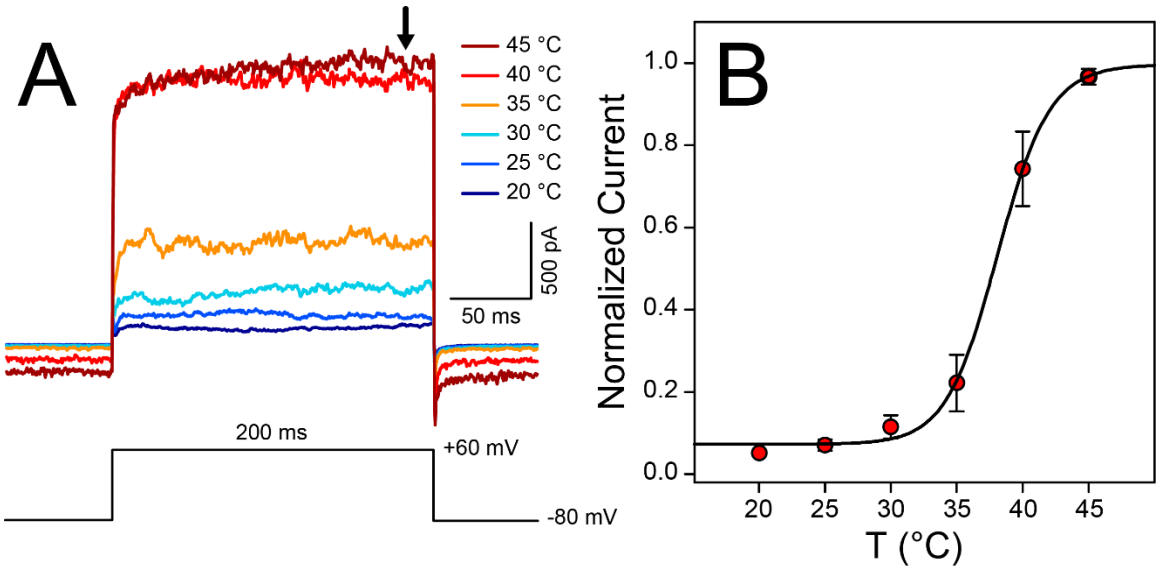

Figure 5.2 Temperature-controlled electrophysiology measurements of human TRPV1. (A) Representative current traces from a single cell. Membrane potential was held at -80 mV and briefly pulsed to +60 mV for the series of temperatures shown. (B) Steady state currents at each temperature (taken at the time point marked by the arrow in (A)) from 7 individual cells were plotted and fit to a two-state model (Equation 9) to extract $\Delta H°$, which was found to be 98 ± 12 kcal/mol, with a $T_{1/2}$ of 38 ± 0.3 °C. Error bars in (B) represent standard error of the mean.

To corroborate the Δ*H*° values measured by the temperature step method illustrated in Figure 5.2, a second method was used in which TRPV1-expressing HEK-293 cells were subjected to continuous temperature ramps. Membrane potential was clamped at +60 mV and current was continuously recorded while the temperature of the solution was ramped from 20 to ~50 °C. The currents were then plotted as a function of temperature (Figure 5.3A). The full temperature response of TRPV1 is difficult to experimentally interrogate due to biological limitations at high temperatures. In this case, the first part of the sigmoidal curve can be approximated by a simplified Boltzmann exponential [9]:

$$P_O = e^{-\frac{\Delta H}{RT}+\frac{\Delta S}{R}} \quad 10$$

This function assumes an equilibrium between the open and closed states. The temperature ramp used here had a heating rate of ~1 °C/s; because TRPV1 has a heat activation time constant in the low millisecond time regime, these measurements were considered to be pseudo steady-state [20]. The calculated Δ*H*° value using this method was 93 ±13 kcal/mol (*n* = 2), in good agreement with that measured using the steady-step temperature step method described above.

5.3.3 Heat Inactivation of Human TRPV1

Recently, it has been reported that heat activation of TRPV1 leads to an irreversible inactivated state of the channel [18]. Patches that had previously been exposed to high temperatures showed decreased maximum current, decreased activation rate, and a decrease in the enthalpy associated with channel opening. This inactivation resulted in a substantially lower heat response and reflects a decrease in Δ*H*° of

activation, from ~90 kcal/mol in channels not previously exposed to high temperatures, to ~17 kcal/mol after heat stimulation, on par with temperature-insensitive channels. These studies were performed using rat TRPV1 expressed in HEK-293 cells.

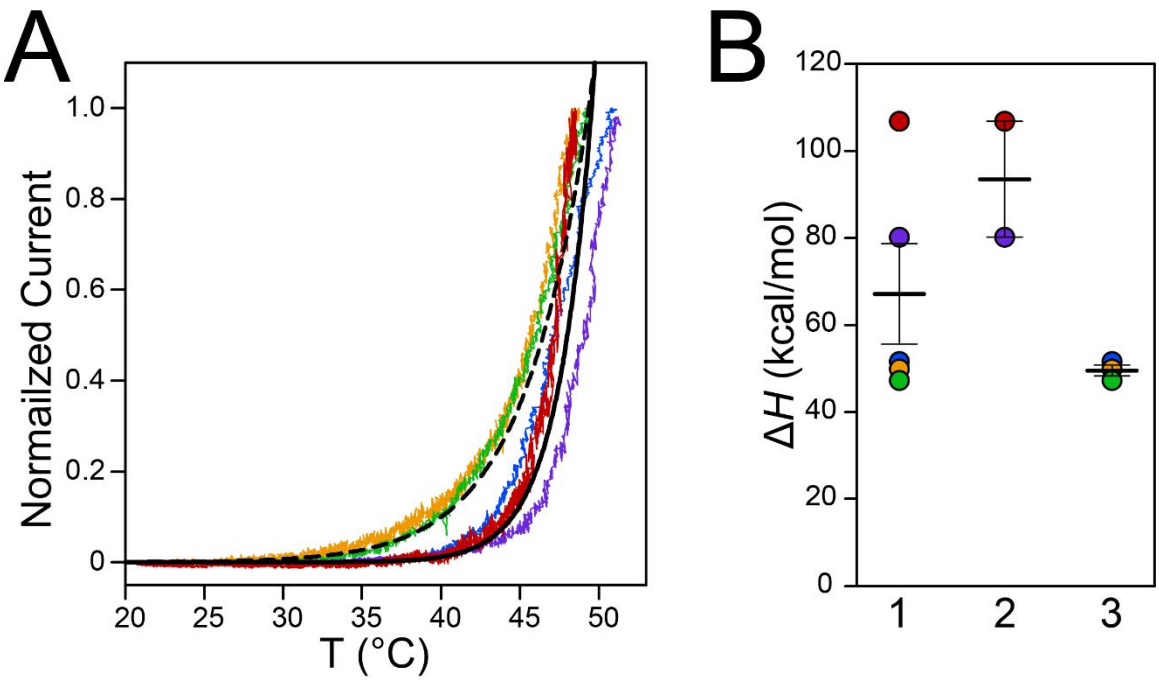

Figure 5.3 (A) Currents were measured as temperature was gradually increased from 20 to 50 °C over ~30 seconds. Each color represents a trace from a different cell (n = 5). Traces were fit individually to (Equation 10), and the average $\Delta H°$ and $\Delta S°$ values from these fits were used to plot the black solid line (average of red and violet traces, not previously exposed to heat) and dashed line (average of blue, green, and orange traces, previously exposed to heat). (B) Calculated $\Delta H°$ values for 1) all five cells (average $\Delta H°$ = 67 ± 26 kcal/mol), 2) cells that were not previously exposed to warm temperatures before temperature ramp recordings (average $\Delta H°$ = 93 ± 19 kcal/mol and 3) cells that were previously heat exposed (average $\Delta H°$ = 50 ± 2 kcal/mol). Thick black lines represent the mean, and colors of the data points correspond to the individual traces in (A). Error bars represent standard error of the mean.

To test whether this heat inactivation mechanism is present in human TRPV1, a second set of temperature ramp measurements were made on cells that had previously been exposed to a series of temperature increases from 20 to 50 °C before the temperature ramp was recorded. Consistent with the results from rat TRPV1, $\Delta H°$ for the

heat-exposed cells showed a clear decrease to 49.5 ± 1.3 kcal/mol (n = 3, Figure 5.3B), compared to $\Delta H°$ of 93 ±13 kcal/mol for cells that had not been previously subjected to warm temperatures. These results indicated that human TRPV1 has a heat inactivation mechanism similar to rat TRPV1 [18].

The $\Delta H°$ values of heat-induced gating of TRPV1 as measured by the two methods reported here are generally in agreement; however, some discrepancies must be pointed out. The temperature step method shown in Figure 5.2 resulted in a saturating maximum current as the temperature approached 45 °C. This is in contrast to the results from current ramps shown in Figure 5.3, which continued on an exponential curve at temperatures between 45 to 50 °C. Additionally, the $T_{1/2}$ values between the two sets of experiments are clearly different. Although the temperature ramp measurements do not reveal an accurate value of $T_{1/2}$ because the currents do not reach an inflection point, they are clearly shifted several degrees higher than the ~38 °C $T_{1/2}$ calculated from the temperature step measurements. These discrepancies in the results of the two measurement methods are likely caused by heat inactivation of TRPV1 channels during the longer heat exposures required to complete the temperature step measurements. The temperature ramp measurements were completed over the course of ~1 minute, much shorter than the several minutes it took to complete temperature step measurements. Therefore the leveling of the curve in Figure 5.2B may be due to a fewer number of active channels as an increasing number of channels became heat inactivated over the course of the measurements.

5.3.4 The R557A Mutation Abolishes TRPV1 Heat Sensitivity

NMR experiments using ^{15}N NOESY-TROSY showed that R557 in the TRPV1 S1–S4 domain normally resides within the membrane mimic; however, at elevated temperatures (~45 °C) a water cross-peak appears in the spectrum, indicating that R557 becomes solvent-exposed (Van Horn lab, unpublished data). To test whether this residue has a functional role in temperature sensing, a human TRPV1 R557A mutant was generated and transiently expressed in HEK-293 cells. Currents from the mutant and from wild-type TRPV1 were measured at different temperatures. Consistent with previous studies using rat TRPV1 [21], this mutant showed no significant response to elevated temperatures that evoked robust currents in wild-type TRPV1 (Figure 5.4). These functional experiments support the notion that R557 is important for TRPV1 thermosensation.

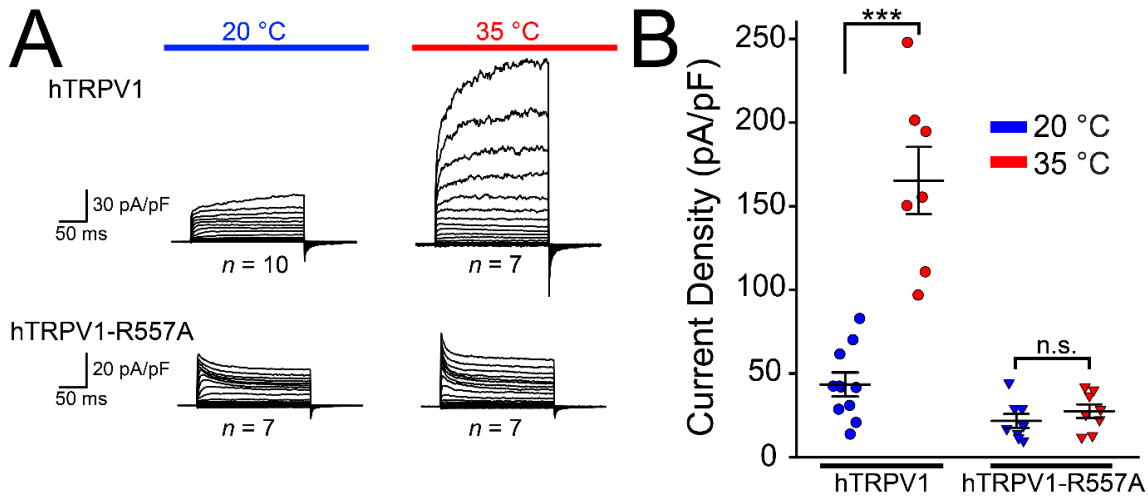

Figure 5.4 The role of R557 in heat sensitivity. (A) Average traces from the indicated number of cells expressing wild-type or R557A TRPV1 measured at potentials from -100 to +100 mV in 10 mV steps. (B) Steady-state current density from individual cells used to generate the traces in (A). As expected, wild-type TRPV1 showed robust response at 35 °C (Student's *t*-test, $p = 0.00002$), while the R557A mutant showed no significant change ($p = 0.194$). Error bars represent standard error of the mean.

5.4 Probing TRPM8 Cold Sensing With TRPM2-TRPM8 Chimeras

Much energy has been expended in the effort to understand mechanisms of thermosensation by TRP channels, but the domains and conformational changes involved are not fully understood. However, the theoretical thermodynamic framework for temperature sensitive proteins was expounded by Clapham and Miller [19]. In brief, because a conformational change of a protein involves a change in molar heat capacity (ΔC_p), thermodynamics imposes that $\Delta H°$ and $\Delta S°$ for that process are both temperature dependent. This results in a U-shaped curve of ln(K) as a function of temperature, where K represents the equilibrium constant between open and closed states of the channel. The curve is greater for larger values of ΔC_p; thus, the conformational change associated with temperature-dependent TRP channel gating must involve relatively large values of ΔC_p. These changes in heat capacity are the result of hydrophobic moieties becoming exposed to water as the protein changes conformation [19]. As large tetrameric complexes, TRP channels contain many such moieties available to contribute to this phenomenon.

This hypothesis was tested empirically by Chowdhury et al. using the canonical voltage-sensitive potassium channel known as Shaker K_V [22]. This channel shows very little native temperature sensitivity. Eight polar residues within the voltage-sensing domain of Shaker were identified as likely to become solvent-exposed upon channel activation. Two of these residues, Y323 and E293, showed correlation between polarity of the substituted residue and temperatures sensitivity of the channel. Furthermore, combining two mutations that individually result in a more temperature sensitive channel caused a marked increase in temperature sensitivity. This result is expected if the

mutations indeed increase ΔC_p for channel gating; since ΔC_p is an additive property, the combination of two mutants should increase ΔC_p further and lead to a steeper slope in the ln(K) versus temperature curve.

It is noteworthy that all the residues tested by Chowdhury et al. reside in the voltage-sensing domain of the channel, suggesting that, although the thermodynamic principles apply to the system as a whole, the molecular determinants can plausibly be contained in a relatively small domain of the channel. This possibility is further strengthened by a second study from Zhang et al. [17], in which the pore domain of the rat TRPV1 was exchanged into the scaffold of the Shaker K_V channel. The resulting channel is heat-sensitive, with a Q_{10} value similar to that of wild-type TRPV1 (40.8 ± 7.5 for the pore domain-exchanged channel versus 26 ± 7.4 for wild-type rat TRPV1). These data suggest that discreet domains are plausibly responsible for temperature sensing in TRP channels.

TRP channels are structurally homologous but functionally diverse in temperature and ligand sensitivity. In such systems, chimeric channels, in which a region from one ortholog is genetically exchanged for a homologous region from a channel with a different functional property, can prove useful in probing which domains of the channel are important for a given function. For example, chimeras between vanilloid-sensitive mammalian TRPV1 and vanilloid-insensitive avian TRPV1 channels were used to identify the residues involved in binding vanilloid ligands [23]; a similar approach was used to find the functional determinants of icilin sensitivity in mammalian TRPM8 versus icilin-insensitive chicken TRPM8 [24]. In Chapter 3 of this dissertation, human/mouse

chimeras were used to show that the transmembrane domain is key to species specific modulation of TRPM8 by PIRT [25].

The nearest relative to TRPM8 is TRPM2 (Figure 1.1); the human orthologs of these two channels share ~43% sequence identity overall, and ~49% identity within the transmembrane region and post-S6 TRP helix (Figure 5.5). Despite its sequence similarity with TRPM8, TRPM2 is activated by warm temperatures above ~40 °C [26]. It has been characterized as a possible somatic warm sensor in mice, with other temperature-dependent roles in body temperature and circadian rhythm regulation [27, 28]. Given that TRPM2 is closely related to TRPM8 yet not sensitive to cold temperatures, it may be possible to create a cold-sensitive chimeric channel by exchanging the right TRPM8 region into a TRPM2 scaffold. Such a channel could provide valuable insight into the regions of TRPM8 that are important for thermosensing.

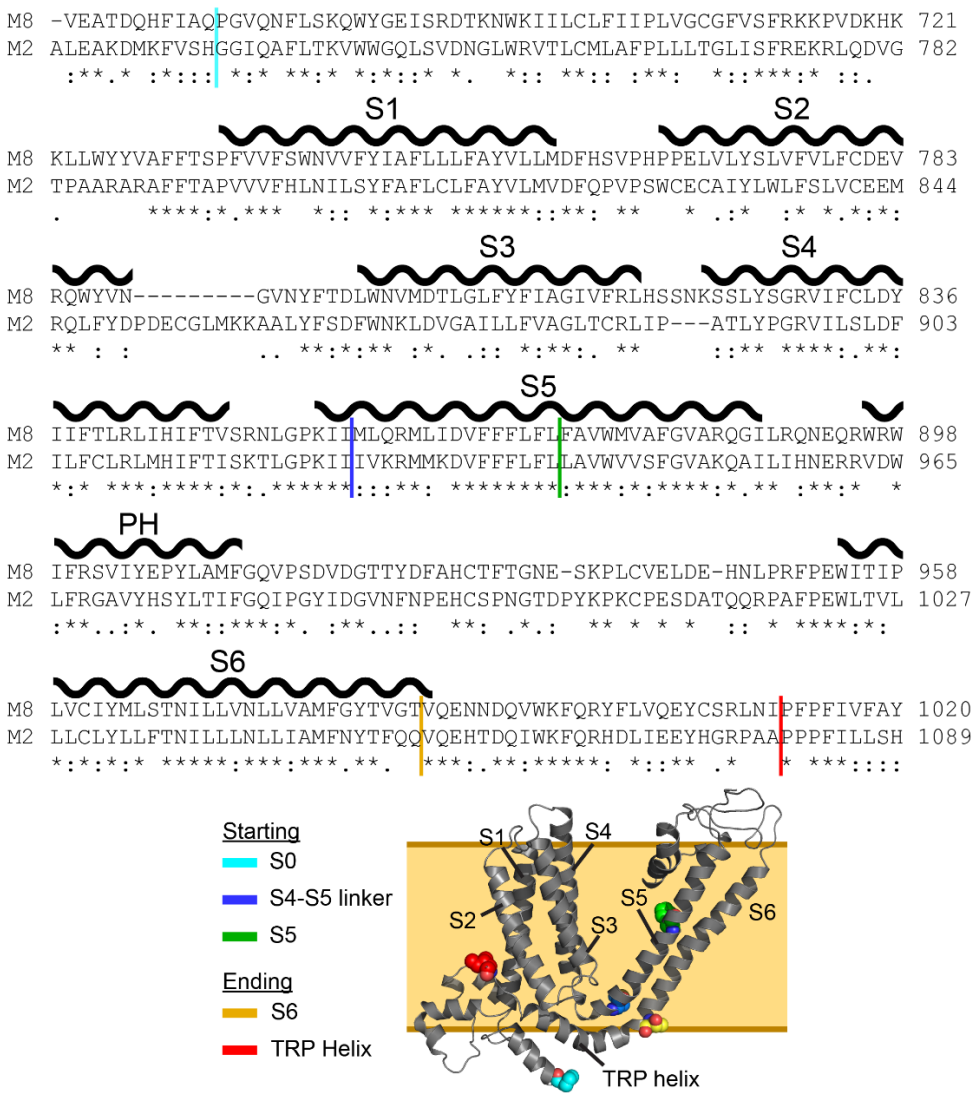

Figure 5.5 Sequence alignment between human TRPM8 and TRPM2 transmembrane domains. Transmembrane helices S1–S6 and the pore helix (PH) as determined from the cryo-EM structure of *Ficedula albicollis* TRPM8 are indicated. Chimeric region beginning and ending sites are indicated by colored lines. Corresponding residues are shown on a single subunit of a human TRPM8 homology model.

To this end, four chimeric channels were generated incorporating varying regions of the TRPM8 transmembrane domain into a TRPM2 scaffold. A sequence alignment was generated with Clustal Omega software, and homologous sequences were selected to generate one chimera exchanging the entire transmembrane domain from TRPM8, and three other chimeras exchanging varying regions of the pore domain from TRPM8

(Figure 5.6). Each was tested by whole-cell patch-clamp electrophysiology in HEK-293 cells. Preliminary recordings were made at room temperature to establish baseline currents. The cells were then stimulated with cold perfusate at 15 °C, then 500 µM menthol at room temperature (23 °C). A final recording was made after washing out the menthol with room temperature perfusate. The results are summarized in (Figure 5.7). None of the chimeras showed obvious cold or menthol sensitivity, although caution is warranted in interpreting these data as only one cell was measured for each chimera.

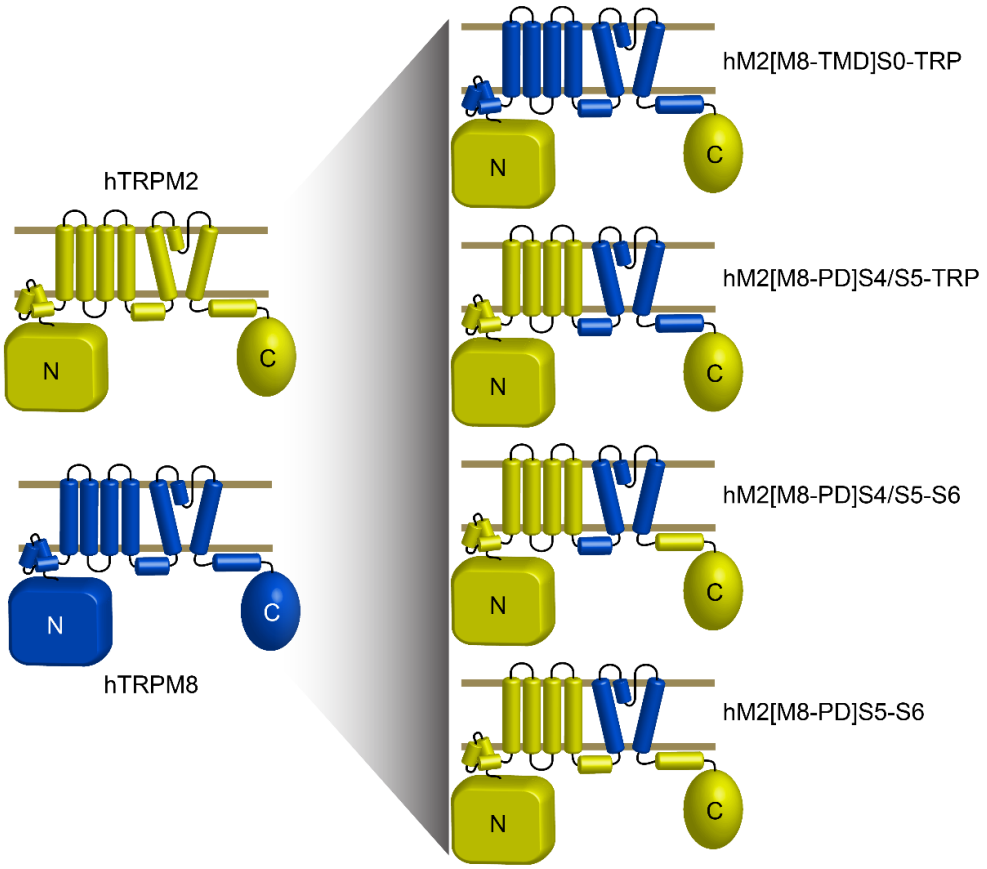

Figure 5.6 Topology plots of TRPM2/TRPM8 chimeras. With human TRPM2 as the scaffold, four different chimeras were made exchanging the indicated regions from human TRPM8.

It is not uncommon for chimeric channels to be nonfunctional; newly introduced sequences can disrupt trafficking to the plasma membrane or interfere with functional

mechanisms that are delicately balanced in the wild-type channel [29, 30]. This is particularly true when homology alignments are not precise due to, for example, lack of structural information. At the time these chimeras were generated and tested in early 2017, no high-resolution structures of channels from the TRPM family had been published. Therefore, the selection of chimeric sequences was inferred based on other methods, including sequence alignment to TRPV1, which has several published structures [31-33], and homology modeling of TRPM8 to TRPV1. After these chimeras were made and tested, a cryo-EM structure of TRPM8 from the collared flycatcher (*Ficedula albicollis*) was published, giving more structural information on these chimeras. The location of chimeric start and stop sequences are shown in Figure 5.5 along with updated transmembrane helix locations based on the TRPM8 structure (PDB: 6BPQ) and a human homology model. The chimeric sequences selected as the beginning of the transmembrane domain and the end of S6 agree well with the structural data. On the other hand, the beginning of the S4-S5 linker likely should have be selected earlier in the sequence, possibly at Asn852 or Leu853. The beginning of S5 was likewise selected too late in the sequence; according to the structure it should be closer to Lys856. In future work, it may be possible to make functional chimeras by taking these newer structural data into account.

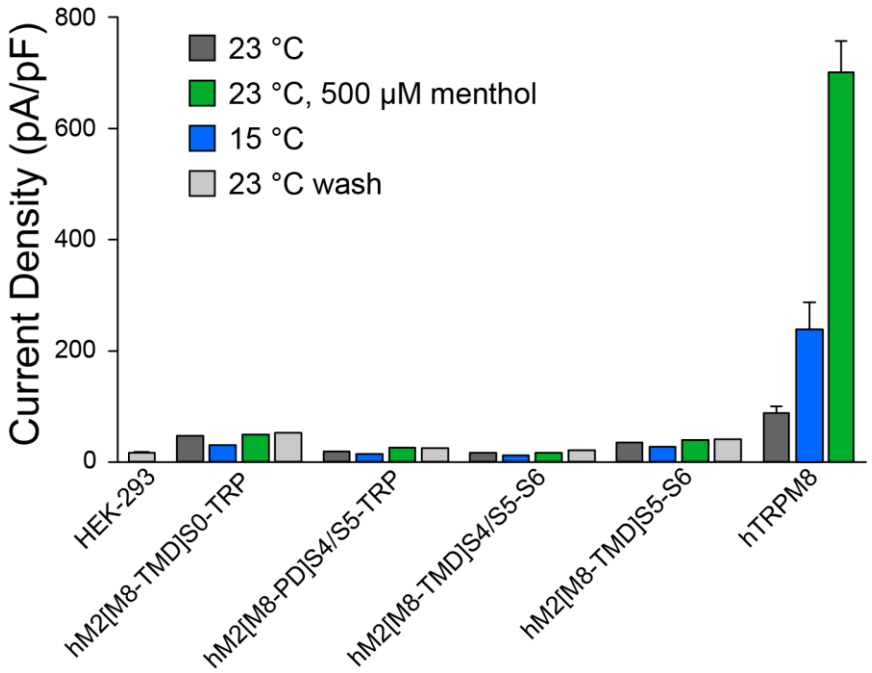

Figure 5.7 Electrophysiology measurements of TRPM2/TRPM8 chimeras. Values were taken from steady state current during a +100 mV voltage pulse and normalized to the measured capacitance of the cell (HEK-293, n = 9; hTRPM8, n = 8; chimeras, n = 1). A baseline measurement (dark gray bars) at room temperature was taken. Cells were then subjected to perfusate pre-cooled to 15 °C (blue), followed by a 500 µM menthol solution at 23 °C (green). Cells were then washed with regular bath solution at 23 °C (light gray). The chimeras do not show obvious sensitivity to cold temperatures or menthol.

5.5 TRPM8 Compound 103 Antagonism

Beyond the temperature sensitivity discussed above, TRP channels are also sensitive to other diverse stimuli. Like other ion channels TRP channels can be activated or inhibited by a variety of ligands [34]. Given their broad role in physiology and potential for modulation by small molecules, TRP channels have long been an attractive target for pharmacological interventions [35]. In particular, TRPM8 is a potential target for a variety of conditions including bladder disorders [36, 37], obesity or weight regulation [38], and several types of cancer [39]. However, one factor limiting

therapeutic targeting of TRPM8 has been the availability of potent, selective antagonists [40].

To help address this gap, tested the potency of compound 103 (C103), a novel TRPM8 antagonist (Figure 5.8). Whole-cell patch-clamp electrophysiology was used to more directly probe the potency of this antagonist against TRPM8. Human TRPM8 was expressed in HEK-293 cells and a series of solutions containing 500 µM menthol and C103 at different concentrations was tested. As shown in Figure 5.9, C103 inhibited menthol-evoked currents in a dose-response manner, with an IC_{50} of 64 ± 2 nM. The discrepancy between IC_{50} in Ca^{2+} imaging and whole-cell patch-clamp measurements, and between competitive antagonism of icilin versus menthol, highlights how different experimental conditions and techniques can give different results. These differences should be taken into account when assessing the ligand in question.

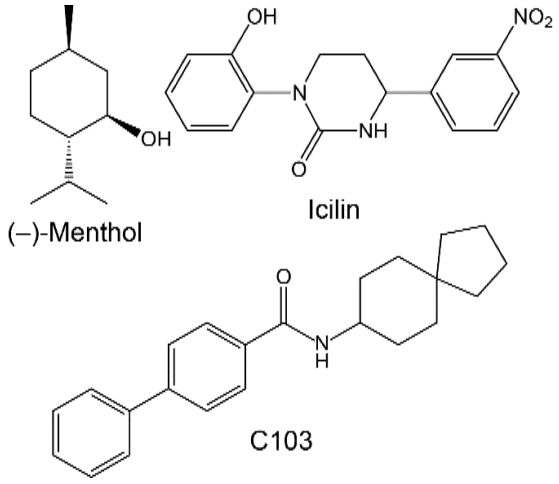

Figure 5.8 Chemical structures of TRPM8 agonists menthol and icilin, and antagonist Compound 103.

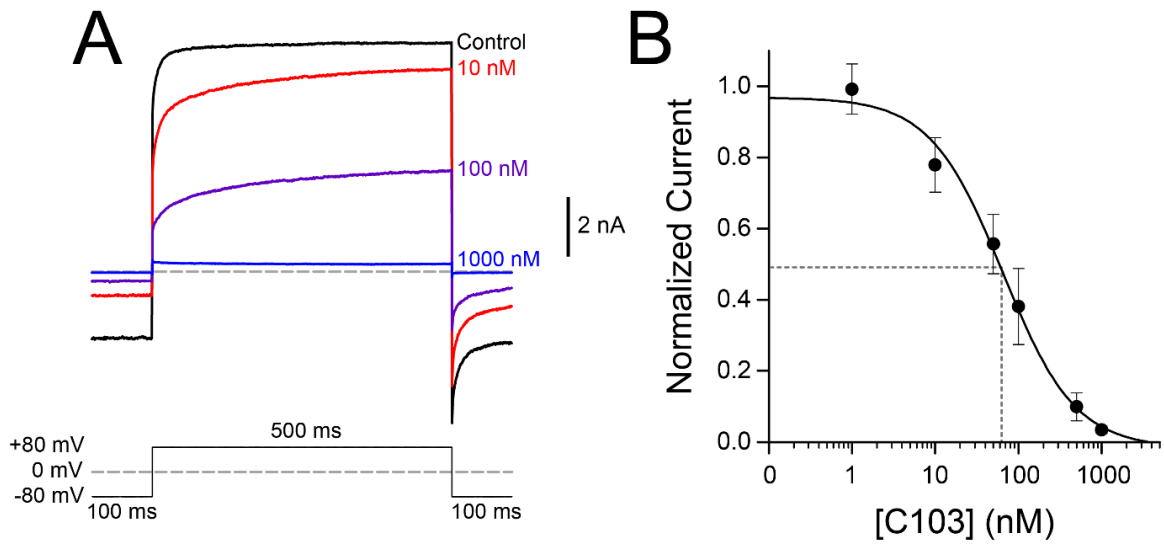

Figure 5.9 Inhibition of menthol-evoked TRPM8 currents by C103. Currents were measured by whole-cell patch-clamp electrophysiology of HEK-293 cells transiently transfected with human TRPM8. (A) Average current traces (n = 4) measured by a +80 mV voltage pulse upon exposure to a saturating concentration of 500 µM menthol and varying concentrations of Compound 103. (B) Dose response of C103 measured at concentrations from 1 nM to 1 µM at +80 mV. Current response was normalized to the maximum current magnitude measured without antagonist for each cell. Data was fit with a single binding site Hill equation, and the IC_{50} was calculated to be 64 ± 2 nM (n = 6 cells). Error bars represent standard error of the mean.

5.6 References

1. Miyazaki, K. (2011) MEGAWHOP cloning: a method of creating random mutagenesis libraries via megaprimer PCR of whole plasmids. *Methods Enzymol.* **498**, 399-406

2. Yao, J., Liu, B., and Qin, F. (2010) Kinetic and energetic analysis of thermally activated TRPV1 channels. *Biophys. J.* **99**, 1743-1753

3. Vriens, J., Nilius, B., and Voets, T. (2014) Peripheral thermosensation in mammals. *Nature reviews. Neuroscience* **15**, 573-589

4. Cao, E., Cordero-Morales, J. F., Liu, B., Qin, F., and Julius, D. (2013) TRPV1 channels are intrinsically heat sensitive and negatively regulated by phosphoinositide lipids. *Neuron* **77**, 667-679

5. Gracheva, E. O., Cordero-Morales, J. F., Gonzalez-Carcacia, J. A., Ingolia, N. T., Manno, C., Aranguren, C. I., Weissman, J. S., and Julius, D. (2011) Ganglion-specific splicing of TRPV1 underlies infrared sensation in vampire bats. *Nature* **476**, 88-91

6. Laursen, W. J., Schneider, E. R., Merriman, D. K., Bagriantsev, S. N., and Gracheva, E. O. (2016) Low-cost functional plasticity of TRPV1 supports heat tolerance in squirrels and camels. *Proc. Natl. Acad. Sci. U. S. A.* **113**, 11342-11347

7. Myers, B. R., Sigal, Y. M., and Julius, D. (2009) Evolution of Thermal Response Properties in a Cold-Activated TRP Channel. *PLoS One* **4**, e5741

8. Matos-Cruz, V., Schneider, E. R., Mastrotto, M., Merriman, D. K., Bagriantsev, S. N., and Gracheva, E. O. (2017) Molecular Prerequisites for Diminished Cold Sensitivity in Ground Squirrels and Hamsters. *Cell reports* **21**, 3329-3337

9. Feng, Q. (2014) Temperature sensing by thermal TRP channels: thermodynamic basis and molecular insights. *Curr. Top. Membr.* **74**, 19-50

10. Meyer, R., and Heinemann, S. (1997) Temperature and pressure dependence of *Shaker* K^+ channel N- and C-type inactivation. *Eur. Biophys. J.* **26**, 433-445

11. Correa, A. M., Bezanilla, F., and Latorre, R. (1992) Gating kinetics of Batrachotoxin-modified Na^+ channels in the squid giant axon. *Biophys. J.* **61**, 1332-1352

12. Vlachova, V., Teisinger, J., Sušánková, K., Lyfenko, A., Ettrich, R., and Vyklicky, L. (2003) Functional Role of C-Terminal Cytoplasmic Tail of Rat Vanilloid Receptor 1. *J. Neurosci.* **23**, 1340-1350

13. Liu, B., Hui, K., and Qin, F. (2003) Thermodynamics of Heat Activation of Single Capsaicin Ion Channels VR1. *Biophys. J.* **85**, 2988-3006

14. Yang, F., Cui, Y., Wang, K., and Zheng, J. (2010) Thermosensitive TRP channel pore turret is part of the temperature activation pathway. *Proc. Natl. Acad. Sci. U. S. A.* **107**, 7083-7088

15. Yao, J., Liu, B., and Qin, F. (2011) Modular thermal sensors in temperature-gated transient receptor potential (TRP) channels. *Proc. Natl. Acad. Sci. U. S. A.* **108**, 11109-11114

16. Sun, X., and Zakharian, E. (2015) Regulation of the temperature-dependent activation of transient receptor potential vanilloid 1 (TRPV1) by phospholipids in planar lipid bilayers. *J. Biol. Chem.* **290**, 4741-4747

17. Zhang, F., Jara-Oseguera, A., Chang, T. H., Bae, C., Hanson, S. M., and Swartz, K. J. (2018) Heat activation is intrinsic to the pore domain of TRPV1. *Proc. Natl. Acad. Sci. U. S. A.* **115**, E317-E324

18. Sanchez-Moreno, A., Guevara-Hernandez, E., Contreras-Cervera, R., Rangel-Yescas, G., Ladron-de-Guevara, E., Rosenbaum, T., and Islas, L. D. (2018) Irreversible temperature gating in trpv1 sheds light on channel activation. *eLife* **7**, e36372

19. Clapham, D. E., and Miller, C. (2011) A thermodynamic framework for understanding temperature sensing by transient receptor potential (TRP) channels. *Proc. Natl. Acad. Sci. U. S. A.* **108**, 19492-19497

20. Yao, J., Liu, B., and Qin, F. (2009) Rapid temperature jump by infrared diode laser irradiation for patch-clamp studies. *Biophys. J.* **96**, 3611-3619

21. Boukalova, S., Marsakova, L., Teisinger, J., and Vlachova, V. (2010) Conserved residues within the putative S4-S5 region serve distinct functions among thermosensitive vanilloid transient receptor potential (TRPV) channels. *J Biol Chem* **285**, 41455-41462

22. Chowdhury, S., Jarecki, B. W., and Chanda, B. (2014) A molecular framework for temperature-dependent gating of ion channels. *Cell* **158**, 1148-1158

23. Jordt, S. E., and Julius, D. (2002) Molecular Basis for Species-Specific Sensitivity to "Hot" Chili Peppers. *Cell* **108**, 421-430

24. Chuang, H. H., Neuhausser, W. M., and Julius, D. (2004) The super-cooling agent icilin reveals a mechanism of coincidence detection by a temperature-sensitive TRP channel. *Neuron* **43**, 859-869

25. Hilton, J. K., Salehpour, T., Sisco, N. J., Rath, P., and Van Horn, W. D. (2018) Phosphoinositide-interacting regulator of TRP (PIRT) has opposing effects on human and mouse TRPM8 ion channels. *J. Biol. Chem.* **293**, 9423-9434

26. Togashi, K., Hara, Y., Tominaga, T., Higashi, T., Konishi, Y., Mori, Y., and Tominaga, M. (2006) TRPM2 activation by cyclic ADP-ribose at body temperature is involved in insulin secretion. *EMBO J.* **25**, 1804-1815

27. Tan, C. H., and McNaughton, P. A. (2016) The TRPM2 ion channel is required for sensitivity to warmth. *Nature* **536**, 460-463

28. Song, K., Wang, H., Kamm, G. B., Pohle, J., Fernanda de Castro, R., Heppenstall, P., Wende, H., and Siemens, J. (2016) The TRPM2 channel is a hypothalamic heat sensor that limits fever and can drive hypothermia. *Science* **353**, 1393-1398

29. Voets, T., Owsianik, G., Janssens, A., Talavera, K., and Nilius, B. (2007) TRPM8 voltage sensor mutants reveal a mechanism for integrating thermal and chemical stimuli. *Nat. Chem. Biol.* **3**, 174-182

30. Kalia, J., and Swartz, K. J. (2013) Exploring structure-function relationships between TRP and Kv channels. *Scientific reports* **3**, 1523

31. Cao, E., Liao, M., Cheng, Y., and Julius, D. (2013) TRPV1 structures in distinct conformations reveal activation mechanisms. *Nature* **504**, 113-118

32. Gao, Y., Cao, E., Julius, D., and Cheng, Y. (2016) TRPV1 structures in nanodiscs reveal mechanisms of ligand and lipid action. *Nature* **534**, 347-351

33. Liao, M., Cao, E., Julius, D., and Cheng, Y. (2013) Structure of the TRPV1 ion channel determined by electron cryo-microscopy. *Nature* **504**, 107-112

34. Calixto, J. B., Kassuya, C. A., Andre, E., and Ferreira, J. (2005) Contribution of natural products to the discovery of the transient receptor potential (TRP) channels family and their functions. *Pharmacol. Ther.* **106**, 179-208

35. Kaneko, Y., and Szallasi, A. (2014) Transient receptor potential (TRP) channels: a clinical perspective. *Br. J. Pharmacol.* **171**, 2474-2507

36. Beccari, A. R., Gemei, M., Lo Monte, M., Menegatti, N., Fanton, M., Pedretti, A., Bovolenta, S., Nucci, C., Molteni, A., Rossignoli, A., Brandolini, L., Taddei, A., Za, L., Liberati, C., and Vistoli, G. (2017) Novel selective, potent naphthyl TRPM8 antagonists identified through a combined ligand- and structure-based virtual screening approach. *Scientific reports* **7**, 10999

37. Aizawa, N., Ohshiro, H., Watanabe, S., Kume, H., Homma, Y., and Igawa, Y. (2019) RQ-00434739, a novel TRPM8 antagonist, inhibits prostaglandin E2-induced hyperactivity of the primary bladder afferent nerves in rats. *Life Sci.* **218**, 89-95

38. Ma, S., Yu, H., Zhao, Z., Luo, Z., Chen, J., Ni, Y., Jin, R., Ma, L., Wang, P., Zhu, Z., Li, L., Zhong, J., Liu, D., Nilius, B., and Zhu, Z. (2012) Activation of the cold-sensing TRPM8 channel triggers UCP1-dependent thermogenesis and prevents obesity. *J. Mol. Cell. Biol.* **4**, 88-96

39. Yee, N. S. (2016) TRPM8 Ion Channels as Potential Cancer Biomarker and Target in Pancreatic Cancer. *Adv. Protein Chem. Struct. Biol.* **104**, 127-155

40. Journigan, V. B., and Zaveri, N. T. (2013) TRPM8 ion channel ligands for new therapeutic applications and as probes to study menthol pharmacology. *Life Sci.* **92**, 425-437

CHAPTER 6

SUMMARY AND CONCLUSIONS

TRP channels are complex polymodal sensors that play crucial roles in physiology. The fifty years since the discovery of the first TRP channel in *Drosophila* have seen great progress in understanding their function and structure. The work presented here contributes to that understanding with experiments to investigate regulation of TRP channels by temperature, by small molecule ligands, and by the modulatory subunit PIRT.

Chapter 2 of this work discusses the role of thermosensitive TRP channels in physiology. Although they are best known for as the primary somatic thermosensors, these channels also involved in a variety of other related processes. Body temperature regulation requires detecting and responding to the internal and external environment of the organism, and these channels are key to that process. This regulation intersects with other physiological processes including body weight regulation and nociception via interaction with opioid receptors. Species diversity between orthologs presents a challenge in experimentally studying these channels and must be taken into account when designing experiments and interpreting results. The molecular mechanism of intrinsic thermosensation by TRP channels to date remains unclear, and Chapter 2 discusses suitable methods of probing this mechanism, such as calorimetry, spectroscopic techniques, structure determination by cryo-EM and X-ray crystallography, and molecular dynamics simulations.

Chapter 3 presents a specific example of TRP channel speciation in a study of the TRPM8 modulatory subunit PIRT. In contrast to previously reported results from mouse studies in which TRPM8 activity is potentiated by PIRT, human PIRT has an attenuating effect on the human ortholog of the channel. PIRT was shown to bind directly to the S1–S4 domain of TRPM8 *in vitro*, with an apparent binding stoichiometry of one PIRT molecule per TRPM8 subunit. Chimeric ion channels demonstrate that the transmembrane domain is key to regulation by PIRT and suggest specific residues that may be important for this regulation. The species-dependent regulation of TRPM8 by PIRT, when considered in the context of other functional speciation of TRP channels, implies that care must be taken when designing experiments and interpreting results in the literature. At the same time, leveraging differences between species can be a useful tool to identify the molecular basis of channel function, as shown with the chimera experiments presented here.

In Chapter 4, a novel mutation in TRPM8 that selectively removes icilin sensitivity is demonstrated. The N852A mutation, at the junction between S4 and the S4-S5 linker, causes a general attenuation of cold- and menthol-evoked channel currents, with a small decrease in menthol sensitivity. However, the potent TRPM8 agonist icilin shows little response in the N852A mutant. NMR experiments with the purified S1–S4 domain from TRPM8 confirm that icilin still binds to this domain; therefore, the mutation appears to disrupt the transduction of the binding event to pore opening. Recently published structures of TRPM8 bound to icilin reveal that the binding causes the bottom of S4 to transition from α- to 3_{10}-helical; this transition moves N852 from the capping

helical position to a loop between S4 and S5. One possible reason for the observed icilin insensitivity in the mutant is that it interferes with this structural transition. Close inspection of the apo and bound structures may suggest coupling mechanisms that could be tested with rational mutations of other residues.

Chapter 5 explores the thermodynamics of TRPV1 heat sensitivity. Temperature-controlled electrophysiology experiments were used to measure the enthalpy of TRPV1 gating in human TRPV1, which has not been previously reported in the literature. Consistent with studies using rat TRPV1, human TRPV1 shows evidence of hysteresis and heat-induced inactivation. In a separate set of experiments, four chimeric channels between cold-sensitive TRPM8 and warm-sensitive TRPM2 were generated to identify regions in the transmembrane domain that may be important for thermosensing. None of these chimeras resulted in functional channels. A cryo-EM structure of TRPM8 published later show that some of the alignment predictions used to make the chimeras did not match with the actual transmembrane helices, one possible reason that they were nonfunctional. Finally, a novel TRPM8 antagonist was tested for inhibition of menthol-evoked currents and found to have an IC_{50} of ~64 nM.

The results presented here provide insight into two of the primary thermosensors in human biology, TRPM8 and TRPV1. Because of their diverse roles in human physiology and disease, understanding these channels is important from a basic science perspective and holds the promise of novel therapeutic strategies in the years to come.

REFERENCES

CHAPTER 1

1. Manning, A., and Cosens, D. J. (1969) Abnormal Electroretinogram from a *Drosophila* mutant. *Nature* **224**, 285-287

2. Minke, B., Wu, C., and Pak, W. L. (1975) Induction of photoreceptor voltage noise in the dark in *Drosophila* mutant. *Nature* **258**, 84-87

3. Montell, C., and Rubin, G. M. (1989) Molecular Characterization of the Drosophila *trp* Locus: A Putative Integral Membrane Protein Required for Phototransduction. *Neuron* **2**, 1313-1323

4. Hardie, R. C., Voss, D., Pongs, O., and Laughlin, S. B. (1991) Novel Potassium Channels Encoded by the *Shaker* Locus in Drosophila Photoreceptors. *Neuron* **6**, 477-486

5. Hardie, R. C., and Minke, B. (1992) The *trp* Gene is Essential for a Light-Activated Ca^{2+} Channel in Drosophila Photoreceptors. *Neuron* **8**, 643-651

6. McKemy, D. D., Neuhausser, W. M., and Julius, D. (2002) Identification of a cold receptor reveals a general role for TRP channels in thermosensation. *Nature* **416**, 52-58

7. Peier, A. M., Moqrich, A., Hergarden, A. C., Reeve, A. J., Andersson, D. A., Story, G. M., Earley, T. J., Dragoni, I., McIntyre, P., Bevan, S., and Patapoutian, A. (2002) A TRP Channel that Senses Cold Stimuli and Menthol. *Cell* **8** 705-715

8. Hofmann, T., Chubanov, V., Gudermann, T., and Montell, C. (2003) TRPM5 Is a Voltage-Modulated and Ca^{2+}-Activated Monovalent Selective Cation Channel. *Curr. Biol.* **13**, 1153-1158

9. Talavera, K., Yasumatsu, K., Voets, T., Droogmans, G., Shigemura, N., Ninomiya, Y., Margolskee, R. F., and Nilius, B. (2005) Heat activation of TRPM5 underlies thermal sensitivity of sweet taste. *Nature* **438**, 1022-1025

10. Caterina, M. J., Schumacher, M. A., Tominaga, M., Rosen, T. A., Levine, J. D., and Julius, D. (1997) The capsaicin receptor: a heat-activated ion channel in the pain pathway. *Nature* **389**, 816-824

11. Myers, B. R., Sigal, Y. M., and Julius, D. (2009) Evolution of Thermal Response Properties in a Cold-Activated TRP Channel. *PLoS One* **4**, e5741

12. Gracheva, E. O., and Bagriantsev, S. N. (2015) Evolutionary adaptation to thermosensation. *Curr. Opin. Neurobiol.* **34**, 67-73

13. Hodgkin, A. L., Huxley, A. F., and Katz, B. (1952) Measurement of current-voltage relations in the membrane of the giant axon of *Loligo*. *J. Physiol.* **116**, 424-448

CHAPTER 2

1. Montell, C., and Rubin, G. M. (1989) Molecular Characterization of the Drosophila trp locus: A Putative Integral Membrane Protein Required for Phototransduction. *Neuron* **2**, 1313-1323

2. Montell, C., Birnbaumer, L., Flockerzi, V., Bindels, R. J., Bruford, E. A., Caterina, M. J., Clapham, D. E., Harteneck, C., Heller, S., Julius, D., Kojima, I., Mori, Y., Penner, R., Prawitt, D., Scharenberg, A. M., Schultz, G., Shimizu, N., and Zhu, M. X. (2002) A Unified Nomenclature for the Superfamily of TRP Cation Channels. *Mol. Cell* **9**, 229-231

3. Caterina, M. J., Schumacher, M. A., Tominaga, M., Rosen, T. A., Levine, J. D., and Julius, D. (1997) The capsaicin receptor: a heat-activated ion channel in the pain pathway. *Nature* **389**, 816-824

4. Cao, E., Cordero-Morales, J. F., Liu, B., Qin, F., and Julius, D. (2013) TRPV1 channels are intrinsically heat sensitive and negatively regulated by phosphoinositide lipids. *Neuron* **77**, 667-679

5. Voets, T., Droogmans, G., Wissenbach, U., Janssens, A., Flockerzi, V., and Nilius, B. (2004) The principle of temperature-dependent gating in cold- and heat-sensitive TRP channels. *Nature* **430**, 748-754

6. Cao, X., Ma, L., Yang, F., Wang, K., and Zheng, J. (2014) Divalent cations potentiate TRPV1 channel by lowering the heat activation threshold. *J. Gen. Physiol.* **143**, 75-90

7. Lukacs, V., Thyagarajan, B., Varnai, P., Balla, A., Balla, T., and Rohacs, T. (2007) Dual regulation of TRPV1 by phosphoinositides. *J. Neurosci.* **27**, 7070-7080

8. Ufret-Vincenty, C. A., Klein, R. M., Hua, L., Angueyra, J., and Gordon, S. E. (2011) Localization of the PIP2 sensor of TRPV1 ion channels. *J. Biol. Chem.* **286**, 9688-9698

9. Kim, A. Y., Tang, Z., Liu, Q., Patel, K. N., Maag, D., Geng, Y., and Dong, X. (2008) Pirt, a phosphoinositide-binding protein, functions as a regulatory subunit of TRPV1. *Cell* **133**, 475-485

10. Prager-Khoutorsky, M., Khoutorsky, A., and Bourque, C. W. (2014) Unique interweaved microtubule scaffold mediates osmosensory transduction via physical interaction with TRPV1. *Neuron* **83**, 866-878

11. De Petrocellis, L., Ligresti, A., Moriello, A. S., Allarà, M., Bisogno, T., Petrosino, S., Stott, C. G., and Marzo, V. D. (2011) Effects of cannabinoids and cannabinoid-enriched Cannabis extracts on TRP channels and endocannabinoid metabolic enzymes. *Br. J. Pharmacol.* **163**, 1479-1494

12. Bohlen, C. J., Priel, A., Zhou, S., King, D., Siemens, J., and Julius, D. (2010) A bivalent tarantula toxin activates the capsaicin receptor, TRPV1, by targeting the outer pore domain. *Cell* **141**, 834-845

13. Szallasi, A., Jonassohn, M., Acs, G., Biro, T., Acs, P., Blumberg, P. M., and Sterner. (1996) The stimulation of capsaicin-sensitive neurones in a vanilloid receptor-mediated fashion by pungent terpenoids possessing an unsaturated 1,4-dialdehyde moiety. *Br. J. Pharmacol.* **119**, 283-290

14. McVey, D. C., and Vigna, S. R. (2005) The Role of Leukotriene B4 in Clostridium difficile Toxin A-Induced Ileitis in Rats. *Gastroenterology* **128**, 1306-1316

15. Shimizu, T., Shibata, M., Toriumi, H., Iwashita, T., Funakubo, M., Sato, H., Kuroi, T., Ebine, T., Koizumi, K., and Suzuki, N. (2012) Reduction of TRPV1 expression in the trigeminal system by botulinum neurotoxin type-A. *Neurobiology of Disease* **48**, 367-378

16. Jordt, S. E., and Julius, D. (2002) Molecular Basis for Species-Specific Sensitivity to "Hot" Chili Peppers. *Cell* **108**, 421-430

17. Gracheva, E. O., Cordero-Morales, J. F., Gonzalez-Carcacia, J. A., Ingolia, N. T., Manno, C., Aranguren, C. I., Weissman, J. S., and Julius, D. (2011) Ganglion-specific splicing of TRPV1 underlies infrared sensation in vampire bats. *Nature* **476**, 88-91

18. Saito, S., and Tominaga, M. (2014) Functional diversity and evolutionary dynamics of thermoTRP channels. *Cell Calcium*

19. Zimmermann, K., Lennerz, J. K., Hein, A., Link, A. S., Kaczmarek, J. S., Delling, M., Uysal, S., Pfieifer, J. D., Riccio, A., and Clapham, D. E. (2011) Transient receptor potential cation channel, subfamily C, member 5 (TRPC5) is a cold-transducer in the peripheral nervous system. *Proc. Natl. Acad. Sci. U. S. A.* **108**, 18114-18119

20. Almeida, M. C., Hew-Butler, T., Soriano, R. N., Rao, S., Wang, W., Wang, J., Tamayo, N., Oliveira, D. L., Nucci, T. B., Aryal, P., Garami, A., Bautista, D.,

Gavva, N. R., and Romanovsky, A. A. (2012) Pharmacological blockade of the cold receptor TRPM8 attenuates autonomic and behavioral cold defenses and decreases deep body temperature. *J. Neurosci.* **32**, 2086-2099

21. Ding, Z., Gomez, T., Werkheiser, J. L., Cowan, A., and Rawls, S. M. (2008) Icilin induces a hyperthermia in rats that is dependent on nitric oxide production and NMDA receptor activation. *European Journal of Pharmacology* **578**, 201-208

22. Gavva, N. R., Davis, C., Sonya, G. L., Rao, S., Wang, W., and Zhu, D. X. (2012) Transient receptor potential melastatin 8 (TRPM8) channels are involved in body temperature regulation. *Molecular Pain* **8**, 36

23. Knowlton, W. M., Daniels, R. L., Palkar, R., McCoy, D. D., and McKemy, D. D. (2011) Pharmacological blockade of TRPM8 ion channels alters cold and cold pain responses in mice. *PLoS One* **6**, e25894

24. Shapovalov, G., Gkika, D., Devilliers, M., Kondratskyi, A., Gordienko, D., Busserolles, J., Bokhobza, A., Eschalier, A., Skryma, R., and Prevarskaya, N. (2013) Opiates modulate thermosensation by internalizing cold receptor TRPM8. *Cell reports* **4**, 504-515

25. Ma, S., Yu, H., Zhao, Z., Luo, Z., Chen, J., Ni, Y., Jin, R., Ma, L., Wang, P., Zhu, Z., Li, L., Zhong, J., Liu, D., Nilius, B., and Zhu, Z. (2012) Activation of the cold-sensing TRPM8 channel triggers UCP1-dependent thermogenesis and prevents obesity. *Journal of molecular cell biology* **4**, 88-96

26. McCoy, D. D., Zhou, L., Nguyen, A. K., Watts, A. G., Donovan, C. M., and McKemy, D. D. (2013) Enhanced insulin clearance in mice lacking TRPM8 channels. *American journal of physiology. Endocrinology and metabolism* **305**, E78-88

27. Vriens, J., Nilius, B., and Voets, T. (2014) Peripheral thermosensation in mammals. *Nature reviews. Neuroscience* **15**, 573-589

28. Riera, C. E., Huising, M. O., Follett, P., Leblanc, M., Halloran, J., Van Andel, R., de Magalhaes Filho, C. D., Merkwirth, C., and Dillin, A. (2014) TRPV1 pain receptors regulate longevity and metabolism by neuropeptide signaling. *Cell* **157**, 1023-1036

29. Rossi, F., Bellini, G., Torella, M., Tortora, C., Manzo, I., Giordano, C., Guida, F., Luongo, L., Papale, F., Rosso, F., Nobili, B., and Maione, S. (2014) The genetic ablation or pharmacological inhibition of TRPV1 signalling is beneficial for the restoration of quiescent osteoclast activity in ovariectomized mice. *Br. J. Pharmacol.* **171**, 2621-2630

30. Jang, Y., Lee, M. H., Lee, J., Jung, J., Lee, S. H., Yang, D. J., Kim, B. W., Son, H., Lee, B., Chang, S., Mori, Y., and Oh, U. (2014) TRPM2 mediates the lysophosphatidic acid-induced neurite retraction in the developing brain. *European Journal of Pharmacology* **466**, 1987-1998

31. Oda, S., Uchida, K., Wang, X., Lee, J., Shimada, Y., Tominaga, M., and Kadowaki, M. (2013) TRPM2 contributes to antigen-stimulated Ca^{2+} influx in mucosal mast cells. *European Journal of Pharmacology* **465**, 1023-1030

32. Numata, T., Sato, K., Christmann, J., Marx, R., Mori, Y., Okada, Y., and Wehner, F. (2012) The DeltaC splice-variant of TRPM2 is the hypertonicity-induced cation channel in HeLa cells, and the ecto-enzyme CD38 mediates its activation. *J. Physiol.* **590**, 1121-1138

33. Kaneko, Y., and Arpadd, S. (2014) Transient receptor potential (TRP) channels: a clinical perspective. *Br. J. Pharmacol.* **171**, 2474-2507

34. Story, G. M., Peier, A. M., Reeve, A. J., Eid, S. R., Mosbacher, J., Hricik, T. R., Earley, T. J., Hergarden, A. C., Andersson, D. A., Hwang, S. W., McIntyre, P., Jegla, T., Bevan, S., and Patapoutian, A. (2003) ANKTM1, a TRP-like Channel Expressed in Nociceptive Neurons, Is Activated by Cold Temperatures. *Cell* **112**, 819-829

35. Chen, J., Kang, D., Xu, J., Lake, M., Hogan, J. O., Sun, C., Walter, K., Yao, B., and Kim, D. (2013) Species differences and molecular determinant of TRPA1 cold sensitivity. *Nat. Commun.* **4**, 2501

36. Saito, S., Banzawa, N., Fukuta, N., Saito, C. T., Takahashi, K., Imagawa, T., Ohta, T., and Tominaga, M. (2014) Heat and noxious chemical sensor, chicken TRPA1, as a target of bird repellents and identification of its structural determinants by multispecies functional comparison. *Mol. Biol. Evol.* **31**, 708-722

37. Klionsky, L., Tamir, R., Gao, B., Wang, W., Immke, D., Nishimura, N., and Gavva, N. (2007) Species-specific pharmacology of Trichloro(sulfanyl)ethyl benzamides as transient receptor potential ankyrin 1 (TRPA1) antagonists. *Molecular Pain* **3**, 39

38. Nagatomo, K., Ishii, H., Yamamoto, T., Nakajo, K., and Kubo, Y. (2010) The Met268Pro Mutation of Mouse TRPA1 Changes the Effect of Caffeine from Activation to Suppression. *Biophys. J.* **99**, 3609-3618

39. Nagatomo, K., and Kubo, Y. (2008) Caffeine activates mouse TRPA1 channels but suppresses human TRPA1 channels. *Proc. Natl. Acad. Sci. U. S. A.* **105**, 17373-17378

40. Jabba, S., Goyal, R., Sosa-Pagán, J. O., Moldenhauer, H., Wu, J., Kalmeta, B., Bandell, M., Latorre, R., Patapoutian, A., and Grandl, J. (2014) Directionality of temperature activation in mouse TRPA1 ion channel can be inverted by single-point mutations in ankyrin repeat six. *Neuron* **82**, 1017-1031

41. Geng, J., Liang, D., Jiang, K., and Zhang, P. (2011) Molecular evolution of the infrared sensory gene TRPA1 in snakes and implications for functional studies. *PLoS One* **6**

42. Kang, K., Panzano, V. C., Chang, E. C., Ni, L., Dainis, A. M., Jenkins, A. M., Regna, K., Muskavitch, M. A. T., and Garrity, P. A. (2012) Modulation of TRPA1 thermal sensitivity enables sensory discrimination in Drosophila. *Nature* **481**, 76-80

43. Viswanath, V., Story, G. M., Peier, A. M., Petrus, M. J., Lee, V. M., Hwang, S. W., Patapoutian, A., and Jegla, T. (2003) Ion channels: Opposite thermosensor in fruitfly and mouse. *Nature* **423**, 822-823

44. Chen, J., and Kym, P. R. (2009) TRPA1: the species difference. *J. Gen. Physiol.* **133**, 623-625

45. Zhong, L., Bellemer, A., Yan, H., Honjo, K., Robertson, J., Hwang, R. Y., Pitt, G. S., and Tracey, W. D. (2012) Thermosensory and Nonthermosensory Isoforms of Drosophila melanogaster TRPA1 Reveal Heat-Sensor Domains of a ThermoTRP Channe. *Cell Rep* **1**, 43-55

46. Gracheva, E. O., Cordero-Morales, J. F., González-Carcacía, J. A., Ingolia, N. T., Manno, C., Aranguren, C. I., Weissman, J. S., and Julius, D. (2011) Ganglion-specific splicing of TRPV1 underlies infrared sensation in vampire bats. *Nature* **476**, 88-91

47. Saito, S., Fukuta, N., Shingai, R., and Tominaga, M. (2011) Evolution of vertebrate transient receptor potential vanilloid 3 channels: opposite temperature sensitivity between mammals and western clawed frogs. *PLoS Genet.* **7**, e1002041

48. Huang, S., Li, X., Yu, Y., Wang, J., and Caterina, M. (2011) TRPV3 and TRPV4 ion channels are not major contributors to mouse heat sensation. *Molecular Pain* **7**, 37

49. Myers, B. R., Sigal, Y. M., and Julius, D. (2009) Evolution of Thermal Response Properties in a Cold-Activated TRP Channel. *PLoS One* **4**, e5741

50. Jordt, S.-E., and Julius, D. (2002) Molecular Basis for Species-Specific Sensitivity to "Hot" Chili Peppers. *Cell* **108**, 421-430

51. Papakosta, M., Dalle, C., Haythornthwaite, A., Cao, L., Stevens, E. B., Burgess, G., Russell, R., Cox, P. J., Phillips, S. C., and Grimm, C. (2011) The chimeric approach reveals that differences in the TRPV1 pore domain determine species-specific sensitivity to block of heat activation. *J. Biol. Chem.* **286**, 39663-39672

52. Phillips, E., Reeve, A., Bevan, S., and McIntyre, P. (2004) Identification of Species-specific Determinants of the Action of the Antagonist Capsazepine and the Agonist PPAHV on TRPV1. *J. Biol. Chem.* **279**, 17165-17172

53. McPartland, J. M., Glass, M., Matias, I., Norris, R., and Kilpatrick, C. W. (2007) A shifted repertoire of endocannabinoid genes in the zebrafish (Danio rerio). *Mol. Genet. Genomics* **277**, 555-570

54. Neeper, M. P., Liu, Y., Hutchinson, T. L., Wang, Y., Flores, C. M., and Qin, N. (2007) Activation Properties of Heterologously Expressed Mammalian TRPV2 EVIDENCE FOR SPECIES DEPENDENCE. *J. Biol. Chem.* **282**, 15894-15902

55. Rohacs, T. (2014) Phosphoinositide Regulation of TRP Channels. *Handbook of Experimental Pharmacology* **223**, 1143-1176

56. Cao, E., Cordero-Morales, Julio F., Liu, B., Qin, F., and Julius, D. (2013) TRPV1 Channels Are Intrinsically Heat Sensitive and Negatively Regulated by Phosphoinositide Lipids. *Neuron* **77**, 667-679

57. Estacion, M., Sinkins, W. G., and Schilling, W. P. (2001) Regulation of Drosophila transient receptor potential-like (TrpL) channels by phospholipase C-dependent mechanisms. *J. Physiol.* **530**, 1-19

58. Huang, J., Liu, C.-H., Hughes, S. A., Postma, M., Schwiening, C. J., and Hardie, R. C. (2010) Activation of TRP Channels by Protons and Phosphoinositide Depletion in Drosophila Photoreceptors. *Curr. Biol.* **20**, 189-197

59. Otsuguro, K.-i., Tang, J., Tang, Y., Xiao, R., Freichel, M., Tsvilovskyy, V., Ito, S., Flockerzi, V., Zhu, M. X., and Zholos, A. V. (2008) Isoform-specific Inhibition of TRPC4 Channel by Phosphatidylinositol 4,5-Bisphosphate. *J. Biol. Chem.* **283**, 10026-10036

60. Patel, K. N., Liu, Q., Meeker, S., Undem, B. J., and Dong, X. (2011) Pirt, a TRPV1 modulator, is required for histamine-dependent and -independent itch. *PLoS One* **6**, e20559

61. Tang, Z., Kim, A., Masuch, T., Park, K., Weng, H., Wetzel, C., and Dong, X. (2013) Pirt functions as an endogenous regulator of TRPM8. *Nat. Commun.* **4**, 2179

62. Zakharian, E., Cao, C., and Rohacs, T. (2010) Gating of transient receptor potential melastatin 8 (TRPM8) channels activated by cold and chemical agonists in planar lipid bilayers. *J. Neurosci.* **30**, 12526-12534

63. Clapham, D. E., and Miller, C. (2011) A thermodynamic framework for understanding temperature sensing by transient receptor potential (TRP) channels. *Proc. Natl. Acad. Sci. U. S. A.* **108**, 19492-19497

64. Voets, T. (2014) TRP channels and thermosensation. *Handbook of Experimental Pharmacology* **223**, 729-741

65. Feng, Q. (2014) Temperature sensing by thermal TRP channels: thermodynamic basis and molecular insights. *Curr. Top. Membr.* **74**, 19-50

66. Yao, J., Liu, B., and Qin, F. (2011) Modular thermal sensors in temperature-gated transient receptor potential (TRP) channels. *Proc. Natl. Acad. Sci. U. S. A.* **108**, 11109-11114

67. Grandl, J., Kim, S. E., Uzzell, V., Bursulaya, B., Petrus, M., Bandell, M., and Patapoutian, A. (2010) Temperature-induced opening of TRPV1 ion channel is stabilized by the pore domain. *Nature neuroscience* **13**, 708-714

68. Brauchi, S., Orta, G., Salazar, M., Rosenmann, E., and Latorre, R. (2006) A hot-sensing cold receptor: C-terminal domain determines thermosensation in transient receptor potential channels. *J. Neurosci.* **26**, 4835-4840

69. Kim, S. E., Patapoutian, A., and Grandl, J. (2013) Single residues in the outer pore of TRPV1 and TRPV3 have temperature-dependent conformations. *PLoS One* **8**, e59593

70. Vlachova, V., Teisinger, J., Sušánková, K., Lyfenko, A., Ettrich, R., and Vyklicky, L. (2003) Functional Role of C-Terminal Cytoplasmic Tail of Rat Vanilloid Receptor 1. *J. Neurosci.* **23**, 1340-1350

71. Yang, F., Cui, Y., Wang, K., and Zheng, J. (2010) Thermosensitive TRP channel pore turret is part of the temperature activation pathway. *Proc. Natl. Acad. Sci. U S A* **107**, 7083-7088

72. Cui, Y., Yang, F., Cao, X., Yarov-Yarovoy, V., Wang, K., and Zheng, J. (2012) Selective disruption of high sensitivity heat activation but not capsaicin activation of TRPV1 channels by pore turret mutations. *J. Gen. Physiol.* **139**, 273-283

73. Valente, P., Garcia-Sanz, N., Gomis, A., Fernandez-Carvajal, A., Fernandez-Ballester, G., Viana, F., Belmonte, C., and Ferrer-Montiel, A. (2008) Identification of molecular determinants of channel gating in the transient

receptor potential box of vanilloid receptor I. *FASEB journal : official publication of the Federation of American Societies for Experimental Biology* **22**, 3298-3309

74. Brauchi, S., Orta, G., Mascayano, C., Salazar, M., Raddatz, N., Urbina, H., Rosenmann, E., Gonzalez-Nilo, F., and Latorre, R. (2007) Dissection of the components for PIP_2 activation and thermosensation in TRP channels. *Proc. Natl. Acad. Sci. U. S. A.* **104**, 10246-10251

75. Caordero-Morales, J. F., Gracheva, E. O., and Julius, D. (2011) Cytoplasmic ankyrin repeats of transient receptor potential A1 (TRPA1) dictate sensitivity to thermal and chemical stimuli. *Proc. Natl. Acad. Sci. U. S. A.* **108**, E1184-E1191

76. Wang, H., Schupp, M., Zurborg, S., and Heppenstall, P. A. (2013) Residues in the pore region of Drosophila transient receptor potential A1 dictate sensitivity to thermal stimuli. *J. Physiol.* **591**, 185-201

77. Grandl, J., Hu, H., Bandell, M., Bursulaya, B., Schmidt, M., Petrus, M., and Patapoutian, A. (2008) Pore region of TRPV3 ion channel is specifically required for heat activation. *Nature neuroscience* **11**, 1007-1013

78. Brauchi, S., Orio, P., and Latorre, R. (2004) Clues to understanding cold sensation: thermodynamics and electrophysiological analysis of the cold receptor TRPM8. *Proc. Natl. Acad. Sci. U. S. A.* **101**, 15494-15499

79. Yao, J., Liu, B., and Qin, F. (2010) Kinetic and energetic analysis of thermally activated TRPV1 channels. *Biophys. J.* **99**, 1743-1753

80. Privalov, P. L. (1997) Thermodynamics of protein folding. *J. Chem. Thermodyn.* **29**, 447-474

81. Liu, B., Hui, K., and Qin, F. (2003) Thermodynamics of Heat Activation of Single Capsaicin Ion Channels VR1. *Biophys. J.* **85**, 2988-3006

82. Becktel, W. J., and Schellman, J. A. (1987) Protein Stability Curves. *Biopolymers* **26**, 1859-1877

83. Bond, C. S., and Schuttelkopf, A. W. (2009) ALINE: a WYSIWYG protein-sequence alignment editor for publication-quality alignments. *Acta crystallographica. Section D, Biological crystallography* **65**, 510-512

84. Larkin, M. A., Blackshields, G., Brown, N. P., Chenna, R., McGettigan, P. A., McWilliam, H., Valentin, F., Wallace, I. M., Wilm, A., Lopez, R., Thompson, J. D., Gibson, T. J., and Higgins, D. G. (2007) Clustal W and Clustal X version 2.0. *Bioinformatics* **23**, 2947-2948

85. Konagurthu, A. S., Whisstock, J. C., Stuckey, P. J., and Lesk, A. M. (2006) MUSTANG: a multiple structural alignment algorithm. *Proteins* **64**, 559-574

86. Barton, G. J. (1993) ALSCRIPT: a tool to format multiple sequence alignments. *Protein engineering* **6**, 37-40

87. Liao, M., Cao, E., Julius, D., and Cheng, Y. (2013) Structure of the TRPV1 ion channel determined by electron cryo-microscopy. *Nature* **504**, 107-112

88. Cao, E., Liao, M., Cheng, Y., and Julius, D. (2013) TRPV1 structures in distinct conformations reveal activation mechanisms. *Nature* **504**, 113-118

89. *Thermal Sensors, Current Topics in Membranes*. (2014) Vol. 74, Islas, L. D., and Qin, F., Elsevier, Amsterdam

90. de Mendoza, D. (2014) Temperature sensing by membranes. *Annual review of microbiology* **68**, 101-116

91. Shapiro, R. S., and Cowen, L. E. (2012) Thermal control of microbial development and virulence: molecular mechanisms of microbial temperature sensing. *mBio* **3**, e00238-00212

92. Inda, M. E., Vandenbranden, M., Fernandez, A., de Mendoza, D., Ruysschaert, J. M., and Cybulski, L. E. (2014) A lipid-mediated conformational switch modulates the thermosensing activity of DesK. *Proc. Natl. Acad. Sci. U. S. A.* **111**, 3579-3584

93. Chowdhury, S., Jarecki, B. W., and Chanda, B. (2014) A molecular framework for temperature-dependent gating of ion channels. *Cell* **158**, 1148-1158

94. Greenfield, N. J. (2006) Using circular dichroism collected as a function of temperature to determine the thermodynamics of protein unfolding and binding interactions. *Nat Protoc* **1**, 2527-2535

95. Chill, J. H., Louis, J. M., Miller, C., and Bax, A. (2006) NMR study of the tetrameric KcsA potassium channel in detergent micelles. *Protein Sci.* **15**, 684-698

96. Butterwick, J. A., and MacKinnon, R. (2010) Solution structure and phospholipid interactions of the isolated voltage-sensor domain from KvAP. *J. Mol. Biol.* **403**, 591-606

97. Peng, D., Kim, J. H., Kroncke, B. M., Law, C. L., Xia, Y., Droege, K. D., Van Horn, W. D., Vanoye, C. G., and Sanders, C. R. (2014) Purification and structural study of the voltage-sensor domain of the human KCNQ1 potassium ion channel. *Biochemistry* **53**, 2032-2042

98. Hwang, P. M., Bishop, R. E., and Kay, L. E. (2004) The integral membrane enzyme PagP alternates between two dynamically distinct states. *Proc. Natl. Acad. Sci. U. S. A.* **101**, 9618-9623

99. White, H. D., Thirumurugan, K., Walker, M. L., and Trinick, J. (2003) A second generation apparatus for time-resolved electron cryo-microscopy using stepper motors and electrospray. *J. Struct. Biol.* **144**, 246-252

100. Kupitz, C., Basu, S., Grotjohann, I., Fromme, R., Zatsepin, N. A., Rendek, K. N., Hunter, M. S., Shoeman, R. L., White, T. A., Wang, D., James, D., Yang, J. H., Cobb, D. E., Reeder, B., Sierra, R. G., Liu, H., Barty, A., Aquila, A. L., Deponte, D., Kirian, R. A., Bari, S., Bergkamp, J. J., Beyerlein, K. R., Bogan, M. J., Caleman, C., Chao, T. C., Conrad, C. E., Davis, K. M., Fleckenstein, H., Galli, L., Hau-Riege, S. P., Kassemeyer, S., Laksmono, H., Liang, M., Lomb, L., Marchesini, S., Martin, A. V., Messerschmidt, M., Milathianaki, D., Nass, K., Ros, A., Roy-Chowdhury, S., Schmidt, K., Seibert, M., Steinbrener, J., Stellato, F., Yan, L., Yoon, C., Moore, T. A., Moore, A. L., Pushkar, Y., Williams, G. J., Boutet, S., Doak, R. B., Weierstall, U., Frank, M., Chapman, H. N., Spence, J. C., and Fromme, P. (2014) Serial time-resolved crystallography of photosystem II using a femtosecond X-ray laser. *Nature* **513**, 261-265

101. Lau, S. Y., Procko, E., and Gaudet, R. (2012) Distinct properties of Ca^{2+}-calmodulin binding to N- and C-terminal regulatory regions of the TRPV1 channel. *J. Gen. Physiol.* **140**, 541-555

102. Lishko, P. V., Procko, E., Jin, X., Phelps, C. B., and Gaudet, R. (2007) The ankyrin repeats of TRPV1 bind multiple ligands and modulate channel sensitivity. *Neuron* **54**, 905-918

103. Moiseenkova-Bell, V. Y., Stanciu, L. A., Serysheva, II, Tobe, B. J., and Wensel, T. G. (2008) Structure of TRPV1 channel revealed by electron cryomicroscopy. *Proc. Natl. Acad. Sci. U. S. A.* **105**, 7451-7455

104. Huynh, K. W., Cohen, M. R., Chakrapani, S., Holdaway, H. A., Stewart, P. L., and Moiseenkova-Bell, V. Y. (2014) Structural insight into the assembly of TRPV channels. *Structure* **22**, 260-268

105. Jin, X., Touhey, J., and Gaudet, R. (2006) Structure of the N-terminal ankyrin repeat domain of the TRPV2 ion channel. *J. Biol. Chem.* **281**, 25006-25010

106. McCleverty, C. J., Koesema, E., Patapoutian, A., Lesley, S. A., and Kreusch, A. (2006) Crystal structure of the human TRPV2 channel ankyrin repeat domain. *Protein Sci.* **15**, 2201-2206

107. Shi, D. J., Ye, S., Cao, X., Zhang, R., and Wang, K. (2013) Crystal structure of the N-terminal ankyrin repeat domain of TRPV3 reveals unique conformation of finger 3 loop critical for channel function. *Protein Cell* **4**, 942-950

108. Inada, H., Procko, E., Sotomayor, M., and Gaudet, R. (2012) Structural and biochemical consequences of disease-causing mutations in the ankyrin repeat domain of the human TRPV4 channel. *Biochemistry* **51**, 6195-6206

109. Shigematsu, H., Sokabe, T., Danev, R., Tominaga, M., and Nagayama, K. (2010) A 3.5-nm structure of rat TRPV4 cation channel revealed by Zernike phase-contrast cryoelectron microscopy. *J. Biol. Chem.* **285**, 11210-11218

110. Phelps, C. B., Huang, R. J., Lishko, P. V., Wang, R. R., and Gaudet, R. (2008) Structural analyses of the ankyrin repeat domain of TRPV6 and related TRPV ion channels. *Biochemistry* **47**, 2476-2484

111. Cvetkov, T. L., Huynh, K. W., Cohen, M. R., and Moiseenkova-Bell, V. Y. (2011) Molecular architecture and subunit organization of TRPA1 ion channel revealed by electron microscopy. *J. Biol. Chem.* **286**, 38168-38176

112. Maruyama, Y., Ogura, T., Mio, K., Kiyonaka, S., Kato, K., Mori, Y., and Sato, C. (2007) Three-dimensional reconstruction using transmission electron microscopy reveals a swollen, bell-shaped structure of transient receptor potential melastatin type 2 cation channel. *J. Biol. Chem.* **282**, 36961-36970

113. Fujiwara, Y., and Minor, D. L., Jr. (2008) X-ray crystal structure of a TRPM assembly domain reveals an antiparallel four-stranded coiled-coil. *J. Mol. Biol.* **383**, 854-870

114. Yamaguchi, H., Matsushita, M., Nairn, A. C., and Kuriyan, J. (2001) Crystal structure of the atypical protein kinase domain of a TRP channel with phosphotransferase activity. *Mol. Cell* **7**, 1047-1057

115. Mio, K., Ogura, T., Kiyonaka, S., Hiroaki, Y., Tanimura, Y., Fujiyoshi, Y., Mori, Y., and Sato, C. (2007) The TRPC3 channel has a large internal chamber surrounded by signal sensing antennas. *J. Mol. Biol.* **367**, 373-383

116. Petri, E. T., Celic, A., Kennedy, S. D., Ehrlich, B. E., Boggon, T. J., and Hodsdon, M. E. (2010) Structure of the EF-hand domain of polycystin-2 suggests a mechanism for Ca^{2+}-dependent regulation of polycystin-2 channel activity. *Proc. Natl. Acad. Sci. U. S. A.* **107**, 9176-9181

117. Yu, Y., Ulbrich, M. H., Li, M. H., Buraei, Z., Chen, X. Z., Ong, A. C., Tong, L., Isacoff, E. Y., and Yang, J. (2009) Structural and molecular basis of the assembly of the TRPP2/PKD1 complex. *Proc. Natl. Acad. Sci. U. S. A.* **106**, 11558-11563

118. Yu, Y., Ulbrich, M. H., Li, M. H., Dobbins, S., Zhang, W. K., Tong, L., Isacoff, E. Y., and Yang, J. (2012) Molecular mechanism of the assembly of an acid-sensing receptor ion channel complex. *Nat. Commun.* **3**, 1252

119. Berjanskii, M., Zhou, J., Liang, Y., Lin, G., and Wishart, D. S. (2012) Resolution-by-proxy: a simple measure for assessing and comparing the overall quality of NMR protein structures. *Journal of biomolecular NMR* **53**, 167-180

120. Orozco, M. (2014) A theoretical view of protein dynamics. *Chemical Society reviews* **43**, 5051-5066

121. Dror, R. O., Dirks, R. M., Grossman, J. P., Xu, H., and Shaw, D. E. (2012) Biomolecular simulation: a computational microscope for molecular biology. *Annual review of biophysics* **41**, 429-452

122. Denning, E. J., and Beckstein, O. (2013) Influence of lipids on protein-mediated transmembrane transport. *Chem. Phys. Lipids* **169**, 57-71

123. Khalili-Araghi, F., Gumbart, J., Wen, P.-C., Sotomayor, M., Tajkhorshid, E., and Schulten, K. (2009) Molecular dynamics simulations of membrane channels and transporters. *Curr. Opin. Struct. Biol.* **19**, 128-137

124. Koehler Leman, J., Ulmschneider, M. B., and Gray, J. J. (2015) Computational modeling of membrane proteins. *Proteins* **83**, 1-24

125. Stansfeld, P. J., and Sansom, M. S. P. (2011) Molecular simulation approaches to membrane proteins. *Structure* **19**, 1562-1572

126. Fernandez-Ballester, G., and Ferrer-Montiel, A. (2008) Molecular modeling of the full-length human TRPV1 channel in closed and desensitized states. *The Journal of membrane biology* **223**, 161-172

127. Kornilov, P., Peretz, A., Lee, Y., Son, K., Lee, J. H., Refaeli, B., Roz, N., Rehavi, M., Choi, S., and Attali, B. (2014) Promiscuous gating modifiers target the voltage sensor of K(v)7.2, TRPV1, and H(v)1 cation channels. *FASEB journal : official publication of the Federation of American Societies for Experimental Biology* **28**, 2591-2602

128. Susankova, K., Ettrich, R., Vyklicky, L., Teisinger, J., and Vlachova, V. (2007) Contribution of the putative inner-pore region to the gating of the transient receptor potential vanilloid subtype 1 channel (TRPV1). *J. Neurosci.* **27**, 7578-7585

129. Cao, E., Liao, M., Cheng, Y., and Julius, D. (2013) TRPV1 structures in distinct conformations reveal activation mechanisms. *Nature* **504**, 113-118

130. Darré, L., Furini, S., and Domene, C. (2015) Permeation and Dynamics of an Open-Activated TRPV1 Channel. *J. Mol. Biol.* **427**, 537-549

131. Poblete, H., Oyarzún, I., Olivero, P., Comer, J., Zuñiga, M., Sepulveda, R. V., Báez-Nieto, D., González Leon, C., González-Nilo, F., and Latorre, R. (2015) Molecular Determinants of Phosphatidylinositol 4,5-Bisphosphate (PI(4,5)P2) Binding to Transient Receptor Potential V1 (TRPV1) Channels. *J. Biol. Chem.* **290**, 2086-2098

132. Shaw, D. E., Dror, R. O., Salmon, J. K., Grossman, J. P., Mackenzie, K. M., Bank, J. A., Young, C., Deneroff, M. M., Batson, B., Bowers, K. J., Chow, E., Eastwood, M. P., Ierardi, D. J., Klepeis, J. L., Kuskin, J. S., Larson, R. H., Lindorff-Larsen, K., Maragakis, P., Moraes, M. A., Piana, S., Shan, Y., and Towles, B. (2009) Millisecond-scale molecular dynamics simulations on Anton. in *SC '09: Proceedings of the Conference on High Performance Computing Networking, Storage and Analysis*, ACM, New York, NY, USA

133. Liwo, A., Czaplewski, C., Ołdziej, S., and Scheraga, H. A. (2008) Computational techniques for efficient conformational sampling of proteins. *Curr. Opin. Struct. Biol.* **18**, 134-139

134. Okamoto, Y. (2004) Generalized-ensemble algorithms: enhanced sampling techniques for Monte Carlo and molecular dynamics simulations. *J. Mol. Graphics Modell.* **22**, 425-439

135. Seyler, S. L., and Beckstein, O. (2014) Sampling of large conformational transitions: Adenylate kinase as a testing ground. *Molec. Simul.* **40**, 855-877

136. van der Vaart, A. (2006) Simulation of conformational transitions. *Theor. Chem. Acc.* **116**, 183-193

137. Chodera, J. D., Mobley, D. L., Shirts, M. R., Dixon, R. W., Branson, K., and Pande, V. S. (2011) Alchemical free energy methods for drug discovery: progress and challenges. *Curr. Opin. Struct. Biol.* **21**, 150-160

138. Roux, B., Allen, T., Bernèche, S., and Im, W. (2004) Theoretical and computational models of biological ion channels. *Quart. Rev. Biophys.* **37**, 15-103

139. Sugita, Y., and Okamoto, Y. (1999) Replica-exchange molecular dynamics method for protein folding. *Chem. Phys. Lett.* **314**, 141-151

140. Wang, L., Friesner, R. A., and Berne, B. J. (2011) Replica exchange with solute scaling: a more efficient version of replica exchange with solute tempering (REST2). *J. Phys. Chem. B* **115**, 9431-9438

141. Jensen, M. Ø., Jogini, V., Borhani, D. W., Leffler, A. E., Dror, R. O., and Shaw, D. E. (2012) Mechanism of Voltage Gating in Potassium Channels. *Science* **336**, 229-233

142. Köpfer, D. A., Song, C., Gruene, T., Sheldrick, G. M., Zachariae, U., and de Groot, B. L. (2014) Ion permeation in K^+ channels occurs by direct Coulomb knock-on. *Science* **346**, 352-355

143. Tarek, M., and Delemotte, L. (2013) Omega currents in voltage-gated ion channels: what can we learn from uncovering the voltage-sensing mechanism using MD simulations? *Acc Chem Res* **46**, 2755-2762

144. Ulmschneider, M. B., Bagnéris, C., McCusker, E. C., Decaen, P. G., Delling, M., Clapham, D. E., Ulmschneider, J. P., and Wallace, B. A. (2013) Molecular dynamics of ion transport through the open conformation of a bacterial voltage-gated sodium channel. *Proc. Natl. Acad. Sci. U. S. A.* **110**, 6364-6369

145. Venkatachalam, K., and Montell, C. (2007) TRP Channels. *Annu. Rev. Biochem.* **76**, 387-417

146. Peng, G., Shi, X., and Kadowaki, T. (2014) Evolution of TRP channels inferred by their classification in diverse animal species. *Molecular phylogenetics and evolution* **84**, 145-157

CHAPTER 3

1. McKemy, D. D., Neuhausser, W. M., and Julius, D. (2002) Identification of a cold receptor reveals a general role for TRP channels in thermosensation. *Nature* **416**, 52-58

2. Peier, A. M., Moqrich, A., Hergarden, A. C., Reeve, A. J., Andersson, D. A., Story, G. M., Earley, T. J., Dragoni, I., McIntyre, P., Bevan, S., and Patapoutian, A. (2002) A TRP Channel that Senses Cold Stimuli and Menthol. *Cell* **108**, 705-715

3. Andersson, D. A., Chase, H. W., and Bevan, S. (2004) TRPM8 activation by menthol, icilin, and cold is differentially modulated by intracellular pH. *J. Neurosci.* **24**, 5364-5369

4. Rohacs, T. (2014) Phosphoinositide Regulation of TRP Channels. *Handb. Exp. Pharmacol.* **223**, 1143-1176

5. Knowlton, W. M., Daniels, R. L., Palkar, R., McCoy, D. D., and McKemy, D. D. (2011) Pharmacological blockade of TRPM8 ion channels alters cold and cold pain responses in mice. *PLoS One* **6**, e25894

6. Almeida, M. C., Hew-Butler, T., Soriano, R. N., Rao, S., Wang, W., Wang, J., Tamayo, N., Oliveira, D. L., Nucci, T. B., Aryal, P., Garami, A., Bautista, D., Gavva, N. R., and Romanovsky, A. A. (2012) Pharmacological blockade of the cold receptor TRPM8 attenuates autonomic and behavioral cold defenses and decreases deep body temperature. *J. Neurosci.* **32**, 2086-2099

7. Ding, Z., Gomez, T., Werkheiser, J. L., Cowan, A., and Rawls, S. M. (2008) Icilin induces a hyperthermia in rats that is dependent on nitric oxide production and NMDA receptor activation. *European Journal of Pharmacology* **578**, 201-208

8. Gavva, N. R., Davis, C., Lehto, S. G., Rao, S., Wang, W., and Zhu, D. X. D. (2012) Transient receptor potential melastatin 8 (TRPM8) channels are involved in body temperature regulation. *Mol. Pain* **8**, 36

9. Ma, S., Yu, H., Zhao, Z., Luo, Z., Chen, J., Ni, Y., Jin, R., Ma, L., Wang, P., Zhu, Z., Li, L., Zhong, J., Liu, D., Nilius, B., and Zhu, Z. (2012) Activation of the cold-sensing TRPM8 channel triggers UCP1-dependent thermogenesis and prevents obesity. *J. Mol. Cell Biol.* **4**, 88-96

10. Sun, J., Yang, T., Wang, P., Ma, S., Zhu, Z., Pu, Y., Li, L., Zhao, Y., Xiong, S., Liu, D., and Zhu, Z. (2014) Activation of cold-sensing transient receptor potential melastatin subtype 8 antagonizes vasoconstriction and hypertension through attenuating RhoA/Rho kinase pathway. *Hypertension* **63**, 1354-1363

11. Quallo, T., Vastani, N., Horridge, E., Gentry, C., Parra, A., Moss, S., Viana, F., Belmonte, C., Andersson, D. A., and Bevan, S. (2015) TRPM8 is a neuronal osmosensor that regulates eye blinking in mice. *Nat. Commun.* **6**, 7150

12. Tang, Z., Kim, A., Masuch, T., Park, K., Weng, H., Wetzel, C., and Dong, X. (2013) Pirt functions as an endogenous regulator of TRPM8. *Nat. Commun.* **4**, 2179

13. Tang, M., Wu, G. Y., Dong, X. Z., and Tang, Z. X. (2016) Phosphoinositide interacting regulator of TRP (Pirt) enhances TRPM8 channel activity in vitro via increasing channel conductance. *Acta Pharmacol. Sin.* **37**, 98-104

14. Kim, A. Y., Tang, Z., Liu, Q., Patel, K. N., Maag, D., Geng, Y., and Dong, X. (2008) Pirt, a phosphoinositide-binding protein, functions as a regulatory subunit of TRPV1. *Cell* **133**, 475-485

15. Wang, C., Wang, Z., Yang, Y., Zhu, C., Wu, G., Yu, G., Jian, T., Yang, N., Shi, H., Tang, M., He, Q., Lan, L., Liu, Q., Guan, Y., Dong, X., Duan, J., and Tang, Z. (2015) Pirt contributes to uterine contraction-induced pain in mice. *Mol. Pain* **11**, 57

16. Gao, X. F., Feng, J. F., Wang, W., Xiang, Z. H., Liu, X. J., Zhu, C., Tang, Z. X., Dong, X. Z., and He, C. (2015) Pirt reduces bladder overactivity by inhibiting purinergic receptor P2X3. *Nat. Commun.* **6**, 7650

17. Patel, K. N., Liu, Q., Meeker, S., Undem, B. J., and Dong, X. (2011) Pirt, a TRPV1 modulator, is required for histamine-dependent and -independent itch. *PLoS One* **6**, e20559

18. Hilton, J. K., Rath, P., Helsell, C. V., Beckstein, O., and Van Horn, W. D. (2015) Understanding thermosensitive transient receptor potential channels as versatile polymodal cellular sensors. *Biochemistry* **54**, 2401-2413

19. Jordt, S.-E., and Julius, D. (2002) Molecular Basis for Species-Specific Sensitivity to "Hot" Chili Peppers. *Cell* **108**, 421-430

20. Myers, B. R., Sigal, Y. M., and Julius, D. (2009) Evolution of Thermal Response Properties in a Cold-Activated TRP Channel. *PLoS One* **4**, e5741

21. Janssens, A., and Voets, T. (2011) Ligand stoichiometry of the cold- and menthol-activated channel TRPM8. *J. Physiol.* **589**, 4827-4835

22. Gkika, D., Lemonnier, L., Shapovalov, G., Gordiencko, D., Poux, C., Bernardini, M., Bokhobza, A., Bidaux, G., Degerny, C., Verreman, K., Guarmit, B., Benahmed, M., de Launoit, Y., Bindels, R. J. M., Pla, A. F., and Prevarskaya, N. (2015) TRP channel-associated factors are a novel protein family that regulates TRPM8 trafficking and activity. *J. Cell Biol.* **208**, 89-107

23. Ufret-Vincenty, C. A., Klein, R. M., Hua, L., Angueyra, J., and Gordon, S. E. (2011) Localization of the PIP2 sensor of TRPV1 ion channels. *J. Biol. Chem.* **286**, 9688-9698

24. Matos-Cruz, V., Schneider, E. R., Mastrotto, M., Merriman, D. K., Bagriantsev, S. N., and Gracheva, E. O. (2017) Molecular Prerequisites for Diminished Cold Sensitivity in Ground Squirrels and Hamsters. *Cell reports* **21**, 3329-3337

25. Chuang, H. H., Neuhausser, W. M., and Julius, D. (2004) The super-cooling agent icilin reveals a mechanism of coincidence detection by a temperature-sensitive TRP channel. *Neuron* **43**, 859-869

26. Kroncke, B. M., Van Horn, W. D., Smith, J., Kang, C., Welch, R. C., Song, Y., Nannemann, D. P., Taylor, K. C., Sisco, N. J., George, A. L., Jr., Meiler, J., Vanoye, C. G., and Sanders, C. R. (2016) Structural basis for KCNE3 modulation of potassium recycling in epithelia. *Sci. Adv.* **2**, e1501228

27. Yin, Y., Wu, M., Zubcevic, L., Borschel, W. F., Lander, G. C., and Lee, S. Y. (2018) Structure of the cold- and menthol-sensing ion channel TRPM8. *Science* **359**, 237-241

28. Jensen, M. Ø., Jogini, V., Borhani, D. W., Leffler, A. E., Dror, R. O., and Shaw, D. E. (2012) Mechanism of Voltage Gating in Potassium Channels. *Science* **336**, 229-233

29. Rath, P., Hilton, J. K., Sisco, N. J., and Van Horn, W. D. (2016) Implications of Human Transient Receptor Potential Melastatin 8 (TRPM8) Channel Gating from Menthol Binding Studies of the Sensing Domain. *Biochemistry* **55**, 114-124

30. Yang, F., Xiao, X., Cheng, W., Yang, W., Yu, P., Song, Z., Yarov-Yarovoy, V., and Zheng, J. (2015) Structural mechanism underlying capsaicin binding and activation of the TRPV1 ion channel. *Nat. Chem. Biol.* **11**, 518-524

31. Zhou, J., Tang, Y., Zheng, Q., Li, M., Yuan, T., Chen, L., Huang, Z., and Wang, K. (2015) Different KChIPs Compete for Heteromultimeric Assembly with Pore-Forming Kv4 Subunits. *Biophys. J.* **108**, 2658-2669

32. Weng, H. J., Patel, K. N., Jeske, N. A., Bierbower, S. M., Zou, W., Tiwari, V., Zheng, Q., Tang, Z., Mo, G. C., Wang, Y., Geng, Y., Zhang, J., Guan, Y., Akopian, A. N., and Dong, X. (2015) Tmem100 Is a Regulator of TRPA1-TRPV1 Complex and Contributes to Persistent Pain. *Neuron* **85**, 833-846

33. Guo, W., Sui, Q. Q., Gao, X. F., Feng, J. F., Zhu, J., He, C., Knight, G. E., Burnstock, G., and Xiang, Z. (2016) Co-localization of Pirt protein and P2X2 receptors in the mouse enteric nervous system. *Purinergic Signalling*

34. Sun, X., Zaydman, M. A., and Cui, J. (2012) Regulation of Voltage-Activated K(+) Channel Gating by Transmembrane beta Subunits. *Front. Pharmacol.* **3**, 63

35. McCrossan, Z. A., and Abbott, G. W. (2004) The MinK-related peptides. *Neuropharmacology* **47**, 787-821

36. Barhanin, J., Lesage, F., Guillemare, E., Fink, M., Lazdunski, M., and Romey, G. (1996) K_VLQT1 and IsK (minK) proteins associate to form the I_{Ks} cardiac potassium current. *Nature* **384**, 78-80

37. Grunnet, M., Jespersen, T., Rasmussen, H. B., Ljungstrøm, T., Jorgensen, N. K., Olesen, S.-P., and Klaerke, D. A. (2002) KCNE4 is an inhibitory subunit to the KCNQ1 channel. *J. Physiol.* **542**, 119-130

38. Manderfield, L. J., and George, A. L., Jr. (2008) KCNE4 can co-associate with the I_{Ks} (KCNQ1-KCNE1) channel complex. *FEBS J.* **275**, 1336-1349

39. Abbott, G. W., and Goldstein, S. A. N. (2002) Disease-associated mutations in KCNE potassium channel subunits (MiRPs) reveal promiscuous disruption of multiple currents and conservation of mechanism. *FASEB journal : official publication of the Federation of American Societies for Experimental Biology* **16**, 390-400

40. Ramanathan, K., Michael, T. H., Jiang, G.-J., Hiel, H., and Fuchs, P. A. (1999) A Molecular Mechanism for Electrical Tuning of Cochlear Hair Cells. *Science* **283**, 215-217

41. Bai, J. P., Surguchev, A., and Navaratnam, D. (2011) beta4-subunit increases Slo responsiveness to physiological Ca2+ concentrations and together with beta1 reduces surface expression of Slo in hair cells. *Am. J. Physiol. Cell Physiol.* **300**, C435-446

42. Martinez-Espinosa, P. L., Yang, C., Gonzalez-Perez, V., Xia, X. M., and Lingle, C. J. (2014) Knockout of the BK beta2 subunit abolishes inactivation of BK currents in mouse adrenal chromaffin cells and results in slow-wave burst activity. *J. Gen. Physiol.* **144**, 275-295

43. Liao, M., Cao, E., Julius, D., and Cheng, Y. (2013) Structure of the TRPV1 ion channel determined by electron cryo-microscopy. *Nature* **504**, 107-112

44. Gao, Y., Cao, E., Julius, D., and Cheng, Y. (2016) TRPV1 structures in nanodiscs reveal mechanisms of ligand and lipid action. *Nature* **534**, 347-351

45. Velisetty, P., Borbiro, I., Kasimova, M. A., Liu, L., Badheka, D., Carnevale, V., and Rohacs, T. (2016) A molecular determinant of phosphoinositide affinity in mammalian TRPV channels. *Scientific reports* **6**, 27652

46. Survery, S., Moparthi, L., Kjellbom, P., Hogestatt, E. D., Zygmunt, P. M., and Johanson, U. (2016) The N-terminal Ankyrin Repeat Domain Is Not Required for Electrophile and Heat Activation of the Purified Mosquito TRPA1 Receptor. *J. Biol. Chem.* **291**, 26899-26912

47. Moparthi, L., Survery, S., Kreir, M., Simonsen, C., Kjellbom, P., Hogestatt, E. D., Johanson, U., and Zygmunt, P. M. (2014) Human TRPA1 is intrinsically cold- and chemosensitive with and without its N-terminal ankyrin repeat domain. *Proc. Natl. Acad. Sci. U. S. A.* **111**, 16901-16906

48. Winkler, P. A., Huang, Y., Sun, W., Du, J., and Lu, W. (2017) Electron cryo-microscopy structure of a human TRPM4 channel. *Nature* **552**, 200-204

49. Duan, J., Li, Z., Li, J., Santa-Cruz, A., Sanchez-Martinez, S., Zhang, J., and Clapham, D. E. (2018) Structure of full-length human TRPM4. *Proc. Natl. Acad. Sci. U. S. A.* **115**, 2377-2382

50. Autzen, H. E., Myasnikov, A. G., Campbell, M. G., Asarnow, D., Julius, D., and Cheng, Y. (2018) Structure of the human TRPM4 ion channel in a lipid nanodisc. *Science* **359**, 228-232

51. Saito, S., Fukuta, N., Shingai, R., and Tominaga, M. (2011) Evolution of vertebrate transient receptor potential vanilloid 3 channels: opposite temperature sensitivity between mammals and western clawed frogs. *PLoS Genet.* **7**, e1002041

52. Chen, J., Kang, D., Xu, J., Lake, M., Hogan, J. O., Sun, C., Walter, K., Yao, B., and Kim, D. (2013) Species differences and molecular determinant of TRPA1 cold sensitivity. *Nat. Commun.* **4**, 2501

53. Gracheva, E. O., and Bagriantsev, S. N. (2015) Evolutionary adaptation to thermosensation. *Curr. Opin. Neurobiol.* **34**, 67-73

54. Khoury, M. K., Parker, I., and Aswad, D. W. (2010) Acquisition of chemiluminescent signals from immunoblots with a digital single-lens reflex camera. *Anal. Biochem.* **397**, 129-131

55. Miyazaki, K. (2011) MEGAWHOP Cloning: A Method of Creating Random Mutagenesis Libraries via Megaprimer PCR of Whole Plasmids. *Methods in Enzymology* **498**, 399-406

56. Peng, D., Kim, J. H., Kroncke, B. M., Law, C. L., Xia, Y., Droege, K. D., Van Horn, W. D., Vanoye, C. G., and Sanders, C. R. (2014) Purification and structural study of the voltage-sensor domain of the human KCNQ1 potassium ion channel. *Biochemistry* **53**, 2032-2042

57. Delaglio, F., Grzesiek, S., Vuister, G. W., Zhu, G., Pfeifer, J., and Bax, A. (1995) NMRPipe - A Multidimensional Spectral Processing System Based on UNIX Pipes. *Journal of biomolecular NMR* **6**, 277-293

58. Vranken, W. F., Boucher, W., Stevens, T. J., Fogh, R. H., Pajon, A., Llinas, P., Ulrich, E. L., Markley, J. L., Ionides, J., and Laue, E. D. (2005) The CCPN data model for NMR spectroscopy: Development of a software pipeline. *Proteins: Struct., Funct., Bioinf.* **59**, 687-696

CHAPTER 4

1. Andersson, D. A., Chase, H. W., and Bevan, S. (2004) TRPM8 activation by menthol, icilin, and cold is differentially modulated by intracellular pH. *J. Neurosci.* **24**, 5364-5369

2. Chuang, H. H., Neuhausser, W. M., and Julius, D. (2004) The super-cooling agent icilin reveals a mechanism of coincidence detection by a temperature-sensitive TRP channel. *Neuron* **43**, 859-869

3. Bandell, M., Dubin, A. E., Petrus, M. J., Orth, A., Mathur, J., Hwang, S. W., and Patapoutian, A. (2006) High-throughput random mutagenesis screen reveals TRPM8 residues specifically required for activation by menthol. *Nature neuroscience* **9**, 493-500

4. Voets, T., Owsianik, G., Janssens, A., Talavera, K., and Nilius, B. (2007) TRPM8 voltage sensor mutants reveal a mechanism for integrating thermal and chemical stimuli. *Nat. Chem. Biol.* **3**, 174-182

5. Autzen, H. E., Myasnikov, A. G., Campbell, M. G., Asarnow, D., Julius, D., and Cheng, Y. (2018) Structure of the human TRPM4 ion channel in a lipid nanodisc. *Science* **359**, 228-232

6. Huang, Y., Winkler, P. A., Sun, W., Lu, W., and Du, J. (2018) Architecture of the TRPM2 channel and its activation mechanism by ADP-ribose and calcium. *Nature* **562**, 145-149

7. Yin, Y., Wu, M., Zubcevic, L., Borschel, W. F., Lander, G. C., and Lee, S. Y. (2018) Structure of the cold- and menthol-sensing ion channel TRPM8. *Science* **359**, 237-241

8. Yin, Y., Le, S. C., Hsu, A. L., Borgnia, M. J., Yang, H., and Lee, S. Y. (2019) Structural basis of cooling agent and lipid sensing by the cold-activated TRPM8 channel. *Science* **363**, eaav9334

9. Rath, P., Hilton, J. K., Sisco, N. J., and Van Horn, W. D. (2016) Implications of Human Transient Receptor Potential Melastatin 8 (TRPM8) Channel Gating from Menthol Binding Studies of the Sensing Domain. *Biochemistry* **55**, 114-124

10. Bidaux, G., Borowiec, A. S., Gordienko, D., Beck, B., Shapovalov, G. G., Lemonnier, L., Flourakis, M., Vandenberghe, M., Slomianny, C., Dewailly, E., Delcourt, P., Desruelles, E., Ritaine, A., Polakowska, R., Lesage, J., Chami, M., Skryma, R., and Prevarskaya, N. (2015) Epidermal TRPM8 channel isoform controls the balance between keratinocyte proliferation and differentiation in a cold-dependent manner. *Proc. Natl. Acad. Sci. U. S. A.* **112**, E3345-E3354

11. Cao, E., Liao, M., Cheng, Y., and Julius, D. (2013) TRPV1 structures in distinct conformations reveal activation mechanisms. *Nature* **504**, 113-118

12. Gao, Y., Cao, E., Julius, D., and Cheng, Y. (2016) TRPV1 structures in nanodiscs reveal mechanisms of ligand and lipid action. *Nature* **534**, 347-351

13. Yang, F., Xiao, X., Cheng, W., Yang, W., Yu, P., Song, Z., Yarov-Yarovoy, V., and Zheng, J. (2015) Structural mechanism underlying capsaicin binding and activation of the TRPV1 ion channel. *Nat. Chem. Biol.* **11**, 518-524

14. Yang, F., Xiao, X., Lee, B. H., Vu, S., Yang, W., Yarov-Yarovoy, V., and Zheng, J. (2018) The conformational wave in capsaicin activation of transient receptor potential vanilloid 1 ion channel. *Nat. Commun.* **9**, 2879

15. Zhang, F., Hanson, S. M., Jara-Oseguera, A., Krepkiy, D., Bae, C., Pearce, L. V., Blumberg, P. M., Newstead, S., and Swartz, K. J. (2016) Engineering vanilloid-sensitivity into the rat TRPV2 channel. *eLife* **5**, e16409

16. Zhang, F., Swartz, K. J., and Jara-Oseguera, A. (2019) Conserved allosteric pathways for activation of TRPV3 revealed through engineering vanilloid-sensitivity. *eLife* **8**, e42756

17. Yang, F., Vu, S., Yarov-Yarovoy, V., and Zheng, J. (2016) Rational design and validation of a vanilloid-sensitive TRPV2 ion channel. *Proc. Natl. Acad. Sci. U. S. A.* **113**, E3657-3666

18. Andersen, K. R., Leksa, N. C., and Schwartz, T. U. (2013) Optimized E. coli expression strain LOBSTR eliminates common contaminants from His-tag purification. *Proteins* **81**, 1857-1861

19. Miles, A. J., and Wallace, B. A. (2018) CDtoolX, a downloadable software package for processing and analyses of circular dichroism spectroscopic data. *Protein Sci.* **27**, 1717-1722

20. Liao, M., Cao, E., Julius, D., and Cheng, Y. (2013) Structure of the TRPV1 ion channel determined by electron cryo-microscopy. *Nature* **504**, 107-112

21. Talavera, K., and Nilius, B. (2011) Electrophysiological Methods for the Study of TRP Channels. in *TRP Channels* (Zhu, M. X. ed.), CRC Press/Taylor & Francis, Boca Raton, FL. pp

22. Bödding, M., Wissenbach, U., and Flockerzi, V. (2007) Characterisation of TRPM8 as a pharmacophore receptor. *Cell Calcium* **42**, 618-628

23. McKemy, D. D., Neuhausser, W. M., and Julius, D. (2002) Identification of a cold receptor reveals a general role for TRP channels in thermosensation. *Nature* **416**, 52-58

24. El-Arabi, A. M., Salazar, C. S., and Schmidt, J. J. (2012) Ion channel drug potency assay with an artificial bilayer chip. *Lab Chip* **12**, 2409-2413

25. Sherkheli, M. A., Vogt-Eisele, A. K., Bura, D., Márques, L. R. B., Gisselmann, G., and Hatt, H. (2010) Characterization of Selective TRPM8 Ligands and their Structure Activity Response (S.A.R) Relationship. *J. Pharm. Pharm. Sci.* **13**, 242-253

26. Gong, X. M., Franzin, C. M., Thai, K., Yu, J., and Marassi, F. M. (2007) Nuclear Magnetic Resonance Structural Studies of Membrane Proteins in Micelles and Bilayers. *Methods Mol. Biol.* **400**, 515-529

27. Wakita, K., Yoshimoto, M., Miyamoto, S., and Watanabe, H. (1986) A Method for Calculation of the Aqueous Solubility of Organic Compounds by Using New Fragment Salubility Constants. *Chem. Pharm. Bull.* **34**, 4663-4681

28. Barrett, P. J., Song, Y., Van Horn, W. D., Hustedt, E. J., Schafer, J. M., Hadziselimovic, A., Beel, A. J., and Sanders, C. R. (2012) The Amyloid Precursor Protein Has a Flexible Transmembrane Domain and Binds Cholesterol. *Science* **336**, 1168-1171

29. Barrett, P. J., Song, Y., Van Horn, W. D., Hustedt, E. J., Schafer, J. M., Hadziselimovic, A., Beel, A. J., and Sanders, C. R. (2012) Structural studies of the transmembrane C-terminal domain of the amyloid precursor protein (APP): does APP function as a cholesterol sensor? *Biochemistry* **47**, 9428– 9446

30. López-Arenas, L., Solís-Mendiola, S., and Hernández-Arana, A. (1999) Estimating the Degree of Expansion in the Transition State for Protein Unfolding: Analysis of the pH Dependence of the Rate Constant for Caricain Denaturation. *Biochemistry* **38**, 15936-15943

31. Consalvi, V., Chiaraluce, R., Giangiacomo, L., Scandurra, R., Christova, P., Karshikoff, A., Knapp, S., and Ladenstein, R. (2000) Thermal unfolding and conformational stability of the recombinant domain II of glutamate dehydrogenase from the hyperthermophile *Thermotoga maritima*. *Protein engineering* **13**, 501-507

32. Manning, M. C., and Woody, R. W. (1991) Theoretical CD studies of polypeptide helices: examination of important electronic and geometric factors. *Biopolymers* **31**, 569-586

33. Toniolo, C., Polese, A., Formaggio, F., Crisma, M., and Kamphuis, J. (1996) Circular Dichroism Spectrum of a Peptide 3_{10}-Helix. *J. Am. Chem. Soc.* **118**, 2744-2745

34. Banerjee, R., and Sheet, T. (2017) Ratio of ellipticities between 192 and 208 nm (R_1): An effective electronic circular dichroism parameter for characterization of the helical components of proteins and peptides. *Proteins* **85**, 1975-1982

CHAPTER 5

1. Miyazaki, K. (2011) MEGAWHOP cloning: a method of creating random mutagenesis libraries via megaprimer PCR of whole plasmids. *Methods Enzymol.* **498**, 399-406

2. Yao, J., Liu, B., and Qin, F. (2010) Kinetic and energetic analysis of thermally activated TRPV1 channels. *Biophys. J.* **99**, 1743-1753

3. Vriens, J., Nilius, B., and Voets, T. (2014) Peripheral thermosensation in mammals. *Nature reviews. Neuroscience* **15**, 573-589

4. Cao, E., Cordero-Morales, J. F., Liu, B., Qin, F., and Julius, D. (2013) TRPV1 channels are intrinsically heat sensitive and negatively regulated by phosphoinositide lipids. *Neuron* **77**, 667-679

5. Gracheva, E. O., Cordero-Morales, J. F., Gonzalez-Carcacia, J. A., Ingolia, N. T., Manno, C., Aranguren, C. I., Weissman, J. S., and Julius, D. (2011) Ganglion-specific splicing of TRPV1 underlies infrared sensation in vampire bats. *Nature* **476**, 88-91

6. Laursen, W. J., Schneider, E. R., Merriman, D. K., Bagriantsev, S. N., and Gracheva, E. O. (2016) Low-cost functional plasticity of TRPV1 supports heat tolerance in squirrels and camels. *Proc. Natl. Acad. Sci. U. S. A.* **113**, 11342-11347

7. Myers, B. R., Sigal, Y. M., and Julius, D. (2009) Evolution of Thermal Response Properties in a Cold-Activated TRP Channel. *PLoS One* **4**, e5741

8. Matos-Cruz, V., Schneider, E. R., Mastrotto, M., Merriman, D. K., Bagriantsev, S. N., and Gracheva, E. O. (2017) Molecular Prerequisites for Diminished Cold Sensitivity in Ground Squirrels and Hamsters. *Cell reports* **21**, 3329-3337

9. Feng, Q. (2014) Temperature sensing by thermal TRP channels: thermodynamic basis and molecular insights. *Curr. Top. Membr.* **74**, 19-50

10. Meyer, R., and Heinemann, S. (1997) Temperature and pressure dependence of *Shaker* K^+ channel N- and C-type inactivation. *Eur. Biophys. J.* **26**, 433-445

11. Correa, A. M., Bezanilla, F., and Latorre, R. (1992) Gating kinetics of Batrachotoxin-modified Na^+ channels in the squid giant axon. *Biophys. J.* **61**, 1332-1352

12. Vlachova, V., Teisinger, J., Sušánková, K., Lyfenko, A., Ettrich, R., and Vyklicky, L. (2003) Functional Role of C-Terminal Cytoplasmic Tail of Rat Vanilloid Receptor 1. *J. Neurosci.* **23**, 1340-1350

13. Liu, B., Hui, K., and Qin, F. (2003) Thermodynamics of Heat Activation of Single Capsaicin Ion Channels VR1. *Biophys. J.* **85**, 2988-3006

14. Yang, F., Cui, Y., Wang, K., and Zheng, J. (2010) Thermosensitive TRP channel pore turret is part of the temperature activation pathway. *Proc. Natl. Acad. Sci. U. S. A.* **107**, 7083-7088

15. Yao, J., Liu, B., and Qin, F. (2011) Modular thermal sensors in temperature-gated transient receptor potential (TRP) channels. *Proc. Natl. Acad. Sci. U. S. A.* **108**, 11109-11114

16. Sun, X., and Zakharian, E. (2015) Regulation of the temperature-dependent activation of transient receptor potential vanilloid 1 (TRPV1) by phospholipids in planar lipid bilayers. *J. Biol. Chem.* **290**, 4741-4747

17. Zhang, F., Jara-Oseguera, A., Chang, T. H., Bae, C., Hanson, S. M., and Swartz, K. J. (2018) Heat activation is intrinsic to the pore domain of TRPV1. *Proc. Natl. Acad. Sci. U. S. A.* **115**, E317-E324

18. Sanchez-Moreno, A., Guevara-Hernandez, E., Contreras-Cervera, R., Rangel-Yescas, G., Ladron-de-Guevara, E., Rosenbaum, T., and Islas, L. D. (2018) Irreversible temperature gating in trpv1 sheds light on channel activation. *eLife* **7**, e36372

19. Clapham, D. E., and Miller, C. (2011) A thermodynamic framework for understanding temperature sensing by transient receptor potential (TRP) channels. *Proc. Natl. Acad. Sci. U. S. A.* **108**, 19492-19497

20. Yao, J., Liu, B., and Qin, F. (2009) Rapid temperature jump by infrared diode laser irradiation for patch-clamp studies. *Biophys. J.* **96**, 3611-3619

21. Boukalova, S., Marsakova, L., Teisinger, J., and Vlachova, V. (2010) Conserved residues within the putative S4-S5 region serve distinct functions among thermosensitive vanilloid transient receptor potential (TRPV) channels. *J Biol Chem* **285**, 41455-41462

22. Chowdhury, S., Jarecki, B. W., and Chanda, B. (2014) A molecular framework for temperature-dependent gating of ion channels. *Cell* **158**, 1148-1158

23. Jordt, S. E., and Julius, D. (2002) Molecular Basis for Species-Specific Sensitivity to "Hot" Chili Peppers. *Cell* **108**, 421-430

24. Chuang, H. H., Neuhausser, W. M., and Julius, D. (2004) The super-cooling agent icilin reveals a mechanism of coincidence detection by a temperature-sensitive TRP channel. *Neuron* **43**, 859-869

25. Hilton, J. K., Salehpour, T., Sisco, N. J., Rath, P., and Van Horn, W. D. (2018) Phosphoinositide-interacting regulator of TRP (PIRT) has opposing effects on human and mouse TRPM8 ion channels. *J. Biol. Chem.* **293**, 9423-9434

26. Togashi, K., Hara, Y., Tominaga, T., Higashi, T., Konishi, Y., Mori, Y., and Tominaga, M. (2006) TRPM2 activation by cyclic ADP-ribose at body temperature is involved in insulin secretion. *EMBO J.* **25**, 1804-1815

27. Tan, C. H., and McNaughton, P. A. (2016) The TRPM2 ion channel is required for sensitivity to warmth. *Nature* **536**, 460-463

28. Song, K., Wang, H., Kamm, G. B., Pohle, J., Fernanda de Castro, R., Heppenstall, P., Wende, H., and Siemens, J. (2016) The TRPM2 channel is a hypothalamic heat sensor that limits fever and can drive hypothermia. *Science* **353**, 1393-1398

29. Voets, T., Owsianik, G., Janssens, A., Talavera, K., and Nilius, B. (2007) TRPM8 voltage sensor mutants reveal a mechanism for integrating thermal and chemical stimuli. *Nat. Chem. Biol.* **3**, 174-182

30. Kalia, J., and Swartz, K. J. (2013) Exploring structure-function relationships between TRP and Kv channels. *Scientific reports* **3**, 1523

31. Cao, E., Liao, M., Cheng, Y., and Julius, D. (2013) TRPV1 structures in distinct conformations reveal activation mechanisms. *Nature* **504**, 113-118

32. Gao, Y., Cao, E., Julius, D., and Cheng, Y. (2016) TRPV1 structures in nanodiscs reveal mechanisms of ligand and lipid action. *Nature* **534**, 347-351

33. Liao, M., Cao, E., Julius, D., and Cheng, Y. (2013) Structure of the TRPV1 ion channel determined by electron cryo-microscopy. *Nature* **504**, 107-112

34. Calixto, J. B., Kassuya, C. A., Andre, E., and Ferreira, J. (2005) Contribution of natural products to the discovery of the transient receptor potential (TRP) channels family and their functions. *Pharmacol. Ther.* **106**, 179-208

35. Kaneko, Y., and Szallasi, A. (2014) Transient receptor potential (TRP) channels: a clinical perspective. *Br. J. Pharmacol.* **171**, 2474-2507

36. Beccari, A. R., Gemei, M., Lo Monte, M., Menegatti, N., Fanton, M., Pedretti, A., Bovolenta, S., Nucci, C., Molteni, A., Rossignoli, A., Brandolini, L., Taddei, A., Za, L., Liberati, C., and Vistoli, G. (2017) Novel selective, potent naphthyl TRPM8 antagonists identified through a combined ligand- and structure-based virtual screening approach. *Scientific reports* **7**, 10999

37. Aizawa, N., Ohshiro, H., Watanabe, S., Kume, H., Homma, Y., and Igawa, Y. (2019) RQ-00434739, a novel TRPM8 antagonist, inhibits prostaglandin E2-

induced hyperactivity of the primary bladder afferent nerves in rats. *Life Sci.* **218**, 89-95

38. Ma, S., Yu, H., Zhao, Z., Luo, Z., Chen, J., Ni, Y., Jin, R., Ma, L., Wang, P., Zhu, Z., Li, L., Zhong, J., Liu, D., Nilius, B., and Zhu, Z. (2012) Activation of the cold-sensing TRPM8 channel triggers UCP1-dependent thermogenesis and prevents obesity. *J. Mol. Cell. Biol.* **4**, 88-96

39. Yee, N. S. (2016) TRPM8 Ion Channels as Potential Cancer Biomarker and Target in Pancreatic Cancer. *Adv. Protein Chem. Struct. Biol.* **104**, 127-155

40. Journigan, V. B., and Zaveri, N. T. (2013) TRPM8 ion channel ligands for new therapeutic applications and as probes to study menthol pharmacology. *Life Sci.* **92**, 425-437

APPENDIX A

SUPPLEMENT TO CHAPTER 3: ADDITIONAL HUMAN-MOUSE TRPM8 CHIMERA DATA

In addition to the mouse-human TRPM8 chimeras described in Chapter 3 of this dissertation, a hTRPM8[mM8-TMD] and a hTRPM8[mM8-SD] chimera were constructed and tested with and without human and mouse PIRT. The following figure show the results of these experiments. These experiments were carried out using the methods described in Chapter 3.

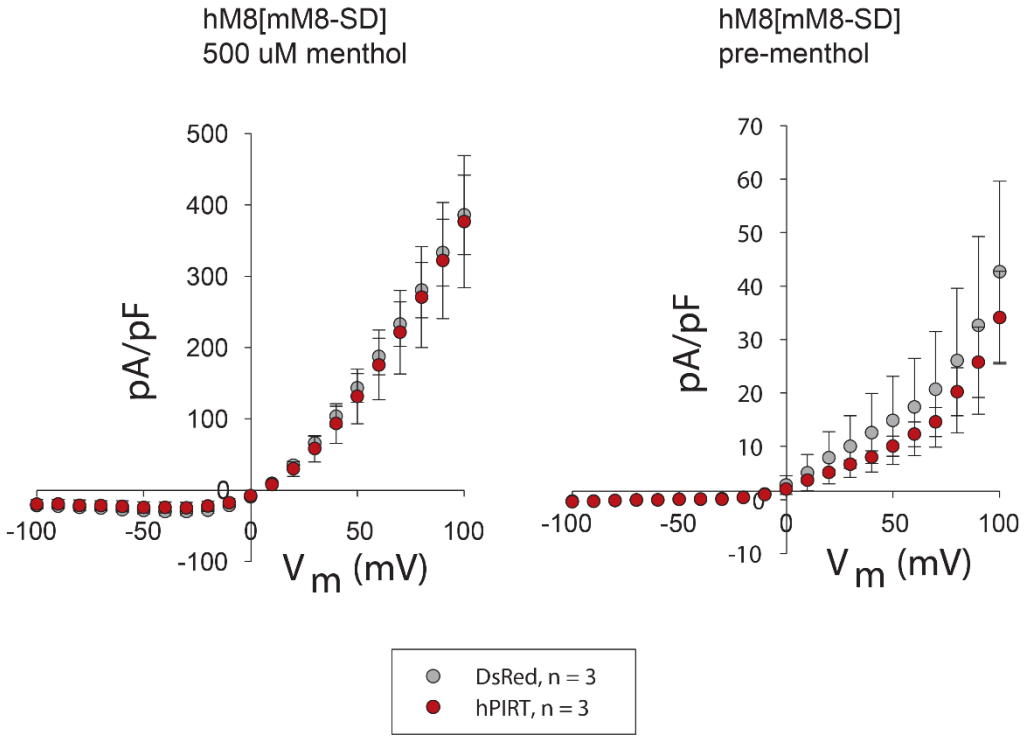

Figure A.1 Current-voltage plots of the hTRPM8[mM8-SD] channel expressed in HEK-293 cells under conditions indicated in the figure. Human PIRT had no significant effect on this chimera.

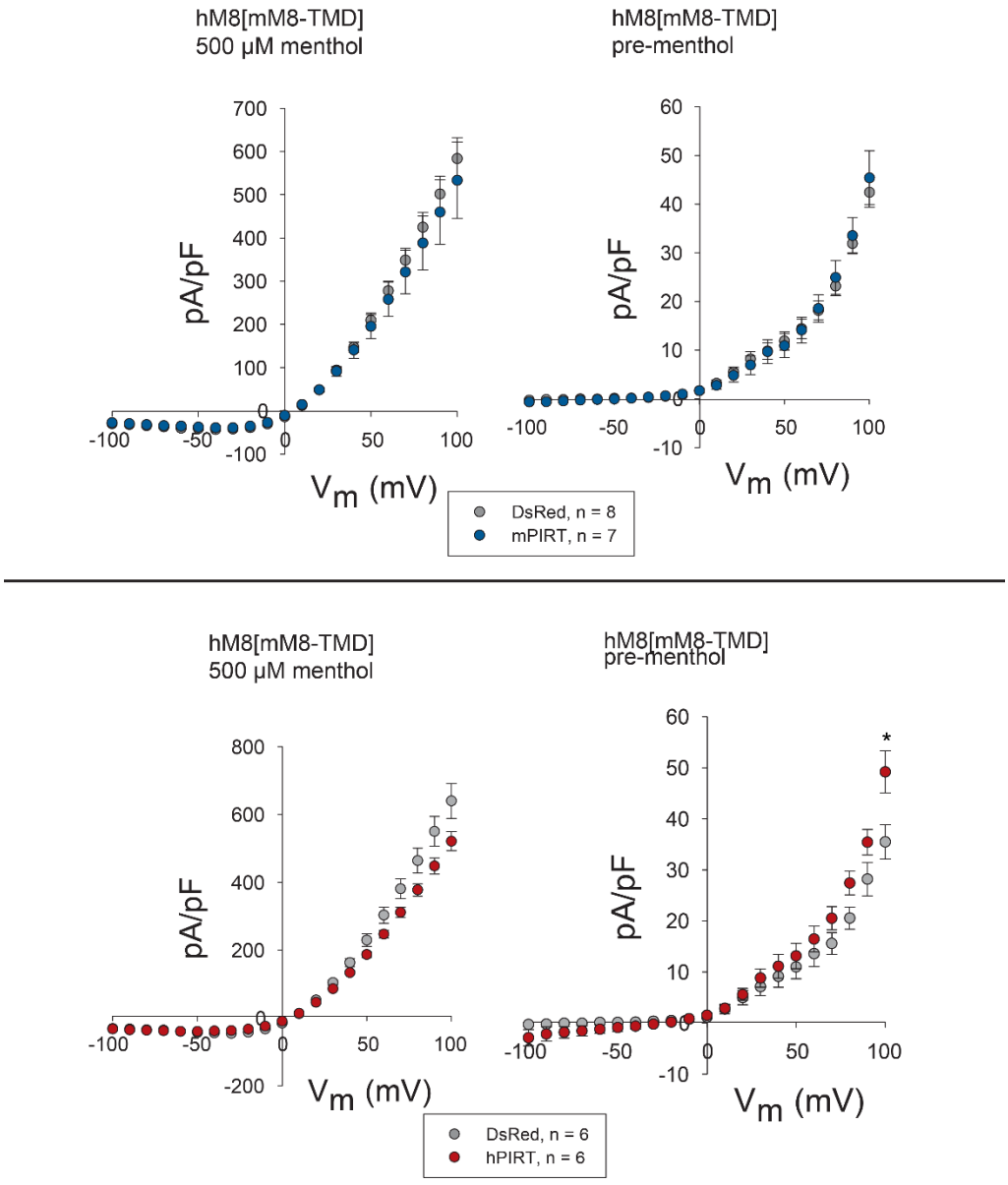

Figure A.2 Current-voltage plots of the hTRPM8[mM8-TMD] channel expressed in HEK-293 cells. Conditions are indicated in the figure. Besides a single point at +100 mV in the absence of menthol, neither PIRT ortholog had a significant effect on this chimera.

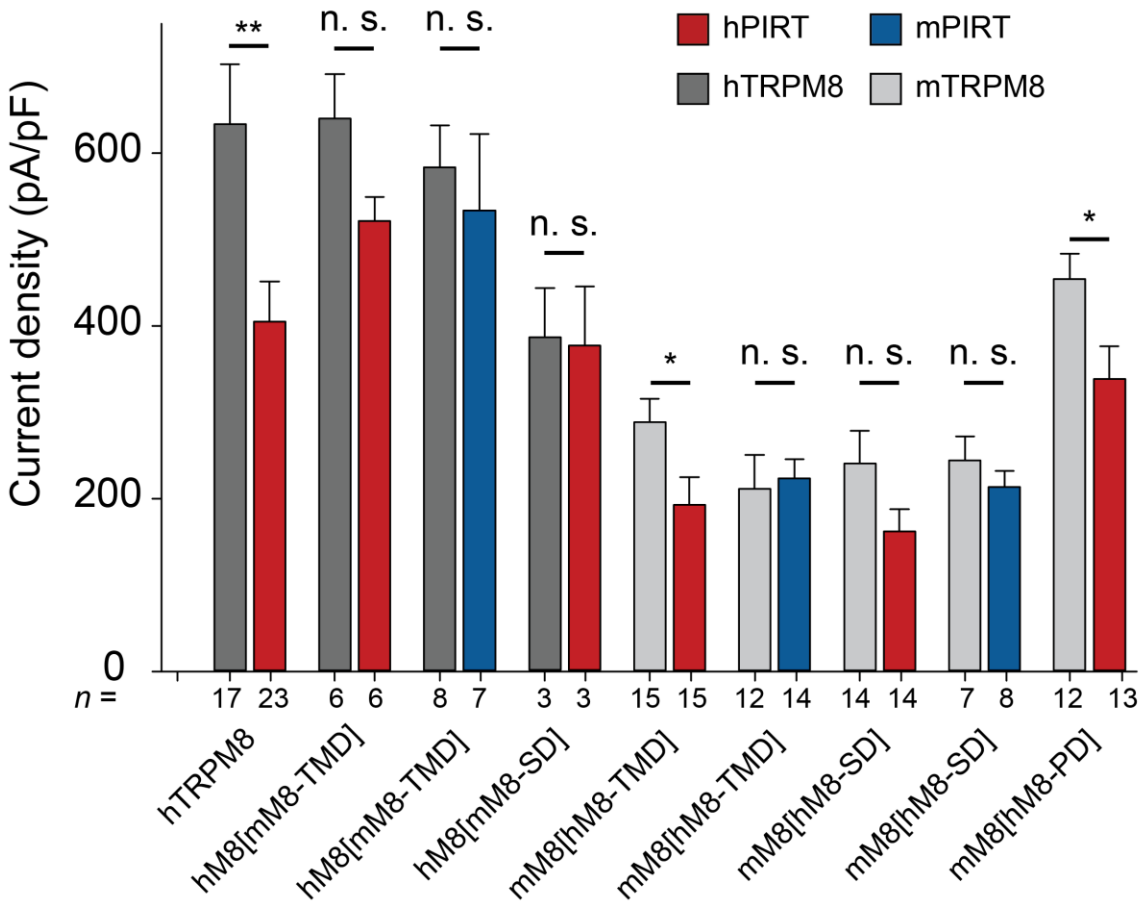

Figure A.3 Summary of chimera results. Values shown are steady-steady current density at +100 mV in the presence of 500 µM menthol. Error bars represent standard error of the mean.

APPENDIX B

PUBLISHED PORTIONS

Portions of this dissertation have been previously published. These portions were included with permission from all co-authors.

Chapter 2:

Reproduced with permission from Hilton, J. K., Rath, P., Helsell, C. V. M., Beckstein, O., and Van Horn, W. D. Understanding Thermosensitive Transient Receptor Potential Channels as Versatile Polymodal Cellular Sensors. *Biochemistry* 2015, 54:2401-2403. Copyright 2015 American Chemical Society.

Chapter 3:

This research was originally published in *The Journal of Biological Chemistry*. Hilton, J. K., Salehpour, T., Sisco, N. J., Rath, P., and Van Horn, W. D. Phosphoinositide-interacting regulator of TRP (PIRT) has opposing effects on human and mouse TRPM8 ion channels. *J. Biol. Chem.* 2018; 293:9423-9434. © the American Society for Biochemistry and Molecular Biology.